BEHAVIOUR OF LIGHT-FRAME WOOD STUD WALLS SUBJECTED TO BLAST LOADING

by
Daniel Lacroix

Thesis submitted to the
Faculty of Graduate and Postdoctoral Studies
in partial fulfillment of the requirements for the degree of
Master of Applied Science
in Civil Engineering

Under the auspices of the Ottawa-Carleton Institute for Civil Engineering

uOttawa

Departments of Civil Engineering
University of Ottawa
June 2013

ABSTRACT

Deliberate and accidental explosions along with the heightened risk of loss of life and property damage during such events have highlighted the need for research in the behaviour of materials under high strain rates. Where an extensive body of research is available on steel and concrete structures, little to no details on how to address the design or retrofitting of wood structures subjected to a blast threat are available. Studies reported in the literature that focused on full scale light-frame wood structures did not quantify the increase in capacity due to the dynamic loading while the studies that did quantify the increase mostly stems from small clear specimens that are not representative of the behaviour of structural size members with defects. Tests on larger-scale specimens have mostly focused on the material properties and not the structural behaviour of subsystems. Advancements in design and construction techniques have greatly contributed to the emergence of taller and safer wood structures which increase potential for blast threat. This thesis presents results on the flexural behaviour of light-frame wood stud walls subjected to shock wave loading using the University of Ottawa shock tube. The emphasis is on the overall behaviour of the wall subsystem, especially the interaction between the sheathing and the studs through the nailed connection.

The approach employed in this experimental program was holistic, where the specimens were investigated at the component and the subsystem levels. Twenty walls consisting of 38 mm x 140 mm machine stress-rated (MSR) studs spaced 406 mm on center and sheathed with two different types and sheathing thicknesses were tested to failure under static and dynamic loads. The experimental results were used to determine dynamic increase factors (DIFs) and a material predictive model was validated using experimental data. The implications of the code are also discussed and compared to the experimental data.

Once validated, an equivalent single-degree-of-freedom (SDOF) model incorporating partial composite action was used to evaluate current analysis and design assumptions. The results showed that a shock tube can effectively be used to generate high strain-rate flexural response in wood members and that the material predictive model was found suitable to effectively predict the displacement resulting from shock wave loading. Furthermore, it was found that current analysis and design approaches overestimated the wall displacements.

SOMMAIRE

Les explosions à la fois délibérées et accidentelles, en plus des risques élevés de décès et de dommages matériels que peuvent entrainer ces dernières, ont su mettre en évidence la nécessité de mener des recherches approfondies sur le comportement des matériaux soumis à de hautes vitesses de déformation. Bien qu'il existe un vaste répertoire de recherches disponibles sur les infrastructures de métaux et de bétons, peu de recherches fournissent des indices sur la façon d'aborder la conception et/ou la modification des infrastructures de bois soumises à de telles explosions. En effet, de nombreuses études précédemment effectuées sur les structures de bois à ossature légère n'ont su quantifier l'augmentation de la capacité en raison de la charge dynamique. Quant à elles, les études qui ont quantifié cette augmentation proviennent de petits spécimens non-représentatifs du comportement des éléments de tailles réelles présentant des défauts, tels que des noeuds. De plus, les tests menés sur des échantillons de plus grande envergure ont surtout porté sur les propriétés des matériaux et non sur les comportements structurels de sous-systèmes. Par ailleurs, les améliorations dans la conception et dans les techniques de construction ont largement contribué à l'émergence d'infrastructures en bois plus hautes et plus sûres, ce qui augmente inévitablement leur potentiel de menace à l'explosion. Cette thèse présente donc des résultats relatifs au comportement de murs de bois à ossature légère soumis à un chargement d'ondes de choc en faisant usage du tube à chocs de l'Université d'Ottawa. Dès lors, l'accent est mis sur le comportement global du sous-système mural, et plus particulièrement sur l'interaction entre le revêtement et les colombages à travers la connexion clouée.

L'approche utilisée dans ce programme expérimental fut holistique, dans le sens où le comportement et les sous-systèmes des spécimens furent étudiés. Vingt murs construits de poutres de bois (colombages) de 38 mm x 140 mm espacés au centre de 406 mm avec deux épaisseurs de revêtement furent testé sous des charges statiques et dynamiques menant à la défaillance du système. Les résultats expérimentaux furent utilisés afin de déterminer l'augmentation de la capacité sous une charge dynamique causant des déformations à haute vitesse. Un modèle considérant l'action partiel entre le revêtement et les goujons (colombages) fut utilisé et validé avec les résultats expérimentaux. Les implications du code sont également discutées et comparées aux données expérimentales.

Une fois validée, un système équivalant à un seul degré de liberté intégrant l'action partielle entre le revêtement et les colombages fut utilisé dans le but d'évaluer l'analyse actuelle du code et les hypothèses de conception. Les résultats ont démontré qu'un tube à chocs peut effectivement être utilisé pour générer un taux de déformation élevé dans les structures en bois et que le modèle prédictif élaboré a été jugé apte à prédire efficacement le déplacement causé par les ondes de choc. En outre, les résultats ont démontré que l'analyse actuelle d'après le code ainsi que les approches utilisées dans la conception ont surestimé les déplacements des murs étudiés.

ACKNOWLEDGEMENTS

Through the course of my master's, I have been fortunate to have a supervisor and family members that believed in my potential and without their continuous moral support nothing of this would be possible, and for that I am grateful. I would like to thank my thesis supervisor, Dr. Ghasan Doudak, for his guidance and time, the many opportunities arising from this project, as well as for financial support.

I would like to extend my appreciation to my spouse, Ms. Alexandra Cross, and my son, Jayden, for understanding the many commitments I had undertaken and for always supporting me. Again, none of this would be possible without your support.

I would also like to thank my fellow graduate students, Mr. Alan Lloyd and Mr. Eric Jacques, for their guidance and help as well as always having time to discuss research related topics. To all of the people who helped me with experimental testing, especially over the weekends, I am infinitely indebted: Mr. Kevin Rocchi, Mr. Benoit Guindon, Mr. Francis Blanchard, Mr. Sebastien Bernard, Mr. Dominic Camiré, Mr. Gino Vaillancourt and Mr. Raymond Piette.

I would like to acknowledge the financial support received, which allowed me to focus on my research, from NSERC, OGS and the University of Ottawa.

Last but not least, I will never be able to thank my parents enough for believing in me and supporting me throughout the course of life.

Table of Contents

LIST OF TABLES

LIST OF FIGURES

GLOSSARY

Acronym		Definition
API	=	American petroleum institute
ASTM	=	American society for testing and materials
BAIT	=	Blast and Injury Tests
BASS	=	Barrier Assessment for Safe Standoff
CEDAW	=	Component explosive damage assessment workbook
COV	=	Coefficient of variation
CSL	=	Coated structural lumber
DIF	=	Dynamic increase factor
FE	=	Finite element
FRP	=	Fiber-reinforced polymer
KE	=	Kinetic energy
LSL	=	Laminated strand lumber
LVDT	=	Linear variable displacement transducer
MDOF	=	Multi-degree-of-freedom
MOE	=	Modulus of elasticity
MOR	=	Modulus of rupture
MSR	=	Machine stress rated
OSB	=	Oriented-strandboard
P-I	=	Pressure-impulse
PSL	=	Parallel strand lumber
RODS	=	Retrofits and Overpressure Design of Structures
ROL	=	Rate of loading
RP	=	Recommended Practice
SDOF	=	Single-degree-of-freedom
SE	=	Strain energy
SEA Hut	=	Southeast Asia Hut
TNT	=	Trinitrotoluene
VCE	=	Vapour cloud explosion
WD	=	Work done by the system
WWII	=	Second World War

Symbol		Definition
$\phi(x)$	=	Shape function
$(P_{max})_{Avg}$	=	Average applied load at failure
$(P_{Xe})_{Avg}$	=	Average applied load at elastic limit
$(X_e)_{Avg}$	=	Average elastic deflection limit
$(X_{max})_{Avg}$	=	Average elastic deflection at failure
$\dot{\epsilon}_{avg}$	=	Average strain rate of four middle studs
H_{EXP}^{d}	=	Heat of detonation of explosive considered
H_{TNT}^{d}	=	Heat of detonation of TNT
P/δ	=	Load-slip relationship
$\bar{m}(x)$	=	Distributed mass per length
$\ddot{y}$	=	Acceleration
μ	=	Ductility ratio
a	=	Acceleration
A	=	Loaded area
b	=	Blast waveform parameter
c	=	Damping constant
C_r	=	Coefficient of reflection
$d_{max\text{-}avg}$	=	Average maximum experimental mid-span displacement
$EI_{P.C.}$	=	Composite bending stiffness
F	=	Total load
F(t)	=	Total external force as a function of time
F_1	=	External force applied indefinitely
f_b	=	Bending strength
F_e	=	Equivalent load
I^-	=	Negative impulse
I^+	=	Positive impulse
I_R	=	Experimental reflected impulse
k	=	Spring constant or stiffness
K_L	=	Load transformation factor
K_{LM}	=	Load-mass transformation factor

K_M	=	Mass transformation factor
K_R	=	Resistance transformation factor
L	=	Clear span length
L_D	=	Driver length
m	=	Mass
MOE_{Dyn}	=	Dynamic modulus of elasticity
MOR_{Dyn}	=	Dynamic modulus of rupture
$MOR_{Exp\text{-}Stud}$	=	Experimental MOR of studs
MOR_{Static}	=	Static modulus of rupture
M_p	=	Dynamic moment capacity
m_w	=	Experimental mass of studs
P(t)	=	Pressure-time history
p(x,t)	=	Distributed load per unit length
P_D	=	Driver pressure
P_{max}	=	Applied load at failure
P_o	=	Ambient pressure
P_r	=	Reflected pressure
P_R	=	Experimental reflected pressure
P_s	=	Incident peak pressure
P_{Xe}	=	Applied load at elastic limit
R	=	Standoff distance
R(t)	=	Total internal force as a function of time
R(y)	=	Non-linear resistance term
R_e	=	Resistance at elastic deflection limit
R_u	=	Ultimate resistance
S	=	Interlayer stiffness
s	=	Nail spacing
S_D	=	Dynamic bending resistance
SIF	=	Strength increase factor
$S_{P.C.}$	=	Composite section modulus
S_S	=	Static bending resistance
t	=	time
t_a	=	Time of arrival of shock wave
t_d	=	Positive phase duration of explosion

t_d^-	=	Negative phase duration of explosion
$t_{d\text{-}exp}$	=	Experimental positive phase duration
$t_{max\text{-}avg}$	=	Average time to average maximum displacement
W	=	Charge weight
W_E	=	Effective charge weight in TNT
W_{EXP}	=	Weight of explosive considered
x_e	=	Elastic deflection
X_e	=	Deflection at elastic limit
x_{max}	=	Maximum deflection
X_{max}	=	Deflection at failure
y	=	Displacement
$\dot{y}$	=	Velocity
y_o	=	Initial displacement
$\dot{y}_o$	=	Initial velocity
y_{st}	=	Displacement resulting from dynamic force applied statically
Z	=	Scaled distance
α_i	=	Angle of incidence
ω	=	Circular frequency

CHAPTER 1-Introduction

1.1 General introduction and research needs

In the past few decades, the response of structures to blast loadings, such as deliberate attacks on buildings (e.g. World Trade Center, 2001) and accidental explosions (e.g. Ronan Point, 1968; BP Texas City, 2005), has become a topic of interest for researchers and engineers. This is in part due to the political and socio-economic issues associated with such tragic events. The heightened risk of loss of life and property damage has highlighted the need for research in the behaviour of materials under high strain rates. The focus, for the most part, has been on the behaviour of concrete and steel as most high-risk and high-profile structures consist of a combination of these two materials. As a result, provisions have been enacted in the United-Kingdom (Office of the Deputy Prime Minister, 2004) and the United-States of America (TM 5-1300, 1990; Unified Facilities Criteria (UFC) 4-023-03, 2009; US Federal Emergency Management Agency (FEMA), 2011) in which provisions covering loads on structures resulting from explosions, fragment analysis, and dynamic analysis are available. An extensive body of research is currently available on concrete and steel structures, however, little to no details on how to address the design or retrofitting of wood structures subjected to a blast threat are available. Wood may not be a designer's first choice as a blast resistant material, but the advancements in design and construction techniques have greatly contributed to the emergence of taller (mid-rise) and safer wood structures in a way where wood is no longer limited to low-rise light-frame residential structures. It is also important to recognize that high-profile timber structures (e.g. the roof of the Olympic Oval skating arena in British Columbia) are being built in Canada and elsewhere throughout the world. Initiatives such as the “Wood First Act” in British Columbia has also helped facilitate a culture of wood by requiring the use of wood as the primary building material in all new provincially funded buildings (Bill 9, 2009). Wood structures may also be located within a given radius of a target or even subjected to an accidental explosion.

The current building code in Canada (NBCC, 2010) does not explicitly require blast loads to be considered in the design of structures. The Canadian Standard Association (CSA) has recently developed a standard that addresses the analysis and design requirements for

structures under blast loading titled "Design and assessment of buildings subjected to blast loads" (CSA S850-12, 2012). Although wood is included in the CSA S850 standard as a material option, research on wood structures under blast loading has been very scarce. Existing literature on the behaviour of wood under high strain rate loading mostly stems from small clear specimens that are free of defects. Tests on larger-scale specimens have mostly focused on the material properties and not the structural behaviour of subsystems.

The current design approach in the CSA S850 standard predicts the performance of light-frame stud walls based on the static design strength of a single stud component, modified for dynamic strength through a dynamic increase factor (DIF) applied on the resistance. Although the increase in resistance of light-frame wood members due to the repetitive nature of the elements has been well established in research and recognized in the CSA O86 design standard under static loads, blast design neglects any load sharing or contribution of the sheathing on the strength and stiffness of the walls.

1.2 Light-frame wood structures

The light weight, ease of construction and material cost has made light-frame platform wood structures the construction technique of choice for low-rise buildings, such as housing.

Light-frame wooden structures behave as assembly of plates and ribs connected together with mechanical fasteners. The primary plate elements are wood-based sheathing materials such as plywood or oriented strandboard (OSB) available in sheets of 1.22 x 2.44 m. Ribs consist of solid sawn dimension lumber such as 38 mm x 140 mm wall studs. A typical wall is shown in Figure 1.1. Sheathed light-frame wood structures provide a high degree of redundancy because the sheathing acts in conjunction with the main structural members to produce a larger effective cross section. This composite action is usually only partly effective because complete shear transfer between the connected sheathing element and the main member is difficult to achieve in wood construction. Typical nailing pattern used to resist lateral loads in light-frame wall construction is shown in Figure 1.2. Current design provisions, both CSA S850 (2012) and CSA O86 (2009), do not account for the increase in stiffness when the framing members are acting together to support a load in a sheathed wall or floor system. This implies that the moment of inertia of the system is that of the stud or

joist member alone. On the other hand, considering full composite action means that the sheathing and the wood member are rigidly attached and the moment of inertia is the one resulting from the transformed area method. Design of wood light-frame structures is based on an assessment of the capacity of isolated rib components such as floor joists, wall studs, or roof trusses. System effects such as load sharing and composite action are allowed for by multiplying the bare rib capacity by a series of factors that reflect: rib spacing, plate thickness, and the type of connection between the plate and ribs. For example, the bending capacity of visually graded dimension lumber ribs can be increased by up to 40% if such members are spaced less than 610 mm apart and if there are at least three members resisting a common load (CSA O86, 2009).

1.3 Blast loading characteristics

1.3.1 Nature of blast loading

Blast loading on structures is the result of a sudden release of energy that can be chemical, physical or nuclear. A nuclear explosion is the result of protons and neutrons being exchanged to form a new nuclei that releases energy, a physical explosion could be the result of failure of a cylinder tank that contains compressed air, and a chemical explosion is the result of an exothermic reaction with rapid oxidation of the carbon and hydrogen elements which all results in the formation of a shock wave (Cormie, Mays, & Smith, 2009) . The formation of a shock wave, causing instantaneous rise to peak pressure, can be referred to as a detonation. In a detonation, the speed of the reaction is greater or equal to the speed of sound in the explosive material. On the other hand, in a deflagration, a pressure wave is generated with a more gradual rise to peak pressure as it propagates through the air. A deflagration can be as destructive as a detonation when found in high concentrations in the air; such explosions are often referred to as 'fuel-air' or 'vapour cloud' explosions (Cormie et al., 2009). The intensity of vapour cloud explosions (VCE) is increased drastically by congestion or confinement as the flammable material, when mixed in the right conditions, will propagate quickly. VCEs are most often observed in refining and petrochemical facilities.

1.3.2 Blast wave characteristics

The detonation of high explosives (e.g. lead azide, trinitrotoluene (TNT), composition C4) results in a blast wave that is also referred to as a shock wave. The latter is a zone of compressed air traveling at the front of a medium (e.g. air) at a speed typically greater than the one of the medium. The shock front, which is propelled by the chemical reaction, is a thin layer of compressed air forcing the surrounding air outward as shown in Figure 1.3. As a result, there is an immediate rise in atmospheric pressure at the time of arrival of the shock front, referred to as the peak incident pressure or pressure above ambient pressure (P_s), as shown in Figure 1.4 (Dusenberry, 2010). In an ideal explosion in free air such as the one shown in Figure 1.4, the shock front propagates spherically without any amplification and thus the rise in pressure at the time of arrival, t_a, is solely due to the energy released. As the shock front propagates, the velocity and temperature decrease along with the peak incident pressure. The overpressure diminishes to ambient pressure, thereby defining the positive phase, t_d, of the blast wave. At time t_a+t_d, the pressure starts decaying below ambient pressure, which denotes the beginning of the negative phase. This occurs due to the rapid return to ambient pressure by the air particles rushing in to fill the voids left by the shock front. Time $t_a+t_d+t_d^-$ denote the end of the negative phase, t_d^-, and the return to ambient pressure. The peak incident pressure in the negative phase, as shown in Figure 1.4, is typically only a fraction of the peak incident pressure observed in the positive phase and is often neglected in analysis (Krauthammer, 2008; Unified Facilities Criteria (UFC) 03-340-02, 2008).

The positive impulse, I^+, is the area under the pressure-time history curve, P(t), during the positive phase while the negative impulse, I^-, is the area under the pressure-time history curve of the negative phase, as expressed in Equations 1.1 and 1.2, respectively.

$$I^+ = \int_{t_a}^{t_a+t_d} P(t)dt \qquad [1.1]$$

$$I^- = \int_{t_a+t_d}^{t_a+t_d+t_d^-} P(t)dt \qquad [1.2]$$

The pressure-time history can be described using the Friedlander equation, reproduced in Equation 1.3 from Cormie et al. (2009).

$$P(t) = P_s\left(1 - \frac{t}{t_d}\right)e^{-\frac{b*t}{t_d}} \quad [1.3]$$

Where P_s is the incident peak pressure, t is the time, t_d is the positive phase duration and b is the blast waveform parameter. It is a common design practice to assume the pressure-time history as an instantaneous rise in pressure, which decreases linearly to ambient pressure. This idealization simplifies the analysis by avoiding the iteration process to determine the waveform parameter, b. This simplified approach also assumes that the pressure and impulse of the idealized and real functions are the same, and therefore the equivalent function can be obtained by varying the positive phase duration (Cormie et al., 2009).

1.3.3 Reflected blast waves

In an actual explosion, the propagation of a shock wave will interact with reflecting surfaces, and thereby lose its spherical form and experience an amplification in magnitude and velocity. The interaction of the blast wave with an object or a medium denser than the one it is travelling in will result in a reflection of the wave, and depending on the size and geometry of the object, the wave might diffract around it. Therefore, the pressure acting on an object will not simply be the incident pressure shown in Figure 1.4 but rather a combination of the incident pressure, stagnation pressure and dynamic pressure that results in a reflected pressure greater than the incident pressure.

1.3.3.1 Normal reflections

In the case of normal reflections, the shock wave propagating in one direction interacts with a wall of infinite height and width at a zero angle of incidence (perpendicular to the direction of the shock wave). The wave arrives to an abrupt stop where the immobilized compressed air particles are additionally compressed by the incoming shock wave. Equation 1.4 (Cormie et al. (2009) shows the reflected pressure, P_r, as a function of the peak overpressure, P_s, and ambient pressure, P_o, for a normal reflection. Equation 1.4 assumes that the air behaves as a real gas and that the specific heat capacity for constant pressure over that of constant volume is equal to 1.4 ($\gamma = c_p/c_v = 1.4$).

$$P_r = 2P_s\left[\frac{7P_o + 4P_s}{7P_o + P_s}\right] \quad [1.4]$$

1.3.3.2 Oblique and mach reflections

In contrast to normal reflections, oblique reflections occur when the angle of incidence, α_i, is between zero and forty degrees (U.S.A.C.E PDC, 2008a). At angles greater than forty degrees, Mach reflection occurs. The angle of incidence is measured from an axis perpendicular to the direction of travel of the shock wave towards the surface of interest as shown in Figure 1.5. At ninety degrees the surface is loaded with the incident over-pressure only, which is sometimes referred to as "side-on" pressure. A shock front more powerful than the reflected shock wave, known as the Mach Stem, is formed when the reflected shock front meets the incident shock front. The point at which the two merge to form the Mach Stem is known as the triple point (U.S.A.C.E PDC, 2008a). Both shock fronts, incident and reflected, intersect at the triple point as the reflected pressure travels much faster and catches up with the incident shock front. The reflected pressure, P_r, for oblique reflections can be expressed as a function of the incident pressure, P_s, and the reflection coefficient, C_r, as shown in Equation 1.5. Reflection coefficients for different angle of incidence can be found in Figure 1.5 (U.S.A.C.E PDC, 2008a).

$$P_r = P_s C_r \qquad [1.5]$$

1.3.3.3 Interaction with Real Structures

The previous discussion on the reflection of blast waves assumed walls of infinite width and height, and where diffraction was not plausible. In reality the dimensions and geometry of a structure would create diffraction as well as drag forces in the blast waves. The loads would therefore need to be determined based on the geometry for the front, side and back walls as well as the roof.

1.3.4 Scaling laws

1.3.4.1 High explosives

The cost of conducting field tests using explosives is high and the procedure is time consuming. The Hopkinson and Cranz scaling law, also known as the cube-root scaling law, is therefore widely implemented to compare the effects of different explosions detonated at different distances for similar atmospheric conditions, explosive geometry, and materials.

According to the scaling law, similar blast waves can be reproduced if two explosive charges of different size are of similar geometry and consisting of the same explosive material in the same atmospheric conditions. The scaled distance, Z, relates the standoff distances, R, to the charge weights, W, as shown in Equation 1.6.

$$Z = \frac{R}{W^{1/3}} \quad [1.6]$$

Therefore, for the same scaled distance, two different charges with different stand-off distances can have the same reflected pressure, and therefore the same response in structural members as illustrated in Figure 1.6 (Baker Engineering & Risk Consultants Inc., 2012). Extending the concept of the cube root scaling, other blast wave parameters such as the impulse and time of arrival can also be scaled (Krauthammer, 2008).

Blast wave parameters generated by the detonation of TNT are well established in literature due to its relative ease of commercial transportation, its pureness as well as its availability. Therefore, TNT has become the benchmark comparison for high explosives, and blast parameters of one type of explosive are converted to an equivalent parameter produced by TNT. The factors applied to modify the release of energy by an explosive other than TNT can be expressed in terms of energy, heat of detonation or combustion, peak pressure, and impulse (Dusenberry, 2010). Table 1.1 shows the equivalency factors for pressure and impulse for common explosives while Equation 1.7 shows how to obtain the equivalent charge weight in TNT based on the heat of detonation (Unified Facilities Criteria (UFC) 03-340-02, 2008).

$$W_E = \left(\frac{H^d_{EXP}}{H^d_{TNT}}\right) W_{EXP} \quad [1.7]$$

Where W_E is the effective charge weight in TNT, W_{EXP} is the weight of the explosive considered, H^d_{EXP} is the heat of detonation of the explosive and H^d_{TNT} is the heat of detonation of TNT.

1.3.4.2 Vapour cloud explosions

A different approach is required to determine the blast loads resulting from VCEs as they are closely related to the flame speed which in turn is a function of the congestion and confinement. Dispersion models can be used to obtain the size, shape and concentration of

the flammable vapour cloud. Simplified methods such as the Baker-Strehlow-Tang (Tang & Baker, 1999) and TNO Multi-energy Method (Van Den Berg, 1985) can be used to determine the scaled pressure and impulse values based on the flame speed. Of interest to the current research study is the simplified analysis method found in the American Petroleum Institute (API) Recommended Practice (RP) 753 to safely locate portable light-frame wood trailers based on stand-off distances from the explosion source (API RP 753, 2012), as shown in Figure 1.7.

1.4 Dynamic analysis

1.4.1 General

Blast loading on structures involves a loading duration that is much smaller than that of earthquakes and wind loading, and therefore the structural response under such short loading can differ quite significantly from the static (i.e. dead and live loads) and the slower dynamic (i.e. earthquakes and wind loads) load cases. In general, it is deemed acceptable to use the equivalent static approach to analyze the slower dynamic loads. The short time duration of a blast load implies that the inertia forces and the kinetic energy cannot be neglected in the analysis of a structure. Equation 1.8 shows the dynamic equilibrium in its most general form while Equation 1.9 shows the principle of conservation of energy.

$$F(t) - R(t) = ma \quad [1.8]$$

$$WD = KE + SE \quad [1.9]$$

Where F(t) is the total external force as a function of time, R(t) is the total internal force as a function of time, m is the mass, a is the acceleration. WD is the work done by the system, KE is the kinetic energy, and SE the strain energy.

The uncertainties associated with blast loads and properties of the components investigated have meant that the use of simplified modelling techniques such as single-degree-of-freedom (SDOF) is justifiable. The accuracy gained from complex analysis methods (e.g. multi-degree-of-freedom (MDOF) and finite element (FE)) is not worth the computational effort (Biggs, 1964). Recent studies have shown that the SDOF method can accurately describe the response of structural elements subjected to blast loads (Burell, 2012; Ciornei, 2012; Jacques,

2011; Lloyd, 2010). Although more complex methods of analysis could be used due to the significant advancement in computational capabilities of computers, complex analysis methods are only beneficial when more than one type of failure mode or when a localized failure mode is investigated.

SDOF analysis method can be deemed acceptable if the motion of the structural member can be described using a specific ordinate along the member. Closed-form solutions and equivalent design methods of SDOF are discussed below.

1.4.2 SDOF closed-form solution

Closed-form solutions are only practical in simple linear elastic systems subjected to forcing functions that can be described by simple mathematical formulations. Figure 1.8 (a) shows simple idealized damped single-degree-of-freedom system with a mass, m, a spring constant, k, a damping constant, c, and a time-varying forcing function, F(t). Figure 1.8 (b) shows the internal equilibrium of the forces, where y, $\dot{y}$ and $\ddot{y}$ are the displacement, velocity and acceleration, respectively. The equilibrium of the system can be represented as shown in Equation 1.10.

$$m\ddot{y} + ky + c\dot{y} = F(t) \qquad [1.10]$$

The effects of damping can be neglected when the load duration is short and where only the maximum dynamic response is of interest (Biggs, 1964). Although not presented here, closed-form solutions that include damping, such as the Duhamel's integral, are readily available in the literature. The resulting equation of motion and displacement solution for an un-damped free vibration response, where the external forcing function and the damping coefficients are equal to zero, are shown in Equations 1.11 and 1.12, respectively.

$$m\ddot{y} + ky = 0 \qquad [1.11]$$

$$y = \frac{\dot{y}_o}{\omega}\sin\omega t + y_o\cos\omega t \qquad [1.12]$$

Where y_o and $\dot{y}_o$ are the initial displacement and velocity, respectively, at time equal to zero. The circular frequency,ω, is a fundamental property of the SDOF system and is defined in Equation 1.13.

$$\omega = \sqrt{\frac{k}{m}} \quad [1.13]$$

The displacement solution for a constant external force, F_1, applied indefinitely, and where damping is omitted is shown in Equation 1.14.

$$y = \frac{F_1}{k}(1 - \cos \omega t) \quad [1.14]$$

More closed-form solutions for different loading scenarios, both for damped and un-damped cases, can be readily found in the literature (Biggs, 1964; Humar, 2005). From the closed-form solutions or through numerical analysis, the dynamic displacement can be obtained and used to find the dynamic load factor (DLF), presented in Equation 1.15. The DLF is defined as the ratio of the maximum dynamic displacement, y, to the maximum static displacement, y_{st}, resulting from the same force applied statically.

$$DLF = \frac{y}{y_{st}} \quad [1.15]$$

1.4.3 Equivalent SDOF analysis

The closed-form solutions for SDOF analysis presented earlier focused on simple linear elastic systems that may not be directly applicable to continuous structural systems such as beams, columns, slabs, and walls. These closed-form solutions assume that the mass of the system or object is concentrated at its center of gravity and that the object experiences the same force as the applied force resulting in the mass moving as a unit. In the case of structural elements, if uniform motion is assumed throughout the element, appreciable error is introduced (Unified Facilities Criteria (UFC) 03-340-02, 2008). Therefore an equivalent system is created by selecting a point where maximum deflection occurs (e.g. mid-span of a beam) and the mass and stiffness of the system along with the applied forces are lumped at that point (Biggs, 1964). In order to transform the mass, stiffness and loads of the real system to an equivalent system, it is necessary to use transformation factors that are determined based on an assumed static deflected shape (Biggs, 1964). The difference between the static deformed shape and the first mode approximations is insignificant for blast loading, thus allowing the use of the static shape, which is more convenient to use (Unified Facilities Criteria (UFC) 03-340-02, 2008). Most importantly, the time-scale between the real and equivalent systems is not altered; therefore, at any instance during the displacement-time history, the displacement of the equivalent system is equal to that of the real structure at the

equivalent ordinate. These transformation factors are based on the loading type and static deformed shape and thereby account for the boundary conditions.

The selection of an appropriate deflected shape is critical to the analysis. Contrary to the closed-form solutions, the equivalent approach can be used for elastic and plastic modes as long as the transformation factors reflect the shape function resulting from the formation of plastic hinges. Equation 1.16 presents the equation of motion of the equivalent system with the mass transformation factor, K_M, load transformation factor, K_L, resistance transformation factor, K_R, and the non-linear resistance term, R(y).

$$K_M m\ddot{y}(t) + K_R R(y) = K_L A P_R \left(1 - \frac{t}{t_d}\right) \quad [1.16]$$

From Equation 1.16, it can be seen that the forcing function introduced in Equation 1.10 has been replaced by the idealized pressure-time history function multiplied by the loaded area, A. Once the time is greater than the positive phase duration of the blast load, the forcing function is assumed to be equal to zero. In equation 1.16, P_R is the maximum reflected pressure that the structure or structural component experiences.

Equating the work done to the kinetic energy and strain energy of the real structural system, the corresponding relationships of the equivalent system will yield the transformation factors. The mass factor, K_M, is expressed in Equations 1.17 and 1.18 for a continuous and a concentrated mass, respectively. The mass factor is obtained by equating the kinetic energy of the real system based on the deflected shape to the one of the equivalent system.

$$K_M = \frac{\int_0^L \bar{m}(x)\emptyset^2(x)dx}{\int_0^L \bar{m}(x)dx} \quad [1.17]$$

$$K_M = \frac{\sum_{r=1}^{i} m_r \emptyset_r^2}{\sum_{r=1}^{i} m_r} \quad [1.18]$$

Where $\bar{m}(x)$ is the distributed mass per length, $\phi(x)$ is the shape function based on the deflected shape along the length of the element resulting from the dynamic loads applied statically, m_r is the r^{th} mass and i is the number of lumped masses.

In general, the resistance factor, K_R, is always equal to the load factor, K_L (Unified Facilities Criteria (UFC) 03-340-02, 2008). The reason is that the resistance factor can be seen as a modifier to the internal force of the element working to return to its unloaded static position; therefore, the maximum resistance of that element is the total load the element can support statically with the same load distribution as assumed for the deflected shape. The load factor is presented in Equations 1.19 and 1.20 for distributed and concentrated loads, respectively.

$$K_L = \frac{F_e}{F} = \frac{\int_0^L p(x,t)\emptyset(x)dx}{\int_0^L p(x,t)dx} \quad [1.19]$$

$$K_L = \frac{F_e}{F} = \frac{\sum_{r=1}^{i} F_r \emptyset_r}{\sum_{r=1}^{i} F_r} \quad [1.20]$$

Where F_e is the equivalent load, F is the total load, p(x,t) is the distributed load per unit length as function of the time, F_r is the r^{th} concentrated load, i is the number of concentrated loads and $\phi(x)$ is the shape function.

The load-mass factor, K_{LM}, can be defined as the ratio between the mass and load factors as shown in Equation 1.21. This enables having only one factor in Equation 1.16 as shown in Equation 1.22. Transformation factors are available in the literature (Biggs, 1964; Unified Facilities Criteria (UFC) 03-340-02, 2008) .

$$K_{LM} = \frac{K_M}{K_L} \quad [1.21]$$

$$K_{LM} m\ddot{y}(t) + R(y) = AP_R\left(1 - \frac{t}{t_d}\right) \quad [1.22]$$

1.4.4 Resistance-deflection function

The resistance-deflection function is an essential part of the dynamic analysis as it expresses the resistance of the element as a function of the displacement at the location of the equivalent ordinate. The resistance can be defined as the sum of the internal forces that try to restore the deflected element to its original position. The resistance can also be thought of as an equivalent force to the external loads applied in an opposite direction or as a restoring force. An example of a resistance-deflection curve for a fix-ended beam, reproduced from Biggs (1964), is shown in Figure 1.9 where the beam undergoes three stages of deflection in

the elastic (a), elastic-plastic (b), and plastic (c) regions. The transition from elastic to plastic behaviour of the beam is characterized by the formation of plastic hinges that need to be accounted for through the transformation factors in the equivalent system.

1.4.5 Pressure-impulse (P-I) diagrams

P-I diagrams describe the performance characteristics for a range of blast loading for a specific type of element. If not normalized, P-I diagrams cannot be generalized and can only be used to assess the behaviour of structural elements of similar geometries and end conditions. P-I diagrams describe the combination of peak pressure and impulse or the equivalent dimensionless quantities for a damage level compared to the response spectrum. The ordinate is generally expressed by the peak pressure since the load distribution resulting from an explosion is described by a pressure profile rather than by a force distribution. The abscissa is the impulse associated with its respective peak pressure, and is defined as the area under the pressure-time history curve.

Damage assessment of a structure or an element to a specific pressure and impulse combination can be undertaken using a P-I diagram. The different curves in a P-I diagram indicate different damage levels. This can be derived using a SDOF analysis method, results from an experimental program or from an actual blast event. In the latter case, P-I curves are less precise as they are based on observations as opposed to the ones obtained from analysis. Figure 1.10 shows a typical P-I diagram for a light-frame wood stud wall system where the predominant failure mode was flexure.

The damage levels provided in Figure 1.10 are based on the Canadian blast standard (CSA S850-12, 2012). The ductility ratio, μ, is defined as the maximum deflection, x_{max}, divided by the elastic deflection, x_e, as shown in Equation 1.23.

$$\mu = \frac{x_{max}}{x_e} \qquad [1.23]$$

Figure 1.11 illustrates that a blast can take place in one of three distinctive loading regimes: impulsive, dynamic and quasi-static. The impulsive loading regime is characterized by its short load duration relative to the response time of the system. In this case, before a structure experiences significant deformation the load would have already occurred. Therefore, the

maximum response is assumed to be independent of the load history. Similarly, the quasi-static regime is only dependent on the peak load (P_r) and the structural stiffness (k) because its load duration is much longer than the response time. The maximum displacement is reached when only a small amount of the load has dissipated (Krauthammer, 2008). The maximum response is also not affected by the load-time history. The dynamic regime differs from the two previous regimes as its maximum response is greatly influenced by load-time history. The dynamic regime is the transient regime located in-between the quasi-static and impulsive regimes.

1.5 Research objectives

The objective of this research project is to assess the flexural behaviour of light-frame wood stud walls subjected to blast loading. More specifically, the goals are to:

1) Investigate the ability of a shock tube to generate high strain-rate flexural response in wood members;
2) Compare analysis from experimental results based on static and dynamic tests in order to establish dynamic increase factors (DIF) for the purpose of design;
3) Develop a material predictive model for the wall system based on component behaviour and interconnectivity between the components through partial composite action;
4) Compare analysis based on the material predictive model with the behaviour of the wood stud walls from full scale tests;
5) Establish damage levels that are appropriate for the wood stud wall system;
6) Investigate the accuracy and validity of the CSA S850 standard provisions related to light-frame wood stud wall systems.

1.6 Scope

The above stated objectives are achieved through the following:

- A detailed literature review on the behaviour of wood light-frame structures subjected to high strain rates and partial composite action between the sheathing and wood members;
- A review of the blast wave characteristics and dynamic analysis procedure;
- Testing of forty studs to capacity and twenty walls both statically and dynamically and establishing the damage levels;
- Developing a material predictive model considering the partial composite action between the sheathing and the studs;
- Determining the required inputs to the material predictive model by conducting component tests;
- Comparing the analytical and experimental results and formulating design recommendations for using a suitable dynamic increase factor;
- Investigating the validity of the current design provisions by comparing analysis conducted based on the design standard with observation from experimental tests and analytical results;
- Discussing the results and implications on the code.

1.7 Structure of thesis

Chapter 1 provides an introduction to the topic of blast analysis and design, and presents the research needs and objectives.

Chapter 2 presents a detailed literature review comprised of studies investigating the dynamic behaviour of wood structures, and relevant studies relating to partial composite action.

Chapter 3 presents the experimental methodology employed in the research program, and provides a detailed description of the components and specimens tested, as well as the test setups used.

Chapter 4 presents the static and dynamic test results for material evaluation tests, destructive tests of individual stud, static and dynamic wall tests, and the load slip relationship between the sheathing and the stud elements.

Chapter 5 provides a description of the methodology used to determine the dynamic increase factors as well as for the development the predictive non-linear material model. The analytical results are also presented in the chapter.

Chapter 6 discusses the analysis and results from the experimental and analytical program, especially the implications of the modelling approach.

Chapter 7 discusses the blast standard and presents the implications of different analysis and design approaches on the results.
Chapter 8 consists of a summary of the most important findings and defines potential future work.

Appendix A and B present details about the test results and analysis for all specimens tested under static and dynamic loading.

Table 1.1: TNT equivalency factors of high explosives

Explosive	Equivalent mass for pressure	Equivalent mass for impulse
ANFO (94/6 Ammonium Nitrate/Fuel Oil)	0.87	0.87[1]
Composition A-3	1.09	1.07
Composition B	1.11	0.98
Composition C-4	1.20	1.19
H-6	1.38	1.15
HBX-1	1.17	1.16
HMX	1.25	1.25[1]
Octal (75/25 HMX/TNT)	1.02	1.06
Pentolite (Cast)	1.42	1.00
RDX/Wax (98/2)	1.16	1.16[1]
Tetryl	1.07	1.07[1]
TNT	1.00	1.00
Tritonal (80/20 TNT/Al)	1.07	0.96

*Reproduced from Dusenberry (2010) [1]Value is estimated

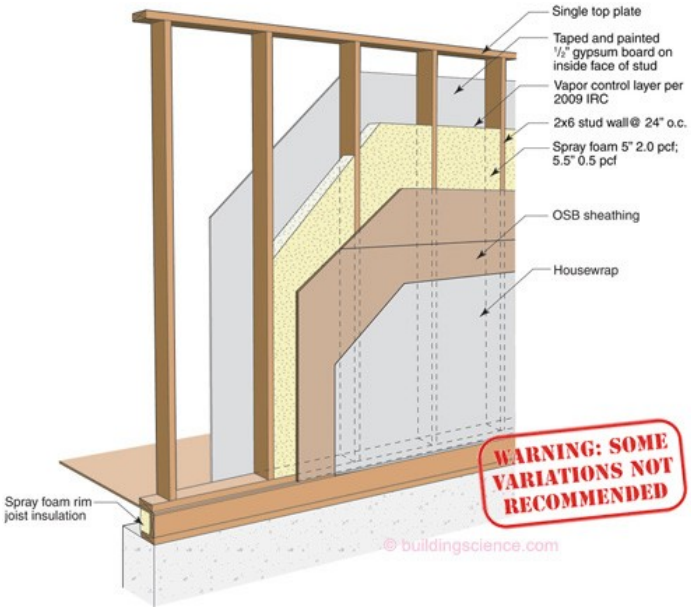

Figure 1.1: Example of the constitution of a typical light-frame wall

*Reproduced from www.buildingscience.com, High R-value wall assemblies, 2009

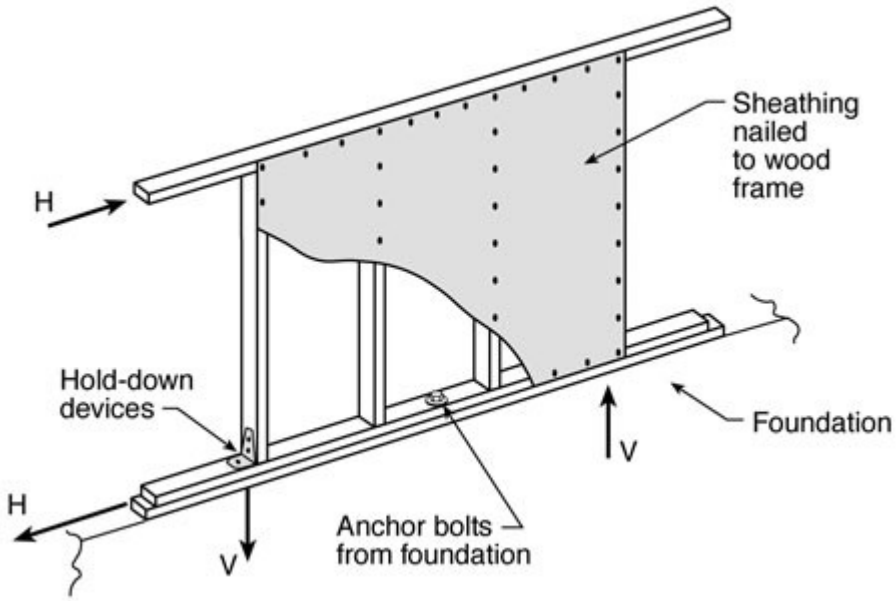

Figure 1.2: Typical light-frame lateral shear wall details

*Reproduced from http://archive.nrc-cnrc.gc.ca, Ensuring good seismic performance with platform-frame wood housing,

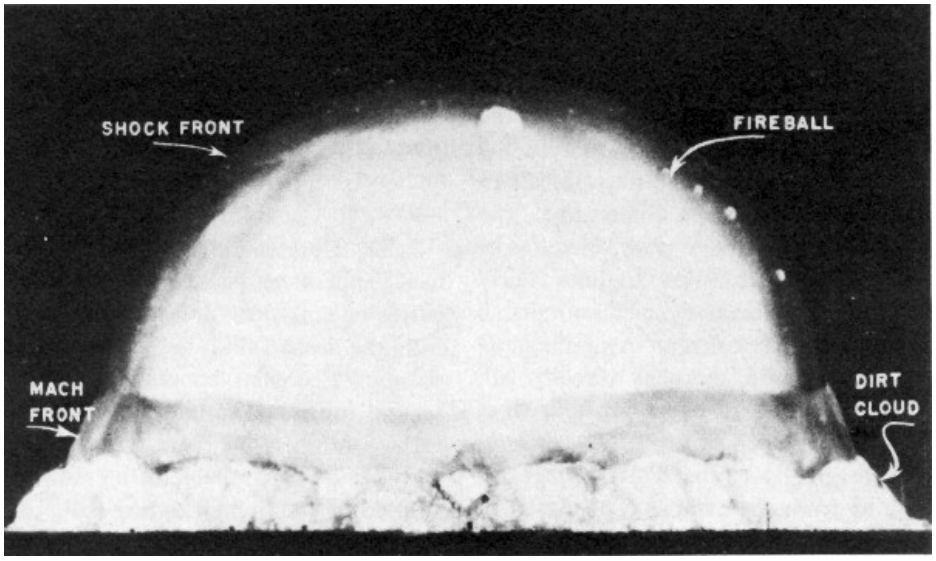

Figure 1.3: Shock front resulting from nuclear explosion

*Reproduced from http://www.cddc.vt.edu/host/atomic/nukeffct/enw77b1.html

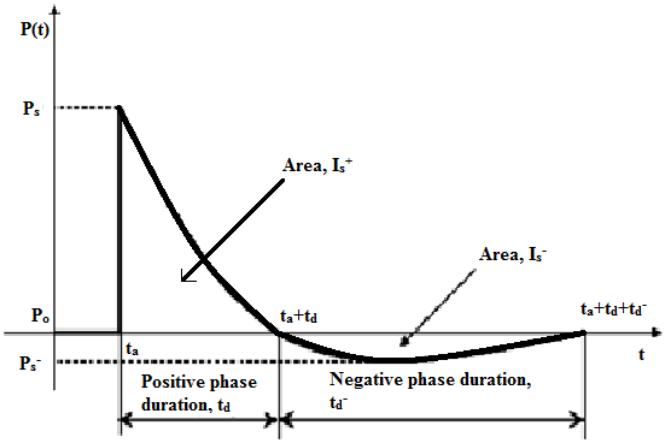

Figure 1.4: Typical blast wave history

*Reproduced from Dusenberry (2010)

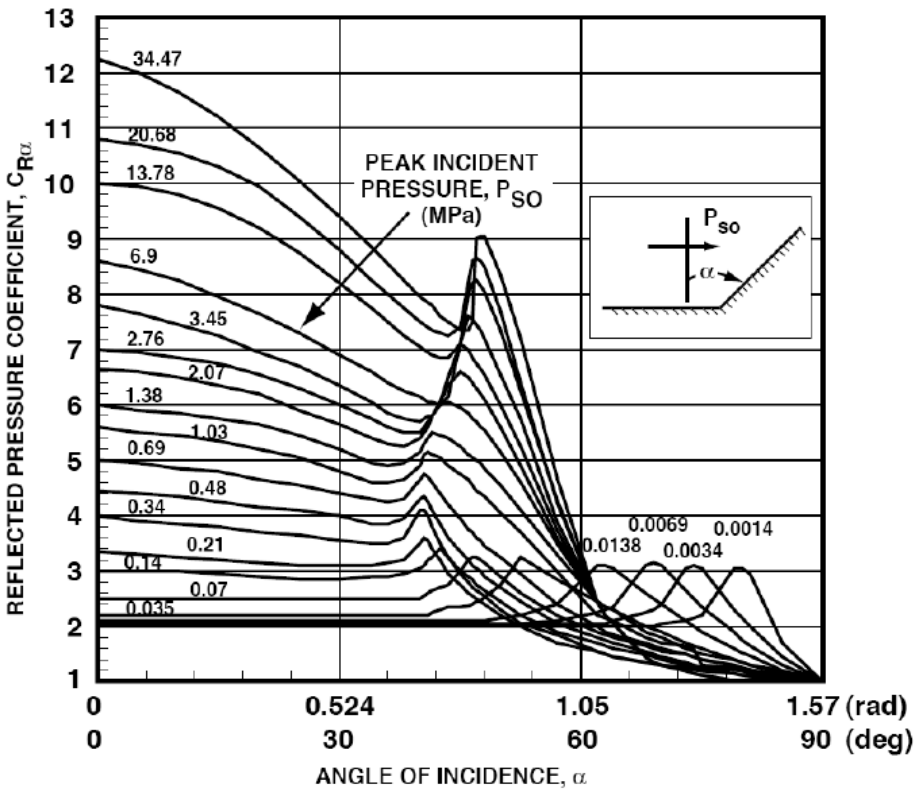

Figure 1.5: Reflected pressure coefficient versus angle of incidence

*Reproduced from U.S.A.C.E PDC (2008a)

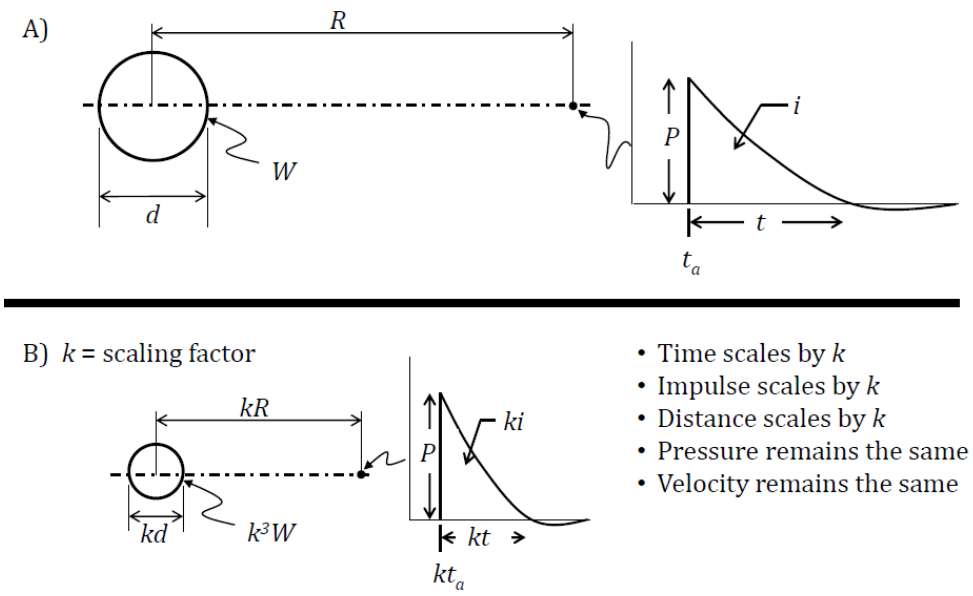

Figure 1.6: Hopkinson-Cranz scaling law

*Reproduced from Baker Engineering & Risk Consultants Inc. course "Design of Blast Resistant Structures" in Chapter 2 "Blast Loads and Explosion Effects", Washington, D.C., 2012

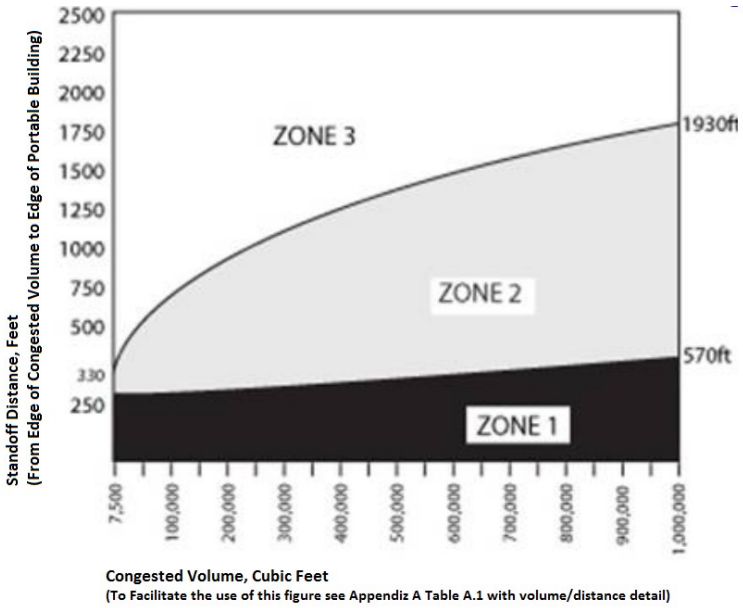

Figure 1.7: API standoff distances

*Reproduced from API RP 753 (2012)

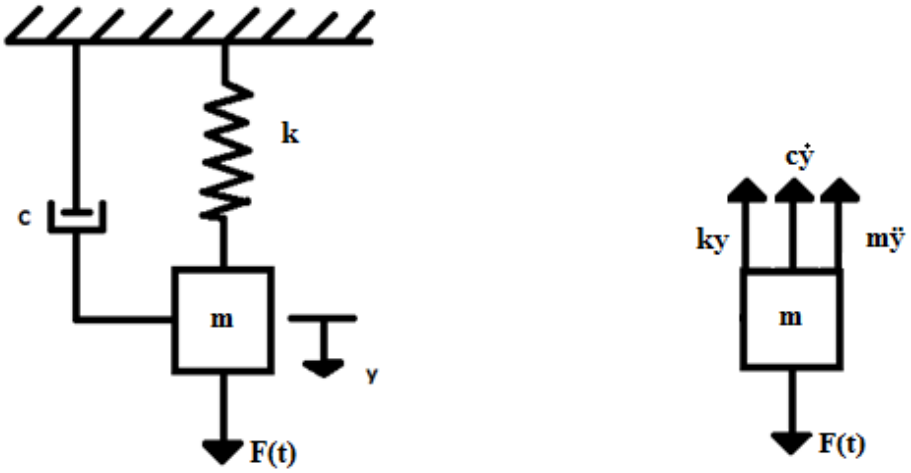

(a) External forces on SDOF (b) Internal equilibrium

Figure 1.8: Dynamic equilibrium of a simple single-degree-of-freedom system

*Reproduced from Biggs (1964)

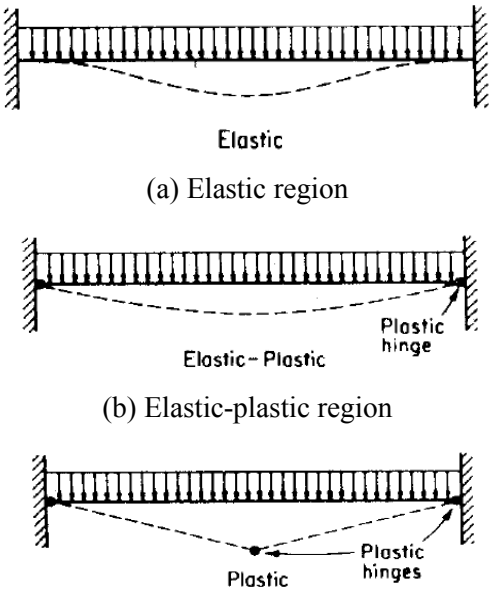

(a) Elastic region

(b) Elastic-plastic region

(c) Plastic region

Figure 1.9: Stages of fixed ended beam response

*Reproduced from Biggs (1964)

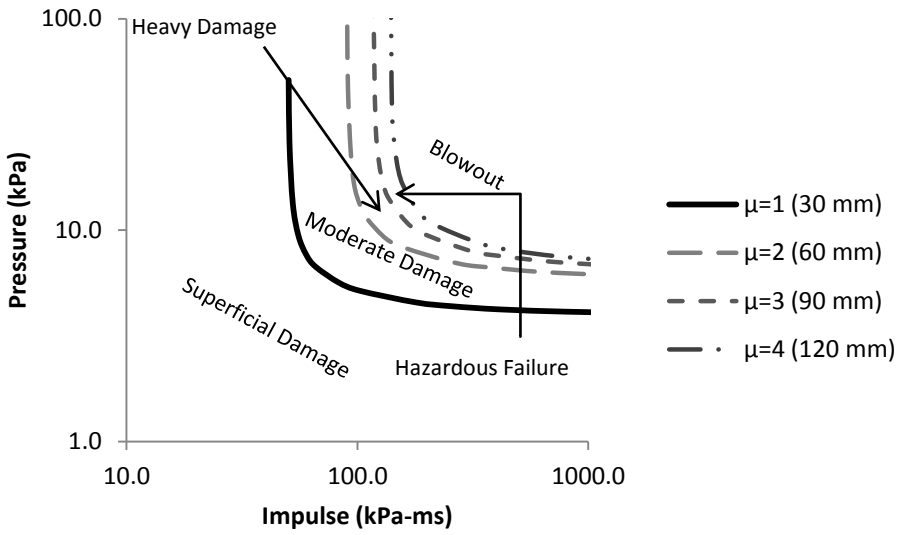

Figure 1.10: Typical pressure-impulse diagram for a typical light-frame wood stud wall

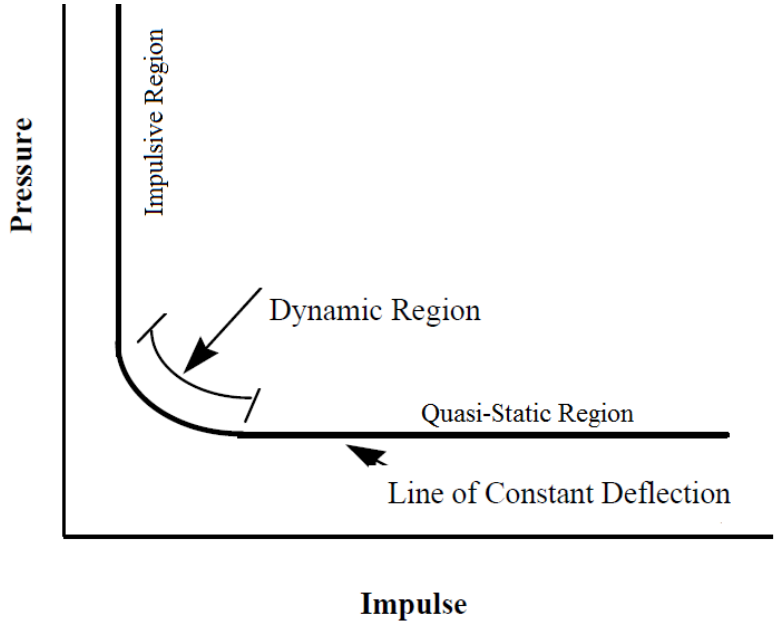

Figure 1.11: Pressure-impulse diagram regimes

*Reproduced from U.S.A.C.E PDC (2008a)

CHAPTER 2-Literature Review

2.1 Effects of blast loading on wood structures

There are much less design information and guidance available and fewer blast tests performed on wood components than other typical structural materials, such as concrete and steel. Some of the limited research available is classified, making it difficult for designers to find sufficient information. Following are selected relevant research projects especially related to wood structures.

2.1.1 Behaviour of buildings subjected to atomic blast

Interest in the ability of buildings and other infrastructures to resist blast loading rose amongst engineers and government defense departments following the Second World War (WWII). Smith (1952) reported on the performance and observed damage levels of various types of structures to the nuclear blast loading. Smith (1952) reported that reinforced concrete structures are the structures that offered the best resistance to blast loads generated by the Hiroshima and Nagasaki bombing compared to any other type of structures. One of the weakest types of structures reported was brick and stone walls with wood roof trusses. The number of these types of structures was, however, limited as their poor performance under seismic loading was already well-known. It was also reported that steel buildings, in general, were stripped of their sidings and roofs, which consisted of corrugated metal panels. Severe distortion of the frames was also observed. Heavy timber and light-frame wood structures were severely destroyed due to blast loading and following fire. It was also stated that "while the workmanship was good in the framing of houses, engineering principles were frequently overlooked" (Smith, 1952). Glasstone and Dolan (1977) summarized the same studies as reported in Smith (1952) and indicated that the construction was not well adapted to resist racking action. This is not uncommon even at present time, where low-rise light-frame wood buildings (mainly residential) are still not designed and detailed by engineers but rather constructed based on prescriptive requirements. Irrespective of the structural material or types, it was noted that debris such as partition walls, infill walls, plaster, fixtures and glass experienced brittle failures and caused many of the casualties.

2.1.2 Behaviour of wood frame houses to nuclear explosions

2.1.2.1 Two-storey wood frame houses, 1953

In 1953, two identical structures with construction details similar to typical North American wood light-frame construction were subjected to blast loading equivalent to the one experienced in the Hiroshima and Nagasaki events. 15 kilotons of TNT equivalent charge was detonated at 91.4 m above ground. The main objective of the project was to determine the adequacy of personal basement shelters to protect the occupants from the blast. The houses were located at two different distances from the point of explosion, in order to simulate different demand and observe the corresponding structural response. The first house was located at 1,067 m from ground zero, and it was anticipated that a level of damage, described as "complete collapse without disintegration", would be achieved (Kimbell & Fies, 1953). The second house was located at 2,286 m from ground zero and a "heavy damage but not collapse" was expected to be observed (Kimbell & Fies, 1953). The walls of both houses were framed with 38 mm x 89 mm studs spaced 406 mm on center and the floor joists and rafters consisted of 38 mm x 184 mm and 38 mm x 140 mm framing elements, respectively.

House #1

Kimbell and Fies (1953) reported that the first house was subjected to an overpressure of 34.5 kPa and that it did collapse, as expected, but it did not completely disintegrate. The study also noted that the basement shelters proved to be adequate as the debris did not fall in the basement. The first storey walls were severely damaged and as a consequence the second floor framing fell onto the main floor. A portion of the roof was lifted from the wall framing and was found 25 feet away from the house. The level of damage is shown in Figure 2.1.

House #2

The second house was subjected to an overpressure of 11.7 kPa. Glasstone and Dolan (1977), who also summarized Kimbell and Fies (1953) work indicated that the second house "was badly damaged both internally and externally, but it remained standing" as shown in Figure 2.2 (a). It was reported that temporary shoring of the living room floor and fixing the building envelope damage would have made the house safe for emergency habitation, but to

restore the house to its original condition would have meant major reconstruction estimated at 50 percent of the original cost. The extent of damage to the floor joists is shown in Figure 2.2 (b). In the damage observations it was also reported that the roof rafters facing the detonation were all split or broken while rafters on the other side were intact. Several studs facing the detonation side had fractures but were not a concern as far as emergency occupancy (Kimbell & Fies, 1953). Kimbell and Fies (1953) concluded that based on the estimated force of impact, the performance of the second house showed an ability to resist stresses that were greater than those allowed in static design for such buildings. The observation was attributed to "lack of credit for the collective action of the integrated elements of a wood frame building, to the impact being of much shorter duration than usually assumed". This statement suggests the need to incorporate a system-level approach in the analysis, and also alludes to the existence of an apparent increase in capacity for wood under short term load duration relative to static capacity. Due to the lack of funding for adequate instrumentation a dynamic increase factor could not be quantified.

2.1.2.2 Wood frame houses, 1955

In 1955, the Federal Civil Defense Administration (FCDA) conducted another series of tests on residential structures similar to the ones reported in 1953 by Kimbell and Fies, where a 30 kilotons TNT equivalent was detonated at 152.4 m above ground. A total of ten residential houses of five different types consisting of wood, brick, lightweight reinforced concrete blocks, and lightweight precast concrete slabs were subjected to load effects similar to those reported by Kimbell and Fies in 1953. The objective of the research was to evaluate the performance of residential houses and to determine possible steps to improve their resistance to blast loading. Of particular interest to the current research project are the two sets of wood frame houses and the "trailer-coach" mobile homes (Glasstone & Dolan, 1977).

The first set of houses consisted of two-storey wood frame houses similar construction to the ones of Kimbell and Fies (1953). An additional cost of enhancing the construction quality was limited to ten percent of the original cost incurred in the project by Kimbell and Fies for the two-storey wood frame houses in the 1955 test. The changes included improvements to the connections between the exterior walls and the foundation and securing the window

frames to the structure. The size of the studs and rafters were also increased to 38 mm x 140 mm and 38 mm x 184 mm, respectively, and their connections were improved accordingly. Interior finish of gypsum lath and plaster was replaced by plywood sheathing, because the gypsum and lath plaster boards were completely destroyed in the previous tests. Finally, the foundation of the basement was upgraded from cinder block to reinforced concrete walls (Randall, 1955).

The second pair of wood house construction consisted of single story wood frame of conventional design, except that the walls of the bathroom were made out of concrete to provide a shelter since the house was built on a poured in place concrete slab. No structural information was provided for the sixteen trailer-coach mobile homes.

House #1, Set 1

The first two-storey house, located 1,676 m from the point of explosion, was subjected to an estimated overpressure of 27.6 kPa and suffered severe damage as shown in Figure 2.3. It was reported that the house would not be suitable for occupancy without extensive major repairs (Randall, 1955). According to Randall (1955), certain upgrades such as the reinforced concrete walls, the connection between the frame walls and concrete foundation walls, as well as securing of the window frames seemed to have fulfilled their purpose. The portion of the roof facing the blast was broken at mid-span and severe racking of the structure was evident (Randall, 1955). The floor joists of the second floor suffered severe damage leaving it near collapse due to the roof debris that fell on it.

House #2, Set 1

The second two-storey house, located 2,377 m from the point of explosion, was subjected to an estimated overpressure of 17.2 kPa. It suffered relatively heavy damage, as shown in Figure 2.4, but it was reported that it could be made available for emergency shelter by shoring some of the structural elements (Randall, 1955). The roof suffered severe damage as it was raised approximately 6 inches. The first floor joists were severely cracked and damaged but no debris was found in the basement as the subflooring remained intact. The pressure on this house was higher than the second two-storey house in tested in 1953 due to

the difference in energy release. The reason for subjecting the house to higher pressure was that it was deemed likely that the redesigned house would withstand the original 11.7 kPa overpressure with only minor damage. Glasstone and Dolan (1977) reported that "the overall damage was much the same degree as that suffered by the corresponding house without the improved features at an overpressure of 11.7 kPa".

House #1, Set 2

The first one-storey house, located 1,433 m from the centre of detonation, was subjected to an estimated overpressure of 34.5 kPa and was demolished beyond repairs while only the bathroom walls remained intact as shown in Figure 2.5 (a). Part of the roof was blown off while the remaining rafters were split and broken.

House #2, Set 2

The second house, located 3,200 m from the centre of detonation, was subjected to an overpressure of 11.7 kPa. It did not suffer heavy structural damage except for one cracked stud, and one broken support beam at mid-span of the rafters on the front side, as shown in Figure 2.5 (b) (Randall, 1955). The structure showed heavy racking evidence and considerable damage to the plaster board walls, ceilings, windows and glass was observed.

Trailer-coach mobile homes

The mobile homes, of which nine were subjected to an overpressure of 11.7 kPa and the remaining seven were subjected to an overpressure of 6.89 kPa, were parked at various angles with respect to the centre of detonation (Glasstone & Dolan, 1977).

At the higher overpressure (11.7 kPa), two trailers were flipped on their sides while the others remained standing (Glasstone & Dolan, 1977). It was reported that there was relatively few ruptures and that the exterior damage on the mobile homes manifested in dents in the walls or roofs. Also, it was noted that even though most windows were broken, there was little or no glass in the interior. Glasstone and Dolan (1977) emphasized that "by rearranging the displaced furniture, repairing cabinets, improvising window coverings, and

cleaning up the debris, all trailer-coaches could have been made habitable for emergency use".

At the 6.89 kPa overpressure, Glasstone and Dolan (1977) reported that "no major damage was sustained" even though some windows were broken. Moreover, it is reported that the trailer-coach mobile homes could be made available for occupancy by replacing the windows or by covering them.

2.1.3 Southeast Asia huts - United States Air Force, 2002

In the development of the "Vehicle Bomb Mitigation Guide" by the United States Air Force (AFH 10-2401, 2006), Southeast Asia Huts (SEA Hut) were tested under blast loading. These blast loads had much shorter durations than those in the 1950s test series modeling nuclear explosions. The tests conducted consisted of three coordinated initiatives, namely the Blast and Injury Tests (BAIT), Barrier Assessment for Safe Standoff (BASS) and Retrofits and Overpressure Design of Structures (RODS). Since the focus was primarily on the personnel vulnerability to explosions, the SEA Huts were tested and the results were evaluated for the purpose of developing retrofit options. The huts consisted of an elevated wood frame structure used as temporary shelters to house military personnel. Damage was mostly observed in rafters, studs, joists and windows as shown in Figure 2.6. It was reported that there was little observed damage to the roof truss system, unless all the load bearing walls failed. No failure of the lateral load resisting systems was observed, indicating that the shear walls were able to resist the side-on loads and dynamic shear loads transferred through the roof diaphragm. To mitigate damage and injuries or fatalities due to high velocity debris, the windows were removed and the window openings were covered with plywood. The SEA Huts were also strengthened by adding another layer of plywood to the floors and walls on the interior side along with the strengthening of the rafters and their connections to the walls.

2.1.4 Accidental explosion - BP Texas, 2005

Following the tragic incident at the BP Products North America Isomerization plant that killed 15 people and injured over 175 workers, a standard was developed to provide guidance on placing portable light-frame structures (API Recommended Practice 753). A total of nine portable trailers were located within 46 m from the explosion point during the incident.

Light-frame wood trailers, intended for occupancy, were not allowed to be placed within zone 1 (refer to Figure 1.2). In order for a trailer to be sited in zone 2, a detailed analysis needs to be undertaken. Any portable light-frame wood trailers can be sited in zone 3. These stand-off distances are for typical portable light-frame trailers found in the US consisting of 38 mm x 89 mm notched stud walls covered with light corrugated metal or wood siding. From the field analysis it was concluded that portable trailers could be deemed safe at an overpressure of 4.13 kPa but shall not be exposed to more than 6.2 kPa overpressure. It should be noted that these types of trailers differ from what is typically used in North American light-frame construction and were therefore also different from what was used in the current research study.

2.1.5 Light-frame wood stud wall damage levels using SDOF modelling, 2005

Oswald and his collaborators collected available information on observed damage levels and used it in the development of the of the Component Explosive Damage Assessment Workbook (CEDAW) Methodology Manual (Oswald, 2005). Limited SDOF-based analysis was performed during development of the blast damage assessment methodology for the wood stud walls on the reflected faces of the BAITS SEA Huts and additional tests on 38 mm x 140 mm and 38 mm x 184 mm stud walls were conducted by BakerRisk and compared with the field observations from the BAITS tests (Oswald, 2005). Normalized pressure-impulse (P-I) diagrams were developed allowing for the development of representative graphs of, for example, walls with dissimilar properties. It was noted that the developed normalized P-I curves predicted well the observed level of protection from experimental testing (Oswald, 2005). When actual strength and stiffness data were not available, published values were used. An allowable static flexural yield strength for wood studs of 1300 psi was assumed based on the published allowable strength for the No. 2 Grade Southern Pine studs used for the shock tube tests. This allowable flexural strength was multiplied by 2.5 (representing a strength increase factor) to calculate an ultimate flexural yield strength and then by 2.0 (representing a dynamic increase factor) for short duration loading to obtain a dynamic flexural tension strength of 6500 psi. The dynamic moment capacity was based on this flexural strength and the elastic section modulus of the studs, ignoring any composite action with the wall cladding. Wood studs with observed medium damage in the tests had

calculated ductility ratios from the SDOF analysis between 1 and 2. Wood studs that failed had calculated ductility ratios of 3 and greater.

2.1.6 Coated structural lumber structure - University of Maine, 2010

An alternative to the SEA Huts was developed at the University of Maine where a blast-resistant structure consisting of a wood based composite material called Coated Structural Lumber (CSL) (Syron, 2010) was investigated. The hybrid material consisted of conventional wood and a Fiber-Reinforced Polymer (FRP) matrix. The CSL building provided higher blast resistance than the conventional SEA Huts and with a consistent failure mode in the plates connecting the wall panels to the roof and floor. The performance of the CSL building was compared to that using conventional light-frame construction technique is shown in Figure 2.7 (a), while the damage to the connection plate can be seen in Figure 2.7 (b).

Laminated Strand Lumber (LSL) was also investigated under high strain rates in compression. It was observed that there was an increase in the compressive strength in both the longitudinal and transverse directions for the two grades of LSL tested, as the strain rate increased. An increase in longitudinal compressive strength between 31% and 37 % was observed for an increase in strain rate from 1E-5 to 1E-3 sec^{-1}. Correspondingly, the transverse compressive strength was observed to increase between 16% and 41%. Furthermore, an increase in the modulus of elasticity was also observed for both directions. The increase in the longitudinal direction was observed to be 16% while in the transverse direction the increase was found to be between 18% and 28%.

2.1.7 FRP-coated light-frame wood stud walls - University of Maine, 2010

The behaviour of FRP-coated light-frame stud walls was investigated statically and dynamically under field explosions (Parlin, 2010). The walls consisted of 38 mm x 89 mm solid sawn lumber sheathed with plywood. The studs were coated with unidirectional e-glass oriented longitudinally and infused with resin. The plywood was coated with multiple layers of 0-90 e-glass on the front and back. The walls were tested dynamically in previous work (Dumais, 2008) while representative T-section samples were tested statically. The predicted displacement history was obtained by using the hysteretic curve determined experimentally

while the forcing function was the one recorded experimentally. In the determination of the fitted parameters for the hysteric curve it was determined that the strength resisting parameters showed an increase that ranged from 11% to 41%. It is later discussed by Parlin that the difference between the pseudo-static properties and blast fitting properties are possibly due to the load rate effects that were not captured in the pseudo-static tests (Parlin, 2010).

2.2 Behaviour of wood specimens subjected to impact and blast loading

Wood has been used in applications where it was subjected to impact loads for a long time but the behaviour has only been quantified recently. For example, wood was used as rams, which consist of a heavy straight piece of timber with a brass cap (to avoid splitting) to break walls of fortresses. Wood was also used to fabricate ships which had to resist the impact loads caused by bullets and cannons (Johnson, 1986). Prior to World War I, it was known that the duration in which the load was applied had an effect on the strength and stiffness of wood members and for that reason, speed of testing requirements were proposed for standard test procedures (Cline, 1908; Tiemann, 1908).

A study conducted at the Forest Products Laboratory investigated the effect of rapid loading on the compressive and flexural strength of wood for two softwood and two hardwood species (Liska, 1950). It was found that the modulus of rupture (MOR) in compression parallel to grain and in flexure increased as the time to maximum load decreased with 10 to 40% of the average standardized control values. Time to maximum loading varied from a third of a second to 550 seconds. It should be noted that this load rate is not in the range typically experienced during blast loading (i.e. this impact loading has much longer load duration than that experience under blast loading). The outcome of this study was reviewed and reaffirmed in 1958 where it is again noted that the ultimate capacity increased with increasing rate of loading both in compression and flexure (Brokaw & Foster, 1958).

Barrett and Lau (1994) reported that the relationship between the rate of loading (ROL) for full-scale members differed from that derived for small clear specimens. It was also shown that the rate of loading effect was smaller for low strength material compared to high strength material. Foschi and Barrett (1982) also reported an increase in strength of

approximately 10% when the specimens were loaded to failure in 0.1s compared 1 minute. Furthermore, for a specimen loaded to failure in 30 hours, a decrease in strength at failure of 10% was found. Tests were conducted on two species (SPF and D. Fir), for two sizes (2x4 and 2x8 nominal sizes), and using three different strain rates ($1.7E^{-5}$ s^{-1}, $1.7E^{-4}$ s^{-1}, and $4.2E^{-4}$ s^{-1}).

The behaviour of parallel strand lumber (PSL) under impact loading was investigated (Sukontasukkul, Lam, & Mindess, 2000) and it was found a strength increase of 30% could be observed relative to static capacity. A total of six specimens were tested statically while 12 specimens were tested using two different impact height. At the higher impact height, it was reported that localized damage attributed to a slight reduction in the increase in apparent bending strength (Sukontasukkul et al., 2000).

Widehammar (2004) reported on the effects of the strain rate, moisture content and direction of loading on the stress-strain relationship of spruce wood. A total of three strain rates: $8E^{-3}$ s^{-1}, 17 s^{-1} and 1000 s^{-1} were used in compression for the axial, tangential and radial directions of the fibers on three state of moisture corresponding to oven dry, fiber saturated and fully saturated. In general, as the water content increases the maximum stress relative to the oven dry tests reduces but the ratio of the maximum stress for the highest strain rate compared to the lower strain rate is always greater than one, thus showing an increase in resistance for increased strain rates, for each water content.

An experimental program was conducted at the University of Ottawa focusing on the dynamic properties of timber members under simulated blast loading (Lloyd et al., 2011). The static and dynamic capacity of the 38 mm x 140 mm x 2440 mm Spruce-Pine-Fir studs was determined by testing 36 specimens under static and shock wave loading . The maximum peak load was applied over a few milliseconds while the failure of the specimens was observed closer to the range of twenty to thirty milliseconds. It is important to note that in this experimental program the specimens were not free of defects as would likely be the case in most of the small specimens used in studies involving impact loading. The study

reported an average increase on the MOR and MOE of 1.45 and 1.19, respectively (Lloyd et al., 2011).

Although almost all of the published research have documented an increase in strength with increased strain rate, a few studies have reported only an increase in ultimate strength for the "stronger" specimens (high grade) and a decrease in ultimate strength in the weaker specimens (low grade) (S Mindess & Madsen, 1986; S. Mindess, Madsen, & Yan, 1988; Spencer, 1978). It was reported that all failures observed under impact loading were similar but they differed from those observed under static loading. It was also noted that the initial crushing of the wood fibres were significantly influenced by the tip of the impact machine. No reasons were provided to explain the drop in the capacity, and no attempt was made to investigate whether the localized damage had any impact on the observed results as was the case in Sukontasukkul et al. (2000).

2.3 Partial composite action between studs and sheathing in floor systems

Partial composite action between the sheathing and studs plays a key role in light-frame systems such as walls and floors. Since floors are usually loaded out-of-plane, several studies have been undertaken to establish the behaviour of such system under uniformly distributed static loading. Since walls consist of elements similar to those found in floors, the concept of partial composite action can be applied to walls loaded out-of-plane as well.

Numerous studies have shown that neglecting the partial composite action between the sheathing and the joists in floors systems will yield spans that are too conservative. For example, the effect of nailing and/or gluing plywood sheathing in a direction perpendicular to the floor joists under uniform distributed load resulted in an average increase in stiffness between 13% and 38% for the nailed and nail-glued floors, respectively (NAHB, 1961). Polensek and his collaborators (Polensek, Atherton, Corder, and Jenkins (1972) also reported an average increase in stiffness between 1.15 and 2.04 for floor joists under distributed loading.

In order to quantify the degree of partial composite action between the sheathing and framing elements, Wilkinson (1972 and 1974) developed a theoretical approach to determine the

lateral resistance of two-member joints. Elastic bearing constants from various wood materials were determined based on theoretical equations developed by Kuenzi and Wilkinson (1971) and it was concluded that there was good agreement between the experimental data and theoretical model.

McCutcheon (1977 and 1986) used the theory developed by Wilkinson to present a method of calculating the deflection of wood floor systems while accounting for the interlayer stiffness and the effects of non-continuous sheathing. In 1986, the theory was extended from a one layered T-beam to systems with sheathing on both sides while still accounting for the interlayer stiffness. The T-beams and I-beams were observed to be 9% to 109% stiffer than that of the framing element alone.

Similar analysis techniques, described further in Chapter 5, have been adopted to establish a better predictive model for wall systems in the current research project.

2.4 Summary

This literature review has highlighted the need for understanding the behaviour of wood structural systems under loading of very short term duration especially for components representative of what is used in construction, i.e. large members containing defects that naturally occur in wood. Unfortunately, the studies conducted on full scale light-frame wood structures reported deficiencies in instrumentation due to lack of funding and could therefore not quantify the increase in capacity due to the dynamic loading. Reported in Table 2.1 is a summary of the observed levels of damage for the different types of wood structures discussed earlier in this Chapter associated with the observed peak free-field pressure. From the literature it can be summarized that for peak free-field pressures above 27.6 kPa will most likely result in a total failure of the light-frame wood houses. Below a peak free-field pressure of 17.2 kPa these low rise light-frame wood structures are not expected to collapse and would be available for emergency occupancy with minimal repairs. These observations provide a general understanding of the behaviour of light-frame wood structures subjected to blast loads, but should not be used to evaluate the performance of other wood structures because the performance is highly influenced by the associated impulse as well as the types of elements used in the light-frame construction.

Experimental studies that measured and reported the load-displacement time histories generally focused on the behaviour of small clear specimens to impact loading. In general, a strength increase between 10% and 90% was observed in the literature when comparing the capacity of specimens tested under short load duration and related those tested under standard load durations, with only few studies reporting on an increase in stiffness. The test results from Barret and Lau (1994), Widehammar (2004), Syron (2010) and Lloyd (2011) are summarized in Figure 2.8, which shows the relative increase in strength against the log-10 based strain rate. From Figure 2.8, a notable increase in strength can be observed with increasing strain rates.

Although the available data is limited, important conclusions that affect the current study can be drawn. Research on the behaviour of light-frame wood structures subjected to nuclear blast highlighted that these types of structures withstood higher loads than what they were designed and constructed for, due to the load sharing and high strain rates effects. Another important finding is that damage to the structures is highly influenced by the damage inflicted to the rafters, studs, joists and windows. Establishing that the predominant failure mode is in flexural failure of wall studs, floor joists and roof purlins was the precursor to deciding to investigate the flexural behaviour of the stud walls while omitting (in the scope of this research work) the consideration of the connections between the wall and roof or wall and floor systems. This information is also helpful for the SDOF analysis because it justifies the simplification of focussing on one failure mode.

The following chapter describes the experimental methodology employed to assess the flexural behaviour of light-frame wood stud walls subjected to blast loading. A detailed description of the components and specimens tests as well as the test setups is provided.

Table 2.1: Summary of observed levels of damage for wood light-frame structures

House type	Peak free-field pressure (MPa)	Observed damage
Two-storey house and one storey house	27.6 to 34.5	Total failure. Collapse of structure. Not suitable for emergency occupancy.
Two-storey house and one storey house	11.7 to 17.2	No collapse, temporary shoring of structural elements and closure of openings would be safe for emergency occupancy. Minimal damage except failed windows and doors.
Trailer-coach mobile homes/ Office trailers	11.7	Possibility of tipping over. Relatively few ruptures of structural elements.
Trailer-coach mobile homes/ Portable trailers	6.2 to 6.89	No major damage. Available for emergency occupancy by covering windows or by replacing them.
Trailer-coach mobile homes/ Portable trailers	4.13	Deemed safe.

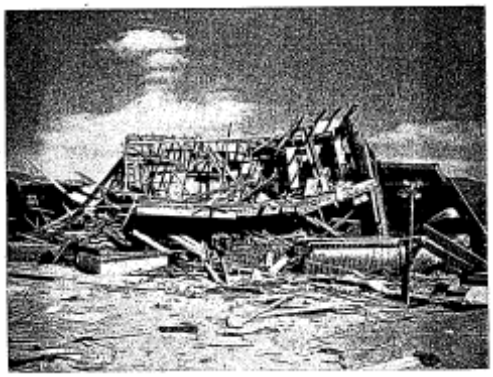

(a) Wall facing detonation

(b) Top view

Figure 2.1: Two-storey wood frame houses, 1953-House #1

*Reproduced from Kimbell and Fies (1953)

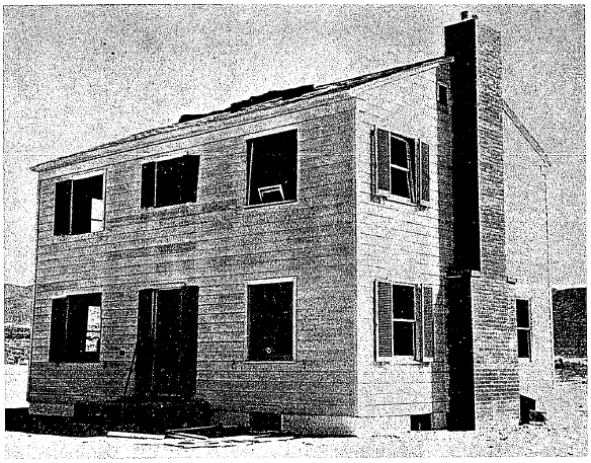

(a) Wall facing detonation

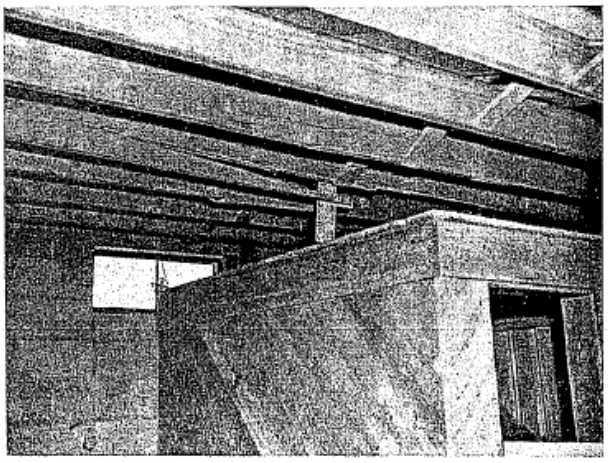

(b) Living room first floor joists

Figure 2.2: Two-storey wood frame houses, 1953-House #2

* Reproduced from Kimbell and Fies (1953)

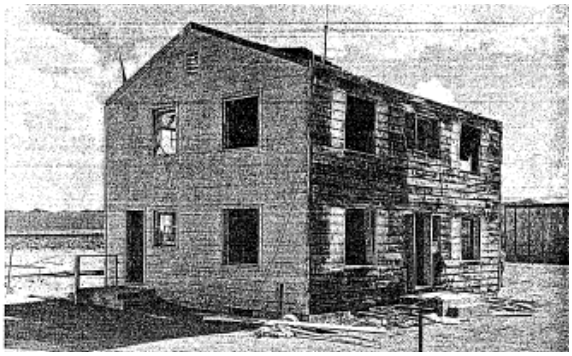

(a) Wall facing detonation

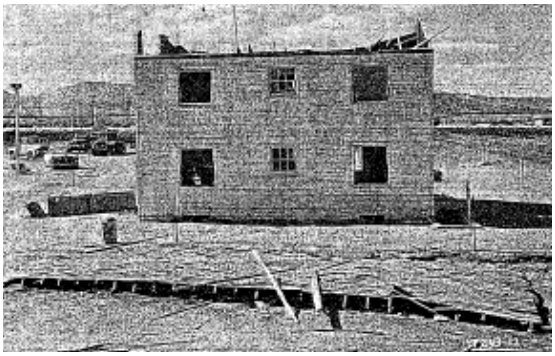

(b) Rear wall

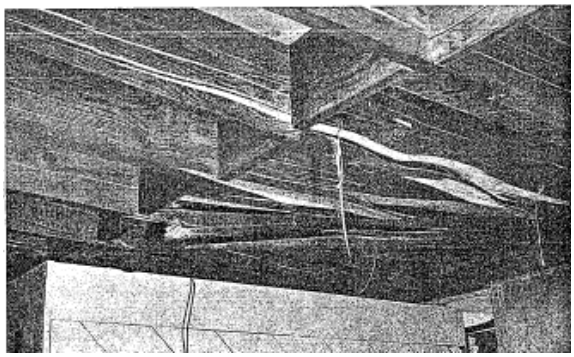

(c) First floor framing under dining room

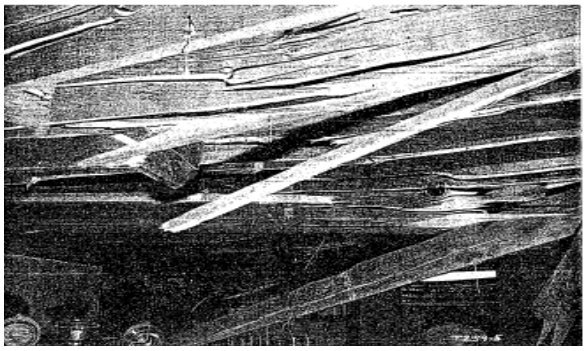

(d) First floor framing under living room

Figure 2.3: Two-storey wood frame houses, 1955-House #1, Set 1

*Reproduced from Randall (1955)

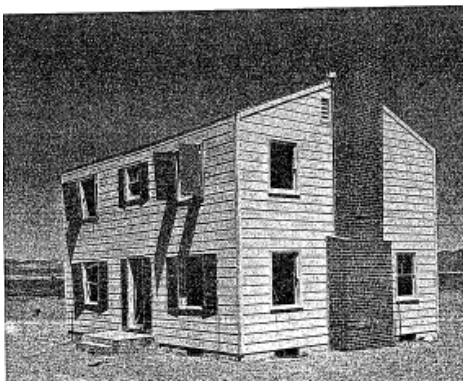

(a) Wall facing detonation

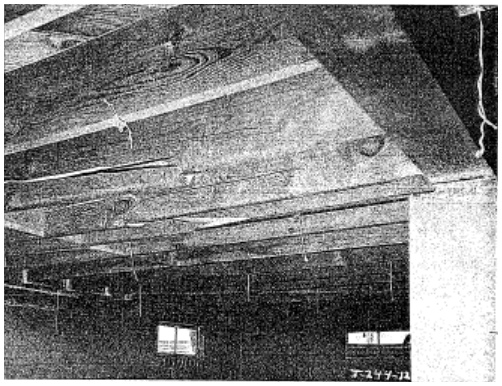

(b) First floor framing

Figure 2.4: Two-storey wood frame houses, 1955-House #1, Set 2

*Reproduced from Randall (1955)

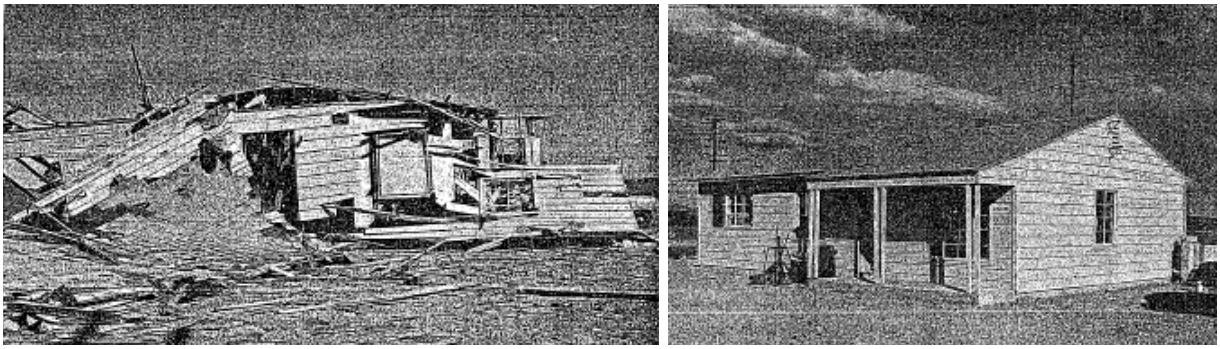

(a) House #1-Wall facing detonation (b) House #2-Wall facing detonation

Figure 2.5: One storey wood frame houses, 1955-Houses #1 and #2, Set 1

*Reproduced from Randall (1955)

(a) Before blast (b) Post blast

Figure 2.6: Southeast Asia Huts, 2002

*Reproduced from AFH 10-2401 (2006)

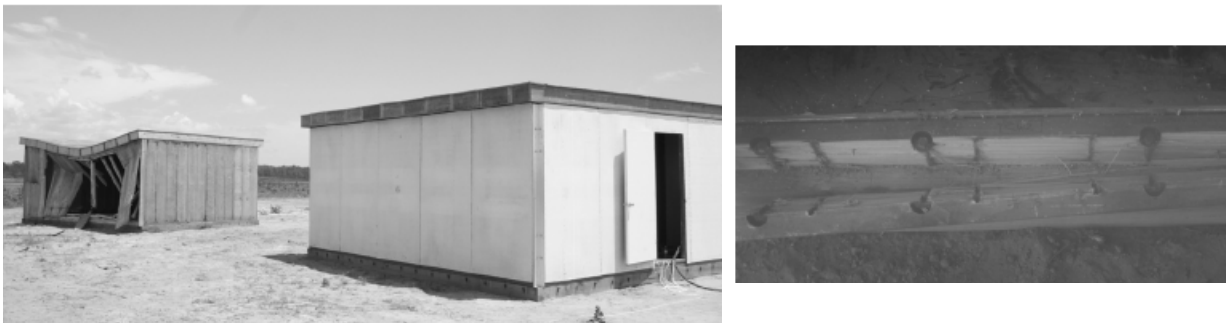

(a) Conventional and CSL building post blast (b) Damage to connection plate

Figure 2.7: Coated structural lumber structure, 2010

*Reproduced from Syron (2010)

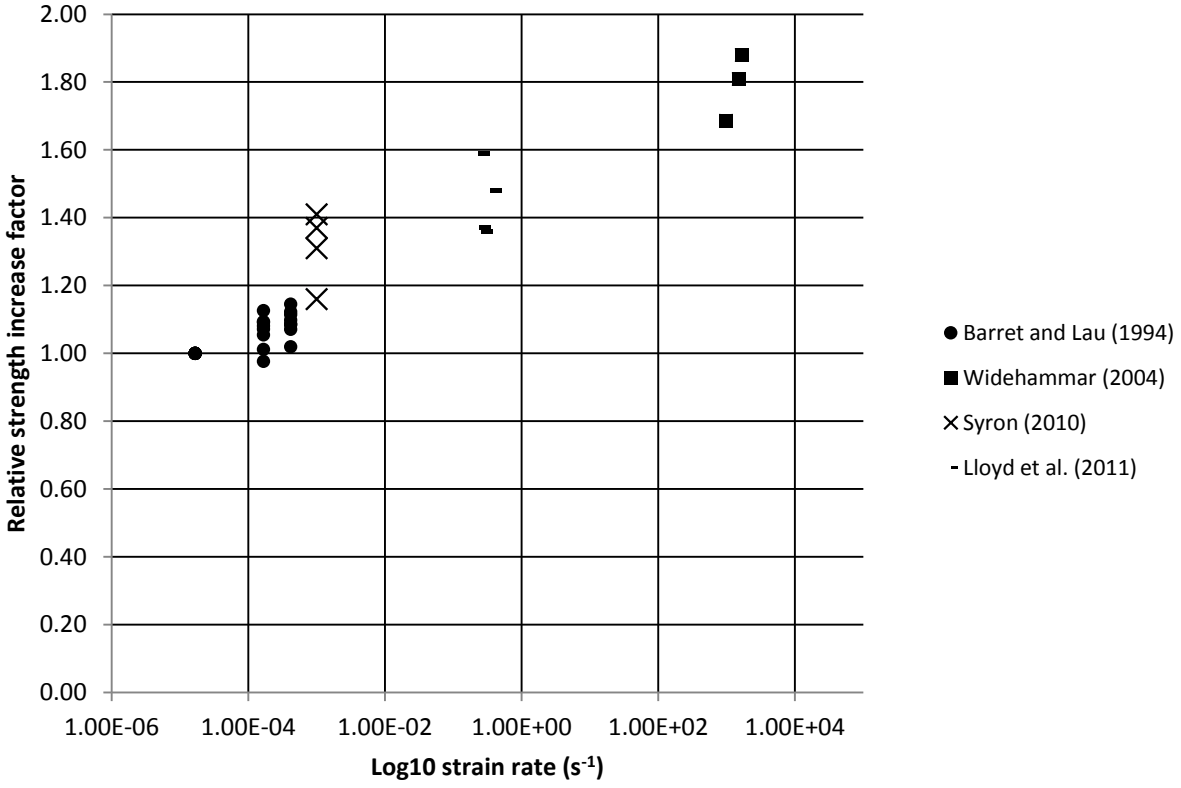

Figure 2.8: Summary of relative increase in strength with strain rate

CHAPTER 3-Experimental Program

The approach employed in this experimental program was holistic, where the specimens were investigated at the component and the system levels. A detailed description of the methodology employed in the experimental program is presented in this section. A summary of the testing program for the walls is provided in Table 3.1. The walls were tested statically prior to being subjected to a number of pressure and impulse combinations simulating blast loads. The specimen description is also shown in Table 3.1. The intent with this approach is to investigate the behaviour of each component individually and develop predictive models such that the behaviour of the wall system as a whole can be evaluated. Testing at full scale would provide a validation to the proposed predictive model.

Twenty light-frame wood stud walls consisting of 38 mm x 140 mm machine-stress-rated (MSR) lumber, spaced 406 mm on center and with a single top and bottom plates, were tested to failure under static and dynamic loading. A total of ten walls were sheathed with 11 mm oriented-strand-board (OSB), attached to the studs with 64 mm long nails with a diameter of 3.50 mm. The other ten walls were sheathed with 18.5 mm plywood and attached with 89 mm long nails with a diameter of 4.24 mm. The nails were fastened using a grid pattern of 150 mm on center for all walls in an attempt to reduce nail withdrawal under dynamic loading observed in earlier testing (Lacroix & Doudak, 2012). The total height of the walls was 2,159 mm with a clear span of 2,032 mm. This dimension ensured that only the response of the studs and sheathing was observed and the possibility of failure of the connection between the studs and top and bottom plates was eliminated. This was also ensured by providing idealized pinned end conditions as described later in this chapter. Complete detailing of the walls is shown in Figures 3.1 and 3.2 for the OSB and plywood walls, respectively.

3.1 Sheathing static tests

Static material properties such as the modulus of elasticity (MOE) and modulus of rupture (MOR) of both the OSB and plywood sheathing were determined in accordance with the American Society for Testing and Materials (ASTM) for Evaluating Properties of Wood-Base Fiber and Particle Panel Materials (ASTM D1037-06a, 2006). Point loads were applied

at mid-span and the resulting mid-span deflection was measured. The results were used in the development of the material predictive model in Chapter 5. A total of 80 specimens, half consisting of plywood and the other half of OSB, were tested. The sample lot sizes were determined based on the standard practice for Sampling and Data-Analysis for Structural Wood and Wood-Based Products (ASTM D2915-10, 2010). The OSB and plywood specimens measured 76 mm x 315 mm and 76 mm x 495 mm, respectively. The test setup is shown in Figure 3.3.

3.2 Load-slip tests

Nail joint tests were performed in order to determine the load-slip relationship between the sheathing and the stud. A total of ten tests were performed at a loading rate of 5 mm/min for each type of sheathing connected with the exact nails used in the construction of the walls specimens. The relative slip between the sheathing and the stud was measured at the end of the specimen through two linear variable displacement transducers (LVDTs) on each side of the stud as shown in Figure 3.4 (a). Figure 3.4 (b) and (c) shows the yielding of the nail and the crushing of the wood, respectively. This information will be used as input in one of the proposed predictive models described in Chapter 5.

3.3 Stud static tests

The MOE of the 160 individual studs was determined using a hand-held grader (Brookhuis Micro-Electronics) as well as a preloading technique prior to assembling the stud wall specimens. Forty studs were randomly selected and tested to failure under four-point loading with simply supported end conditions in accordance with ASTM D198 (2009). The test setup is shown in Figure 3.5. The load application points were located at the third points of the clear span. The stud elements were laterally braced at the load application points as well as at the end supports as required by the testing Standard. In order to avoid crushing of the wood at the load application points, bearing blocks consisting of a denser wood material were used to transfer the load to the test specimens. The applied load was measured using a load cell located between the jack and the reaction frame. The mid-span displacement was measured using a compact string pot wire gauge with a 300 mm stroke. As shown in Figure 3.5, full rotation was ensured at the supports while Figure 3.6 shows the actual setup before and during a test.

3.4 Wall static tests

A total of ten walls, half consisting of OSB and the other half of plywood sheathing, were tested to failure under four-point loading and pinned end conditions. Ten additional walls were only preloaded to approximately 10% of their capacity to obtain their initial stiffness. This information would be used to compare with the stiffness values obtained from the dynamic tests. The test setup used to load the walls is shown in Figure 3.7 and 3.8. A load transfer device was used to transfer the applied load at the third points of the clear span (2032 mm). This span was consistent with that used to test studs in isolation. The applied load was transferred to the studs through the two load spreader beams, as shown in Figures 3.7 and 3.8. The load cell was placed between the hydraulic jack and the spreader beam. The mid-span deflections of the four middle studs were measured using four wire gauges attached to the floor independently from the reaction frame. Idealized pin conditions were provided by attaching a steel angle to both ends of the supporting wood knee wall providing a clear span of 2032 mm. To avoid potential crushing of the wood at the location of load application, 50 mm x 100 mm steel plates were fastened to the studs at each point of contact (Figure 3.8).

3.5 Wall dynamic tests

High strain rates in the stud walls were generated through shock wave loading using the University of Ottawa's Shock Tube. This section describes the Shock Tube as well as the test setup and the methodology employed.

3.5.1 Description of the shock tube

A shock wave, similar to that resulting from far-field detonations of high explosives, was created by adding compressed air in the driver section of the Shock Tube. A wide range of explosions with different pressure and impulse combinations representing different charge-weights and stand-off distances can be obtained. The Shock Tube is shown in Figure 3.9 with its three main components: driver section, spool section and expansion section. The shock wave is created by the release of the compressed air stored in the driver section through the control of the spool section. The mechanism used for firing is referred to as a double diaphragm firing system due to the two set of diaphragms, foils consisting of sheets of aluminium, used to keep the pressure in the spool and driver sections. During the loading stage, compressed air is not only added in the driver section but in the spool section as well,

therefore the combination of the foils between the expansion section and spool section need to be greater than that anticipated in the spool section. The second combination of foils, between the spool and driver section needs to be greater than the differential pressure between the driver and spool section. Once the desired driver pressure is reached, the pressure in the spool section is drained until rupture of the foils occurs between the spool and driver section, leading to the rupture of the second foil set. The quick release of the compressed air forms a shock front that travels along the 6096 mm expansion section and interacts with the specimen mounted to the end frame as shown in Figure 3.9 (c). The opening of the end frame, 2032 mm x 2032 mm, allows for the testing of large scale specimens that can be mounted directly to the rigid end frame. Located near the end of the expansion section are twelve pressure relief vents that allow for a negative pressure phase to be developed as the shock wave tries to return to ambient pressure. This also contributes to the reduction of tertiary shock waves occurring within the Shock Tube caused by the reflection of the shock wave. The maximum peak reflected pressure is controlled by the driver pressure while the reflected impulse, and hence the time duration of the positive phase, is controlled by varying the driver length. The positive phase increases with driver length as there is a higher volume of compressed air in the driver section. The driver section can be varied in 305 mm increments from 305 mm to 5,185 mm. The maximum reflected pressure and reflected impulse that can be achieved with the Shock Tube are 100 kPa and 2200 kPa-ms, respectively, while the range of time durations for the positive phase is 5 to 70 ms. More details on the calibration of the shock tube can be found in Lloyd (2010).

3.5.2 Description of the test setup

The walls were attached to the end frame of the Shock Tube without the need of a load transfer device. Simply supported end conditions that mimicked those used in the static testing were used, as shown in Figure 3.10. Two steel angles were held to the end frame by four 50 mm x 50 mm hollow steel sections to provide a point of contact for the wall. In addition, these angles provided space for the walls to deflect without interacting with the end frame. The angles were placed in such a way that the clear span was equal to 2032 mm, which was consistent with the span in the static testing. As it can be seen in Figure 3.10, no axial load was applied and the wall was held in place by friction with the steel angle. In order

to avoid potential crushing of the wood at the point of contact, the same 50 mm x 100 mm steel plates as used in the static loading tests, were fastened to the studs.

The reflected pressure was measured by two independent dynamic piezoelectric sensors. For each test, strain gauges measured the strain at mid-span on the tension side and LVDTs were attached at mid-span at the neutral axis to measure the deflection of the four middle studs. An additional LVDT was used to measure the displacement of the Shock Tube frame during the test. The strain gauges used were 6 mm x 11 mm general purpose strain gauges with a resistance of 350 ohms while the LVDTs used had a 300 mm stroke. The LVDTs were mounted to a hollow 50 mm x 50 mm steel section which was in turn attached to two shoring jacks independent of the Shock Tube movement. In an attempt to protect the LVDTs from debris, a steel barrier was mounted to the Shock Tube as shown in Figures 3.10 and 3.11. The complete test setup is shown in Figure 3.12. The area on which the strain gauge was applied was hand-sanded and cleaned prior to the installation of the strain gauges. A layer of epoxy was placed and the area was sanded again when the surface was dried. The strain gauges were then glued to the studs at the desired location and covered using duct tape, as shown in Figure 3.13.

The strain gauges, LVDTs and pressure sensors were connected to the data acquisition system which recorded the experimental data at a sampling rate of 100,000 samples per second. The data acquisition system was triggered by the shock wave front as it passed one of the pressure sensors while also initiating the recording of the high speed camera, which recorded at a rate of 500 frames per second with a resolution of 800 x 600 pixels.

3.5.3 Determination of pressure and impulse combinations

The walls were subjected to various pressure and impulse combinations to achieve different response levels. Three driver lengths were used: 305, 2,745 and 4,880 mm in order to achieve pressure-impulse combinations in the impulsive, dynamic and quasi-static regions, respectively. Another motive for varying the driver sections was to verify the accuracy of the proposed model over a wide range of pressure and impulse combinations. The driver lengths were chosen based on preliminary SDOF modeling using the average static resistance curve

of each type of walls obtained through experimental testing and modified for high strain rate effect using the dynamic increase factor values published in the CSA S850 standard.

The walls were subjected to two or three combinations of pressure and impulse. The objective of the first combination was to observe an elastic response without causing any damage in the test specimens. The second combination of pressure and impulse was chosen to provide a pressure approximately equivalent to the load applied statically while the third pressure and impulse combination was chosen to observe failure in the specimen.

Table 3.1: Testing schedule summary

Specimen	Wall static test	Number of pressure-impulse combinations	Driver length (mm)	Configuration
W1	Destructive	-	-	38 mm x 140 mm MSR @ 406 mm o/c 11 mm OSB Nails, 64 mm x 3.50 mm @ 150 mm (field and edge)
W2	Destructive	-	-	
W3	Destructive	-	-	
W4	Destructive	-	-	
W5	Destructive	-	-	
W6	Non-destructive	2	2,745	
W7	Non-destructive	1*	2,745	
W8	Non-destructive	2	305	
W9	Non-destructive	3	2,745	
W10	Non-destructive	2	4,880	
W11	Destructive	-	-	38 mm x 140 mm MSR @ 406 mm o/c 18.5 mm Plywood Nails, 89 mm x 4.24mm @ 150 mm (field and edge)
W12	Destructive	-	-	
W13	Destructive	-	-	
W14	Destructive	-	-	
W15	Destructive	-	-	
W16	Non-destructive	3	2,745	
W17	Non-destructive	2	4,880	
W18	Non-destructive	2	305	
W19	Non-destructive	2	2,745	
W20	Non-destructive	3	2,745	

*One test due to cracks in members prior to test

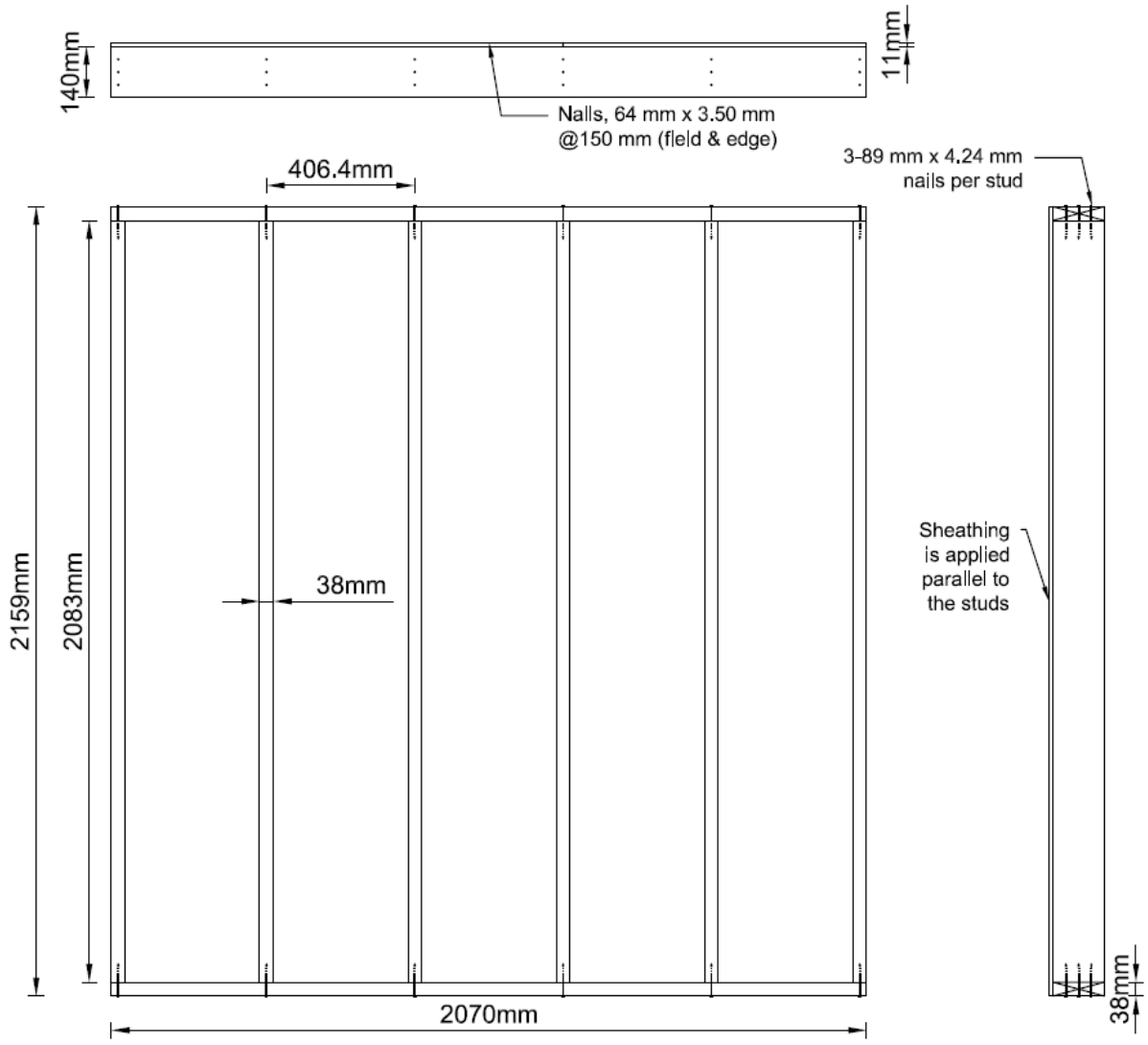

Figure 3.1: Typical OSB wall details

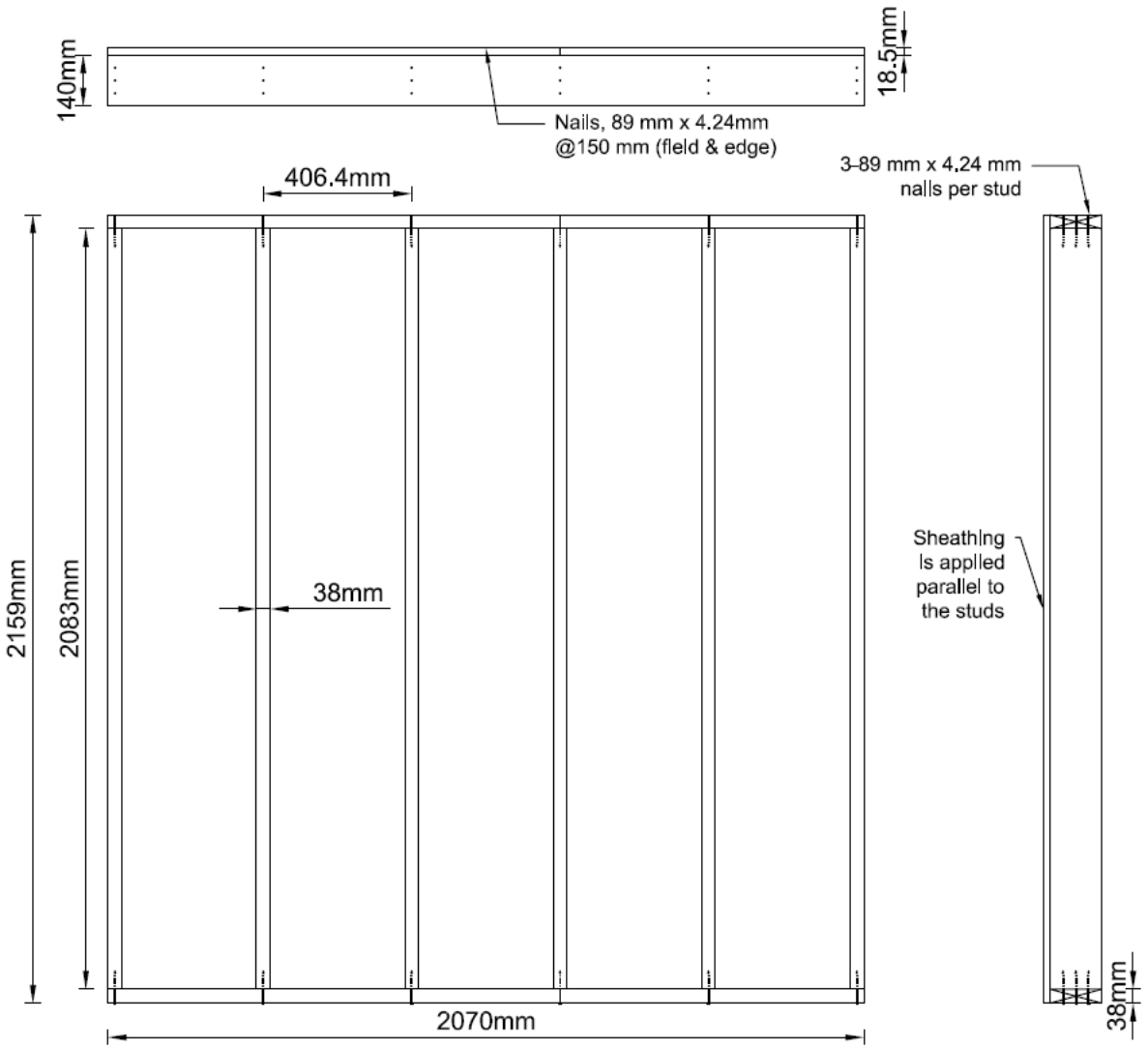

Figure 3.2: Typical plywood wall details

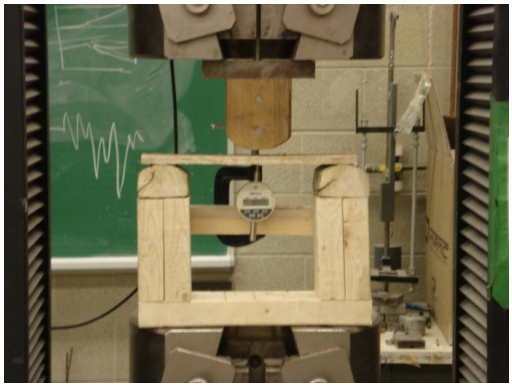

(a) Before testing

(b) Typical failure of sheathing coupons

Figure 3.3: Typical test setup for the sheathing tests

(a) Test setup

(b) Yielding of nails

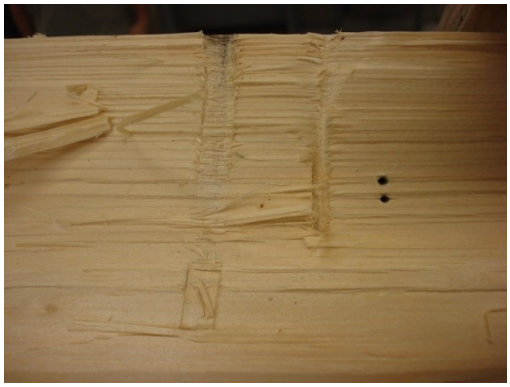

(c) Crushing of wood

Figure 3.4: Typical test setup for the load-slip tests and typical failure mode

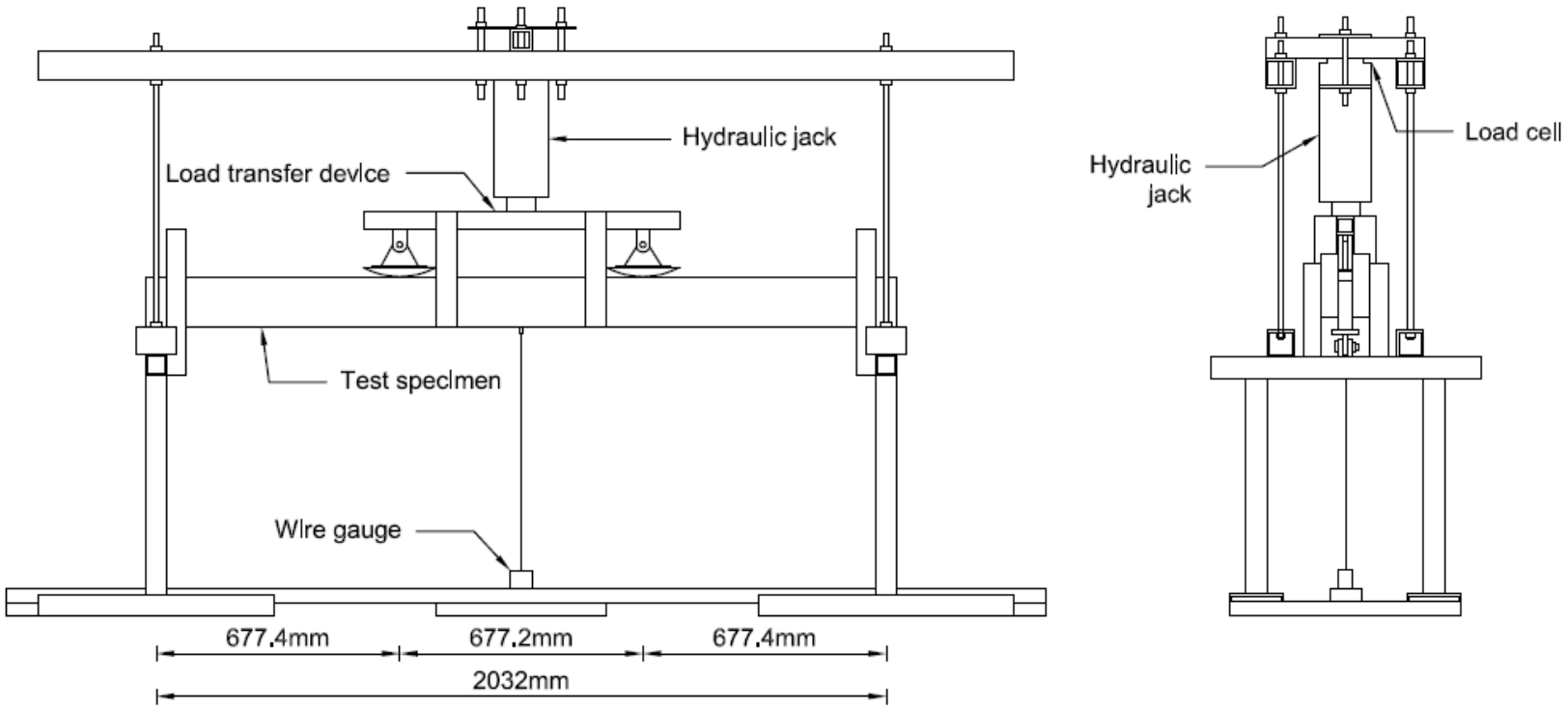

(a) Profile (b) Side

Figure 3.5: Typical test setup for the stud elements in isolation

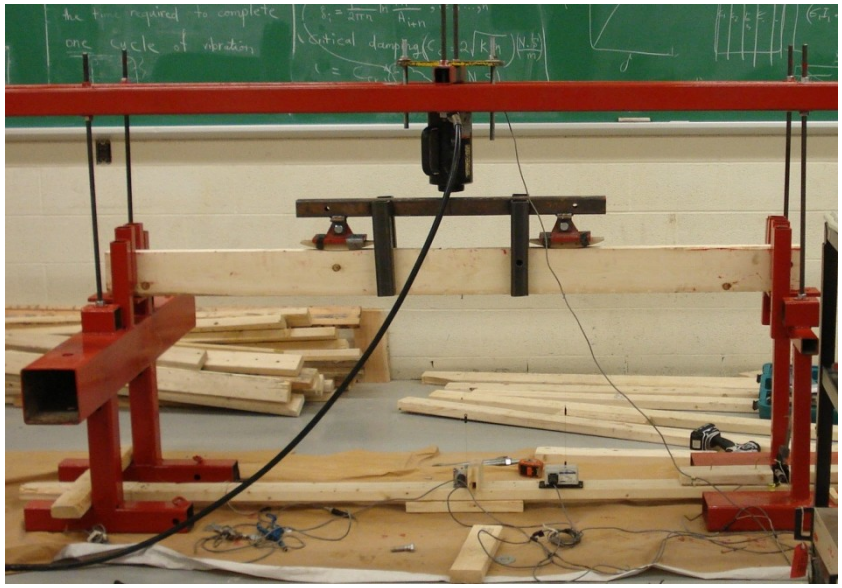

(a) Before testing

(b) Typical failure of studs

Figure 3.6: Static testing of individual studs

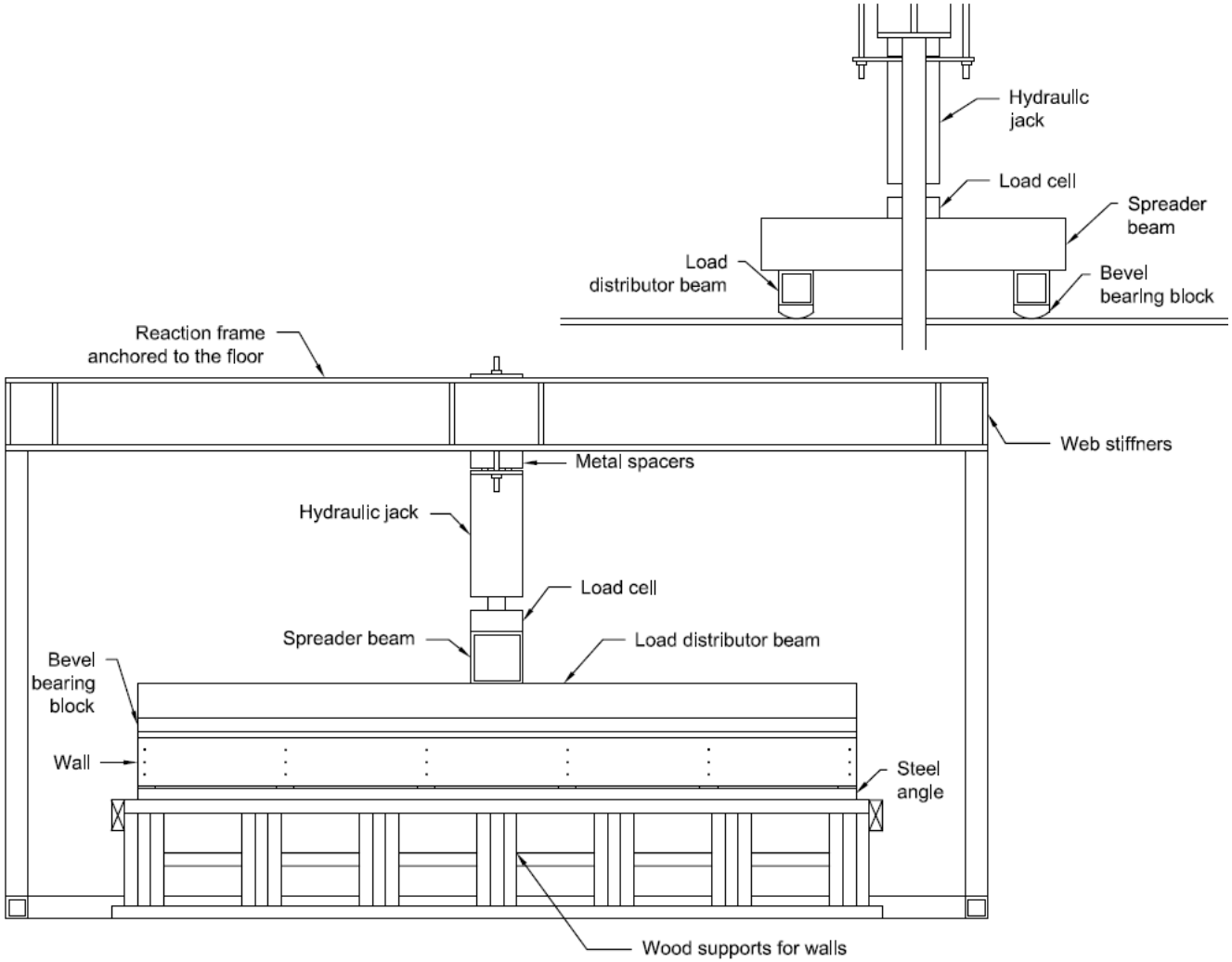

Figure 3.7: Typical wall test setup-Load transfer device details

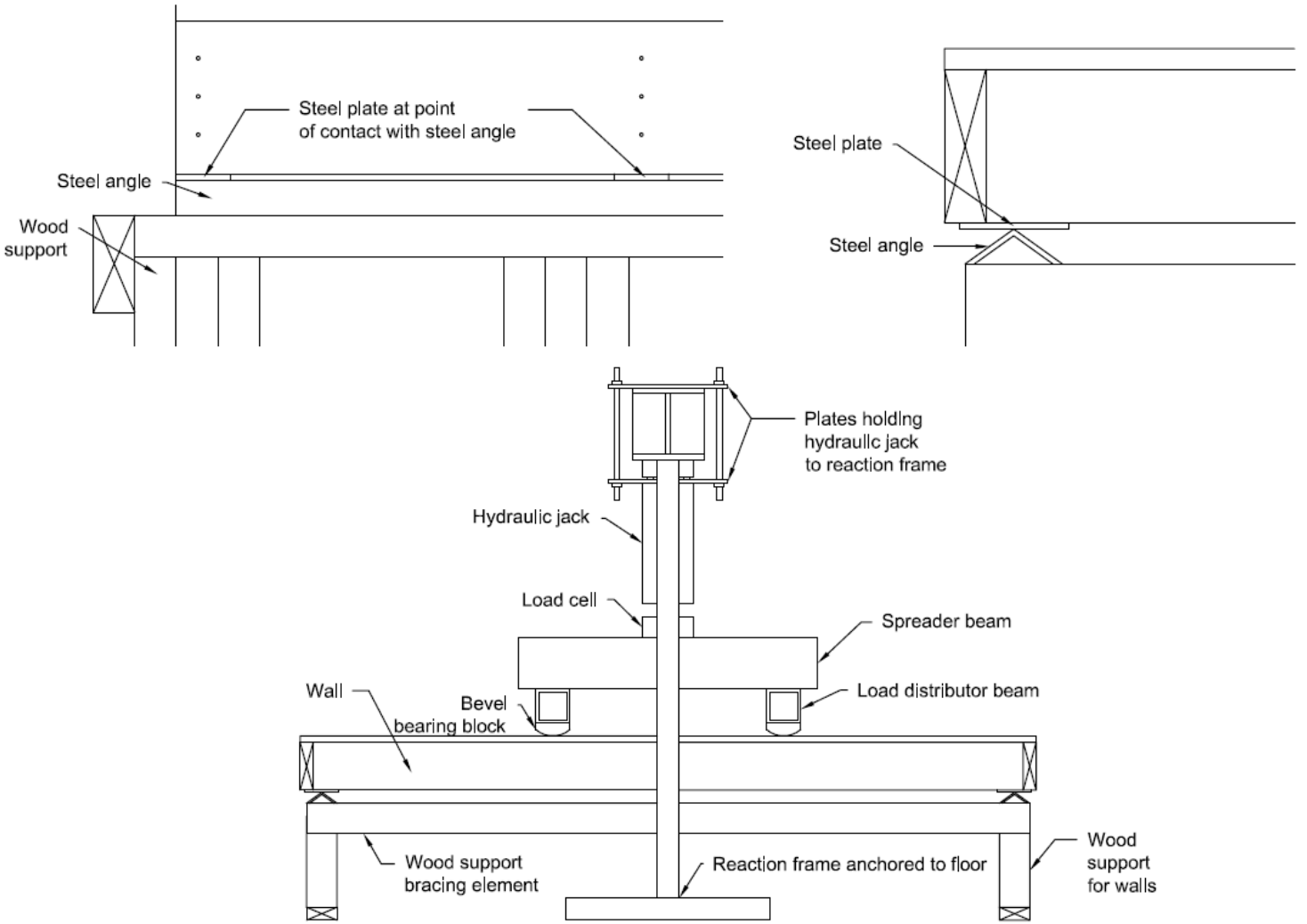

Figure 3.8: Typical wall test setup-Support condition details

(a) Driver and spool section

(b) Expansion section

(c) End frame

Figure 3.9: University of Ottawa's Shock Tube

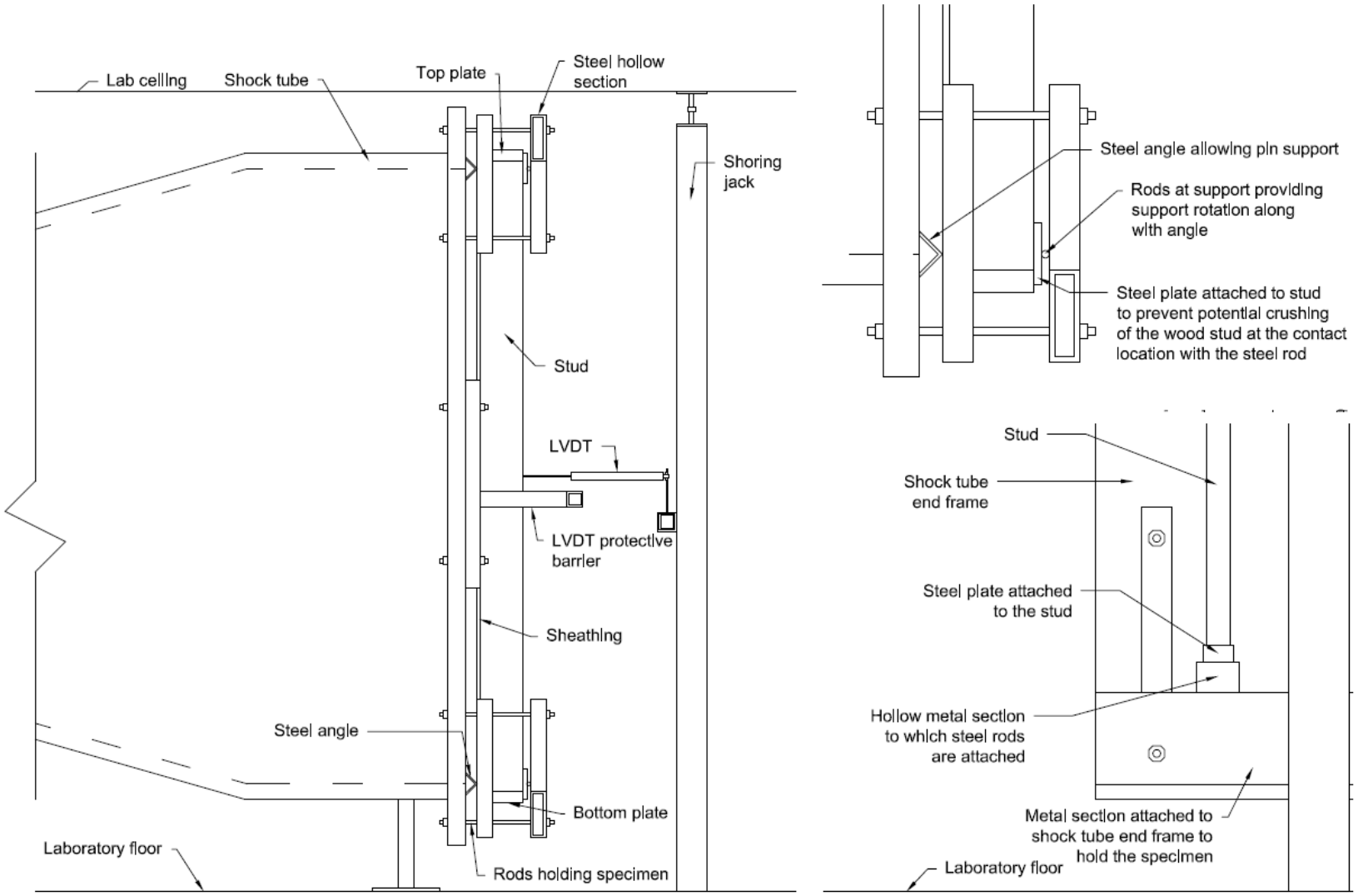

Figure 3.10: Dynamic wall test setup - Support conditions details

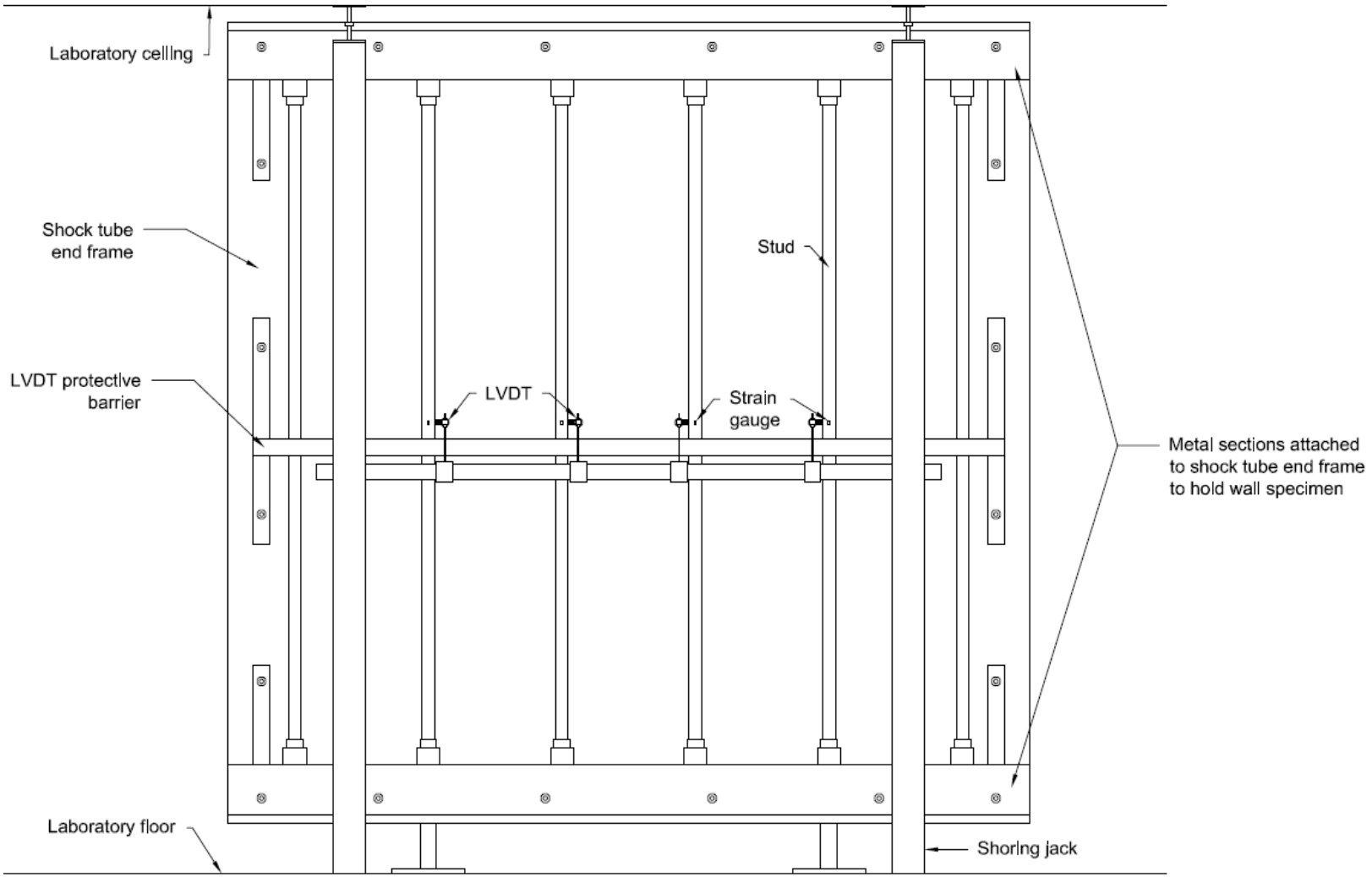

Figure 3.11: Dynamic wall test setup - General

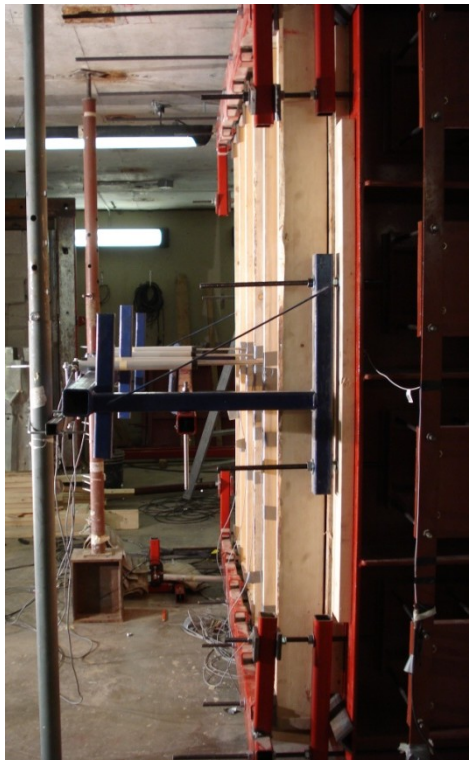

(a) Side view

(b) Oblique view

(c) Back view

Figure 3.12: Actual dynamic test setup

(a) Epoxy layer after sanding wood

(b) Sanding epoxy layer

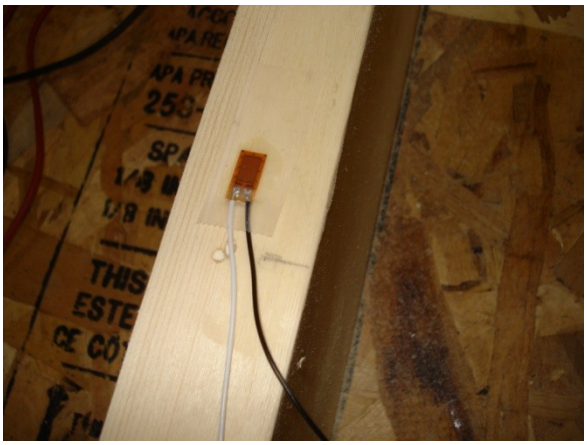

(c) Gluing strain gauge to stud

(d) Protection of strain gauge

Figure 3.13: Process of strain gauges

CHAPTER 4-Experimental Results

4.1 General

The experimental results from the static and dynamic tests are presented in this chapter. This includes the static stiffness and strength properties of the OSB and plywood coupons, individual studs, and the full scale wall tests. A brief description of the specimens' failure modes is also included. For the dynamic tests, a detailed description of the response and failure characteristics is provided along with the shock wave properties. Greater details on the results from each test can be found in Appendix A and B.

4.2 Static tests results

4.2.1 Coupon test results

The average MOE and MOR values for the OSB and plywood coupons are presented in Table 4.1 along with the standard deviation and coefficient of variation (COV). The OSB coupons had an average MOE of 5,550MPa with a COV of 0.24. Figure 4.1 illustrates the results from the forty coupon tests, including the average experimental MOE and the average published E_{50} value of 6,580 MPa, as reported in the wood design manual (CSA O86-09, 2009). The average MOR for the forty OSB coupons was determined to be 28.4 MPa with a COV of 0.31. The results can be seen in Figure 4.2.

The average MOE and MOR values for the forty plywood coupons were 7,120 MPa and 41.0 MPa with a COV of 0.16 and 0.28, respectively. The experimental MOE and MOR values for the plywood coupons can be seen in Figure 4.3 and 4.4, respectively. A typical force-displacement history is shown for a plywood coupon in Figure 4.5.

The densities of the OSB and plywood were determined to be 685.0 kg/m^3 and 470.9 kg/m^3, respectively. The percentage difference between the measured densities and those published (713.6 kg/m^3 for OSB and 509.7 kg/m^3 for plywood) was calculated to be 4 % and 8 %, respectively.

4.2.2 Load-slip test results

Nail-slip tests were conducted on joints consisting of 11 mm OSB sheathing using 64 mm nails and 18.5 mm plywood sheathing using 89 mm nails. The initial stiffness was calculated as the slope from 0 to 40 percent of the peak load of the nail-slip relationship as shown in Figure 4.6. The average initial stiffness of the joints with OSB was found to be 1,770 N/mm with a COV of 0.28 while the average initial stiffness of the joints with plywood was 2,430 N/mm with a COV of 0.12.

4.2.3 Individual stud test results

Individual studs were tested to failure under four-point loading and with simply supported end conditions. The observed predominant failure mode for all stud components was flexural failure. The average MOE of the studs tested was 9,690 MPa and the average MOR was 44.5 MPa with COVs of 0.11 and 0.23, respectively (Table 4.1). The experimental data for the MOE and MOR for the forty studs are plotted in Figures 4.7 and 4.8. Also shown in Figure 4.7 is the published average MOE value (CSA O86-09, 2009) In Figure 4.8, the "in-grade" test value for MSR-1,450f_b is also shown (Barrett & Lau, 1994). Figure 4.9 shows typical force-displacement histories for individual stud tests. Based on the MOE of the studs tested non-destructively, the studs were allocated randomly to different walls such that the average MOE of each wall is similar to each other as shown in Table 4.2.

Tables 4.3 and 4.4 present the stud capacities and stiffnesses for individual studs and as well as part of the sheathed walls for OSB and plywood walls, respectively. An increase factor is calculated for each wall which accounts for the strength increase due to the system effects. The average moisture content of the studs was measured to 15% while the density was found to be 498.0 kg/m^3 with a COV of 0.09.

4.2.4 Wall static test results

A detailed description of the static test results for the walls is shown in Tables 4.3 through 4.6. Tables 4.3 and 4.4 present the stiffness of each stud within a sheathed system for OSB and plywood walls, respectively. As can be seen in Tables 4.3 and 4.4, there is an average increase in ultimate capacity of 1.20 for a stud within a wall system compared to the studs' individual capacity. This factor is consistent with the system effect factor for MSR in the

wood design manual (CSA O86-09, 2009) and accounts for the variability in stiffness and strength between the individual studs. It is not anticipated that any given test would yield such results. The load sharing is dependent on several variables including the thickness of the sheathing panel, the composite action between the sheathing and the studs (i.e. nail diameter and spacing) and the variability in stiffness and strength between the individual studs.

Table 4.5 summarises the applied load and associated deflection at the elastic limit, P_{Xe} and X_e, as well as the applied load and associated deflection at failure, P_{max} and X_{max}, for the four middle studs within each wall. As expected, the deflection values of the four middle studs are similar. The small variability observed in the values could possibility be attributed to a slight bending in the load transfer device as more deflection was observed in the center studs. Other potential source of errors could potentially stem from the workmanship where the wall could be slightly out of square. Table 4.6 presents the average applied load and average deflection, $(P_{Xe})_{Avg}$ and $(X_e)_{Avg}$ at the elastic limit, as well as the average applied load $(P_{max})_{Avg}$, and average deflection, $(X_{max})_{Avg}$, at failure. Figures 4.10 and 4.11 show a representative load-displacement curve for walls under static loading and observed typical failure modes, respectively.

4.3 Dynamic test results

The tests results for all ten walls tested dynamically are summarized in Table 4.7, including information on the driver length, L_D, driver pressure, P_D, reflected pressure, P_R, reflected impulse, I_R, experimental positive phase, $t_{d\text{-}exp}$, maximum average displacement, $d_{max\text{-}avg}$, average time to maximum displacement, $t_{max\text{-}avg}$, average strain rate of the four middle studs, $\dot{\epsilon}_{avg}$, and the quantified damage levels. Complete details for each test are presented in Appendix B. Also provided in Appendix B are the loading and response characteristics as a function of time and the response description. In shots where damage was observed, additional figures are presented showing the progression of deflection up to failure and post-failure photos to help quantify the damage level. The figure numbering format in Appendix B describes the wall identification number and the shot number. For example, in the case of the second test conducted on Wall 6, the fourth figure would in this text be referred to as Figure B6-2.4. The table number also refer to the shot number; for example, the table

containing the test result summary for the second pressure-impulse combination on Wall 6 would be referred to as: Table B6-2.

A representative graph showing the reflected pressure and impulse versus time is shown in Figure 4.12. Figure 4.13 is a typical response history where one stud fails (Stud 2) for the four middle studs along with the time varying forcing function. The major and secondary vertical axes represent the displacement of the four middle studs and the reflected pressure, respectively, while the horizontal axis represents time. A typical strain-time history is shown in Figure 4.14 and is compared to the displacement-time history. The following presents a brief description of the testing and observed damage for walls 6 through 10 and 16 through 20.

4.3.1 Wall 6

Wall 6 was subjected to two different pressure and impulse combinations using a driver length of 2,745 mm. For the first shot, a driver pressure of 63.4 kPa was used. Due to an error of instrumentation there were no reflected pressures, displacements or strains available for this test. An inspection of the wall showed that all studs remained in the elastic region, with no apparent visual damage. This was also corroborated by reviewing the recorded video.

For the second shot, a driver pressure of 260.0 kPa was achieved, resulting in a reflected pressure of 38.3 kPa and a reflected impulse of 403.0 kPa-ms over a positive phase of 22.0 ms. An average experimental displacement of 47 mm, which occurred at an average time of 8.9 ms following the recording of the initial reflected shock wave, was recorded. A total of three studs failed and one other stud cracked. The wall was therefore evaluated to have suffered heavy damage. From analyzing the video of this shot, it was noted that the studs failed at the first positive peak. Sheathing failure, between studs 3 and 4 as well as 5 and 6, was also observed in this shot. No sheathing debris was projected in the room but significant separation between the sheathing and the studs was observed.

4.3.2 Wall 7

Wall 7 was subjected to a single pressure and impulse combination using a driver length of 2,745 mm. A driver pressure of 248.2 kPa was used, which resulted in a reflected pressure of

38.2 kPa and a reflected impulse of 384.9 kPa-ms over a positive phase of 22.0 ms. An average experimental displacement of 59 mm, which occurred at an average time of 9.4 ms following the initial reflected shock wave, was recorded.

A total of four studs failed while no damage was observed on the two other studs. The four studs failed at mid-span during the first positive peak. Sheathing debris was projected in the lab. Furthermore, the sheathing was cracked at mid-span between studs 4 and 6 where the permanent deflection was observed as a result of the studs' failure. Separation between the sheathing and the studs was observed. The wall was quantified to have moderate to heavy damage.

4.3.3 Wall 8

Wall 8 was subjected to two different pressure and impulse combinations using a driver length of 305 mm. For the first shot, a driver pressure of 84.1 kPa was used, which resulted in a reflected pressure of 9.8 kPa and a reflected impulse of 25.1 kPa-ms over a positive phase of 4.4 ms. An average experimental displacement of 8 mm, which occurred at an average time of 6.2 ms following the initial reflected shock wave, was recorded. An inspection of the wall post shot showed that all studs remained in the elastic region, with no apparent visual damage. This was also corroborated by reviewing the recorded video.

For the second shot, a driver pressure of 568.8 kPa was achieved, resulting in a reflected pressure of 52.6 kPa and a reflected impulse of 163.0 kPa-ms over a positive phase of 8.0 ms. An average experimental displacement of 45 mm, at an average time of 7.8 ms following the initial reflected shock wave, was measured. The reflected pressure history left all but one stud with no damage. One stud failed and another was heavily cracked while the others had minor cracks. From analyzing the video from this shot, it was noted that the damage inflicted on the studs was amplified during the successive peaks. The wall was evaluated to have suffered moderate damage. Due to the high pressure that was experienced in the negative phase of the blast history, a portion of the sheathing between Studs 5 and 6 was sucked in the shock tube. Nail withdrawal was observed.

4.3.4 Wall 9

Wall 9 was subjected to three different pressure and impulse combinations using a driver length of 2,745 mm. For the first shot, a driver pressure of 40.7 kPa was achieved, resulting in a reflected pressure of 6.6 kPa and a reflected impulse of 76.1 kPa-ms over a positive phase of 23.5 ms. An average displacement of 8 mm was measured at an average time of 10.6 ms following the initial reflected shock wave. An inspection of the wall post shot showed that all studs remained in the elastic region, with no apparent visual damage. This was also corroborated by reviewing the recorded video.

For the second shot, a driver pressure of 138.6 kPa was achieved, resulting in a reflected pressure of 28.9 kPa and a reflected impulse of 282.3 kPa-ms over a positive phase of 21.5 ms. An average experimental displacement of 39 mm was measured at an average time of 11.7 ms following the initial reflected shock wave. The wall remained elastic throughout its displacement time history with the exception of Stud 4 which was cracked on the tension side but no residual displacement was observed. Neither sheathing, nor nail withdrawal failure was observed. The wall was therefore quantified to have superficial damage.

For the third shot, a driver pressure of 241.3 kPa was achieved, resulting in a reflected pressure of 41.9 kPa and a reflected impulse of 386.5 kPa-ms over a positive phase of 21.5 ms. An average experimental displacement of 60 mm was measured at an average time of 11.7 ms following the initial reflected shock wave. The failure of the Studs 4 and 5 is a result of the exasperation on the rebound displacements of the initial cracking that occurred during the first positive peak. Stud 2 was slightly cracked on the tension side while Studs 3 was slightly cracked at mid-span. A failure of the sheathing was observed between Studs 3 and 4 as well as Studs 5 and 6 but no debris was projected. Some nail withdrawal was also observed for this test. The wall was quantified with moderate damage.

4.3.5 Wall 10

Wall 10 was subjected to two different pressure and impulse combinations using a driver length of 4,880 mm. For the first shot, a driver pressure of 71.7 kPa was used, resulting in a reflected pressure of 11.6 kPa and a reflected impulse of 207.0 kPa-ms over a positive phase

of 35.0 ms. An average experimental displacement of 9 mm was measured at an average time of 9.0 ms following the initial reflected shock wave. Due to an instrumentation error, only displacement data was available for Stud 4 as shown in Table B10-1. An inspection of the wall post shot showed that all studs remained in the elastic region, with no apparent visual damage. This was also corroborated by reviewing the recorded video. The wall was quantified with superficial damage.

For the second shot, a driver pressure of 208.2 kPa was used, resulting in a reflected pressure of 31.3 kPa and a reflected impulse of 495.1 kPa-ms over a positive phase of 44.0 ms. An average experimental displacement of 48 mm was measured at an average time of 12.0 ms following the initial reflected shock wave. The wall was quantified with moderate damage as three studs experienced cracking. Moreover, one stud had a more pronounced crack initiating at mid-span on the tension side towards the top plate while the remaining two damaged studs had minor cracks. The remaining three studs experienced no damage. The sheathing was cracked in the upper portion of the wall between Studs 1 and 2 while no nail withdrawal was observed.

4.3.6 Wall 16

Wall 16 was subjected to three different pressure and impulse combination using a driver length of 2,745 mm. For the first shot, a driver pressure of 68.9 kPa was used, resulting in a reflected pressure of 11.5 kPa and a reflected impulse of 128.1 kPa-ms over a positive phase of 19.5 ms. An average experimental displacement of 11 mm was measured at an average time of 9.8 ms following the initial reflected shock wave. An inspection of the wall post shot showed that all studs remained in the elastic region, with no apparent visual damage. This was also corroborated by reviewing the recorded video. The wall was quantified with superficial damage.

For the second shot, a driver pressure of 216.5 kPa was achieved resulting in a reflected pressure of 32.6 kPa and a reflected impulse of 331.5 kPa-ms over a positive phase of 21.8 ms. An average experimental displacement of 37 mm was measured at an average time of 9.9 ms following the initial reflected shock wave. The wall remained elastic throughout its displacement time history with the exception of Stud 2 which failed during the first positive

peak and Stud 3 where cracks were initiated. Neither sheathing, nor nail withdrawal failure was observed. The wall was therefore quantified to have moderate damage.

For the third shot, a driver pressure of 247.5 kPa was achieved resulting in a reflected pressure of 34.1 kPa and a reflected impulse of 377.6 kPa-ms over a positive phase of 22.0 ms. An average experimental displacement of 45 mm was measured at an average time of 11.4 ms following the initial reflected shock wave. Studs number 1 to 3 failed during the first positive peak and the damage was exasperated during the successive peaks and no damage was observed for studs number 4 to 6. Neither sheathing failure, nor nail withdrawal was observed. The wall was quantified to have heavy damage.

4.3.7 Wall 17

Wall 17 was subjected to two different pressure and impulse combinations using a driver length of 4,880 mm. For the first shot, a driver pressure of 70.3 kPa was achieved, resulting in a reflected pressure of 12.6 kPa and a reflected impulse of 245.7 kPa-ms over a positive phase of 38.5 ms. An average experimental displacement of 13 mm was measured at an average time of 9.9 ms following the initial reflected shock wave. An inspection of the wall post shot showed that all studs remained in the elastic region, with no apparent visual damage. This was also corroborated by reviewing the recorded video. The wall was quantified with superficial damage.

For the second shot, a driver pressure of 266.1 kPa was achieved resulting in a reflected pressure of 40.1 kPa and a reflected impulse of 813.2 kPa-ms over a positive phase of 56.0 ms. An average experimental displacement of 51 mm was measured at an average time of 9.9 ms following the initial reflected shock wave. Studs number 1 to 3 failed during the first positive peak and the damage was exasperated during the successive peaks and minor cracking was observed on Stud 5. Neither sheathing failure, nor nail withdrawal was observed. The wall was quantified to have moderate damage.

4.3.8 Wall 18

Wall 18 was subjected to two different pressure and impulse combinations using a driver length of 305 mm. For the first shot, a driver pressure of 82.7 kPa was achieved, resulting in

a reflected pressure of 9.5 kPa and a reflected impulse of 27.3 kPa-ms over a positive phase of 5.8 ms. An average experimental displacement of 5 mm was measured at an average time of 5.6 ms following the initial reflected shock wave. Due to an instrumentation error, only displacement data was available for Stud 2 as shown in Table B18-1. An inspection of the wall post shot showed that all studs remained in the elastic region, with no apparent visual damage. This was also corroborated by reviewing the recorded video. The wall was quantified with superficial damage.

For the second shot, a driver pressure of 613.6 kPa was achieved resulting in a reflected pressure of 55.0 kPa and a reflected impulse of 172.6 kPa-ms over a positive phase of 8.0 ms. An average experimental displacement of 45 mm was measured at an average time of 8.7 ms following the initial reflected shock wave. Due to an instrumentation error, only displacement data was available for Studs 2 and 4. The wall was quantified with moderate damage as three studs failed leaving all of the studs with some extent of damage with the exception of two studs where no damage was observed. Moreover, one stud had minor cracking. Due to the high pressure experienced during the negative phase of the pressure history, the change from compression to tension observed in the oscillations of positive to negative peaks led to failure of Studs 3, 4 and 5. Neither sheathing failure nor nail withdrawal was observed.

4.3.9 Wall 19

Wall 19 was subjected to two different pressure and impulse combinations using a driver length of 2,745 mm. For the first shot, a driver pressure of 64.8 kPa was achieved resulting in a reflected pressure of 11.0 kPa and a reflected impulse of 122.2 kPa-ms over a positive phase of 19.0 ms. An average experimental displacement of 11 mm was measured at an average time of 9.8 ms following the initial reflected shock wave. An inspection of the wall post shot showed that all studs remained in the elastic region, with no apparent visual damage. This was also corroborated by reviewing the recorded video. The wall was quantified with superficial damage.

For the second shot, a driver pressure of 264.0 kPa was achieved, resulting in a reflected pressure of 42.1 kPa and a reflected impulse of 450.4 kPa-ms over a positive phase of 24.0

ms. An average experimental displacement of 56 mm was measured at an average time of 10.3 ms following the initial reflected shock wave. The wall was quantified with moderate damage as two studs failed leaving all of the studs with some extent of damage with the exception of one stud where no damage was observed. Moreover, Stud 1 had a considerable crack on the tension side while minor cracks were observed in Studs 4 and 5. The damage observed for Studs 2 and 3 was exasperated in the successive peaks while the initial failure occurred during the first positive peak. Neither sheathing failure nor nail withdrawal was observed.

4.3.10 Wall 20

Wall 20 was subjected to three different pressure and impulse combinations using a driver length of 2,745 mm. For the first shot, a driver pressure of 76.5 kPa was achieved, resulting in a reflected pressure of 12.5 kPa and a reflected impulse of 160.3 kPa-ms over a positive phase of 22.0 ms. An average experimental displacement of 16 mm was measured at an average time of 12.1 ms following the initial reflected shock wave. An inspection of the wall post shot showed that all studs remained in the elastic region, with no apparent visual damage. This was also corroborated by reviewing the recorded video. The wall was quantified with superficial damage.

For the second shot, a driver pressure of 200.6 kPa was achieved resulting in a reflected pressure of 31.0 kPa and a reflected impulse of 302.0 kPa-ms over a positive phase of 23.0 ms. An average experimental displacement of 41 mm was measured at an average time of 11.7 ms following the initial reflected shock wave. The wall was quantified with superficial damage as apart from Stud 5 the wall remained elastic throughout its displacement history. Stud 5 was split lengthwise with an additional crack above mid-span initiating towards the top plate but no permanent deflection was observed. Neither sheathing failure nor nail withdrawal was observed.

For the third shot, a driver pressure of 269.6 kPa was achieved resulting in a reflected pressure of 38.7 kPa and a reflected impulse of 427.9 kPa-ms over a positive phase of 23.0 ms. An average experimental displacement of 61 mm was measured at an average time of 11.9 ms following the initial reflected shock wave. The wall was quantified to have heavy

damage. Studs 3, 4 and 5 failed during the first positive peak to maximum displacement. The sheathing failed between Studs 4 and 5 as well as 5 and 6 which were sheathed with the half of the full size plywood sheet compared to studs number 1 to 4 which were covered by a full sheet. Nail withdrawal along Stud 4 was observed on both panel edges.

Table 4.1: Summary of OSB, plywood and stud properties

	OSB		Plywood		Stud	
	Modulus of elasticity, MOE_{OSB}	Modulus of rupture, MOR_{OSB}	Modulus of elasticity, MOE_{Ply}	Modulus of rupture, MOR_{Ply}	Modulus of elasticity, MOE_{Stud}	Modulus of rupture, MOR_{Stud}
Average (MPa)	5,550	28.4	7,120	41.0	9,690	44.5
Standard deviation (MPa)	1,340	8.8	1,140	11.3	1,110	10.3
Coefficient of variation	0.24	0.31	0.16	0.28	0.11	0.23

Table 4.2: Summary of wall studs' MOE

Wall name	Modulus of elasticity, MOE (MPa)						Average of wall
	Stud 1	Stud 2	Stud 3	Stud 4	Stud 5	Stud 6	
W1	9,560	9,330	9,380	9,050	9,770	9,260	9,400
W2	9,070	10,400	10,900	10,200	9,310	8,720	9,770
W3	8,660	9,480	10,400	11,100	9,640	9,110	9,730
W4	8,830	9,400	10,800	11,000	10,000	9,050	9,860
W5	8,240	9,570	10,500	11,600	9,750	8,910	9,750
W6	9,270	9,810	11,300	10,500	9,360	8,810	9,840
W7	8,880	9,970	11,900	8,960	9,310	8,270	9,540
W8	9,240	9,900	11,200	10,700	9,600	8,730	9,900
W9	9,150	9,860	11,400	10,200	9,510	7,880	9,660
W10	9,290	10,000	11,100	10,200	9,590	8,780	9,830
W11	8,960	9,860	11,500	10,200	9,390	8,700	9,760
W12	9,160	9,850	12,500	10,100	9,330	8,850	9,950
W13	8,350	9,590	10,400	11,300	9,780	9,070	9,740
W14	8,670	9,490	10,600	11,100	9,850	9,280	9,830
W15	8,570	9,570	10,500	11,600	9,750	8,910	9,810
W16	9,170	9,910	11,700	10,300	9,430	7,630	9,690
W17	10,400	9,830	12,000	10,400	9,610	8,270	10,100
W18	9,190	9,900	11,600	10,300	9,380	8,810	9,860
W19	9,160	9,710	11,300	10,400	9,600	8,590	9,790
W20	9,250	9,760	11,000	10,700	9,400	8,560	9,780
Average	9,050	9,760	11,100	10,500	9,570	8,710	

Table 4.3: Summary of static tests for OSB walls and corresponding studs

Static test number	Wall name	Stud number	Stud name	Studs within a sheathed system				Individual studs			Capacity increase factor	Stiffness increase factor
				Stiffness (kN/m)	Total applied load kN	Average stiffness (kN/m)	Average resistance per stud (kN)	MOE (MPa)	Stiffness (kN/m)	Average resistance per stud (kN)		
1	W1	1	60A	-	139.3	666	23.2	9,560	560	16.6	1.40	1.15
		2	71A	598				9,330	545			
		3	109A	562				9,380	548			
		4	90A	617				9,050	528			
		5	125A	656				9,770	570			
		6	16A	899				9,260	541			
2	W2	1	99A	707	116.4	639	19.4	9,070	530	16.6	1.17	1.13
		2	49A	611				10,400	607			
		3	40A	561				10,900	634			
		4	45A	581				10,200	598			
		5	67A	614				9,310	543			
		6	82A	759				8,720	509			
3	W3	1	50A	670	127.1	643	21.2	8,660	505	16.6	1.27	1.13
		2	65A	593				9,480	553			
		3	9A	545				10,400	606			
		4	100A	560				11,100	649			
		5	111A	638				9,640	563			
		6	53A	850				9,110	532			
4	W4	1	20A	690	114.8	646	19.1	8,830	515	16.6	1.15	1.12
		2	102A	561				9,400	548			
		3	97A	529				10,800	632			
		4	27A	596				11,000	643			
		5	26A	631				10,000	586			
		6	96A	868				9,050	528			
5	W5	1	118A	674	107.9	619	18.0	8,240	481	16.6	1.08	1.09
		2	105A	560				9,570	558			
		3	91A	522				10,500	612			
		4	88A	558				11,600	675			
		5	35A	615				9,750	569			
		6	57A	786				8,910	520			

Table 4.4: Summary of static tests results for plywood walls and corresponding studs

Static test number	Wall name	Stud number	Stud name	Studs within a sheathed system				Individual studs			Capacity increase factor	Stiffness factor
				Stiffness	Total applied load	Average stiffness	Average resistance per stud	MOE	Stiffness	Average resistance per stud		
				kN/m	kN	kN/m	kN	MPa	kN/m	kN		
6	W11	1	128A	735	103.0	672	17.2	8,960	523	16.6	1.03	1.18
		2	51A	621				9,860	576			
		3	24A	606				11,500	671			
		4	84A	594				10,200	592			
		5	73A	637				9,390	548			
		6	59A	837				8,700	508			
7	W12	1	41A	772	124.6	683	20.8	9,160	534	16.6	1.25	1.18
		2	93A	643				9,850	575			
		3	79A	589				12,500	728			
		4	38A	615				10,100	587			
		5	119A	650				9,330	544			
		6	117A	830				8,850	516			
8	W13	1	124A	755	123.1	664	20.5	8,350	487	16.6	1.23	1.17
		2	37A	610				9,590	560			
		3	11A	567				10,400	604			
		4	101A	594				11,300	660			
		5	74A	614				9,780	571			
		6	69A	840				9,070	529			
9	W14	1	30A	840	130.3	683	21.7	8,670	506	16.6	1.30	1.19
		2	116A	611				9,490	554			
		3	31A	589				10,600	618			
		4	104A	580				11,100	649			
		5	39A	631				9,850	575			
		6	36A	848				9,280	542			
10	W15	1	78A	758	99.4	682	16.6	8,570	500	16.6	1.00	1.18
		2	105A	560				9,570	558			
		3	91A	521				10,500	612			
		4	88A	558				11,600	675			
		5	35A	615				9,750	569			
		6	57A	786				8,910	520			

Table 4.5: Load and deflection values at elastic limit and failure of studs within a sheathed system

Test name	Stud 2				Stud 3				Stud 4				Stud 5			
	P_{X_e} kN	X_e mm	P_{max} kN	X_{max} mm	P_{X_e} kN	X_e mm	P_{max} kN	X_{max} mm	P_{X_e} kN	X_e mm	P_{max} kN	X_{max} mm	P_{X_e} kN	X_e mm	P_{max} kN	X_{max} mm
W1	13.4	23	23.2	55	13.5	25	23.2	58	13.5	24	23.2	88	13.4	22	23.2	49
W2	18.7	33	19.4	62	18.6	35	19.4	98	18.6	35	19.4	57	18.6	33	19.4	50
W3	15.4	26	21.2	51	15.8	30	21.2	54	15.1	27.	21.2	68	16.0	26	21.2	47
W4	15.1	28	19.1	65	15.1	30	19.1	65	15.0	26	19.1	48	15.1	26	19.3	68
W5	15.0	30	18.0	36	15.1	30	18.0	37	15.4	28	18.0	34	15.4	26	18.0	31
W11	15.8	25	17.2	29	15.8	26	17.2	30	15.8	27	17.2	31	15.7	26	17.2	29
W12	18.5	31	20.8	68	18.3	33	20.8	80	18.3	31	20.7	50	18.4	29	20.7	39
W13	14.5	25	20.4	63	14.4	27	20.7	56	14.4	26	20.3	46	13.3	24	20.7	39
W14	14.6	24	21.7	58	14.7	26	21.6	43	14.7	27	21.7	45	14.6	24	21.8	41
W15	15.9	26	16.6	27	16.6	31	16.6	61	16.6	29	16.6	29	16.6	26	16.6	26

*P_{Xe}=Applied load at elastic limit *X_e=Elastic limit

*P_{max}=Applied load at failure *X_{max}=Deflection at failure

Table 4.6: Summary of wall properties under static loading

	OSB walls	Plywood walls
Average applied load at elastic limit, $(P_{X_e})_{Avg}$ (kN)	15.6	15.9
Average elastic deflection limit, $(X_e)_{Avg}$ (mm)	28	27
Average applied load at failure, $(P_{max})_{Avg}$ (kN)	20.2	19.3
Average deflection at failure, $(X_{max})_{Avg}$ (mm)	56	44

Table 4.7: Summary of dynamic tests results

Test name	m_w kg	L_D mm	P_D kPa	P_R kPa	I_R kPa-ms	$t_{d\text{-}exp}$ ms	$d_{max\text{-}avg}$ mm	$t_{max\text{-}avg}$ ms	$\dot{\varepsilon}_{avg}$ s^{-1}	Quantified wall damage
W6- 1	76.0	2,745	63.4	No data						Superficial
2		2,745	260.0	38.3	403.0	22.0	47	8.9	5.24E-1	Heavy
W7- 1	74.2	2,745	248.2	38.2	384.9	22.0	59	9.4	5.48E-1	Heavy
W8- 1	71.7	305	84.1	9.8	25.1	4.4	8	6.2	1.54E-1	Superficial
2		305	568.8	52.6	163.0	8.0	46	7.9	5.31E-1	Moderate
W9- 1	77.5	2,745	40.7	6.6	76.1	23.5	8	23.1	No data	Superficial
2		2,745	138.6	28.9	282.3	21.5	39	19.6	2.54E-1	Superficial
3		2,745	241.3	41.9	386.5	21.5	60	11.7	4.66E-1	Moderate
W10- 1	73.5	4,880	71.7	11.6	207.0	35.0	9	9.0	1.23E-1	Superficial
2		4,880	208.2	31.3	495.1	44.0	48	12.0	3.12E-1	Moderate
W16- 1	85.3	2,745	68.9	11.5	128.1	19.5	11	9.8	1.20E-1	Superficial
2		2,745	216.5	32.6	331.5	21.8	37	9.9	3.02E-1	Moderate
3		2,745	247.5	34.1	377.6	22.0	45	11.4	3.06E-1	Heavy
W17- 1	84.0	4,880	70.3	12.6	245.7	38.5	13	9.9	1.45E-1	Superficial
2		4,880	266.1	40.1	813.2	56.0	51	9.9	3.57E-1	Moderate
W18- 1	83.8	305	82.7	9.5	27.3	5.8	5	5.6	1.04E-1	Superficial
2		305	613.6	55.0	172.6	8.0	45	8.7	5.40E-1	Moderate
W19- 1	83.1	2,745	64.8	11.0	122.2	19.0	11	9.8	1.24E-1	Superficial
2		2,745	264.0	42.1	450.4	24.0	56	10.3	4.64E-1	Moderate
W20- 1	85.2	2,745	76.5	12.5	160.3	22.0	16	12.1	1.46E-1	Superficial
2		2,745	200.6	31.0	302.0	23.0	41	11.7	3.82E-1	Superficial
3		2,745	269.6	38.7	427.9	23.0	61	11.9	5.34E-1	Heavy

*m_w=Measured wall mass *L_D=Driver length *P_R=Reflected pressure *I_R=Reflected pressure

*$t_{d\text{-}exp}$=Experimental positive phase duration * $d_{max\text{-}avg}$=Maximum average displacement

*$t_{max\text{-}avg}$=Average time to maximum displacement * $\dot{\varepsilon}_{avg}$=Average strain rate of four middle studs

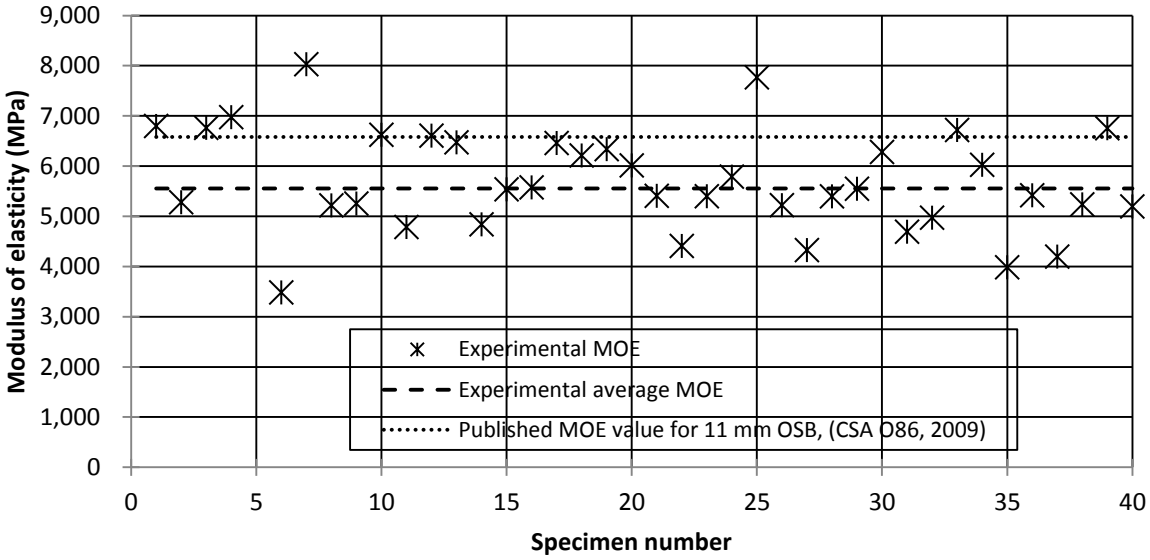

Figure 4.1: Experimental MOE for OSB coupons

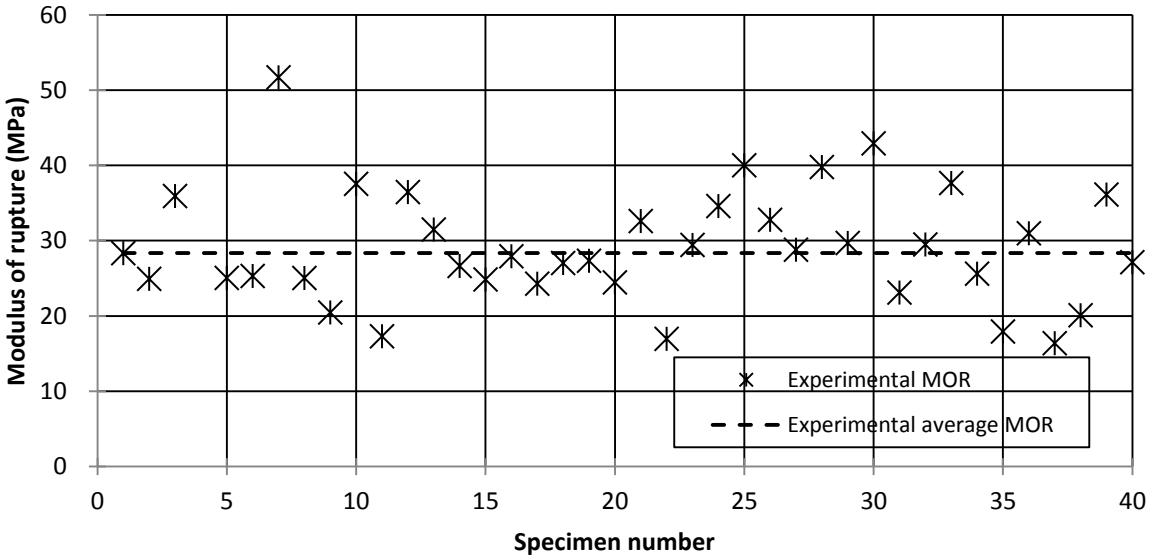

Figure 4.2: Experimental MOR for OSB coupons

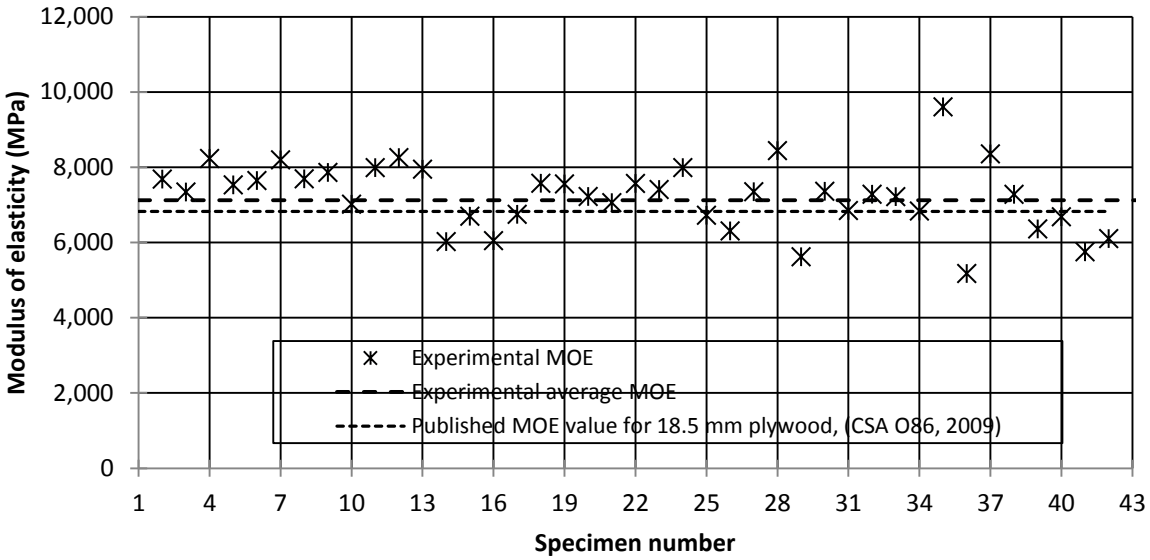

Figure 4.3: Experimental MOE for plywood coupons

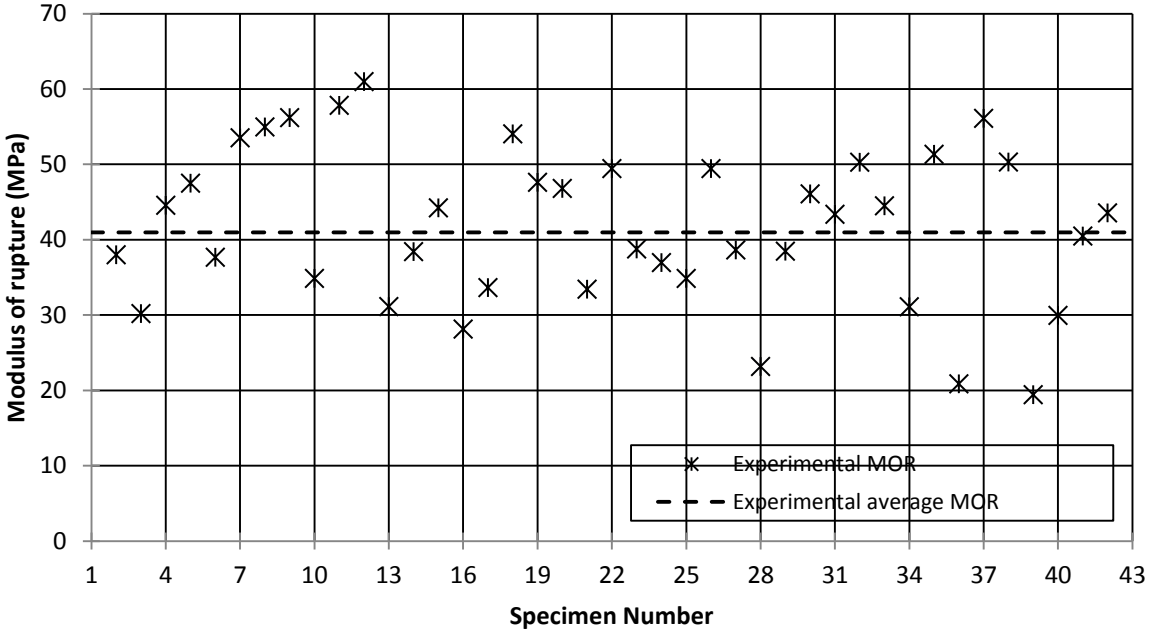

Figure 4.4: Experimental MOR for plywood coupons

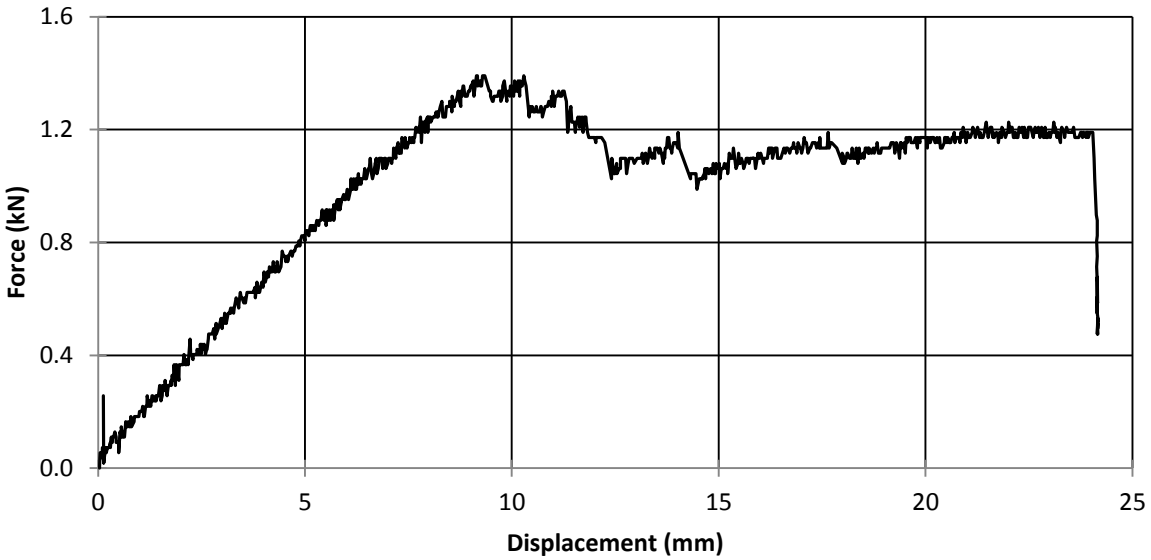

Figure 4.5: Typical force-displacement history for plywood coupon tests

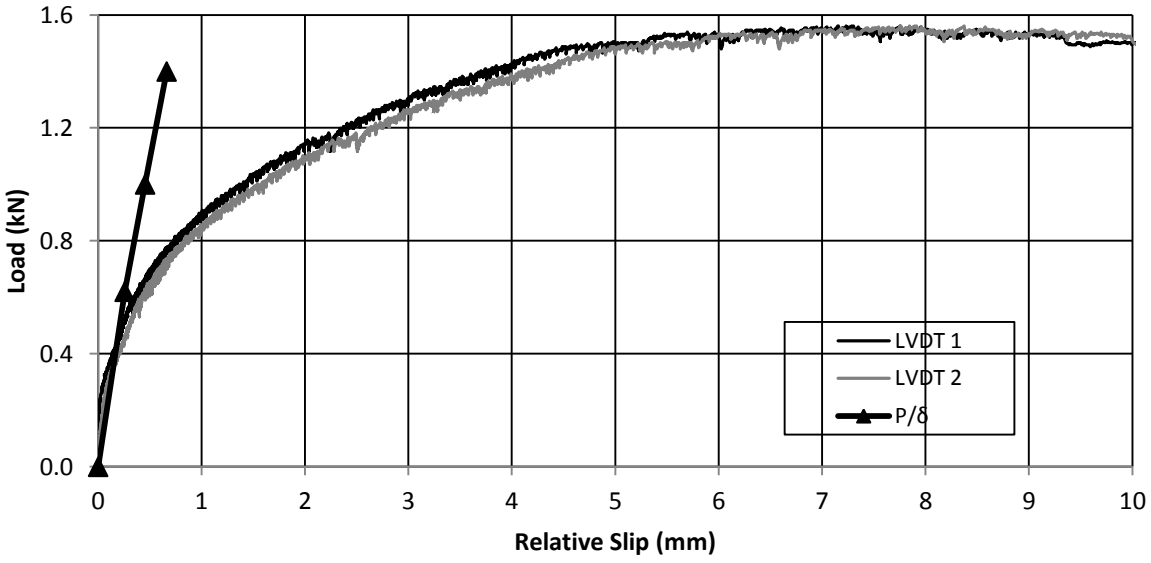

Figure 4.6: Typical load-slip for plywood specimen

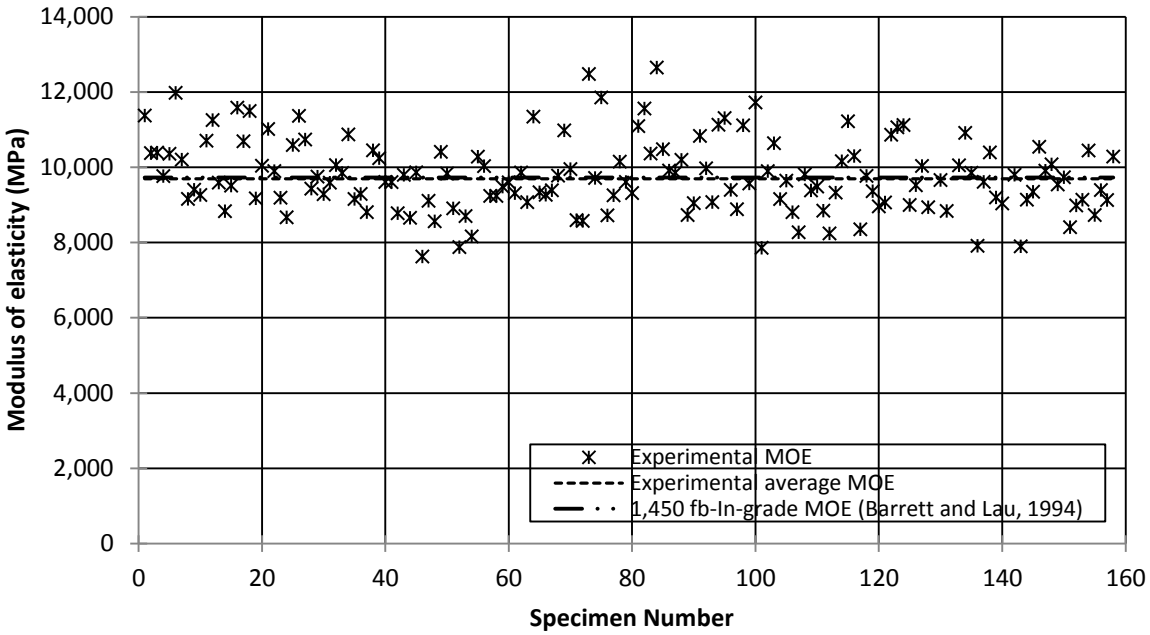

Figure 4.7: Experimental MOE of studs

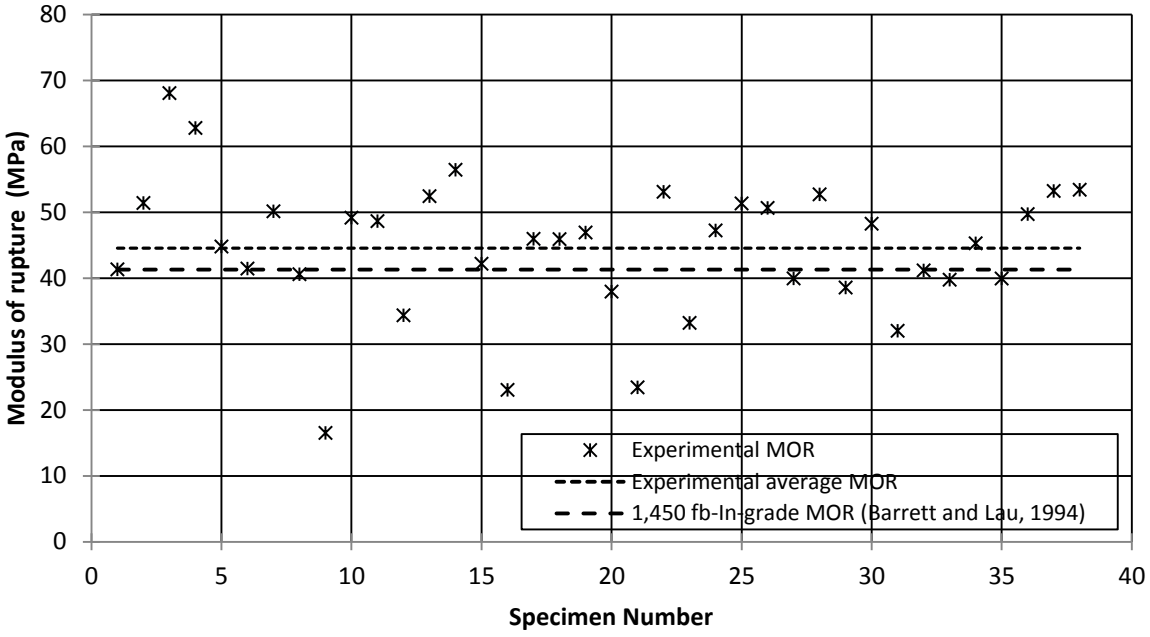

Figure 4.8: Experimental MOR of studs

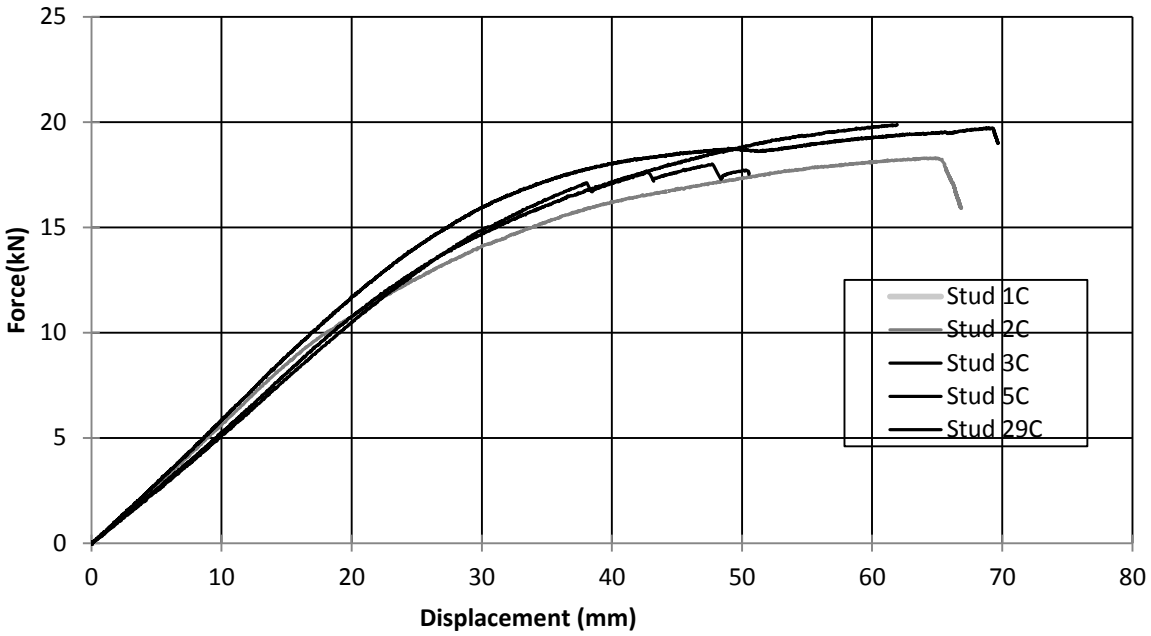

Figure 4.9: Typical force-displacement histories for individual stud tests

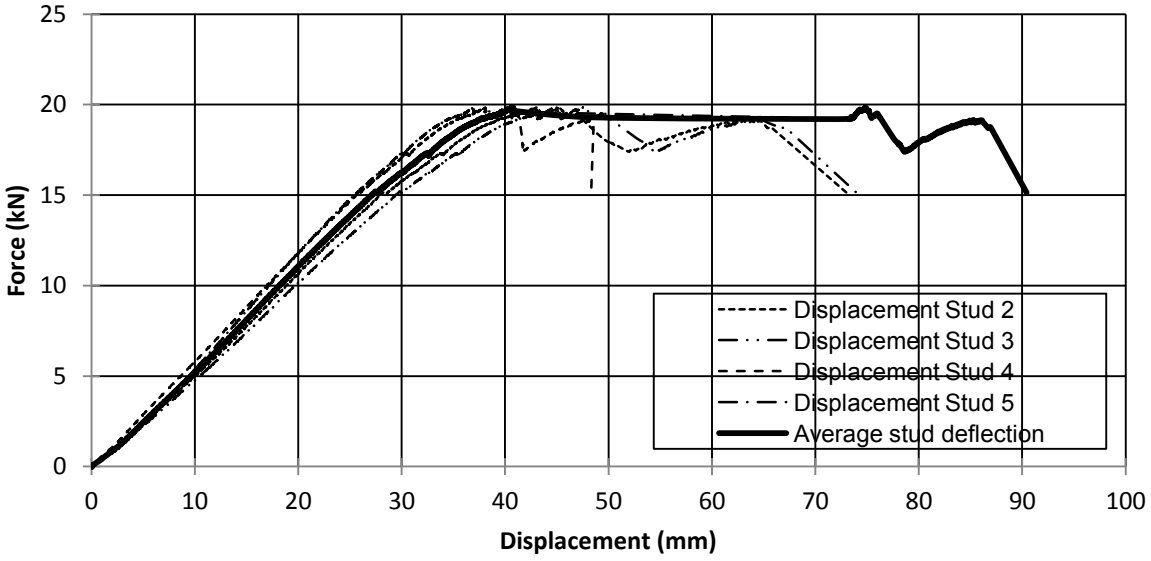

Figure 4.10: Typical force-displacement graph for walls under static loading

(a) View from right side

(b) View from left side

Figure 4.11: Typical damage for walls under static loading

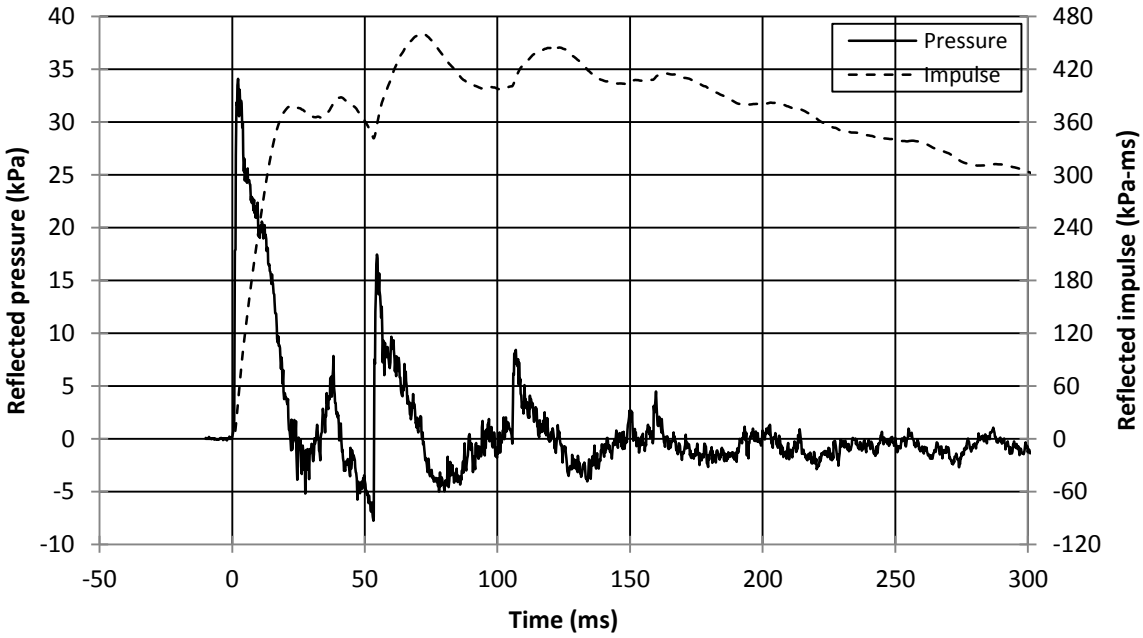

Figure 4.12: Typical dynamic time varying loading function

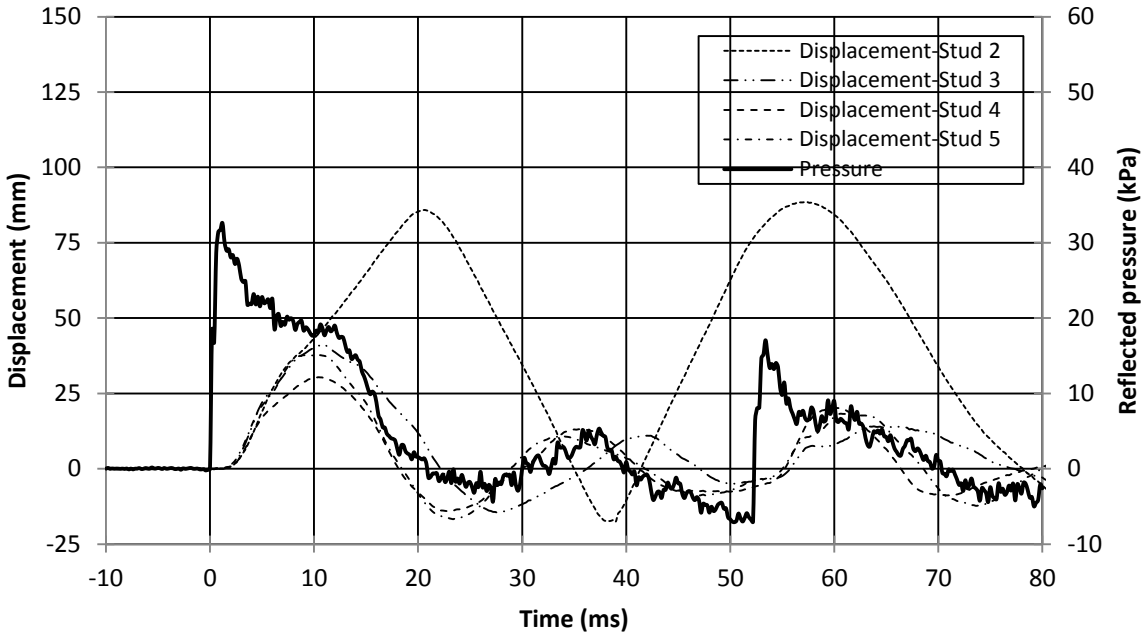

Figure 4.13: Displacement and pressure time histories for Wall 16 Shot 2

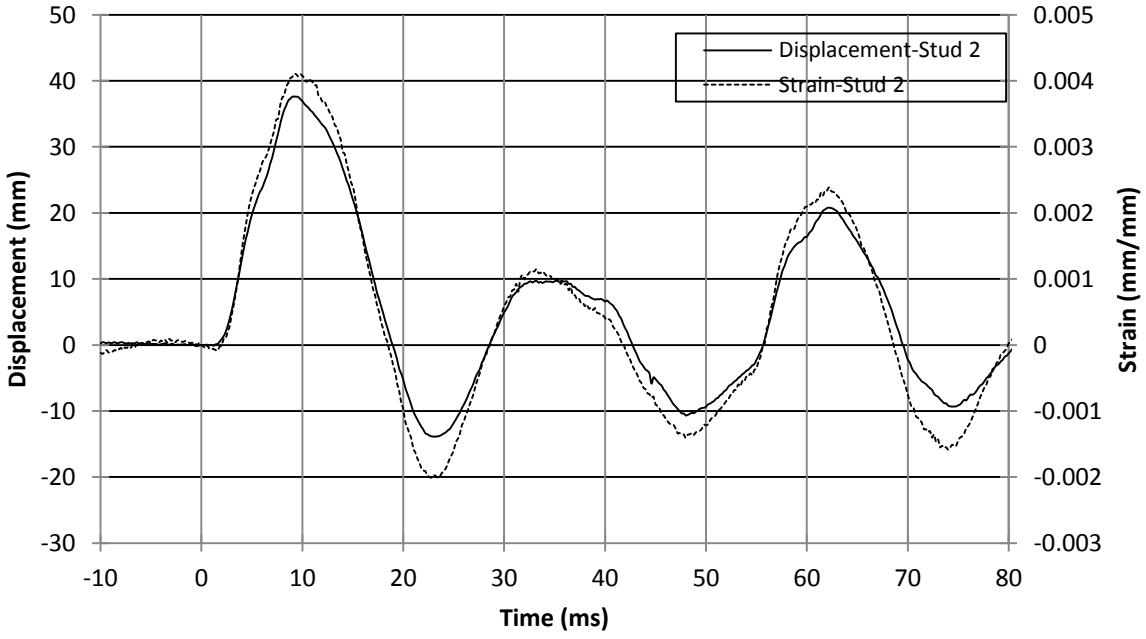

Figure 4.14: Displacement and strain time histories for Wall 20 Shot 2

CHAPTER 5-Analytical Modelling and Results

5.1 General

This chapter describes the analytical methodology used to determine the DIFs as well as the two constitutive models used along with their respective inputs. Since it was not feasible to measure the dynamic reactions directly, an iterative procedure was employed to determine the DIFs.

A constitutive model considering the partial composite action between the sheathing and the stud is presented. The ultimate goal of the model is to predict a static resistance curve for the entire wall by adapting a mechanics based approach that was developed for floors. In this chapter, two different resistance curves are presented: one using the experimental nail-slip relationship and the other using an established theoretical expression. By using the experimental values from component tests, it is possible to obtain the same resistance function as that obtained from full-scale static tests.

The inputs, common to both approaches, used to solve the equation of motion are presented in section 5.2. Constitutive models based on full scale wall static tests and component tests are presented in sections 5.3 and 5.4.

5.2 Model description and inputs

The dynamic response of the walls is established by conducting dynamic analysis using the SDOF methodology described in section 1.4.3. The average flexural response of the OSB and plywood walls was modelled using a representative T-section consisting of the sheathing section pertaining to the tributary width (406 mm) and a stud with a clear span of 2,032 mm. SDOF modelling requires that the structural element is idealized as a single equivalent ordinate; therefore the degree of freedom used here was the mid-span deflection. The assumed deflected shape in all the SDOF analyses conducted is that of a simply supported beam subjected to a uniformly distributed load along with a bi-linear resistance curve. In Equation 5.1, it is required to use two different load-mass factors to account for the change in the assumed deformed static shape from the elastic to plastic mode. These load-mass factors

can be determined using the assumed deflected shape along with Equations 1.17, 1.19 and 1.21 or by simply using the values established in the literature (Biggs, 1964; U.S.A.C.E PDC, 2008a). Load-mass factors of 0.78 and 0.66 were used to reflect for the change in the assumed deformed static shape from the elastic to plastic mode, respectively.

$$K_{LM} m\ddot{y}(t) + R(y) = AP_R\left(1 - \frac{t}{t_d}\right) \quad [5.1]$$

The mass of the section considered for dynamic analysis was that of the T-section while the participation of mass outside the clear span was assumed to be negligible. Measured densities of 498 kg/m^3, 685 kg/m^3 and 471 kg/m^3 were used to calculate the mass of the studs, OSB and plywood sheathing elements, respectively. This resulted in masses of 11.6 kg and 12.8 kg for the representative T-section with OSB and plywood sheathing, respectively.

The forcing function used in all dynamic analyses was the idealized pressure-time history described in sections 1.3.2 and 1.4.3 multiplied by the loaded area. The loaded area was taken as 0.83 m^2, which is equal to the stud spacing multiplied by the clear span. An example of the good fit between the idealized pressure-time history and the actual pressure-history is shown in Figure 5.1. All the resistance curves were described by idealized linear elastic-plastic curves as confirmed from the static tests.

5.3 Determining the increase factors using an iterative solution

5.3.1 General

The term Dynamic Increase Factor (DIF) is defined as the ratio between the capacity under dynamic loading and that obtained under static loading. Since the increase is due to the fact that the material is subjected to a higher strain rate under the dynamic load, it is meaningless to talk about a DIF without concurrently specifying what strain rate is associated with each capacity. Furthermore, for wood materials, there is an additional increase between capacity obtained under static loading and capacity representing design level load duration. The load duration factor, K_d, is equal to 1.15 for short term loading (i.e. capacity based on static test to that assumed in design) (CSA O86-09, 2009), however, this factor is conservatively assumed to be 1.0 in the blast design code due to the lack of full scale tests supporting otherwise (CSA S850-12, 2012). Due to this ambiguity in the definition, the terminology “dynamic increase factor” (or DIF) is used as a general description of the increase due to higher strain rate

relative to static tests. How this relates to the DIF value provided in the blast code will also be further clarified in Chapter 7.

5.3.2 Methodology and results

The dynamic increase factors for each wall were determined by iteratively changing the stiffness and ultimate resistance until the predicted maximum displacement and time to maximum displacement of the model matched those obtained from the experimental program along with the inputs described in section 5.2. Increase factors for resistance were determined by using the dynamic modulus of rupture, $MOR_{Dyn.}$, and comparing it to the average static modulus of rupture, MOR_{Static}. Increase factors for the stiffness were determined by comparing the modulus of elasticity values from the dynamic testing, MOE_{Dyn}, to those obtained from the statically tested walls. Only pressure-impulse combinations from the ultimate shots were used to calculate the DIF. The results are presented in Table 5.1. Using the dynamic increase factors, the shots from all the walls tested (including shots not causing failure) were compared with the SDOF results. Average increase factors of 1.40 and 1.18 on the resistance and stiffness, respectively, were found. A summary of the comparison, including ratios of SDOF results to measured displacement values, as well as time to maximum displacement is presented in Table 5.2. A sample of the predicted SDOF displacement-time history is plotted with the experimental displacement-time histories of the four middle studs in Figure 5.2 (a) and (b), for a pressure-impulse combination resulting in a response in the elastic and plastic range, respectively. The response resulting from the iterative solution can be seen in Appendix B for all pressure and impulse combinations conducted on each wall.

5.4 Constitutive models

5.4.1 General

Failure in timber connections is generally dominated by a combination of steel connector yielding and/or wood crushing, making it difficult to achieve a fully rigid connection. Assuming that the connections are semi-rigid is therefore valid and reflective of the real behaviour of such joints. The implication of this is that the full transformed area of the cross section cannot be used in calculating the stiffness or resistance. Capturing the behaviour of the walls including the semi-rigid joints can be achieved by either using the stiffness and

resistance resulting from full scale tests or by using a model that incorporates the partial composite action. A non-linear material predictive model considering the effects of partial composite action through the incorporation of the nail-slip between the sheathing and the stud is therefore proposed in the following sections. The methodology is described and the resulting resistance curves based on nail-slip relationship determined experimentally and using an established theoretical approach are compared.

5.4.2 Constitutive model methodology and results

The resistance curves used in the model are generated using Equations 5.2 and 5.3 for capacity and stiffness, respectively.

$$R_e = R_u = \frac{8M_p}{L} \quad [5.2]$$

Where M_p is the ultimate moment capacity amplified for dynamic strength and L is the clear span length. The stiffness, K, for simply supported end conditions and a uniformly distributed load is given in Equation 5.3.

$$K = \frac{384EI_{P.C.}}{5L^3} \quad [5.3]$$

Where $EI_{P.C.}$ is the composite bending stiffness, and L the clear span length.

The dynamic flexural capacity, M_p, is calculated using Equation 5.4.

$$M_p = MOR_{Exp-Stud} * S_{P.C.} \quad [5.4]$$

Where $MOR_{Exp\text{-}Stud}$ is the experimental MOR determined from testing the studs individually and $S_{P.C.}$ is the section modulus resulting from partial composite action.

The partial composite action is accounted for through the modification of the axial flange stiffness by considering the interlayer slip between the sheathing and the stud. The composite bending stiffness, $EI_{P.C}$, and the modified axial stiffness of the flange, $\overline{EA}_f$, can be determined according to Equations 5.5 and 5.6, respectively (McCutcheon, 1986).

$$EI_{P.C.} = EI_u + \frac{\left(\overline{EA}_f\right)(EA_w)}{\overline{EA}_f + EA_w} h^2 \quad [5.5]$$

$$\overline{EA}_f = \frac{EA_f}{1 + 10\frac{EA_f}{SL_f^2}} \quad [5.6]$$

Where EI_u is the bending stiffness of the web only, EA_w is the axial stiffness of the web, h is the distance between the centroid of the web and flange, EA_f is the axial stiffness of the flange, S is the interlayer stiffness, and L_f is the distance between the sheathing gaps (see Figure 5.3 (a)). In this experimental program L_f is equal to the clear span of the panels, because they were applied in a direction parallel to the studs. A more general application of the theory covers composite I-beams as illustrated in Figure 5.3 (b).

The shear-slip per unit length, also referred to as the interlayer stiffness, can be defined as shown in Equation 5.7 as function of the load slip for one nail, P/δ, divided by the nail spacing.

$$S = \frac{P/\delta}{s} \quad [5.7]$$

Material properties used as inputs for Equations 5.4 through 5.6 were obtained experimentally as described in Chapters 3 and 4 and are summarized in Table 5.3. The interlayer stiffness can either be determined experimentally or theoretically. Determining the load-slip relationship experimentally help eliminate all of the uncertainties associated with the assumed elastic bearing constants and fastener properties. The slope of the experimental load-deformation curve is used directly as input in Equation 5.7. Using the average experimental P/δ curves reported in Chapter 4 for the OSB and plywood joints yields interlayer stiffness values of 11.79 MPa and 16.23 MPa, respectively. The resulting static resistance curves can be seen in Figure 5.4. Table 5.4 present a summary of the displacement and time to maximum displacement determined using this material predictive model compared to the experimental results.

The load slip relationship (P/δ) can also be determined analytically for a two-member nailed joint using the elastic bearing constants and the mechanical properties of the fastener (Wilkinson 1972 and 1974). First, the λ parameters are determined using Equations 5.8 and 5.9.

$$\lambda_1 = 2\sqrt[4]{\frac{k_{o_1}}{\pi E d^3}} \quad [5.8]$$

$$\lambda_2 = 2\sqrt[4]{\frac{k_{o_2}}{\pi E d^3}} \quad [5.9]$$

Where λ_1 and λ_2 are the value of the lambda parameter for the top and bottom members respectively, k_{o1} and k_{o2} are the elastic bearing constants for the top and bottom members respectively, E is the modulus of elasticity of the nail and d is the diameter of the mechanical fastener. Once the values of the lambda parameters are determined, there are two possible cases as presented in Equations 5.10 to 5.12 and Equations 5.13 to 5.16:

Case 1: $\lambda_1 a > 2 \; and \; \lambda_2 b > 2$

$$\frac{P}{\delta} = \frac{E^{1/4} k_{0,1}^{3/4} d^{7/4} \pi^{1/4} \beta_1}{2} \quad [5.10]$$

$$\beta_1 = \frac{r\left(r + r^{3/4}\right)}{2(r + r^{1/4})(r + r^{3/4}) - (r - r^{3/4})^2} \quad [5.11]$$

$$r = \frac{k_{o2}}{k_{o1}} \quad [5.12]$$

Case 2: $\lambda_1 a < 2 \; and \; \lambda_2 b > 2$

$$\frac{P}{\delta} = a d k_{o1} \beta_2 \quad [5.13]$$

$$\beta_2 = \frac{r(3r + \alpha^3)}{2(2r + \alpha)(3r + \alpha^3) - (3r - \alpha^2)^2} \quad [5.14]$$

$$r = \frac{k_{o2}}{k_{o1}} \quad [5.15]$$

$$\alpha = \lambda_2 a \quad [5.16]$$

Where a and b are the thickness of the top and bottom member, respectively.

Table 5.6 presents a summary of published elastic bearing constants as a function of the specific gravity of the material (Wilkinson, 1972). The average elastic bearing constant for plywood was estimated to be 217.2 N/mm^3 (0.8 x10^6 lb/in^3) based on published values (Wilkinson 1974). The input parameters to calculate the interlayer slip are provided in Table 5.7. The nail diameter was determined based on measured sizes of 30, randomly selected,

nails used in the construction of the test specimens. From Table 5.7, it can be seen that the same elastic bearing constant is used for the OSB as that used for the plywood because there were no published values available for the OSB sheathing. The elastic bearing constant for the stud was determined using the equation for a "Smooth shank nails driven with no lead hole and loaded parallel to the grain" presented in Table 5.6. The specific gravity used in the model was also determined experimentally, as described in Chapter 4. As shown in Table 5.8, the interlayer stiffness for the OSB and plywood T-section was determined to be 10.6 MPa and 16.6 MPa, respectively. The incorporation of the load-slip relationship increases the bending stiffness of the OSB and Plywood T-section by 24% and 41 %.

The resulting static resistance curves can be seen in Figure 5.5. Table 5.5 present a summary of the displacement and time to maximum displacement determined using this material predictive model compared to the experimental results. Table 5.9 compares the theoretical P/δ curve to the one obtained experimentally for both the OSB and plywood sections. The percentage difference between the two approaches is 8.4 % and -4.1% for the OSB and plywood T-sections, respectively.

5.5 Dynamic analysis program

An excel-based program was developed by the author to conduct SDOF dynamic analyses. The equation of motion was solved using the constant-velocity method to find the maximum displacement as well as the time to maximum displacement. The excel-based SDOF engine, shown in Figure 5.6, allows the user to enter the factors used in the equivalent dynamic analysis as well as the properties of the SDOF. The user can enter properties such as mass, loaded area, load and mass factors, resistance function, time step, and pressure-time history. The program is designed to find the maximum response using the idealized pressure-time history and does not consider hysteric response. The pressure-time history handled by the program is the one corresponding to the triangular idealization of the blast load described in Chapter 1; therefore an actual pressure-time history cannot be entered. Also, only the positive phase of the idealized equivalent pressure-time history is considered. The program also suggests a maximum recommended time step for the analysis in order to get reasonably accurate results. The recommended time step is based on criteria outlined in U.S.A.C.E PDC (2008a).

The excel-based program was verified using a computer software "RCBLAST" (Jacques, 2013). The comparison between the two programs is highlighted for same idealized pressure-time history and SDOF properties obtained from Figure 5.5 in Figure 5.6. Similar trends were found for all other examples used in the comparison. The way the comparison shown in Figure 5.6 was feasible is due to the fact that RCBLAST has an overlay option where the displacement-time histories can be imported and compared to the one predicted by the program.

As mentioned earlier, an idealized function representing the pressure-time history was used to run the analysis. In order to verify that this assumption is valid, the actual pressure-time history was entered into the RCBLAST program and the results were compared to those using the idealized pressure function, as illustrated in Figure 5.7. In all the cases, using the actual pressure-time history resulted in maximum displacement values that were within 10% of those obtained using the idealized pressure-time history.

Table 5.1: Iterative solution numerical modelling summary

Test Name	Experimental		SDOF		SDOF		Experimental average		Increase factors	
	$d_{max-Avg}$ mm	$t_{max-Avg}$ ms	d_{max} mm	t_{max} ms	$R_u=R_e$ kN	K_e kN/m	$R_u=R_e$ kN	K_e kN/m	Resistance, R	Stiffness, K
W6- 1	No data				42.5	1,125	27.0	874	1.57	1.29
2	47	8.9	47	9.3						
W7- 1	59	9.4	59	11.1	35.7	940			1.32	1.08
W8- 1	8	6.2	8	7.7	33.0	875			1.22	1.00
2	46	7.9	44	7.9						
W9- 1	8	10.6	9	11.4	36.5	980			1.35	1.12
2	39	11.7	38	9.1						
3	60	11.7	63	11.0						
W10- 1	9	9.0	17	9.9	39.0	985			1.44	1.13
2	48	12.0	46	10.1						
W16- 1	11	9.8	14	9.9	37.5	1,350	25.9	920	1.45	1.47
2	37	9.9	39	9.8						
3	45	11.4	43	11.1						
W17- 1	13	9.9	14	9.1	42.0	1,325			1.62	1.44
2	51	9.9	50	10.6						
W18- 1	5	5.6	7	7.8	29.5	925			1.14	1.01
2	45	8.7	43	8.1						
W19- 1	11	9.8	12	10.1	37.8	1,175			1.46	1.28
2	56	10.3	54	10.8						
W20- 1	16	12.0	18	11.7	36.0	925			1.39	1.01
2	41	11.7	41	10.1						
3	61	11.9	59	11.4						

Table 5.2: Summary of experimental response and response predicted by SDOF analysis of iterative procedure

	Maximum displacement ratio, $\frac{d_{SDOF}}{d_{exp-avg}}$			Time-to-maximum displacement ratio, $\frac{d_{SDOF}}{d_{exp-avg}}$			Num. of tests
	Mean	Std dev	COV	Mean	Std dev	COV	
All tests	1.09	0.22	0.20	1.02	0.14	0.13	21
OSB walls	1.11	0.31	0.28	1.03	0.15	0.15	9
Plywood walls	1.08	0.16	0.15	1.01	0.13	0.13	12

Table 5.3: Parameter input to compute partial composite action

Modulus of elasticity for 11 mm OSB, E (N/mm^2)	5,550
Modulus of elasticity for 18.5 mm plywood, $E_{sheathing}$ (N/mm^2)	7,120
Modulus of elasticity for studs, E_{stud} (N/mm^2)	9,690
Modulus of rupture for studs, $MOR_{Exp\text{-}Studs}$ (N/mm^2)	44.5
Length between gaps-Sheathing parallel to studs (Span) (mm)	2,032
Nail spacing for both types of wall, s (mm)	150

Table 5.4: SDOF results using experimental and theoretical nail-slip in partial composite action

Test name	Experimental		SDOF-Experimental nail-slip		SDOF-Theoretical nail-slip	
	$d_{max-Avg}$ mm	$t_{max-Avg}$ ms	d_{max} mm	t_{max} ms	d_{max} mm	t_{max} ms
W6- 1	No data					
2	47	8.9	49	10.3	50	10.3
W7- 1	59	9.4	56	11.2	49	10.4
W8- 1	8	6.2	6	6.9	6	6.9
2	45	7.9	36	7.3	36	7.4
W9- 1	8	10.7	8	11.1	8	10.8
2	39	11.7	32	8.6	33	8.6
3	60	11.7	60	11.2	56	10.7
W10- 1	9	9.0	15	9.2	15	9.3
2	48	12.0	40	9.9	41	10.0
W16- 1	11	9.8	12	9.1	12	9.1
2	37	9.9	33	9.1	33	9.0
3	45	11.4	36	10.3	36	10.3
W17- 1	13	9.9	14	9.2	14	9.2
2	51	9.9	58	12.1	57	12.0
W18- 1	5	5.6	6	7.0	6	7.0
2	45	8.7	34	7.1	34	7.1
W19- 1	11	9.8	12	9.8	11	9.7
2	56	10.3	50	10.5	49	10.4
W20- 1	16	12.0	13	10.4	13	10.4
2	41	11.7	31	8.9	31	8.9
3	61	11.9	43	9.9	43	9.8

Table 5.5: Summary of experimental response and response predicted by SDOF non-linear predictive material model using experimental and theoretical nail-slip

		SDOF maximum displacement ratio, $\frac{d_{SDOF}}{d_{exp-avg}}$			SDOF time-to-maximum displacement ratio, $\frac{d_{SDOF}}{d_{exp-avg}}$			Num. of tests
		Mean	Std dev	COV	Mean	Std dev	COV	
SDOF-Experimental nail-slip	All tests	0.95	0.20	0.21	0.97	0.15	0.15	21
	OSB walls	0.97	0.25	0.25	1.00	0.15	0.15	9
	Plywood walls	0.94	0.17	0.18	0.96	0.15	0.16	12
SDOF-Theoretical nail-slip	All tests	0.94	0.21	0.22	0.97	0.14	0.15	21
	OSB walls	0.96	0.26	0.27	0.98	0.14	0.14	9
	Plywood walls	0.93	0.17	0.18	0.96	0.15	0.16	12

Table 5.6: Summary of elastic bearing constants

Description	**Elastic Bearing Constant, k_0 (N/mm^3) ***
Smooth shank nails driven in prebored holes and loaded parallel to the grain	869*G
Annularly threaded nails driven in prebored holes and loaded parallel to the grain	782*G
Helically threaded nails driven in prebored holes and loaded parallel to the grain	678*G
Smooth shank nails driven with no lead hole and loaded parallel to the grain	582*G
Annularly threaded nails driven with no lead hole and loaded parallel to the grain	608*G
Helically threaded nails driven with no lead hole and loaded parallel to the grain	521*G
Smooth shank nails driven in prebored holes and loaded perpendicular to the grain	348*G
Smooth shank nails driven with no lead hole and loaded perpendicular to the grain	348*G

Table 5.7: Parameter input for theoretical load-slip resistance

Options	Specific gravity of stud	Elastic bearing constant		Nail modulus of elasticity,E_N	Diameter of nail, d_N	Length of nail, L_N	Thickness of	
		Sheathing, k_{01} (N/mm^3)	Stud, k_{02} (N/mm^3)	($x10^3$ N/mm^2)	(mm)	(mm)	Sheathing (mm)	Stud (mm)
OSB	0.498	217	290	200	3.50	63.5	11.0	140.0
Plywood	0.498	217	290	200	4.24	89.0	18.5	140.0

Table 5.8: Computation of interlayer stiffness

Options	Load/slip resistance P/δ (N/mm) Eq. 5.6 or 5.9	Interlayer stiffness S (N/mm^2) Eq. 5.3	Composite bending stiffness, EI ($x10^6$ Nmm^2) [1]	Bending stiffness of joist alone, EI_U ($x10^6$ Nmm^2) [2]	Relative bending stiffness increase [1] / [2]
OSB	1,620	10.6	104,150	84,200	1.24
Plywood	2,540	16.6	118,510	84,200	1.41

Table 5.9: Comparison of theoretical and experimental load-slip

Options	Theoretical load slip, $(P/\delta)_{Theo.}$ (N/mm)	Experimental load slip, $(P/\delta)_{Exp.}$ (N/mm)	Percentage difference (%)
OSB	1,620	1,770	8.4
Plywood	2,540	2,430	-4.1

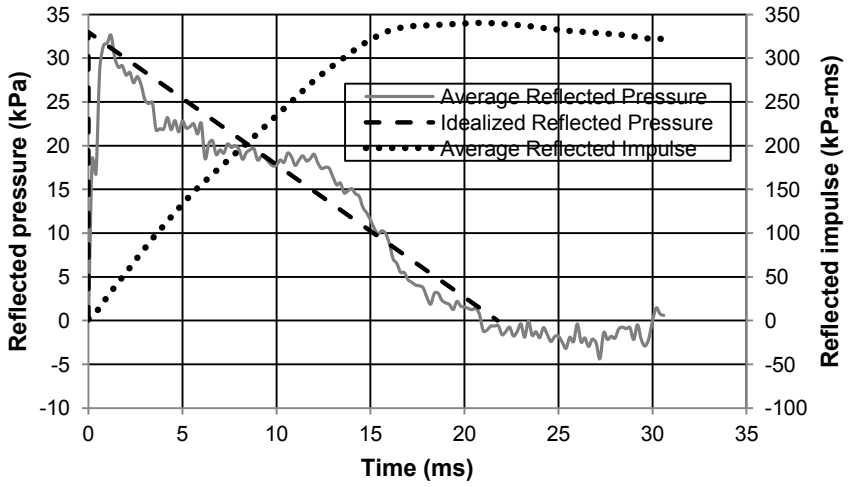

Figure 5.1: Typical Idealized history pressure

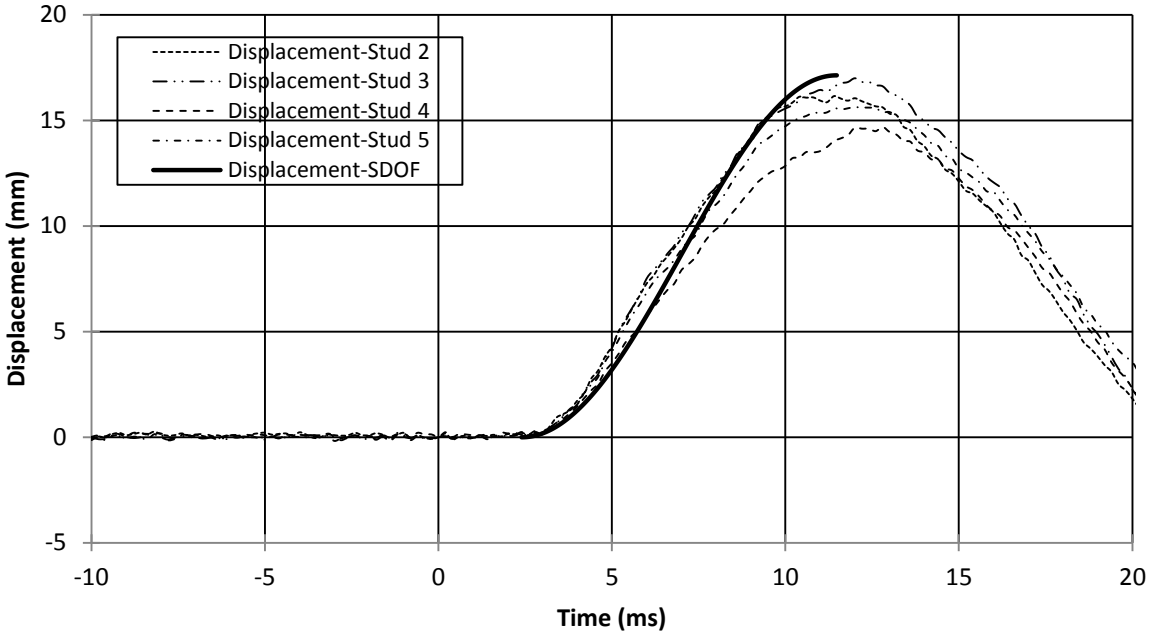

(a) SDOF prediction for Wall 20 Shot 1

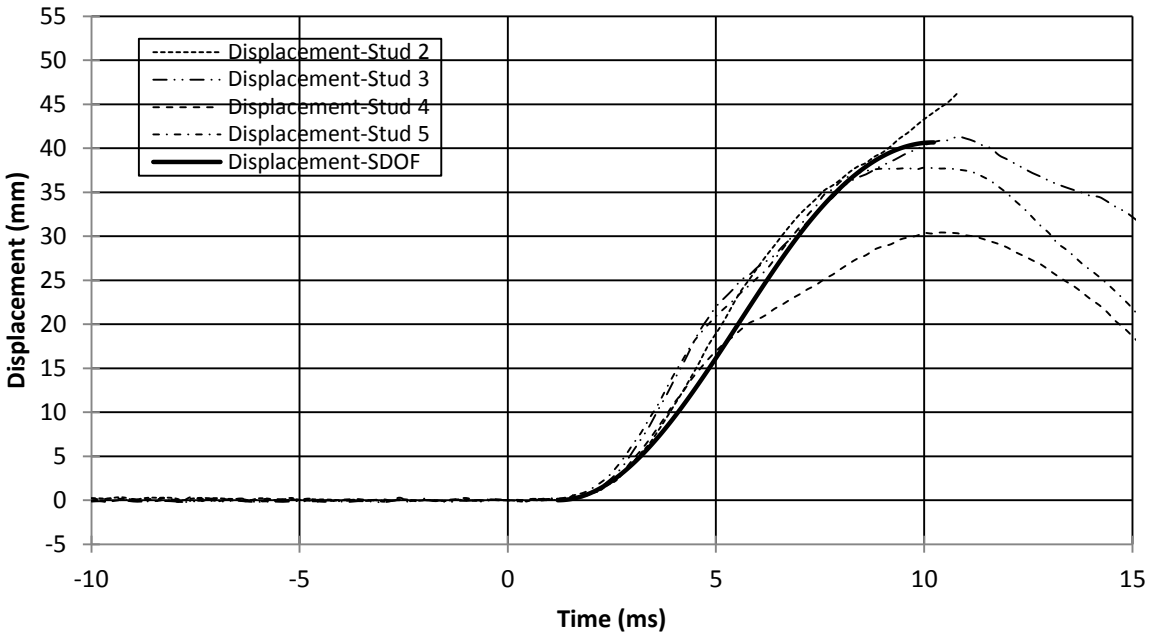

(b) SDOF prediction for Wall 16 Shot 2

Figure 5.2: Comparison between SDOF and experimental displacement-time histories

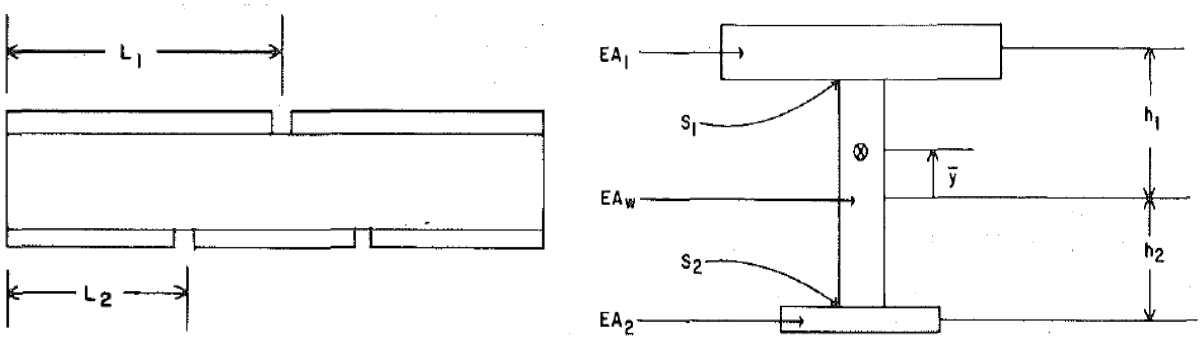

(a) Side view (b) End view

Figure 5.3: Nomenclature for composite I-beam

*Reproduced from McCutcheon (1986)

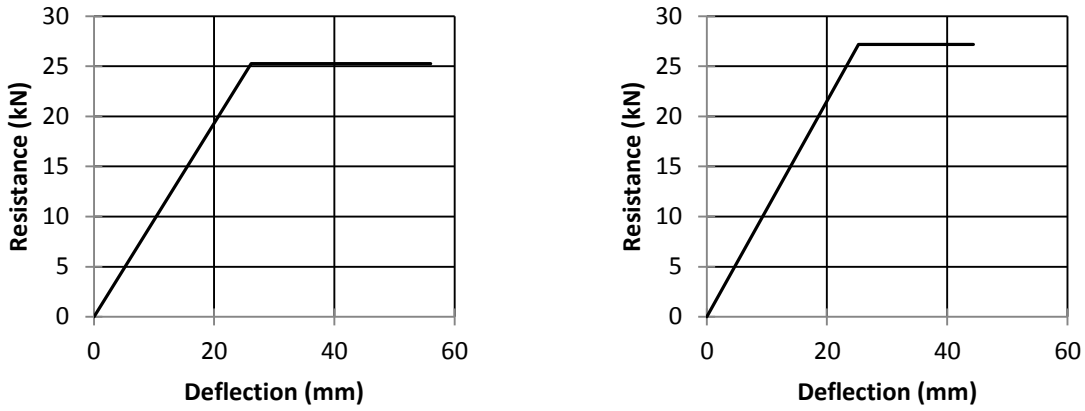

(a) OSB (b) Plywood

Figure 5.4: Static resistance curves using experimental nail-slip for T-sections

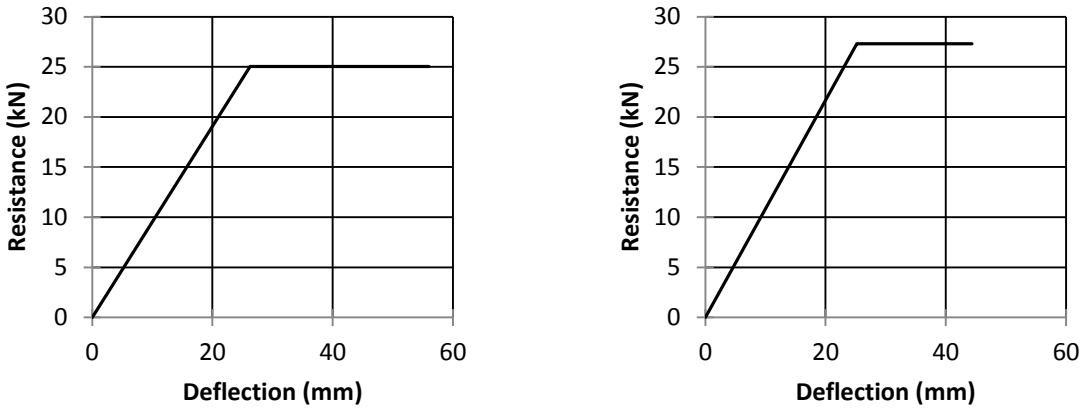

(a) OSB (b) Plywood

Figure 5.5: Static resistance curves using theoretical nail-slip for T-sections

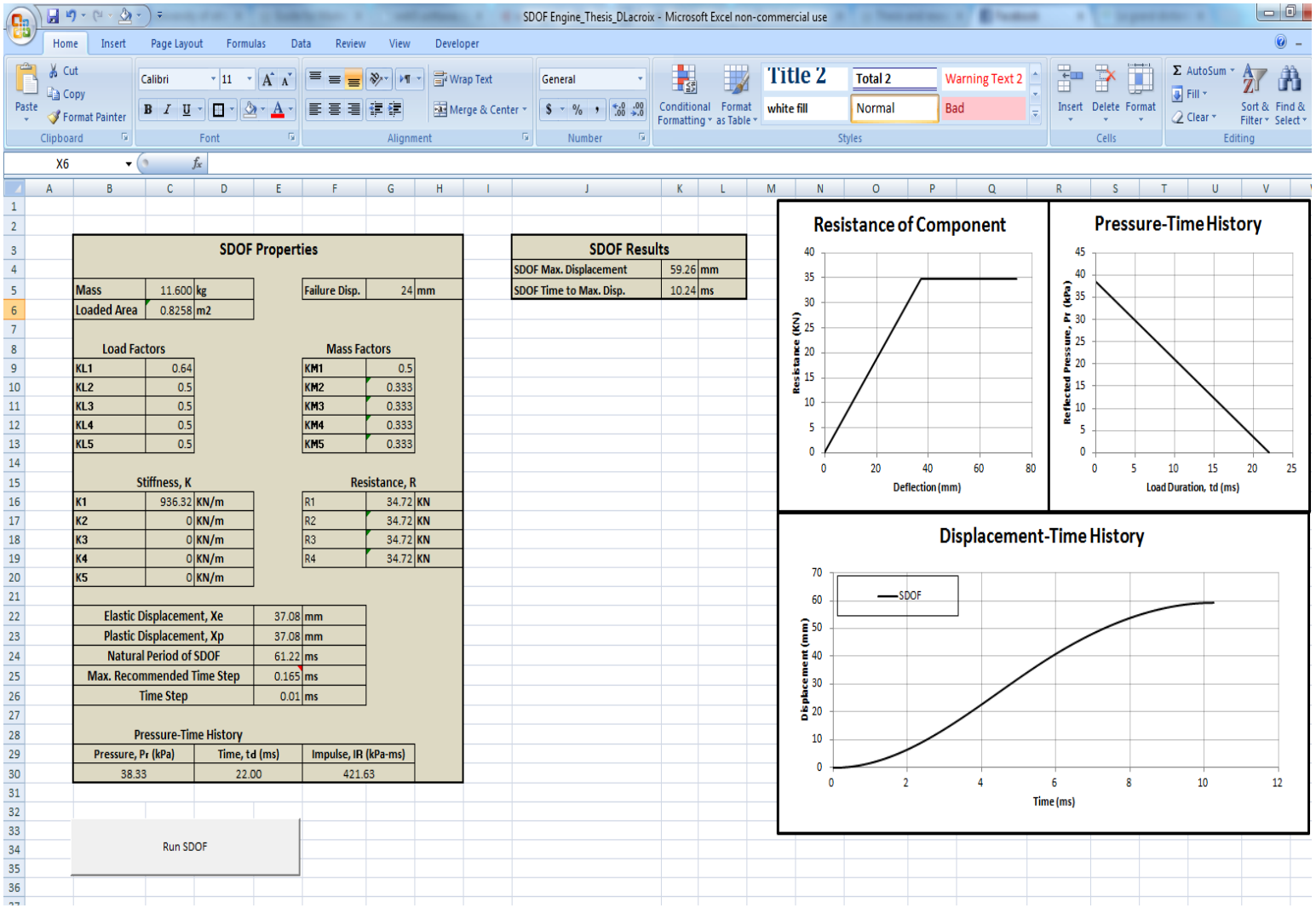

Figure 5.6: SDOF spreadsheet program

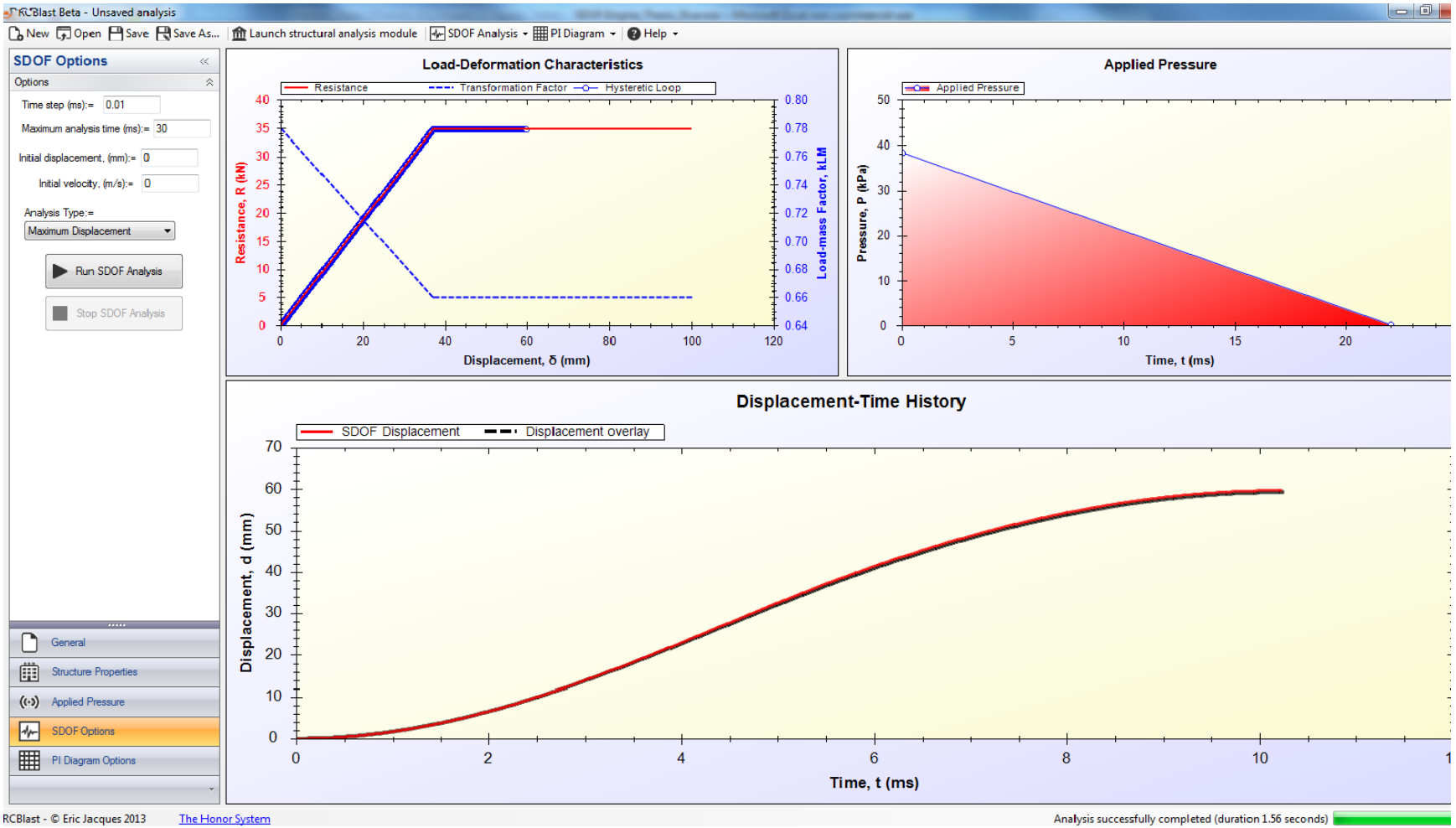

Figure 5.7: Comparison between spread sheet program developed by the author and RCBLAST (Jacques, 2013)

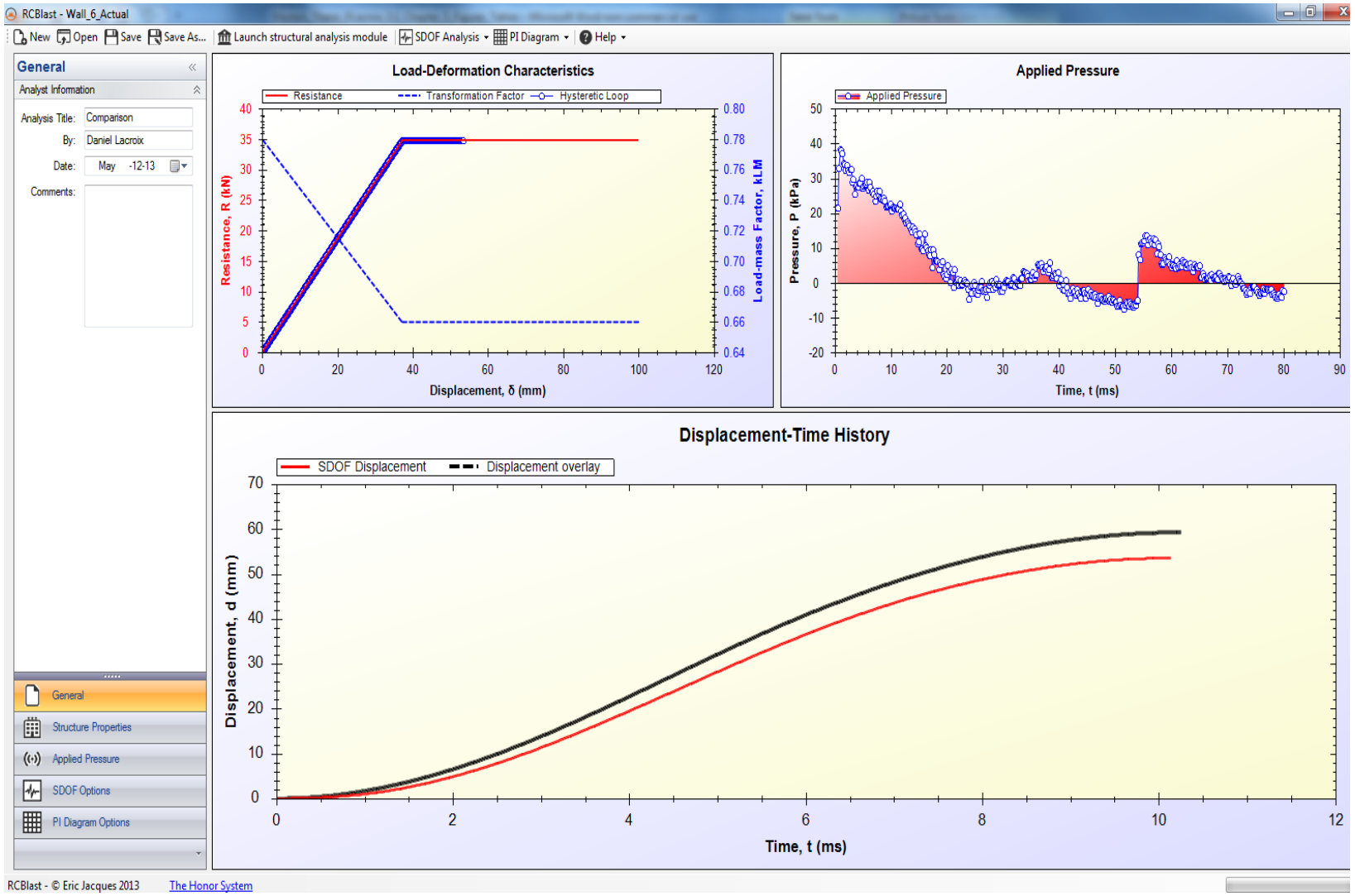

Figure 5.8: Comparison between SDOF and experimental displacement-time histories for idealized vs. actual pressure

CHAPTER 6-Discussion

6.1 General

Light-frame wood structures are highly complex and redundant due to the repetitive nature of the individual components within such system. Even though a stud, a sheathing panel, and a nail by themselves may be considered structural elements, the description of the overall behaviour of the wall substructure cannot simply be described by adding the individual components together. Considerations related to the interactions between the elements, e.g. load sharing effects, need be considered when describing the wall subsystem behaviour. The notation "subsystem" here is also used to illustrate the limitation of the current study to describe the overall behaviour of the light-frame wood system as a whole. Combining subsystems (such as walls, floors, etc) together, presents an added layer of complexity, due to the influence of load paths and boundary conditions. The current study investigated all the individual components separately and as part of the wall subsystem in order to present a predictive model capable of describing the subsystem behaviour from the component behaviour without the need for additional full scale static testing.

One of the fundamental assumptions used in the testing and modelling in the current study is that failure would occur within the wall subsystem and that the failure would be in flexure. The first assumption has been corroborated by field observations as discussed in Chapter 2, where previous research studies had indicated that subsystems such as rafters, floors and walls governed the overall damage under blast loads. This is not suggesting that connections between subsystems should not be studied but rather emphasizes that current study attempted to "isolate" the behaviour of the wall subsystem in order to understand it better. It is recommended that subsequent studies look at the effect of various joints between subsystems and their effect on the overall behaviour of the structure. The static and dynamic tests clearly proved that the second assumption, that failure in the studs is in flexure, is valid (e.g. Figures A1.2 and B6-2.4).

6.2 Load sharing effects

Current design provisions on wood light-frame structures are based on an assessment of the capacity of isolated rib components such as floor joists, wall studs, or roof trusses. System effects such as load sharing and composite action are allowed for by multiplying the bare rib capacity by a "load sharing" factor. Since the study tested individual studs and full scale sheathed walls, it allows for a direct comparison between their respective capacities. Even though data is limited, the results show an increase in the capacity of individual studs as part of a system compared to their capacities in isolation. From Figure 6.1, it can be observed that an increase in capacity of 1.20 was achieved when studs shared the applied load within a wall system.

Even though no increase factor for stiffness is currently provided in the timber design code, based on the testing program, a relative increase in stiffness of 1.15 was obtained in wall systems compared to individually tested studs, as shown in Figure 6.2. It should be noted that the above is merely an observation based on the actual construction details and that the results could be affected by several factors such as: sheathing thickness and bending stiffness, fastener stiffness, variability in modulus of elasticity between members, and the statistical correlation between member stiffness and bending strength, etc. It is for these reasons that above mentioned factors cannot be generalized, although the observation on the strength load sharing factor happened to be the same as what the code provision states. As expected, the values for the load sharing factor obtained here is less than that of visually graded lumber. The reason is that MSR lumber is graded using machine evaluated MOE resulting in less variability in both stiffness and ultimate capacity.

6.3 Failure of wood stud walls under blast loading

6.3.1 Observed failure modes

When a uniformly distributed load is "slowly" applied to a wall system, it is expected that the sheathing would collect the pressure and apply it to the various studs that the wall consist of as shown in several examples in Chapter 4 (e.g. Figure 4.10). Whether this assumption is valid when the wall is subjected to a dynamic load needs to be investigated. From the experimental program in the shock tube, it can be seen that the deflection of all studs occur

in unison up to the point where maximum deflection is reached as shown in Figure 6.3 (a) and (b) for shots within the elastic region and ultimate shots causing failure, respectively. Past the initial peak displacement, the studs are observed to deflect out of phase. This is primarily due to the low out-of-plane stiffness of the sheathing panel and its inability to keep the studs moving in synch. This effect is more pronounced for shots causing failure. Even though more uniform deflection was observed when plywood was used under static loading, a similar conclusive statement cannot be made under dynamic testing.

In limited cases with high pressure in the negative phase, studs that were undamaged in the inbound phase failed during the rebound (e.g. Wall 8 Shot 2). This occurred even though the negative phase maximum pressure was smaller than that measured in the positive phase. Ignoring the negative phase may be appropriate for systems that are symmetric, however, here, the sheathing is only applied on one side and during the negative phase the behaviour of the wall system seems to be different, especially when nail withdrawal occurred.

There were several examples of nail withdrawal (e.g. Wall 8 Shot 2 and Wall 20 Shot 3) primarily due to the negative pressure (see Figure B8-2.3). The nail withdrawal was especially pronounced when the studs were deflecting out of synch. The lack of symmetry in the wall and the very weak nature of the nail joint in withdrawal make the stud wall subsystem vulnerable and possibly susceptible to premature failure. The main function of nails connecting sheathing to studs in a light-frame wood walls is to prevent the studs from buckling laterally and provide capacity, stiffness and ductility to the wall when loaded in plane (as a shearwall). More work is needed to understand the behaviour of stud walls under blast loading post maximum displacement and to improve the withdrawal capacity of joints between sheathing and studs when the wall is subjected to negative pressure. Both these topics are beyond the scope of the current work.

Experience from static testing on wood stud walls shows that typical wall and floor configurations, such as those tested here; do not lead to a failure in the sheathing before the failure of the framing members. Such failure was, however, observed when the walls were loaded dynamically (e.g. Wall 7 Shot 1 and Wall 20). It should be mentioned that this failure

type always occurred concurrently with stud failures. The sheathing failure occurred primarily in the walls sheathed with the 11 mm OSB and not those sheathed with 18.5 mm plywood (with one exception, where a stud failed in a prior shot causing a larger tributary width). Since the ultimate capacities of walls sheathed with plywood and OSB were almost indistinguishable, once the mass and stiffness of the sheathing were accounted for, it can be concluded that the breaching of the sheathing had no significant effect on the transfer of the forces to the studs. However, the breaching of the sheathing panels under blast loading is not considered satisfactory due to the debris generated and also from the perspective of force transfer. Based on the current study, the minimum sheathing thickness needed so that the sheathing does not fail before the studs was found to be 11 mm. It is uncertain whether the sheathing material itself (i.e. OSB) played a role and therefore, more studies are needed to further establish that relationship.

6.3.2 Quantification of damage levels

The observed levels of damage were quantified based on the overall performance of the specimens according to the criteria defined in the "Single Degree of Freedom Structural Response Limits for Antiterrorism" (U.S.A.C.E PDC, 2008b). Although studs are considered "primary structural component", the failure of a single stud does not usually result in a complete wall failure nor does it lead to progressive collapse of the building. Stud wall subsystems are very redundant with an ability to share the applied load as well as redistribute the load after the failure of a single component. This makes characterizing the failure level more difficult than in the case of for example a column. The variability inherited in wood also affects the perceived level of damage of the entire wall if one or more studs with inferior capacity experience a severe level of damage and therefore the whole wall may be characterized for a higher damage level. Since the component level damage may not be representative of the damage at the subsystem level (wall), both the severity of the damage for individual component and the number of failed components were considered in assigning levels of damage to the walls. Although systematic, this evaluation is obviously subjective, and many more stud wall tests need to be conducted before such assessment is reliable.

The quantified levels of damage are presented in Table 4.6. A detailed description of the damage levels for each wall can be seen in Appendix B. In the quantification of the damage

levels, “heavy damage” relates to the structure being at onset of collapse, “moderate damage” corresponds to un-repairable damage where progressive collapse would not occur, and “superficial damage” relates to reparable damage.

6.4 Dynamic increase factors

Similar to other materials, such as concrete and steel, wood is expected to experience an increase in capacity under high strain rate loadings. Commonly, the dynamic increase factor (DIF) is defined as the ratio of the dynamic to the static capacities. Figures 6.4 and 6.5 show the relative increase in resistance and stiffness, respectively, for all the tested walls. Figure 6.6 shows the correlation between the predicted displacement and the experimental displacement for all shots, including the ultimate shots. A strong correlation, with an R^2 value of 0.98, and proximity to the 45-degree line representing “perfect agreement”, can be observed. This was anticipated, as the DIF used are the average values found using the iterative procedure on the ultimate shots; however, it is important to document that the values are also applicable for shots other than those they were derived from.

As it will be elaborated on in Chapter 7, current provisions in the blast design code in Canada (CSA S850-12, 2012) allow for a DIF of 1.4 to be applied on the static capacity of MSR lumber subjected to high strain rates. The DIF in the code was proposed pending substantiation, such as full scale shock tube tests. The value obtained in the current research study seems to provide corroborating evidence that the proposed factor in the code is appropriate. The current blast code does not allow any increase in stiffness for wood light-frame systems. The implication of the findings in this study on the design of light-frame structures under blast will be discussed in Chapter 7.

6.5 Constitutive models

The results and discussion presented under section 6.2 showed the importance of including the sheathing contribution to be able to describe the behaviour of floor and walls systems. This has also been substantiated by other studies (e.g. Polensek et al., 1972; Foshi, 1985; McCutcheon, 1986; and Wheat et al., 1986). A methodology, originally proposed by McCutcheon (1986) for floors, has been employed by the author to account for the partial composite action in the wall system through establishing the interlayer slip between the

sheathing and the stud. In order to verify the proposed approach, a comparison was made with experimental results. Figures 6.7 and 6.8 show the predicted resistance curves compared to the experimental static resistance for the OSB and plywood walls, respectively. For both sheathing types, it was observed that the difference in stiffness and resistance when using the theoretical and experimental nail slip relationship is very small. This confirms the mechanics-based relationship for nail slip once all the parameters are known experimentally.

The calculated stiffness for OSB and plywood walls, appear to be slightly higher than that measured under the static wall test. The calculated capacity based on the partial composite action seems lower in the case of OSB and higher in the case of plywood sheathing. This could be attributed to the variability naturally occurring in the material. It could also be attributed to the selection of the elastic bearing constant for OSB, where, as mentioned in Chapter 4, no such value could be found in the literature and therefore the value used was that of plywood sheathing.

In all cases, it can be concluded that as long as the material properties of the studs, sheathing panel and nails are known, the procedure outlined here would provide reasonably accurate prediction of the wall static behaviour. The implication of this is that it reduces or eliminates the need for testing full scale wall subsystems.

The experimental static resistance curves for OSB and plywood (Figures 6.7 and 6.8) were modified using the average DIF discussed in section 6.5 and used as input to solve the equation of motion (Equation 5.1). As mentioned earlier, these static resistance curves were based on the partial composite action method using the experimental and theoretical nail-slip. Figure 6.9 shows the predicted displacement using the experimental nail slip data compared to the average experimental mid-span displacement. As it can be seen, there is a strong correlation between the predicted and experimental displacement. It is observed in Figure 6.9 that there is a tendency for the model to under-estimate the deflections, especially at the high displacement range.

Figure 6.10 shows the predicted displacement using the theoretical nail slip values to the average experimental mid-span displacement. A strong correlation between the predicted and experimental displacement, similar to that obtained in Figure 6.9, is observed.

A possible explanation for the constitutive model to underestimate the deflection may lie in the way stiffness is estimated. The constitutive model relies on the stiffness defined by the initial stiffness of the load-slip curve up to forty percent of peak load. However, the behaviour of a nailed joint is non-linear (see Figure 4.6). What might be considered as a "representative stiffness" to be used as an input to the model requires further research. This point was not explored further in the current research, because the differences found were considered small given the variability in the material, uncertainty in the load and the simplifications made in the model approach.

6.6 Strain rate effects

As discussed in Chapter 2, the behaviour of wood under the effect of high strain rates is not well established in the literature. Even though an attempt was made to generate different strain rates by selecting different lengths of driver, the strain rates only ranged between $1.20E^{-1}$ to $5.48E^{-1}$ s^{-1}. The difference in the strain rate was simply not large enough to yield significant difference in the results. To expand the range of strain rate, a detailed investigation of the literature was done in Chapter 2 (Barret and Lau, 1994; Widehammar, 2004; Lloyd et al., 2011; Sukontasukkul, 2000; and Syron, 2010), where the relationship between increases in resistance and the associated strain rate was established (see Figure 2.8). These data points were plotted along with the data points resulting from the current research study including the walls tested under static loading. Figure 6.11 shows the relative increase in resistance versus the strain rate, plotted on a logarithmic scale and normalized relative to the results from static loading (i.e. duration of a few minutes). It is noteworthy to mention that what is considered "standard load duration" in the timber design code (CSA O86, 2009) is based on live and snow loads, and a factor K_d of 1.15 can be used to increase the capacity for short term load duration, relative to the standard term capacity. It can be seen that the test data from this study fits well within the trend of behaviour found in the literature, both for the walls tested statically and dynamically. It can be concluded that there is a strong correlation between the increase in strain rate and the relative increase in strength. The

following equation is proposed to relate the relative increase factor (DIF) over a wide range of strain rates, $\dot{\varepsilon}$, based on both literature data points as well as data resulting from this research program.

$$DIF = 1.46 + 0.1 \log_{10} \dot{\varepsilon} \qquad [6.1]$$

It is important to note that the equation can be considered valid over a strain rate range of $1.67E^{-5}$ s^{-1} to $1.65E^{3}$ s^{-1}, as seen in Figure 6.11.

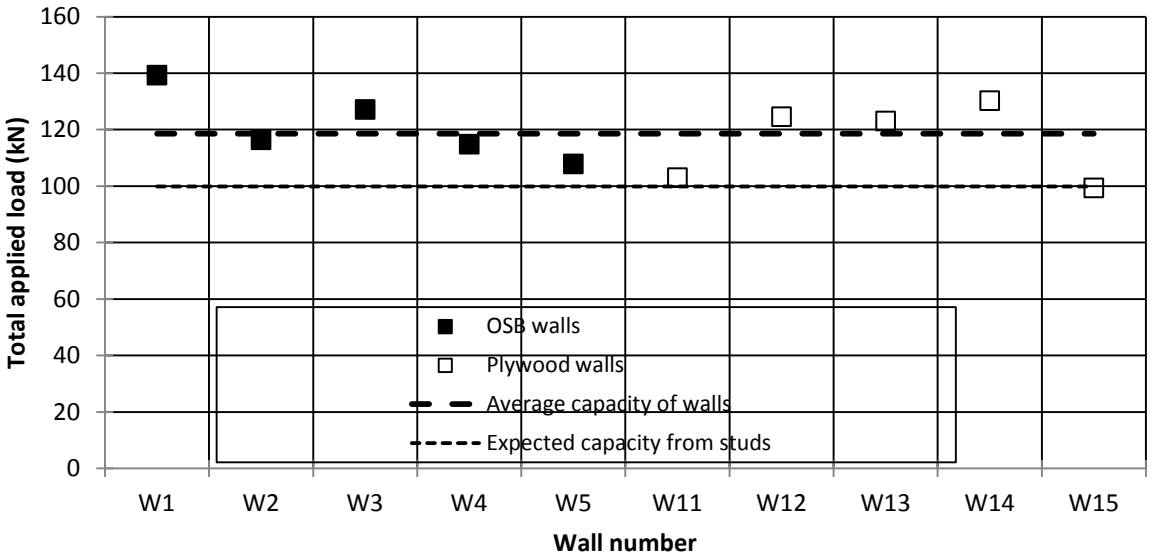

Figure 6.1: Experimental static resistance of OSB and plywood walls compared to the expected static capacity determined from the studs

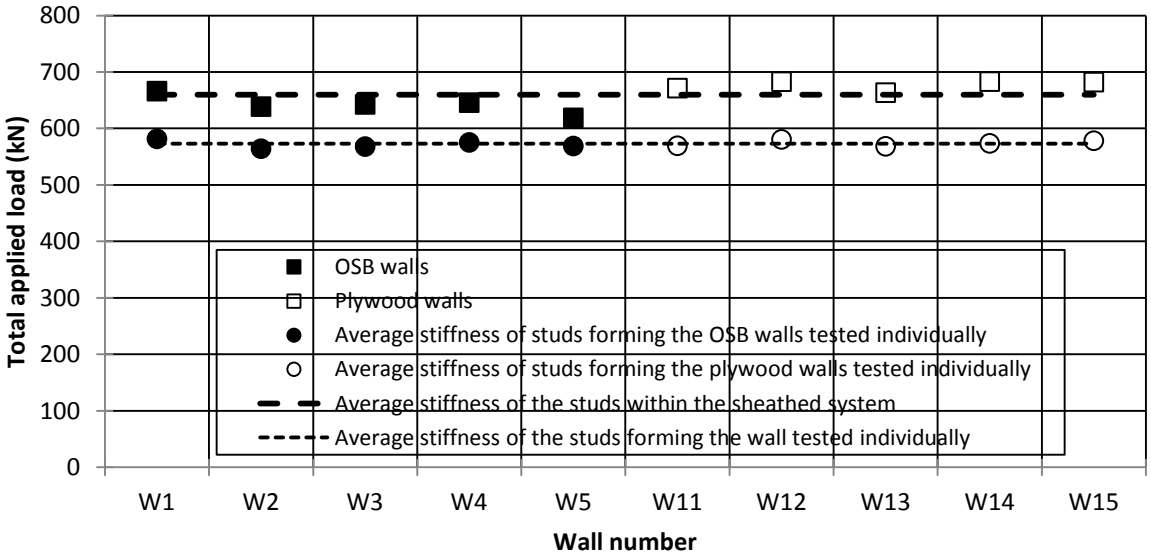

Figure 6.2: Experimental average stiffness of OSB and plywood walls compared to the expected average stiffness determined from the studs

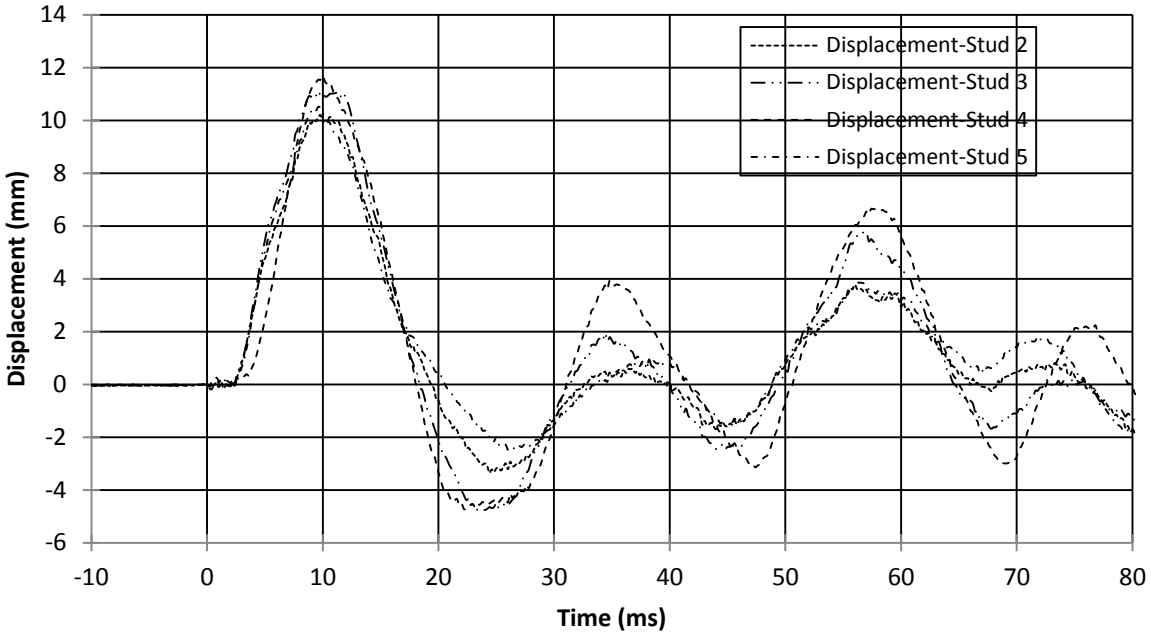

(a) Elastic region-Wall 19 Shot 1

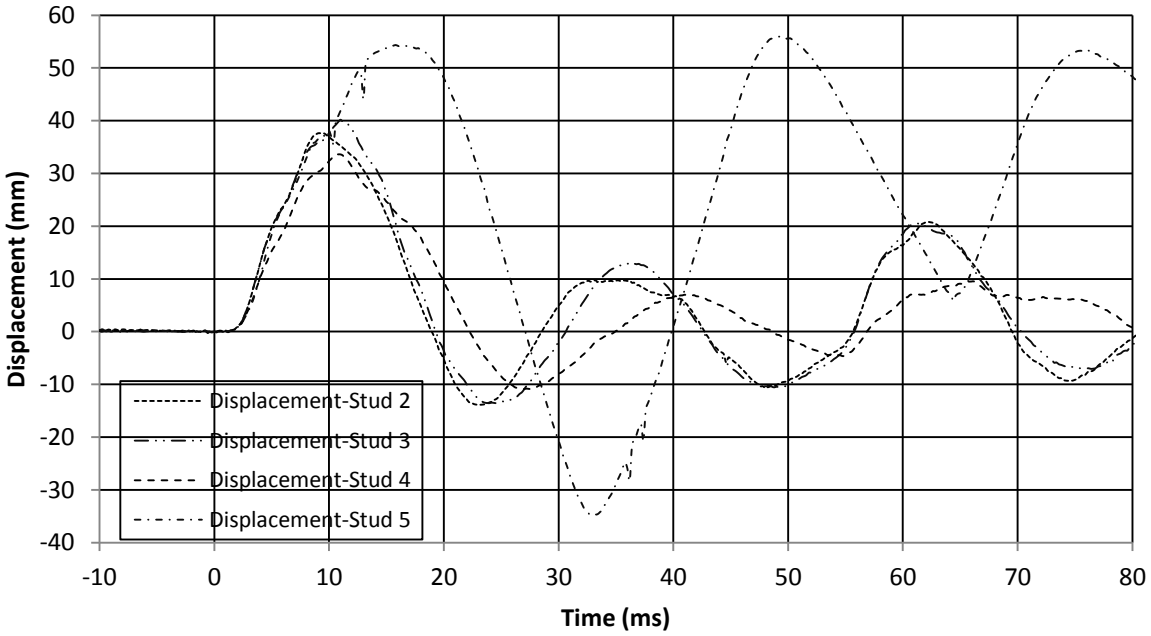

(b) Plastic region-Wall 20 Shot 2

Figure 6.3: Typical displacement histories in the elastic and plastic region for walls subjected to shock wave loading

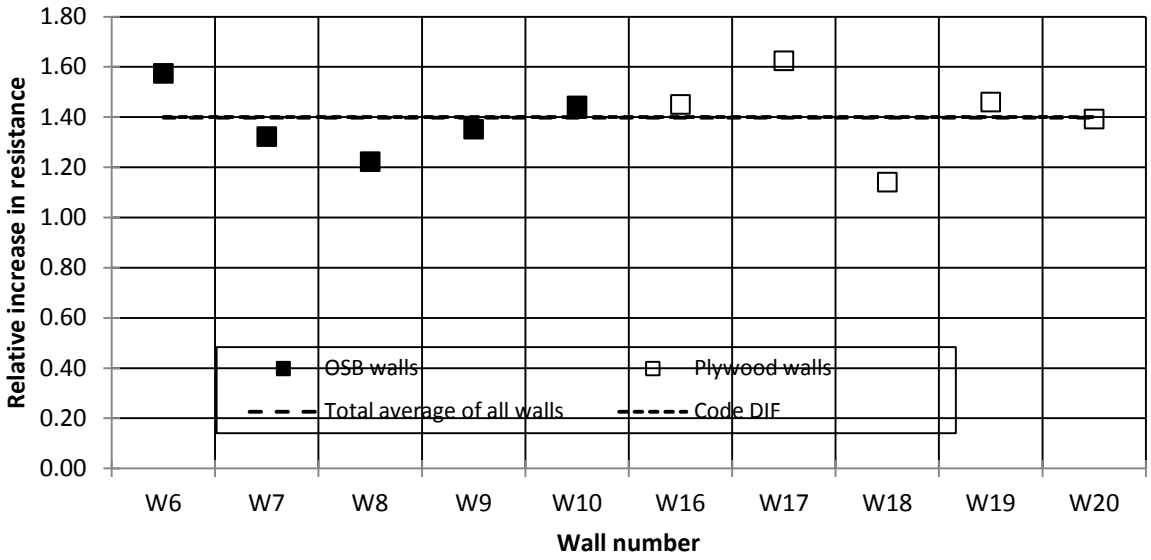

Figure 6.4: Summary of experimental resistance increase

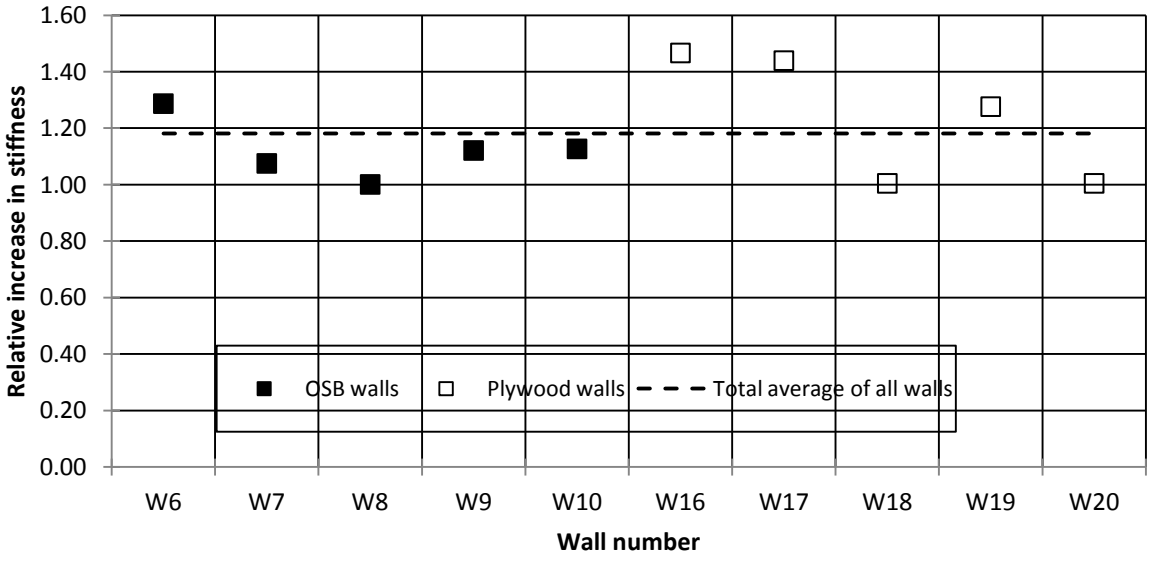

Figure 6.5: Summary of experimental stiffness increase

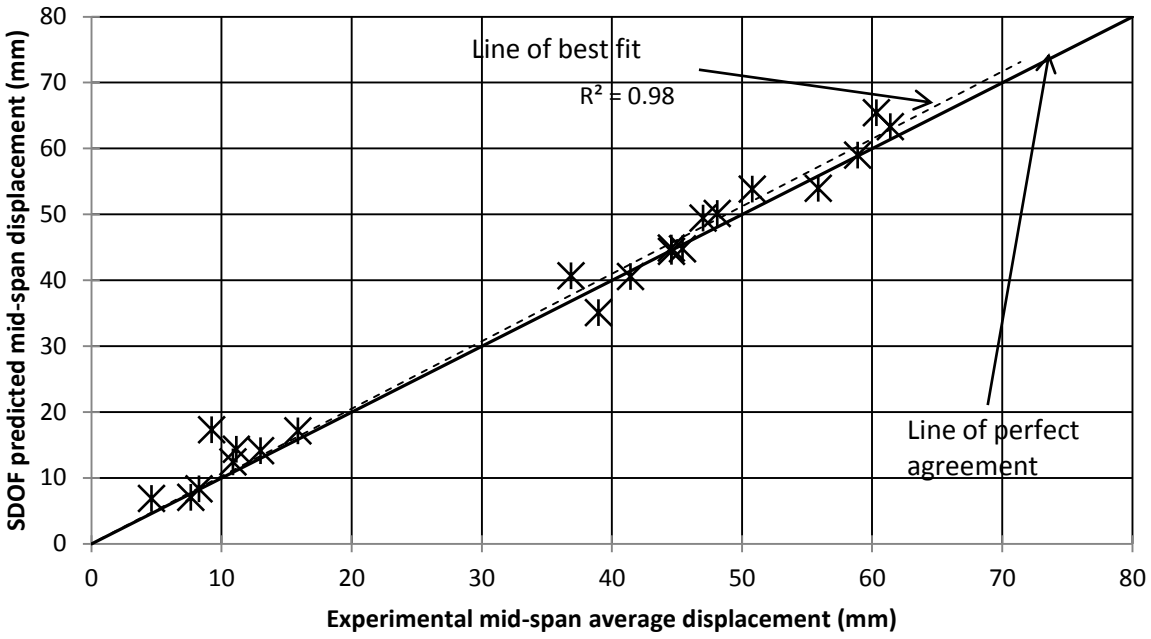

Figure 6.6: Iterative solution SDOF and experimental mid-span displacement comparison

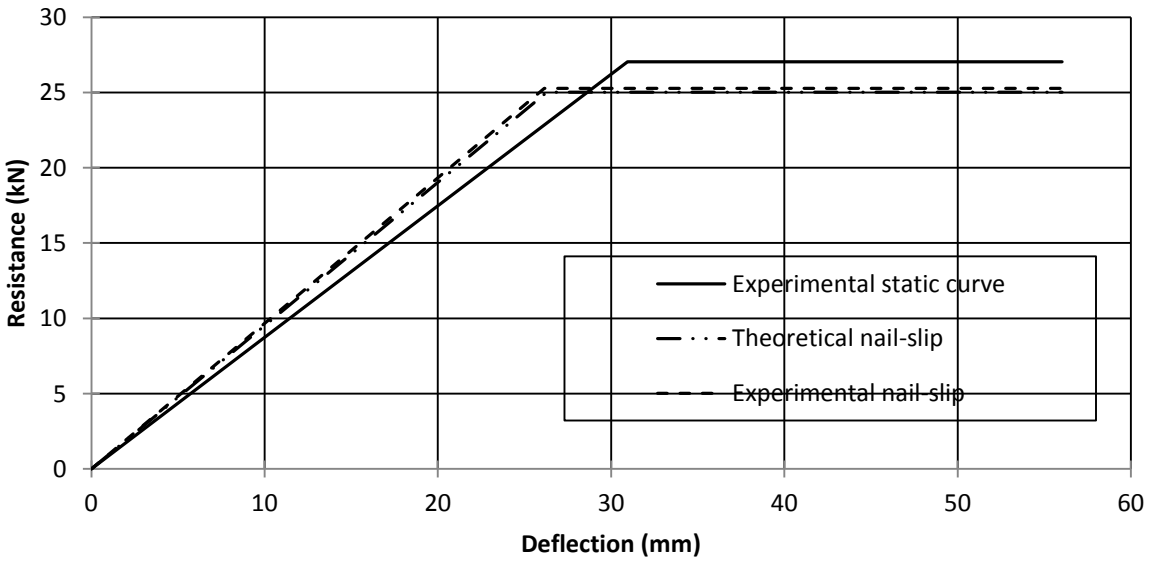

Figure 6.7: Experimental static resistance of OSB T-section compared to that predicted by the partial composite action method

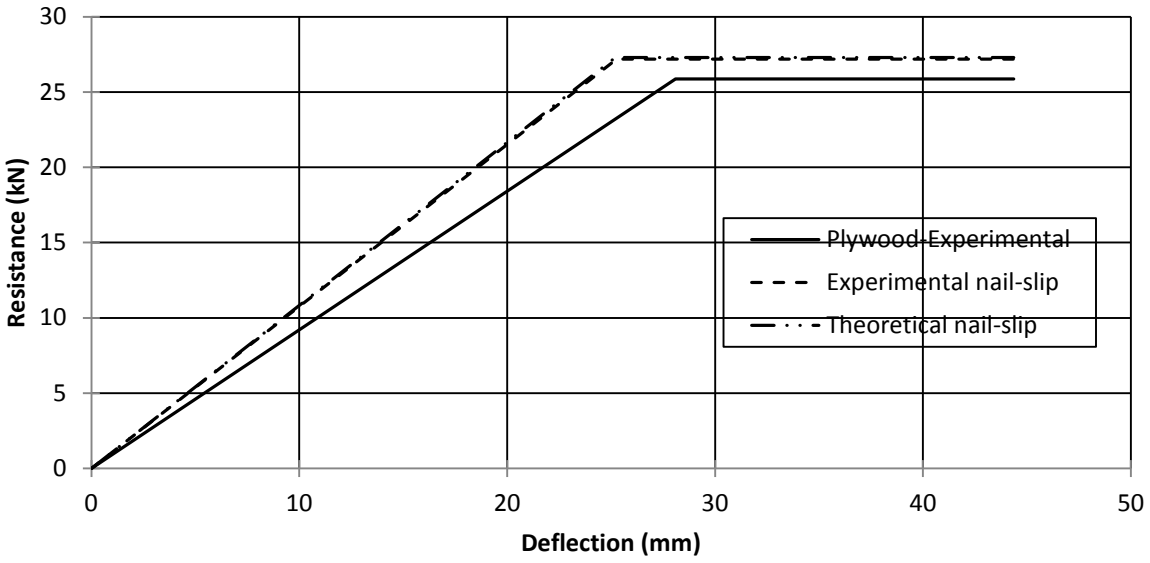

Figure 6.8: Experimental static resistance of plywood T-sections compared to that predicted by the partial composite action method

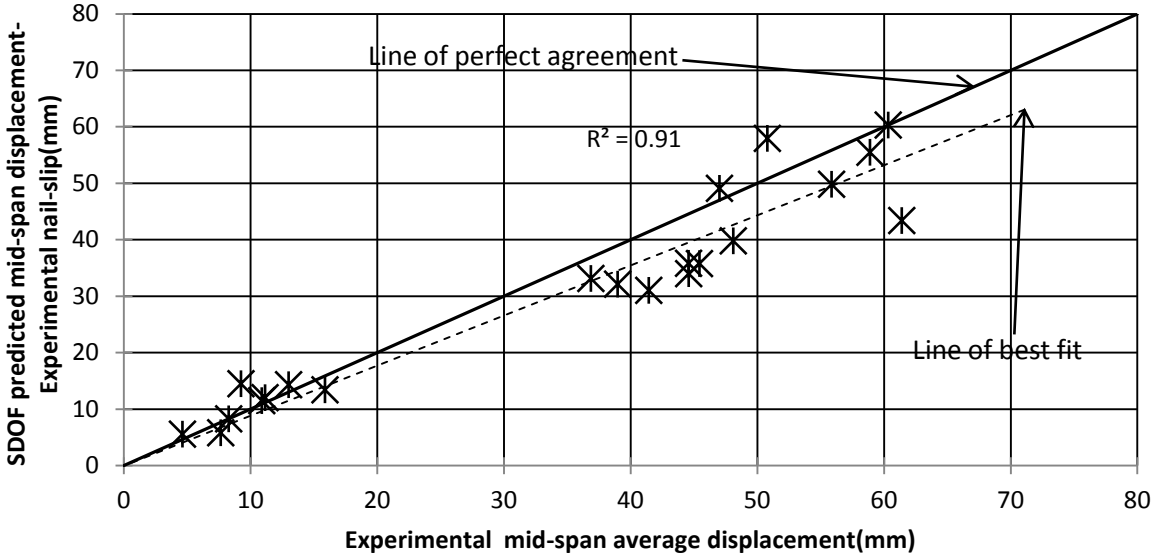

Figure 6.9: Comparison between SDOF predicted displacement using experimental nail-slip to experimental average displacement

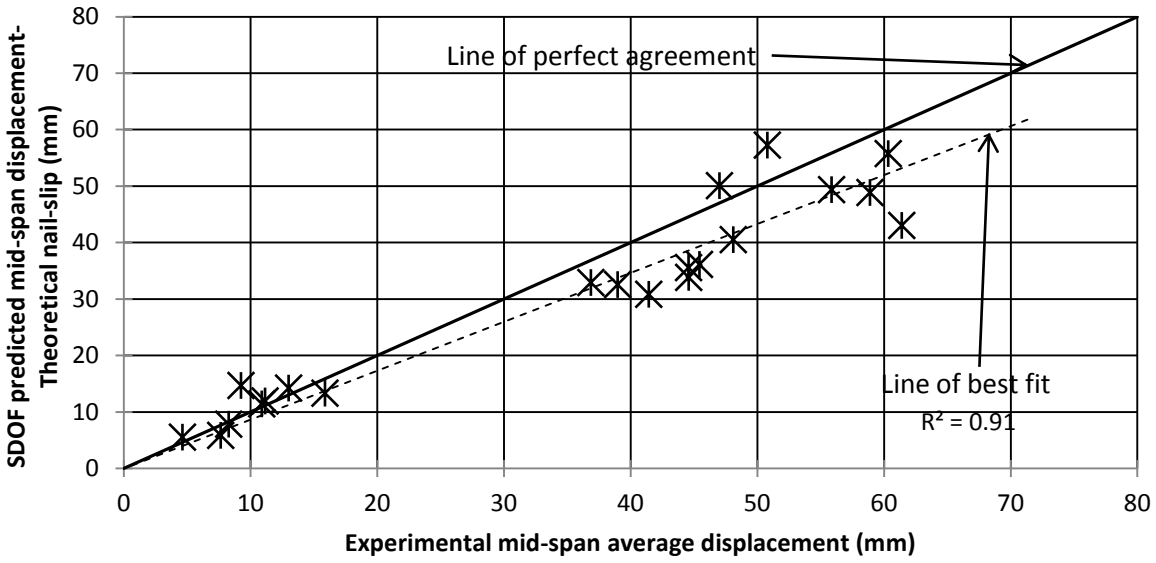

Figure 6.10: Comparison between SDOF predicted displacement using theoretical nail-slip to experimental average displacement

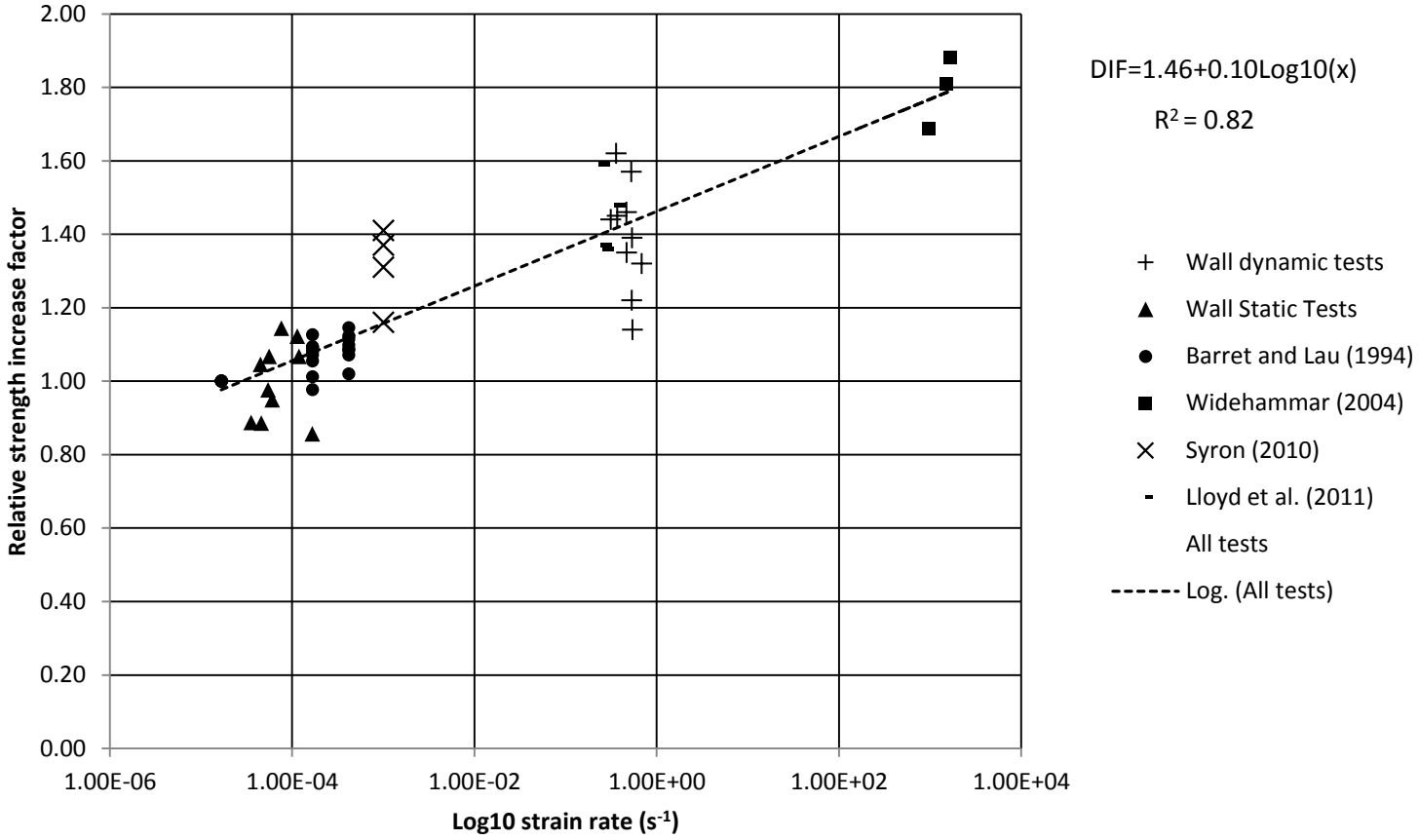

Figure 6.11: Relative increase in strength compared to strain rates

CHAPTER 7-Code Considerations

7.1 Design approach

In order to evaluate the level of safety and conservatism of the design assumptions and code provisions for wood structures, different material models including different analysis assumptions and code simplifications were used. In reality, the designer may not have access to static test data on individual studs or wall systems, thus the model in this chapter includes only published strength and stiffness data. The recently published Canadian blast standard "Design and assessment of buildings subjected to blast loads" (CSA S850-12, 2012) provides guidance on how to obtain the dynamic design strength. Although not specified in the design standard, it was deemed appropriate that a designer would assume that the weight of the wall is that pertaining to the studs and the sheathing whereas the stiffness and resistance of the sheathing is considered negligible. The dynamic bending resistance, S_D, is determined based on the static bending resistance, S_s, modified for high strain rate effects, as shown in Equation 7.1.

$$S_D = SIF\ x\ DIF\ x\ S_s \qquad [7.1]$$

Where SIF is the strength increase factor, DIF is the dynamic increase factor, and S_s is the static bending resistance as calculated using the CSA O86 Standard.

According to the CSA S850, the DIF for MSR lumber is 1.4 and the SIF is 1.5. For the static member strength, shown in Equation 7.2, it is assumed that the load duration factor, K_D, and the material resistance factor, ϕ, are taken as unity as specified in the appendix to the CSA S850.

$$S_s = \emptyset[f_b(K_D K_H K_{Sb} K_T)]SK_{Zb}K_L \qquad [7.2]$$

The service condition for bending at extreme fiber, K_{Sb}, treatment factor, K_T, size factor, K_{Zb}, and lateral stability factor, K_L, are all taken equal to unity. This was deemed appropriate since the experiments were conducted in dry service conditions, the studs were not incised and chemically treated, and the studs were restrained by the sheathing from out-of-plane buckling. Furthermore, for MSR lumber there is no size factor effect. The bending strength,

f_b, of the stud element is based on published strength data for MSR grade 1450f_b-1.3E (21 MPa) and the section modulus, S, is that of the stud alone. The assumption made for calculating the section modulus may vary; here, the approach is the most conservative one, and is believed by the author to be the most common. Figure 7.1 show the resulting dynamic resistance curve for a T-section for both OSB and plywood walls. Since the sheathing is not accounted for in the resistance or the stiffness, the resistance curve for both sheathing types is assumed to be the same. Therefore, the difference between the two T-sections according to the code approach is due to the slight difference in mass between the two systems.

A SDOF analysis was conducted based on the input parameters described here. The analytical results are summarized in Table 7.1, where the ratios of the SDOF displacement and time-to-maximum displacement to those measured experimentally are presented. Figure 7.2 illustrates graphically this approach relative to the displacements measured under the shock tube testing. It is noted that the approach is very conservative. Maximum displacement values obtained here were more than twice those measured. The conservativeness can be attributed to both the strength increase factor value and the contribution of the sheathing to strength and stiffness.

Since the studs were observed to act together until the first peak it can be argued that the load sharing factor should be included in the resistance term. This means that the capacity is increased by a factor of 1.2, as shown in Figure 7.3. The results from the SDOF analysis including the load sharing factor are shown in Table 7.2 and Figure 7.4. It can be observed that the inclusion of the system effect factor in the model reduces the scatter of the data and improves considerably model's capability to predict the displacement, especially at higher deflections.

7.2 Partial composite action method using published values

The theory of partial composite action between the framing member and the sheathing was successfully used by the author to predict the performance of the full scale walls under blast loading. In order to include the sheathing contribution to the stiffness and resistance the method of partial composite action is used together with published strength and stiffness values. The methodology is explained in details in Chapter 5. The input parameters used to

determine the partial composite bending stiffness are shown in Tables 7.5 and 7.6. Since the degree of partial composite action for the OSB and plywood T-sections are not the same, there are two different resistance curves as shown in Figure 7.5 for the method where only the code DIF is applied. The results from the SDOF analysis including the partial composite action with the code DIF only are summarized in Table 7.3 and in Figure 7.6 where the resulting SDOF predicted displacements are compared to the experimental displacements. It can be seen that the accuracy of predicting the displacements at a higher range is greatly improved. The accuracy of predicting the average mid-span displacements is even further improved by replacing the code DIF on the capacity by the ones proposed in this thesis on the capacity and stiffness. The resulting resistance curves are shown in Figure 7.7. The results are summarized in Table 7.3 and Figure 7.8. By including the increase factor on the stiffness the model's fit to the experimental results is further improved for the low and mid-range shots. The model prediction of the high range shots is still too conservative. This can be attributed to the fact that the code's estimate of the SIF. The SIF used in this calculation was based on the code value of 1.5, whereas the actual increase factor for tested walls was on average 1.8. It is to be expected, and desired, that the code provisions yield conservative results especially since the approach in design for extreme loading (e.g. blast, fire) is to use average, rather than design level strength values. It can be concluded that calculating the wall stiffness and strength based on the partial composite action method and incorporating the stiffness increase factor, or simply by adding a load sharing factor, improves the prediction significantly.

7.3 Code implications

Based on the outcome of this research project and the analysis undertaken in section 7.2, the following recommendations for light-frame wood structures are made:

- The DIF of 1.4 on capacity that currently exist in the blast code can be maintained for far field blast loading. For a given strain rate within the range of $1.67E^{-5}$ s^{-1} to $1.65E^{+3}$ s^{-1}, the DIF can be found using Equation 7.3;

$$DIF = 1.46 + 0.1 \log_{10} \dot{\varepsilon} \qquad [7.3]$$

- The resistance function used to determine a wall's behaviour can be that of a bi-linear, elastic-plastic resistance curve;

- The analysis of walls and floors should reflect the system effects either by applying a load sharing factor or by incorporating an expression to account for the contribution of the sheathing to the capacity and stiffness;
- A DIF on the stiffness of 1.18 seems appropriate.

Table 7.1: Summary of experimental response and response predicted by SDOF analysis of code approach

	SDOF maximum displacement ratio, $\frac{d_{SDOF}}{d_{exp-avg}}$			SDOF time-to-maximum displacement ratio, $\frac{d_{SDOF}}{d_{exp-avg}}$			Num. of tests
	Mean	Std dev	COV	Mean	Std dev	COV	
All tests	1.98	0.51	0.26	1.45	0.31	0.22	21
OSB walls	2.07	0.56	0.27	1.52	0.35	0.23	9
Plywood walls	1.91	0.48	0.25	1.40	0.29	0.21	12

Table 7.2: Summary of experimental response and response predicted by SDOF using the system effect factor

	SDOF maximum displacement ratio, $\frac{d_{SDOF}}{d_{exp-avg}}$			SDOF time-to-maximum displacement ratio, $\frac{d_{SDOF}}{d_{exp-avg}}$			Num. of tests
	Mean	Std dev	COV	Mean	Std dev	COV	
All tests	1.64	0.36	0.22	1.29	0.21	0.16	21
OSB walls	1.60	0.46	0.29	1.31	0.23	0.18	9
Plywood walls	1.67	0.28	0.17	1.28	0.20	0.16	12

Table 7.3: Summary of experimental response and response predicted by SDOF using the partial composite action

		SDOF maximum displacement ratio, $\frac{d_{SDOF}}{d_{exp-avg}}$			SDOF time-to-maximum displacement ratio, $\frac{d_{SDOF}}{d_{exp-avg}}$			Num. of tests
		Mean	Std dev	COV	Mean	Std dev	COV	
SDOF-Code DIF	All tests	1.32	0.31	0.23	1.19	0.22	0.19	21
	OSB walls	1.42	0.40	0.28	1.26	0.25	0.20	9
	Plywood walls	1.25	0.20	0.16	1.13	0.18	0.16	12
SDOF-Proposed DIF	All tests	1.18	0.28	0.24	1.14	0.23	0.20	21
	OSB walls	1.28	0.36	0.28	1.22	0.26	0.21	9
	Plywood walls	1.11	0.19	0.17	1.08	0.19	0.17	12

Table 7.4: Parameter input to compute partial composite action

Modulus of elasticity for 11 mm OSB, E (N/mm^2)	6,580
Modulus of elasticity for 18.5 mm plywood, $E_{sheathing}$ (N/mm^2)	6,820
Modulus of elasticity for studs, E_{stud}	9,000
Length between gaps-Sheathing parallel to studs (Span) (mm)	2,032
Nail spacing for both types of wall, s (mm)	150

Table 7.5: Parameter input for theoretical load-slip resistance

Options	Specific gravity of stud	Elastic bearing constant		Nail modulus of elasticity, E_N	Diameter of nail, d_N	Length of nail, L_N	Thickness of	
		Sheathing, k_{01} (N/mm^3)	Stud, k_{02} (N/mm^3)	($x10^3$ N/mm^2)	(mm)	(mm)	Sheathing (mm)	Stud (mm)
OSB	0.498	217	290	200	3.50	63.5	11.0	140.0
Plywood	0.498	217	290	200	4.24	89.0	18.5	140.0

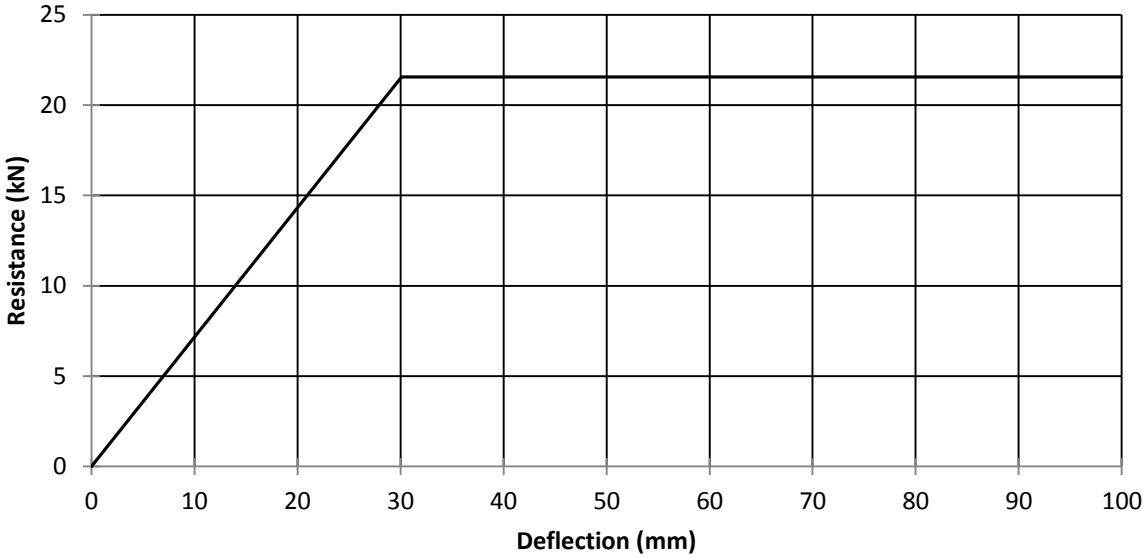

Figure 7.1: Resistance curve using the CSA S850 approach

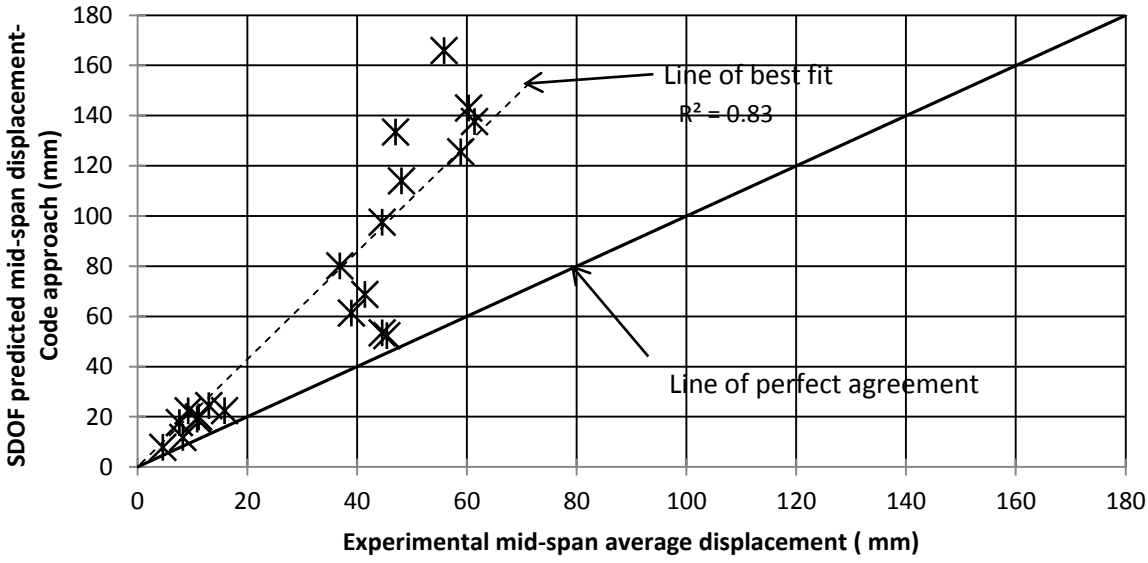

Figure 7.2: Comparison between SDOF predicted displacement using code approach to experimental average displacement

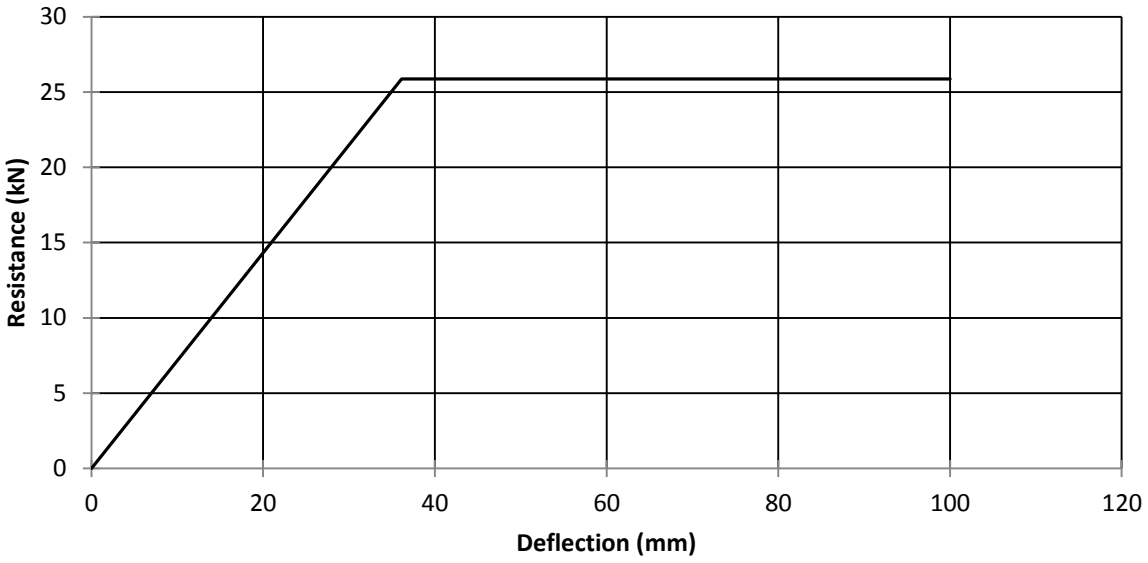

Figure 7.3: Resistance curve using the CSA S850 approach with system effect factor

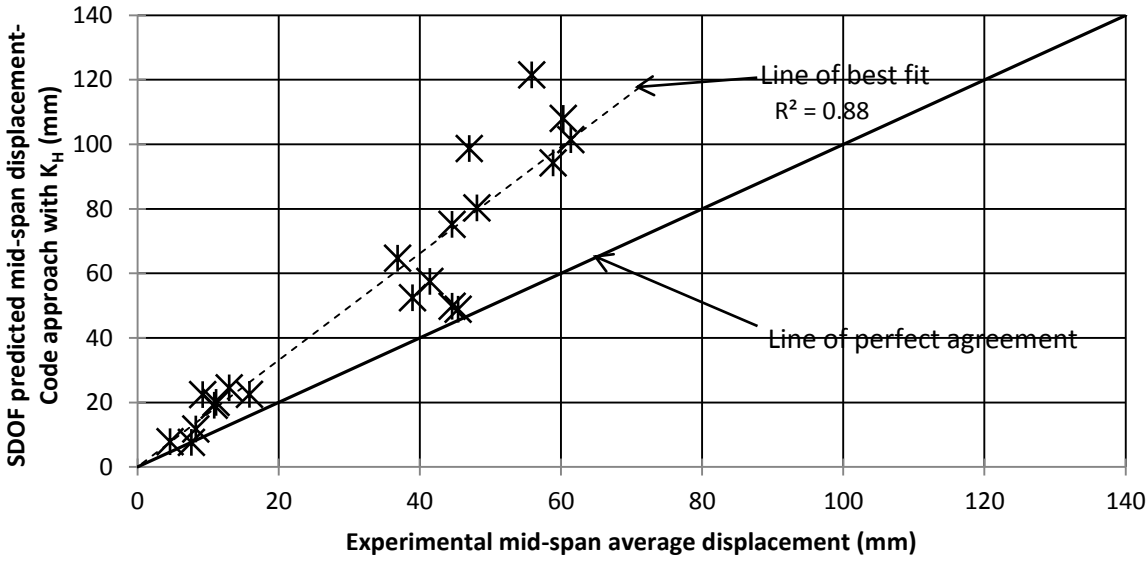

Figure 7.4: Comparison between SDOF predicted displacement using code approach with system effect to experimental average displacement

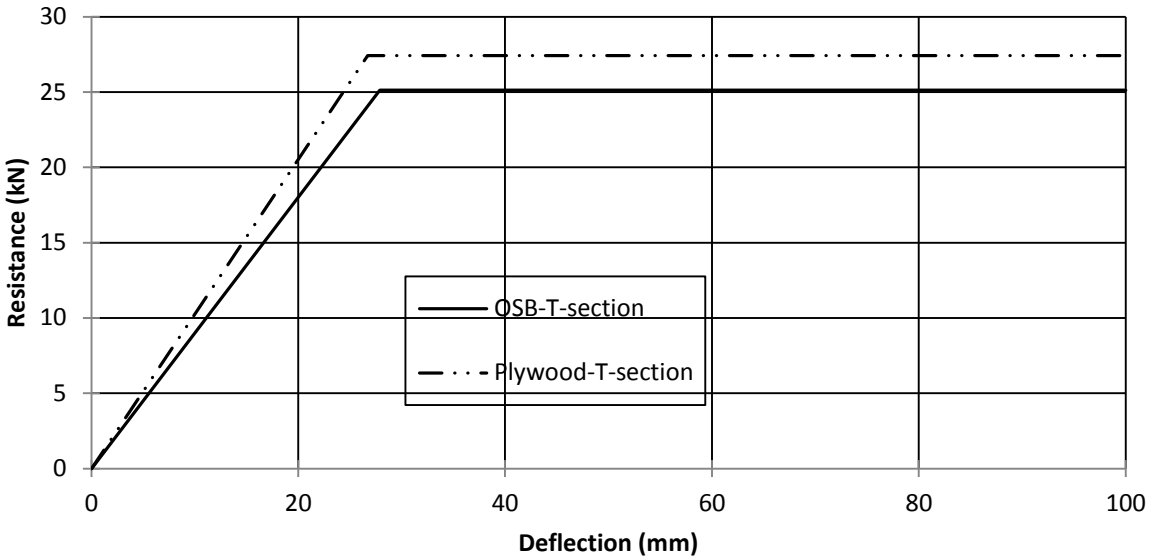

Figure 7.5: Resistance curve using P.C.A along with published values and code DIF

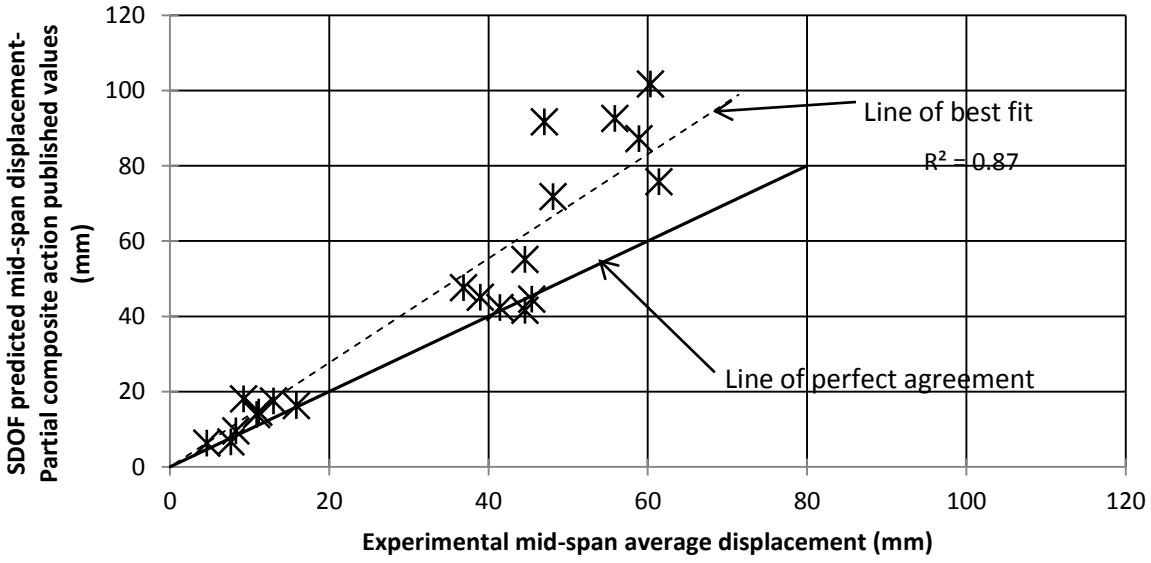

Figure 7.6: Comparison between SDOF predicted displacement using P.C.A along with published values and code DIF to experimental average displacement

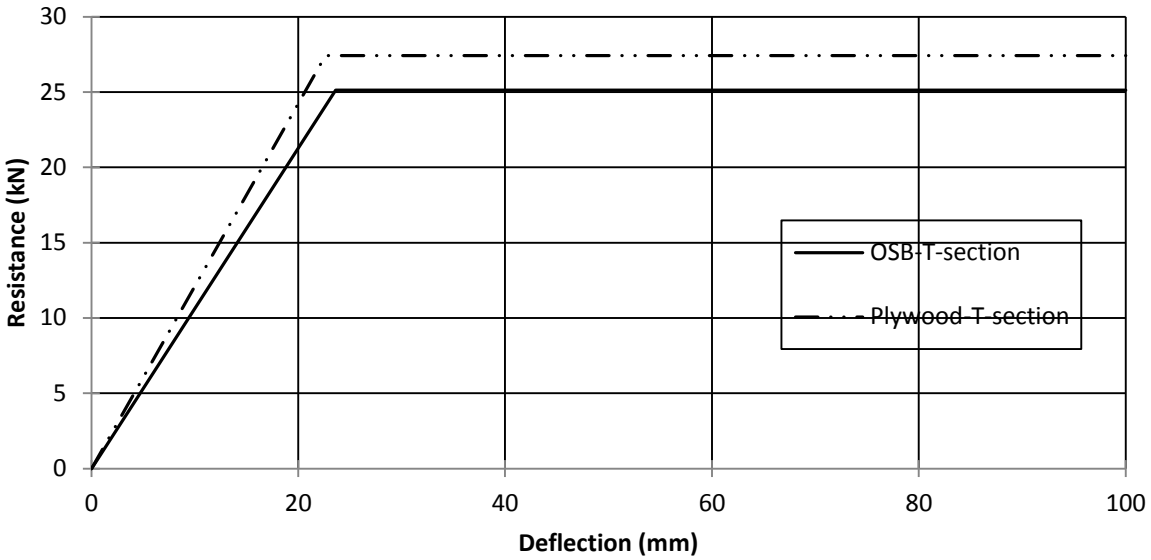

Figure 7.7: Resistance curve using P.C.A along with published values and proposed DIFs

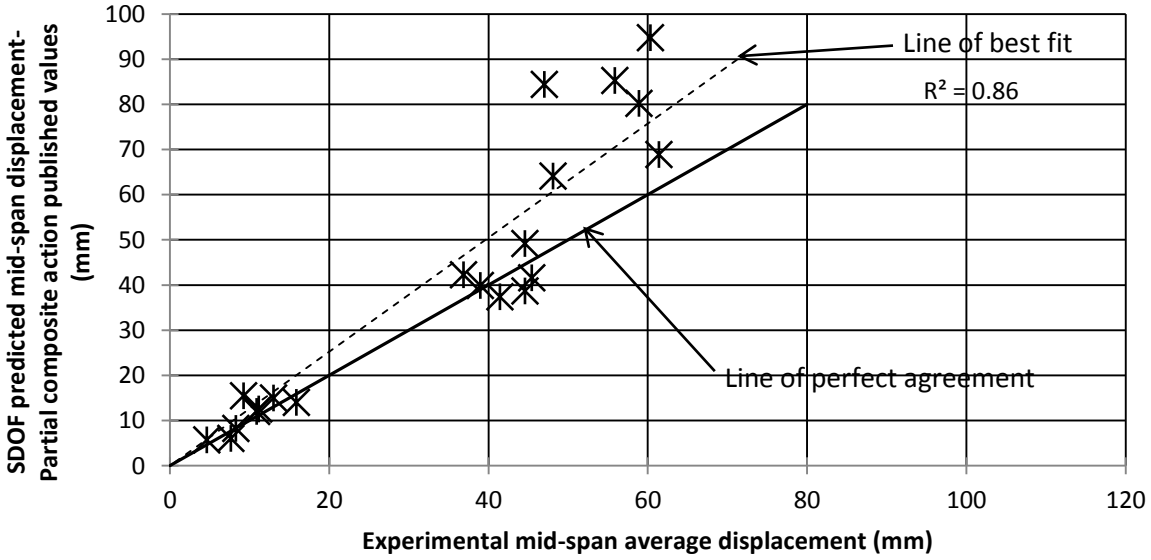

Figure 7.8: Comparison between SDOF predicted displacement using P.C.A. along with published values and proposed DIFs to experimental average displacement

CHAPTER 8-Conclusions

A holistic approach was employed to assess the flexural behaviour of light-frame wood stud walls subjected to blast loading simulated by a shock tube. Strain rates between $1.20E^{-1}$ to $5.48E^{-1}$ s^{-1} were generated. The conclusions that can be made from the current research are:

- A shock tube can be used effectively to generate high strain-rate flexural response in wood members.
- Average dynamic increase factors were derived using SDOF analysis and values of 1.40 and 1.18 on the resistance and stiffness, respectively, were found;
- The resistance curve for walls can be accurately described by a bi-linear elastic-plastic resistance curve.
- An OSB sheathing thickness of 11 mm may not be adequate for blast design as multiple breaching of the sheathing was observed resulting in debris. On the other hand, the 18.5 mm plywood's performance was satisfactory with regard to transferring the load to the stud with minimal or no breaching and debris.
- A material predictive model considering the partial composite action between the sheathing and the stud was found to effectively predict the displacement resulting from blast loading. This novel approach eliminates the need for additional full scale testing of walls.
- Flexural failure of wood light-frame walls was observed in all cases when loaded statically and dynamically. Nail withdrawal was also observed, primarily due to the high negative pressures.
- Damage levels were established based on both the severity of the damage for individual component and the number of failed components. Although systematic, this evaluation was obviously subjective, and many more stud wall tests are needed before such assessment is reliable.
- The material predictive model using only published data and code provisions was found to provide reasonable and conservative estimates of the deflection. Including the load sharing factor seemed to provide a simple method of accounting for the system effects in the wall. Similarly, the material predictive model using published

material data while using the DIFs proposed on the resistance and stiffness was found to provide the best estimates of the deflection.

8.1 Recommendations for future work

Based on the current research, the following areas have been identified for future work:

- One of the main areas of limitation of this study was focusing the research in the behaviour within the wall subsystem, and disregarding the effects of connection between the wall and floor or roof subsystem. If failure is to occur in the connections, the system may fail prematurely because the wall subsystem would not have reached its ultimate capacity. This may also cause the wall to become projectile, injuring or killing the occupants of the building. Developing connections suitable for blast design, where the capacity of the connector exceeds the wall capacity (or dynamic reaction near the ultimate capacity of the wall), would be desirable.
- An investigation of the sequence of failure between studs and sheathing need to be investigated and established. Similar to the argument made in the previous point, a sheathing failure would mean that the studs may not achieve their full capacity and it could also lead to debris throw of the failed sheathing pieces. Recommendations on the interplay between stud spacing, sheathing thickness and stud size could be developed.
- The effect of nail withdrawal on the capacity of the wall subsystem needs to be investigated. It is recommended that an investigation of other types of connectors, such as screws and glue, take place. This would improve the withdrawal capacity of joints between sheathing and studs and enhance the partial composite action when the wall is subjected to negative pressure.
- Finally, the current study dealt with the primary structural elements in the wall with no considerations for the non-structural elements such as gypsum wallboard (GWB), insulation, siding, etc. Some of these non-structural elements could have a significant effect on the global behaviour of the wall as they could potentially add mass and stiffness to the system. However, GWB is known to be a brittle material and when loaded out-of-plane may cause significant debris that could become projectiles and therefore resulting in injuries or casualties. An investigation of replacing the interior

layer of GWB with sheathing panel would be interesting, as this would provide more symmetry to the wall, increase its capacity and possibly its ductility.

REFERENCES

AFH 10-2401. (2006). Force Protection Battlelab Vehicle Bomb Mitigation Guide (pp. 162): USAF Force Protection Battlelab.

API RP 753. (2012). Management of Hazards Associated with Location of Process Plan Portable Buildings. Washington, D.C.: American Petroleum Institute Publishing Services.

ASTM D198-09. (2009). Static Tests of Lumber in Structural Sizes (pp. 26). West Conshohocken, PA: ASTM International.

ASTM D1037-06a. (2006). Evaluating Properties of Wood-Base Fiber and Particle Panel Materials (pp. 30). West Conshohocken, PA: ASTM International.

ASTM D1761-12. (2012). Mechanical Fasteners in Wood (pp. 10). West Conshohocken, PA: ASTM International.

ASTM D2915-10. (2010). Sampling and Data-Analysis for Structural WOod and Wood Based Products (pp. 14). West Conshohocken, PA: ASTM International.

ASTM E2126-11. (2011). Cyclic (Reversed) Load Test for Shear Resistance of Vertical Elements of the Lateral Force Resisting Systems for Buildings (pp. 15). West Conshohocken, PA: ASTM International.

Barrett, J. D., & Lau, W. (1994). Canadian Lumber Properties. Ottawa, Ontario: Canadian Wood Council.

Biggs, J. M. (1964). *Introduction to structural dynamics*. New York,: McGraw-Hill.

Bill 9. (2009). Wood First Act,. Retrieved 27/04/2013, 2013, from http://www.leg.bc.ca/39th1st/1st_read/gov09-1.htm

Brokaw, M., P., & Foster, G., W. (1958). Effect of rapid loading and duration of stress on the strength properties of wood tested in compression and flexure (pp. 69). Madison, Wisconsin: Forest Products Laboratory

Forest Service

U.S. Department of Agriculture.

Burell, R. (2012). *Performance of steel fibre reinforced concrete columns under shock tube induced shock wave loading.* (M.A.Sc.), University of Ottawa, Ottawa, Canada,.

Ciornei, L. (2012). *Performance of polyurea retrofitted unreinforced concrete masonry walls under blast loading.* (M.A.Sc.), University of Ottawa, Ottawa,Canada,.

Cline, M. (1908). Forest Service Tests to Determine the Influence of Different Methods and Rates of Loading on the Strength and Stiffness of Timber. *Proceedings American Society Testing Materials, 8*.

Cormie, D., Mays, G., & Smith, P. (2009). *Blast effects on buildings*. Reston, VA: Thomas Telford.

CSA O86-09. (2009). Engineering design in wood.

CSA S850-12. (2012). Design and assessment of buildings subjected to blast loads (pp. 126). Mississauga, Ontario, Canada: CSA Group.

Dusenberry, D., O. (2010). *Handbook for blast-resistant design of buildings*. Hoboken, N.J.: J. Wiley.

Foschi, R., O. (1985). Wood floor behavior: Experimental Study. *Journal of Structural Engineering, 111*(11), 12.

Glasstone, S., & Dolan, P., J.,. (1977). The Effects of Nuclear Weapons (United States Department of Defense & E. R. a. D. Administration, Trans.) (3rd ed.). Washington, D.C.,: United States Department of Defense,

Energy Research and Development Administration.

Humar, J., L. (2005). *Dynamics of Structures* (2 ed.). AK Leiden, The Netherlands: Taylor & Francis / Balkema.

Jacques, E. (2011). *Blast Retrofit of Reinforced Concrete Walls and Slabs.* (Master of Applied Science), University of Ottawa, Ottawa.

Jacques, E. (2013). RCBLAST (Version 0.4.1). Retrieved from http://www.rcblast.ca

Johnson, W. (1986). Historical and Present-Day References Concerning Impact on Wood. *International Journal of Impact Engineering, 4*(3), 14.

Kimbell, R., G., & Fies, J. (1953). Two Typical Wood Frame Houses Exposed to Energy Released by Nuclear Fission (pp. 16). Washington, D.C.: National Lumber Manufacturers Association.

Krauthammer, T. (2008). *Modern protective structures*. Boca Raton, FL: CEC Press.

Lacroix, D., & Doudak, G. (2012). *Behaviour of typical light-frame wood stud walls subjected to blast loading*, Auckland.

Liska, J., A. (1950). Effect of rapid loading on the compressive and flexural strength of wood (pp. 77). Madison, Wisconsin: United States Department of Agriculture

Forest Service

Forest Products Laboratory.

Lloyd, A. (2010). *Performance of Reinforced Concrete Columns Under Shock Tube Induced Shock Wave Loading.* (Master of Applied Science), University of Ottawa, Ottawa.

Lloyd, A., Jacques, E., Abdelalim, O., Saatcioglu, M., Braimah, A., & Doudak, G. (2011). *High Strain-Rate Effects on the Dynamic Material Properties of Timber Beams*. Paper presented at the 2nd International Engineering Mechanics and Materials Specialty Conference, Ottawa, Ontario, Canada.

McCutcheon, W., J. (1977). Method for predicting the stiffness of wood-joist floor systems with partial composite action (pp. 18). Madison, Wisconsin: U.S.D.A. Forest Service.

McCutcheon, W., J. (1986). Stiffness of framing members with partial composite action. *Journal of Structural Engineering, 112*(7), 15.

Mindess, S., & Madsen, B. (1986). The fracture of wood under impact loading. *Materials and Structures/Materiaux et Constructions, 19*(1), 5.

Mindess, S., Madsen, B., & Yan, C. (1988). *Behaviour of timber beams under impact loading*. Paper presented at the Colloque Scientifique Europeén: Comportement Mécanique du Bois, Bordeaux, France.

NAHB. (1961). The effect of framing and subfloor attachment on the stiffness of residential floors (pp. 59). Rockville, Maryland: National Association of Home Builders.

National Research Council of Canada. (2010). National Building Code of Canada. Ottawa: National Research Council of Canada,.

Office of the Deputy Prime Minister. (2004). Disproportionate Collapse, The Building Regulations 2000 (revised 2004) (pp. 5).

Oswald, C. J. (2005). Component Explosive Damage Assessment Workbook (CEDAW) Methodology Manual V1.0 (pp. 140). San Antonio, TX: Baker Engineering and Risk Consultants, Inc.

Parlin, N. J. (2010). *Behavior of FRP-Coated Wood Panels Under Dynamic Loading.* University of Maine, University of Maine.

Polensek, A., Atherton, G., H., Corder, S., E., & Jenkins, J., L. (1972). Response of nailed wood-joist floors to static loads. *Forest Products Journal, 22*(9), 10.

Randall, P., A. (1955). Damage to Conventional and Special Types of Residences Exposed to Nuclear Effects (W. Housing and Home Finance Agency, D.C., Trans.) (pp. 53). Battle Creek, Michigan.

Smith, S., B. (1952). Reaction of Buildings to Atomic Blast. *The Military Engineer, 44*(301), 9.

Spencer, R. (1978). *Rate of loading effect in bending for Douglas-fir lumber*. Paper presented at the 1st International Conference on Wood Fracture, Banff, Alberta, Canada.

Sukontasukkul, P., Lam, F., & Mindess, S. (2000). Fracture of parallel strand lumber (PSL) under impact loading. *Materials and Structures/Materiaux et Constructions, 33*(August-September), 5.

Syron, W. D. (2010). *Strain Rate-Dependent Behavior of Laminated Strand Lumber.* University of Maine, University of Maine.

Tang, M., J.,, & Baker, Q., A.,. (1999). A new set of blast curves from vapour cloud explosion. *Process Safety Progress, 18*(4), 6.

Tiemann, H., D. (1908). The Effect of Speed of Testing Upon the Strength of Wood and the Standardization of Tests for Speed. *Proceedings American Society Testing Materials, 8*.

TM 5-1300. (1990) Structures to Resist Effects of Accidental Explosions, . *Technical Manual 5-1300*. Washington, DC: Department of the Army, Navy and Air Force.

U.S.A.C.E PDC. (2008a). Methodology Manual for the Single-Degree-of-Freedom Blast Effects Design Spreadsheets (SBEDS) (pp. 227): U.S. Army Corps of Engineers Protective Design Center Technical Report.

U.S.A.C.E PDC. (2008b). Single Degree of Freedom Structural Response Limits for Antiterrorism Design (Revision 1 ed., pp. 35): U.S. Army Corps of Engineers Protective Design Center.

Unified Facilities Criteria (UFC) 03-340-02. (2008). Structures to Resist the Effects of Accidental Explosions (pp. 1943). Washington, D.C.: United States of America Department of Defense.

Unified Facilities Criteria (UFC) 4-023-03. (2009). Design of Buildings to Resist Progressive Collapse (pp. 181). Washington, DC: United States of America Department of Defense,.

US Federal Emergency Management Agency (FEMA). (2011). Reference Manal to Mitigate Potential Terrorist Attacks against Buildings (pp. 514). Washington, DC.

Van Den Berg, A., C.,. (1985). The multi-energy method-A framework for vapour cloud blast prediction. *Journal of Hazardous Materials, 12*(1), 10.

Wheat, D., L., Gromala, D., S., & Moody, R., C. (1986). Static behavior of wood-joist floors at various limit states. *Journal of Structural Engineering, 112*(7), 15.

Widehammar, S. (2004). Stress-Strain Relationships for Spruce Wood: Influence of Strain Rate, Moisture Content and Loading Direction. *Experimental Mechanics, 44*(1), 5. doi: 10.1177/0014485104039748

Wilkinson, T., Lee. (1972). Effect of deformed shanks, prebored lead holes, and grain orientation on the elastic bearing constant for laterally loaded nail joints (pp. 15). Madison, Wisconsin: U.S.D.A. Forest service.

Wilkinson, T., Lee. (1974). Elastic bearing constants for sheathing materials (pp. 10). Madison, Wisconsin: U.S.D.A. Forest Service.

APPENDIX A-Static Test Results

Wall 1, Static Destructive Test

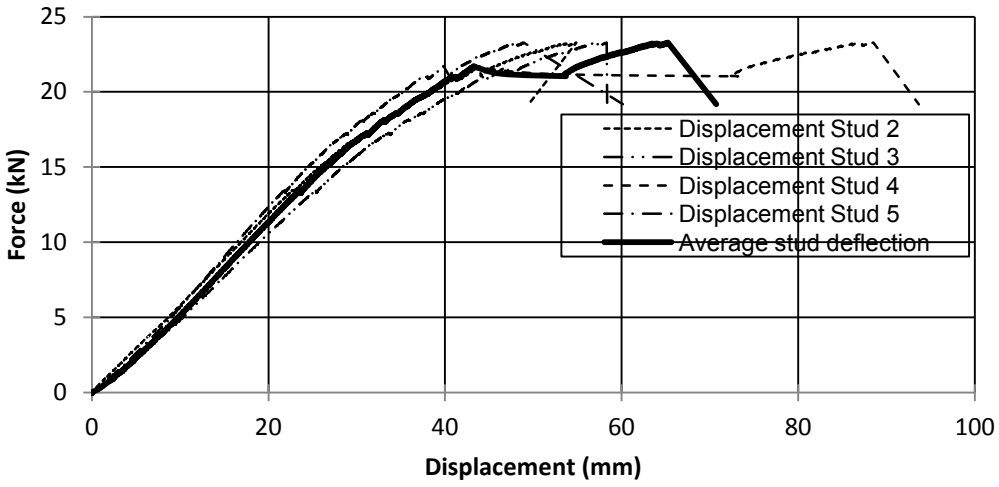

Figure A1.1: Experimental force displacement for Wall 1

(a) View from right side (b) View from left side

Figure A1.2: Static wall damage for Wall 1

*Comments: Studs number 1 to 4 failed in bending while no damage was observed on the remaining studs. Stud 5 experienced minor cracks on the compression side at mid-span. Neither sheathing failure nor nail withdrawal was observed.

Wall 2, Static Destructive Test

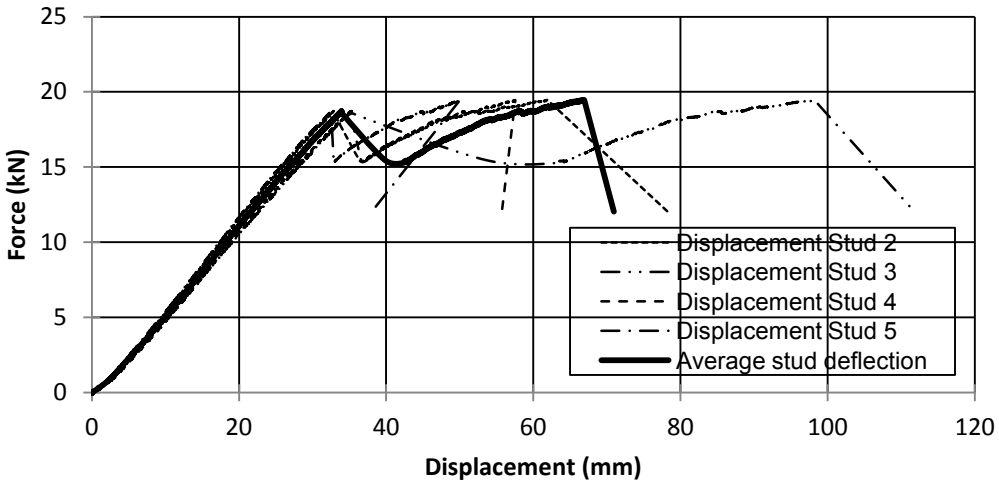

Figure A2.1: Experimental force displacement for Wall 2

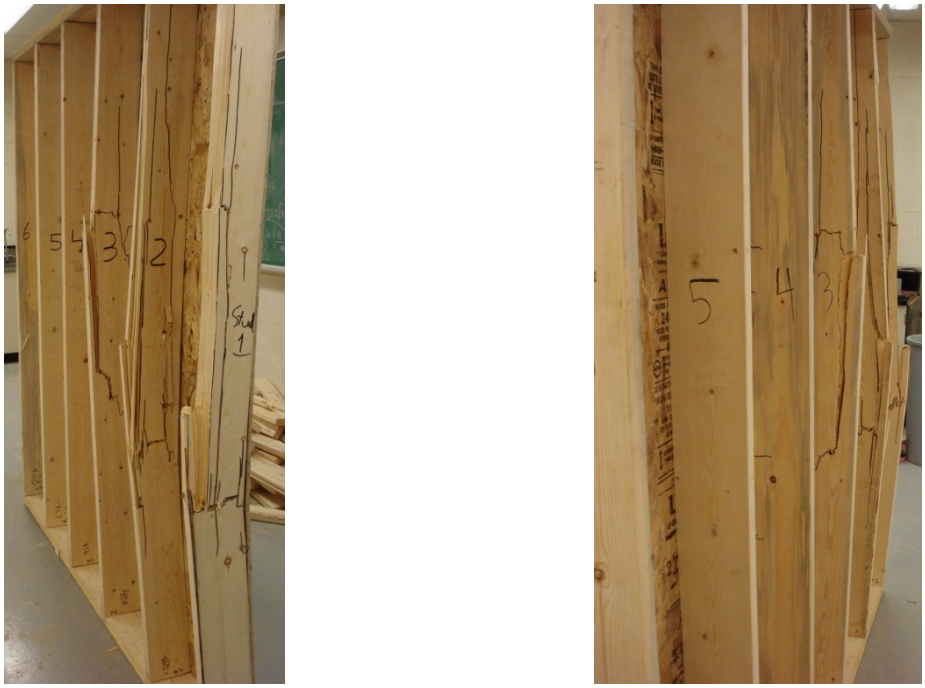

(a) View from right side (b) View from left side

Figure A2.2: Static wall damage for Wall 2

*Comments: Studs number 1 to 3 failed in bending while no damage was observed on the remaining studs. Studs 4 and 5 experienced minor cracks on the compression side at mid-span. Neither sheathing failure nor nail withdrawal was observed.

Wall 3, Static Destructive Test

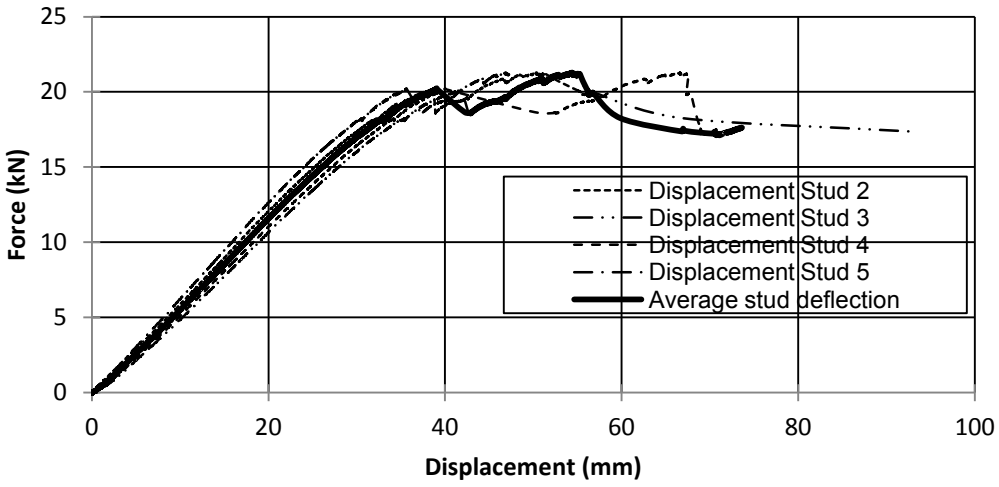

Figure A3.1: Experimental force displacement for Wall 3

(a) View from right side (b) Nail withdrawal

Figure A3.2: Static wall damage for Wall 3

*Comments: Studs number 1 to 4 failed in bending while no damage was observed on the remaining studs. The sheathing was cracked between Studs 1 and 2. Nail withdrawal was observed on the studs that experienced the most deflection.

Wall 4, Static Destructive Test

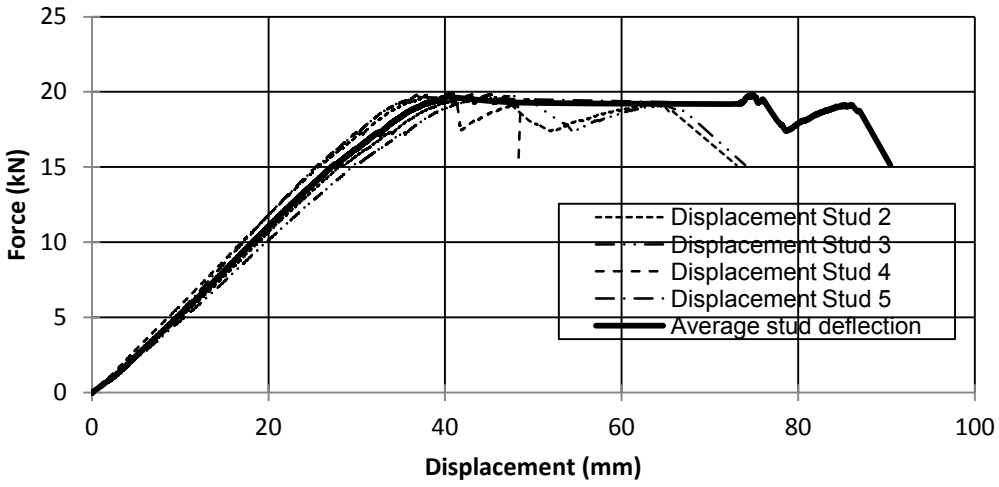

Figure A4.1: Experimental force displacement for Wall 4

(a) View from right side

(b) View from left side

Figure A4.2: Static wall damage for Wall 4

*Comments: Studs number 4 to 6 failed in bending while no damage was observed on the remaining studs except for stud number 2 where minor cracks on the tension side at mid-span were observed. Neither sheathing failure nor nail withdrawal was observed.

Wall 5, Static Destructive Test

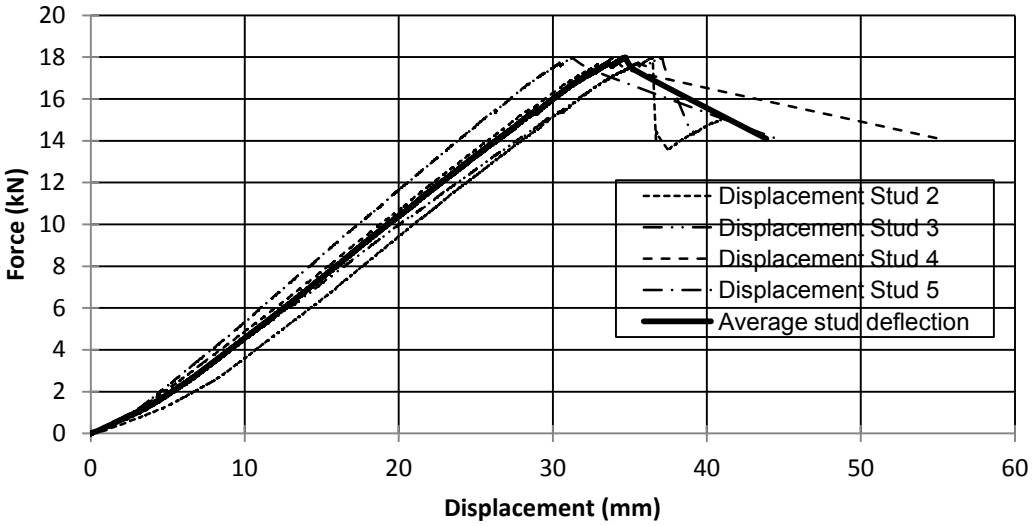

Figure A5.1: Experimental force displacement for Wall 5

(a) View from right side (b) View from left side

Figure A5.2: Static wall damage for Wall 5

*Comments: Studs number 2 to 4 failed in bending. Studs number 5 and 6 had cracks on the tension side at mid-span. Stud number 1 had minor cracks on the compression side at mid-span. Neither sheathing failure nor nail withdrawal was observed.

Wall 11, Static Destructive Test

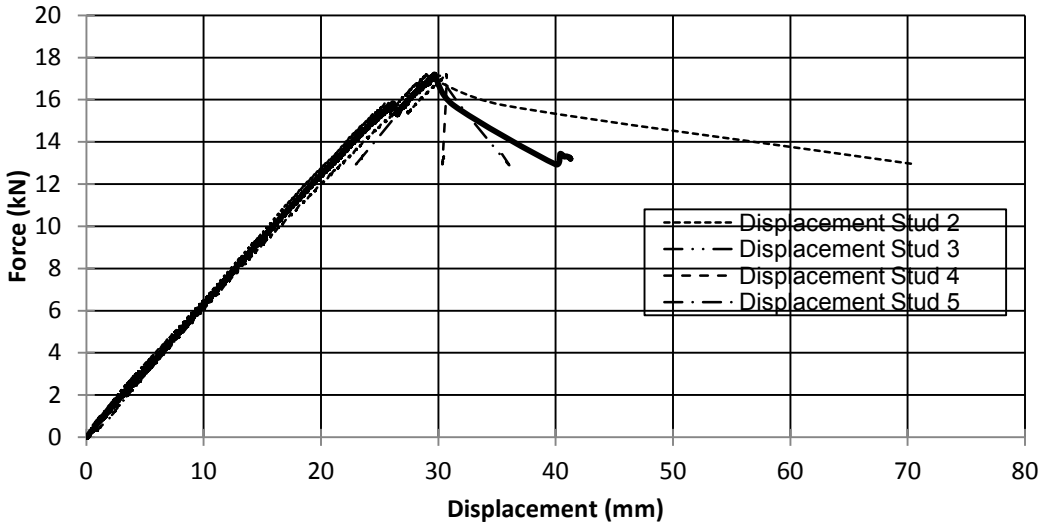

Figure A11.1: Experimental force displacement for Wall 11

(a) View from right side (b) View from left side

Figure A11.2: Static wall damage for Wall 11

*Comments: Studs number 1 to 3 failed in bending. Stud number 5 and 6 experienced minor cracks on the tension side at mid-span. Neither sheathing failure nor nail withdrawal was observed.

Wall 12, Static Destructive Test

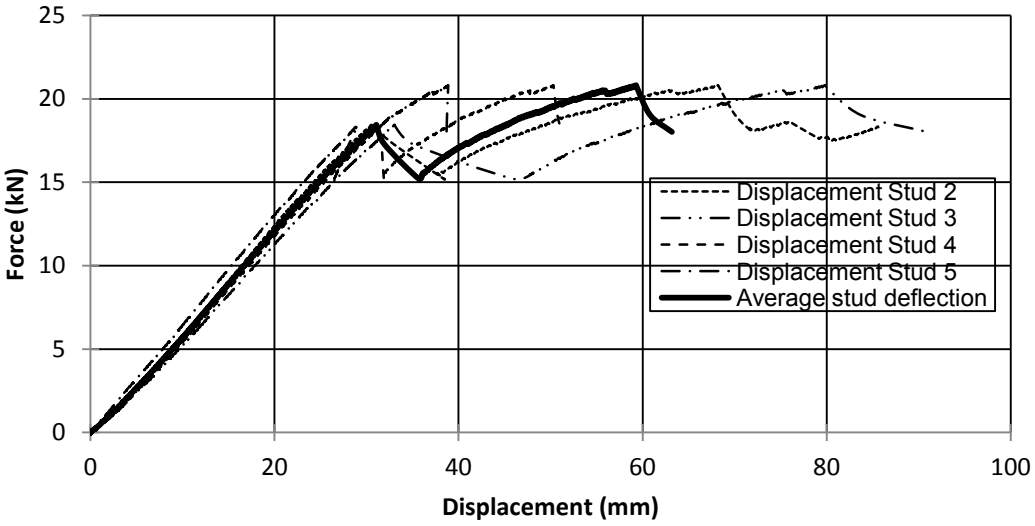

Figure A12.1: Experimental force displacement for Wall 12

(a) View from right side (b) Sheathing failure

Figure A12.2: Static wall damage for Wall 12

*Comments: Studs number 1 to 3 failed in bending. Stud 5 experienced minor cracks on the compression side at mid-span. The sheathing was cracked at mid-span between Studs 1 and 2 as well as Studs 2 and 3. Minor nail withdrawal was observed.

Wall 13, Static Destructive Test

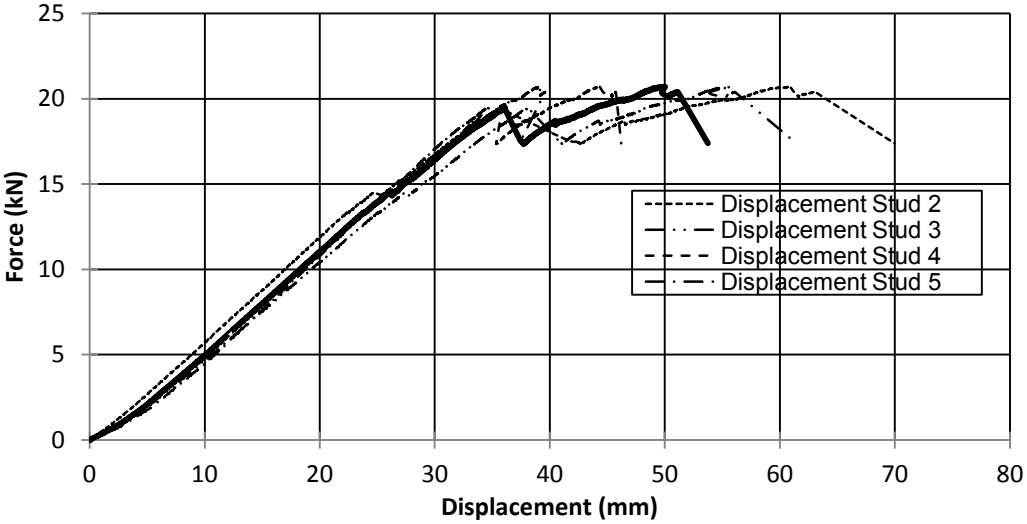

Figure A13.1: Experimental force displacement for Wall 13

(a) View from right side (b) View from left side

Figure A13.2: Static wall damage for Wall 13

*Comments: Studs number 4 to 6 failed in bending while no damage was observed on the remaining studs. Stud 3 had a crack on the tension side along the length of the stud. Neither sheathing failure nor nail withdrawal was observed.

Wall 14, Static Destructive Test

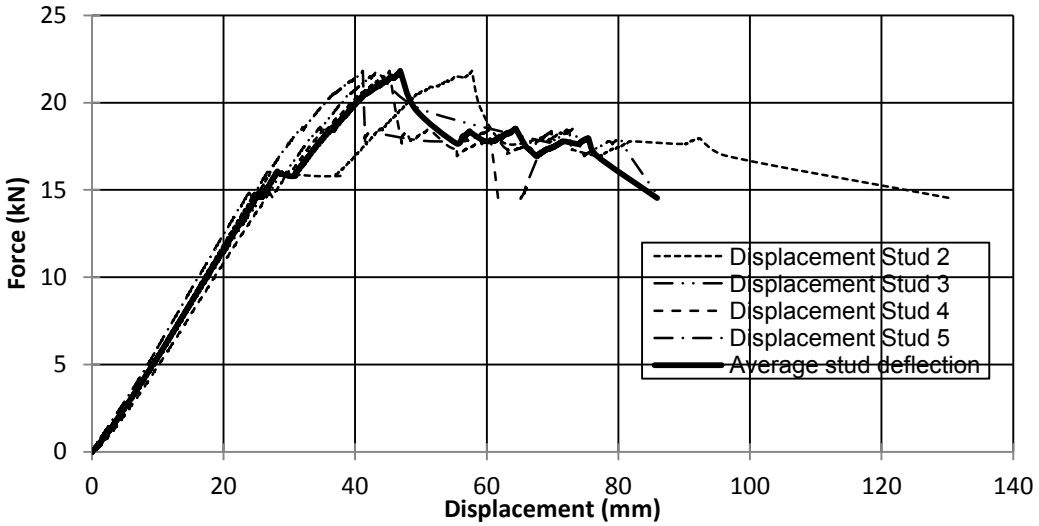

Figure A14.1: Experimental force displacement for Wall 14

(a) View from right side (b) View from left side

Figure A14.2: Static wall damage for Wall 14

*Comments: Studs number 1 to 4 failed in bending. Stud 5 had minor cracks on the tension side. Neither sheathing failure nor nail withdrawal was observed.

Wall 15, Static Destructive Test

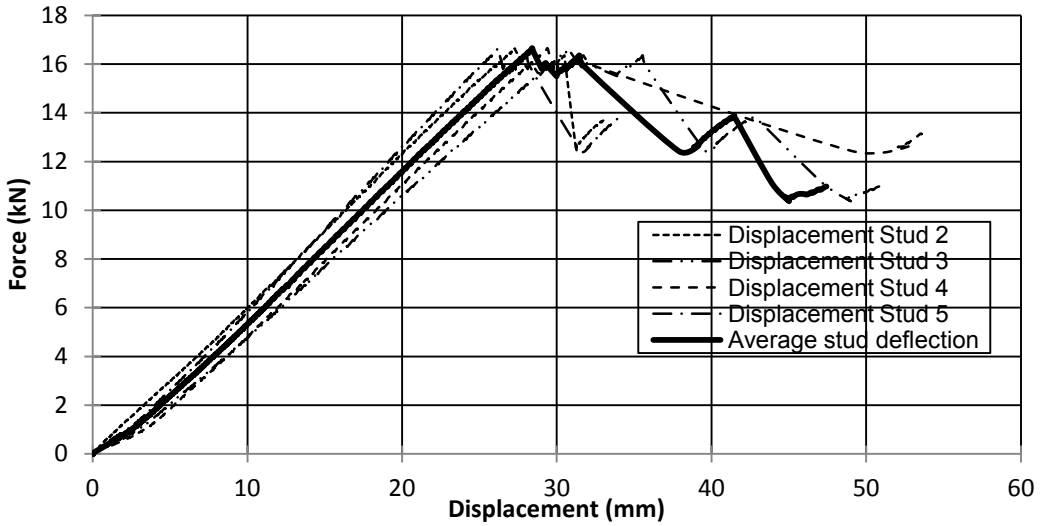

Figure A15.1: Experimental force displacement for Wall 15

(a) View from right side (b) View from left side

Figure A15.2: Static wall damage for Wall 15

*Comments: Studs number 3 to 6 failed in bending while no damage was observed on the remaining studs. Neither sheathing failure nor nail withdrawal was observed.

APPENDIX B-Dynamic Test Results

Wall 6, Pressure-Impulse Combination Number 1

Table B6-1: Wall 6, Shot 1-Test result summary

Light-Frame Stud Wall Dynamic Tests: Wall 6, Pressure-Impulse Combination Number 1

Test name:	Wall_6_Shot_1	**Test date:**	16/12/2012
Driver length:	2,745 **mm**	**Driver pressure:**	63.4 **kPa**

Test specimen description:

-38 mm x 140 mm MSR studs @ 406.4 mm o/c. -11 mm OSB

-Nails, 64 mm x 3.50 mm @150 mm o/c (field and edge)

-2,159 mm total height of wall -2,083 mm long studs -2,032 mm clear span

Average maximum reflected pressure:	-	**kPa**	**Wall mass:**	76.0	**kg**
Average maximum reflected impulse:	-	**kPa-ms**			
Experimental positive phase:	-	**ms**			
Theoretical positive phase:	-	**ms**			
Average deflection of wall studs:	-	**mm**			
Average time to maximum deflection:	-	**ms**			
Quantified wall damage:	**Superficial**				

Stud number	Stud reference name	Max. Disp.	Time to max.	Stud damage
		mm	ms	
1	72A	-	-	No damage
2	114A	-	-	No damage
3	70A	-	-	No damage
4	44A	-	-	No damage
5	127A	-	-	No damage
6	112A	-	-	No damage

General comments and response description:

The wall did not suffer any damage and remained elastic throughout its displacement history. Due to an instrumentation error, no data was recorded to the PC from the data acquisition system for that shot.

Wall 6, Pressure-Impulse Combination Number 2

Table B6-2: Wall 6, Shot 2-Test result summary

Light-Frame Stud Wall Dynamic Tests: Wall 6, Pressure-Impulse Combination Number 2

Test name:	Wall_6_Shot_2	**Test date:**	16/12/2012
Driver length:	2,745 **mm**	**Driver pressure:**	260.0 **kPa**

Test specimen description:

-6-38 mm x 140 mm MSR studs @ 406.4 mm o/c. -11 mm OSB

-Nails, 64 mm x 3.50 mm @150 mm o/c (field and edge)

-2,159 mm total height of wall -2,083 mm long studs -2,032 mm clear span

Average maximum reflected pressure:	38.3	**kPa**	**Wall mass:**	76.0	**kg**
Average maximum reflected impulse:	403.0	**kPa-ms**			
Experimental positive phase:	22.0	**ms**			
Theoretical positive phase:	21.0	**ms**			
Average deflection of wall studs:	47	**mm**			
Average time to maximum deflection:	8.9	**ms**			
Quantified wall damage:	**Heavy**				

Stud number	Stud reference name	Max. Disp.	Time to max.	Stud damage
		mm	ms	
1	72A	-	-	No damage
2	114A	48	7.6	Failed
3	70A	42	12.2	Cracked
4	44A	43	7.2	Failed
5	127A	56	8.6	Failed
6	112A	-	-	Minor Cracking

General comments and response description:

Studs 2, 4 and 5 failed at mid-span upon reaching first positive peak having significant permanent deformations. Studs 3 and 6 cracked upon reaching first positive peak and similar to Stud 2, 4 and 5 no other peaks were experienced. The sheathing failed along the height of the wall between Stud 3 and 4 as well as Stud 5 and 6. Stud 6 was cracked on the tension side for a portion of the depth of the stud. The sheathing was also damaged between Stud 4 and 5 at mid-span. Nail withdrawal was observed throughout the entire wall.

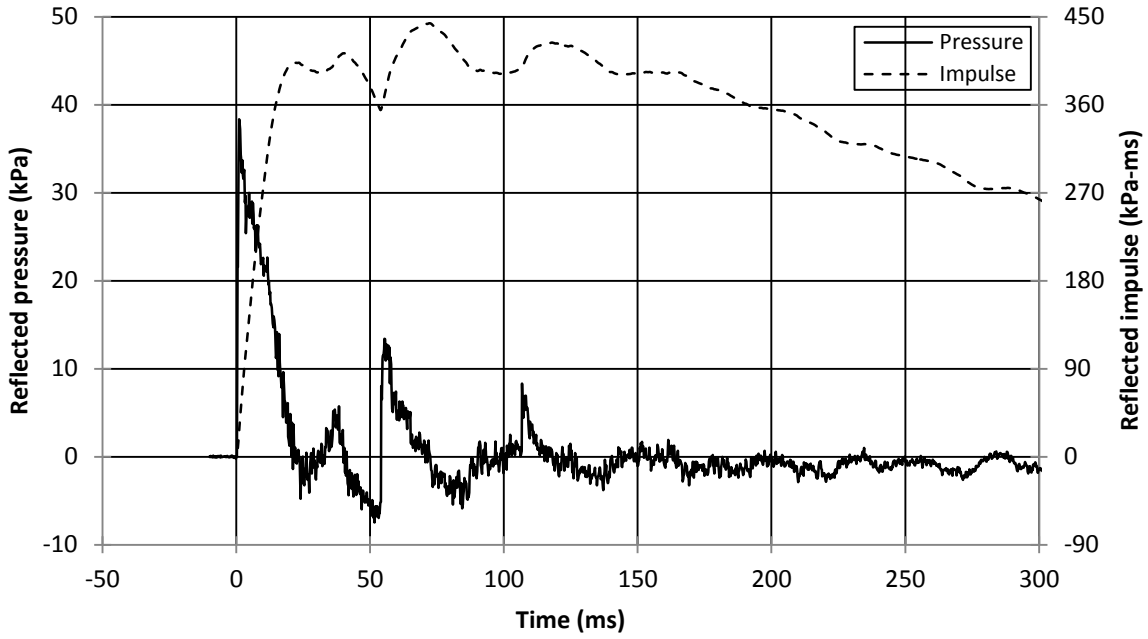

Figure B6-2.1: Reflected pressure and impulse time histories for Wall 6 Shot 2

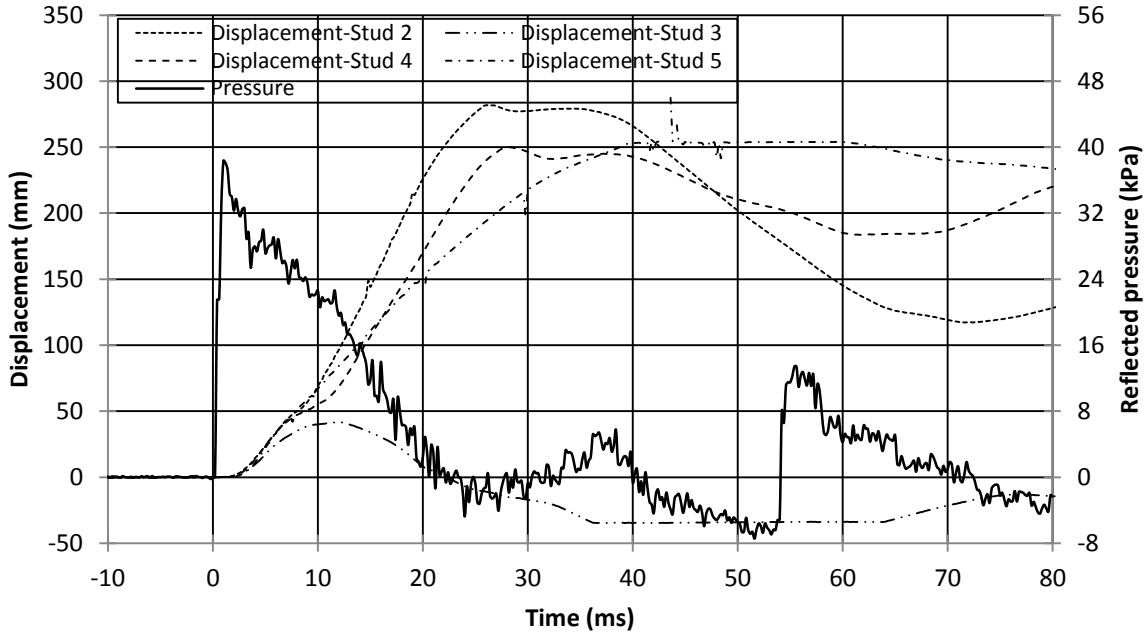

Figure B6-2.2: Displacement and pressure time histories for Wall 6 Shot 2

(a) t=0 ms (b) t=8 ms (c) t=14 ms

(d) t=20 ms (e) t=28 ms (f) t=80 ms

Figure B6-2.3: Evolution of damage with time for Wall 6 Shot 2

(a) View of entire wall

(b) View of sheathing failure

(c) Side view of wall

Figure B6-2.4: Damage of Wall 6 after shot 2

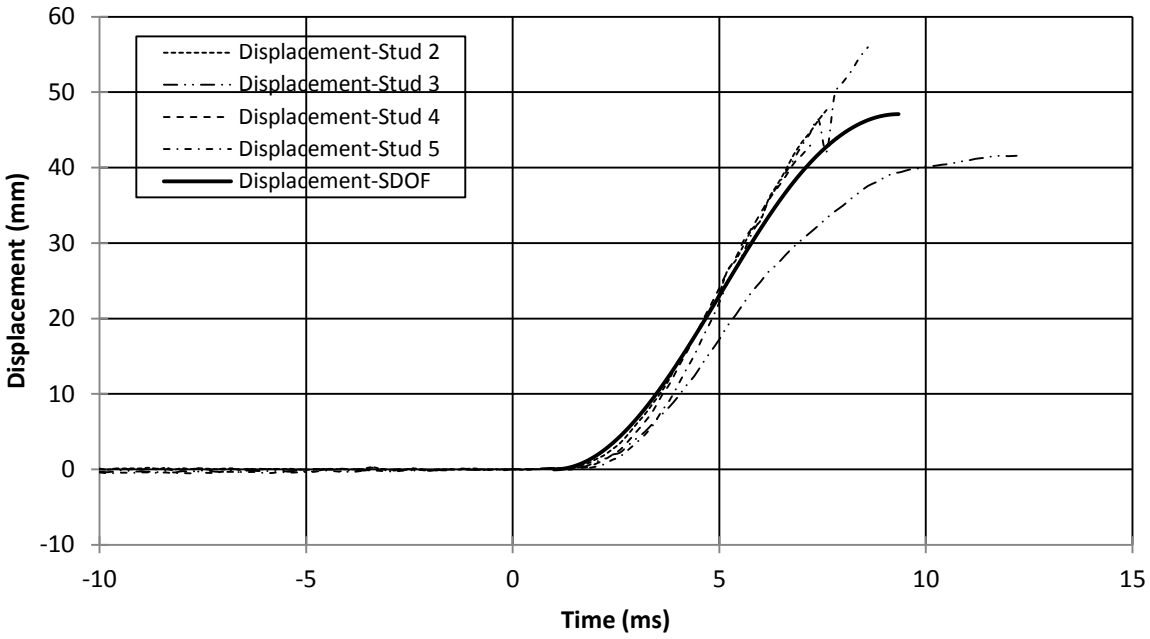

Figure B6-2.5: SDOF prediction for Wall 6 Shot 2

Wall 7, Pressure-Impulse Combination Number 1

Table B7-1: Wall 7, Shot 1-Test result summary

Light-Frame Stud Wall Dynamic Tests: Wall 7, Pressure-Impulse Combination Number 1

Test name:	Wall_7_Shot_1	**Test date:**	15/12/2012
Driver length:	2,745 **mm**	**Driver pressure:**	248.2 **kPa**

Test specimen description:

-6-38 mm x 140 mm MSR studs @ 406.4 mm o/c. -11 mm OSB

-Nails, 64 mm x 3.50 mm @150 mm o/c (field and edge)

-2,159 mm total height of wall -2,083 mm long studs -2,032 mm clear span

Average maximum reflected pressure:	38.2 **kPa**	**Wall mass:**	74.2 **kg**
Average maximum reflected impulse:	384.9 **kPa-ms**		
Experimental positive phase:	22.0 **ms**		
Theoretical positive phase:	20.1 **ms**		
Average deflection of wall studs:	59 **mm**		
Average time to maximum deflection:	9.4 **ms**		
Quantified wall damage:	**Heavy**		

Stud number	Stud reference name	Max. Disp.	Time to max.	Stud damage
		mm	ms	
1	107A	-	-	No damage
2	86A	79	9.8	Failed
3	120A	44	8.4	Failed
4	81A	42	10.2	No damage
5	98A	70	9.2	Failed
6	103A	-	-	Failed

General comments and response description:

Permanent deflection observed in 4 out of 6 studs was observed. All four studs failed at mid-span at the first positive peak. Stud 4, although being located in the center of the wall, did not experience additional damage from the original superficial cracks observed prior to the tests. The sheathing failed between Stud 1 and 2 as well as Stud 3 and 4 causing two holes within the walls. Debris of the sheathing was projected further in the room. The sheathing was cracked between Stud 4 and 5 and Stud 5 and 6 at mid-span. Nail withdrawal was observed.

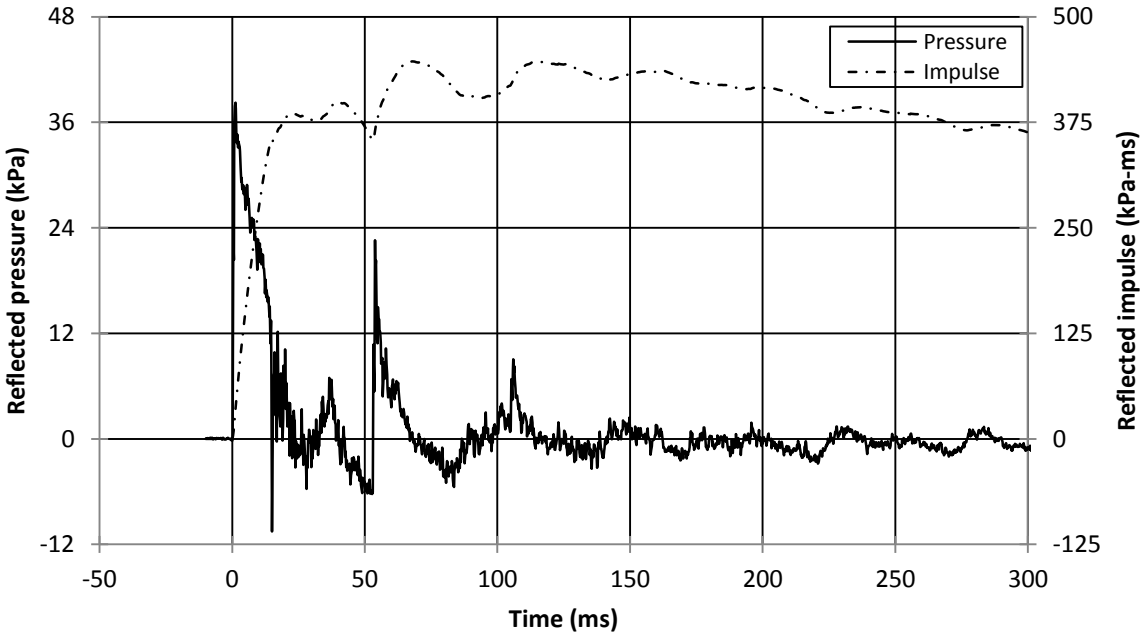

Figure B7-1.1: Reflected pressure and impulse time histories for Wall 7 Shot 1

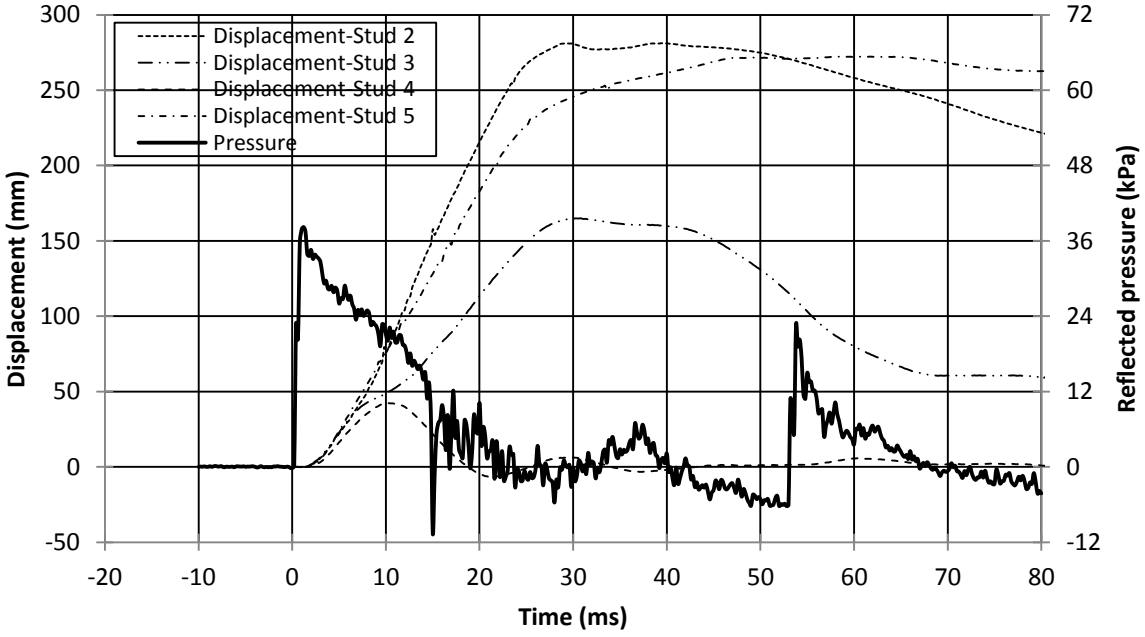

Figure B7-1.2: Displacement and pressure time histories for Wall 7 Shot 1

(a) t=0 ms (b) t=10 ms (c) t=14 ms

(d) t=18 ms (e) t=30 ms (f) t=60 ms

Figure B7-1.3: Evolution of damage with time for Wall 7 Shot 1

e 

(a) View of entire wall

(b) View of sheathing failure

(c) Localized damage-Stud 4 to 6

Figure B7-1.4: Damage of Wall 7 after shot 1

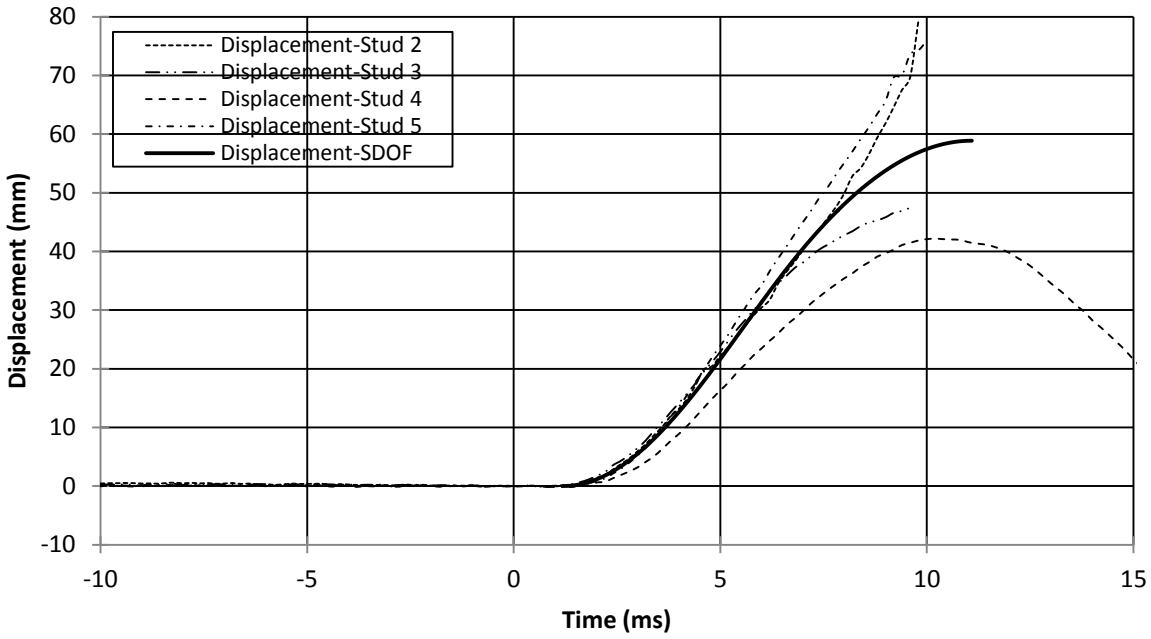

Figure B7-1.5: SDOF prediction for Wall 7 Shot 1

Wall 8, Pressure-Impulse Combination Number 1

Table B8-1: Wall 8, Shot 1-Test result summary

Light-Frame Stud Wall Dynamic Tests: Wall 8, Pressure-Impulse Combination Number 1

Test name:	Wall_8_Shot_1	**Test date:**	17/12/2012
Driver length:	305 **mm**	**Driver pressure:**	84.1 **kPa**

Test specimen description:

-6-38 mm x 140 mm MSR studs @ 406.4 mm o/c. -11 mm OSB

-Nails, 64 mm x 3.50 mm @150 mm o/c (field and edge)

-2,159 mm total height of wall -2,083 mm long studs -2,032 mm clear span

Average maximum reflected pressure:	9.8 **kPa**	**Wall mass:**	71.7 **kg**
Average maximum reflected impulse:	25.1 **kPa-ms**		
Experimental positive phase:	4.4 **ms**		
Theoretical positive phase:	5.1 **ms**		
Average deflection of wall studs:	8 **mm**		
Average time to maximum deflection:	6.2 **ms**		
Quantified wall damage:	**Superficial**		

Stud number	Stud reference name	Max. Disp.	Time to max.	Stud damage
		mm	ms	
1	63A	-	-	No damage
2	108A	8	6.4	No damage
3	121A	6	6.4	No damage
4	23A	9	6.0	No damage
5	47A	8	6.0	No damage
6	95A	-	-	No damage

General comments and response description:

The wall did not suffer any damage and remained elastic throughout its displacement history.

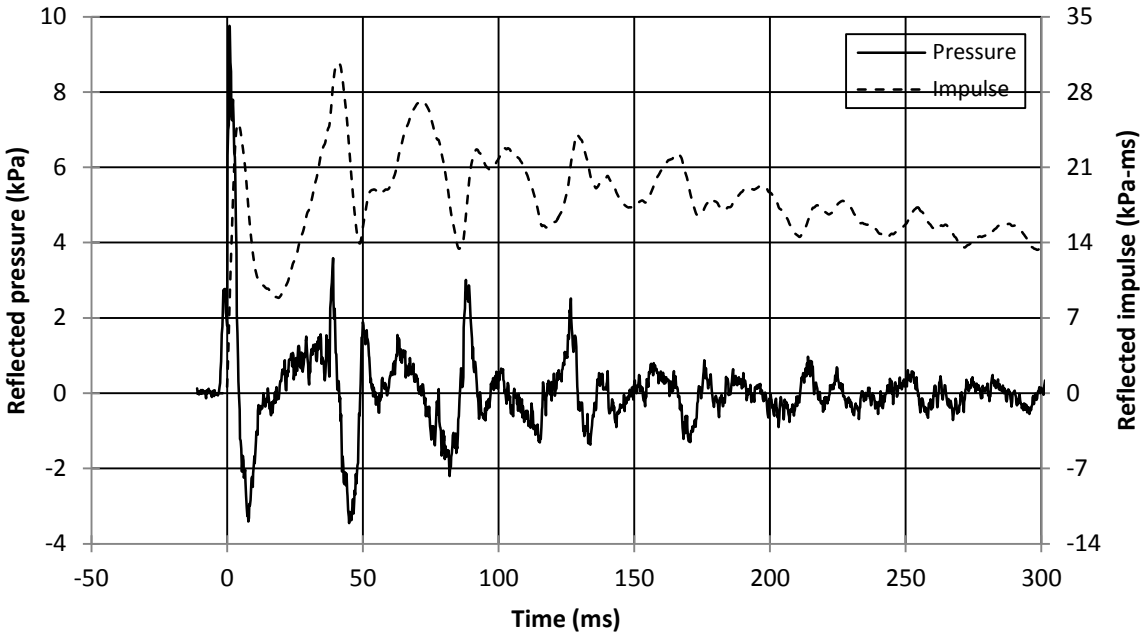

Figure B8-1.1: Reflected pressure and impulse time histories for Wall 8 Shot 1

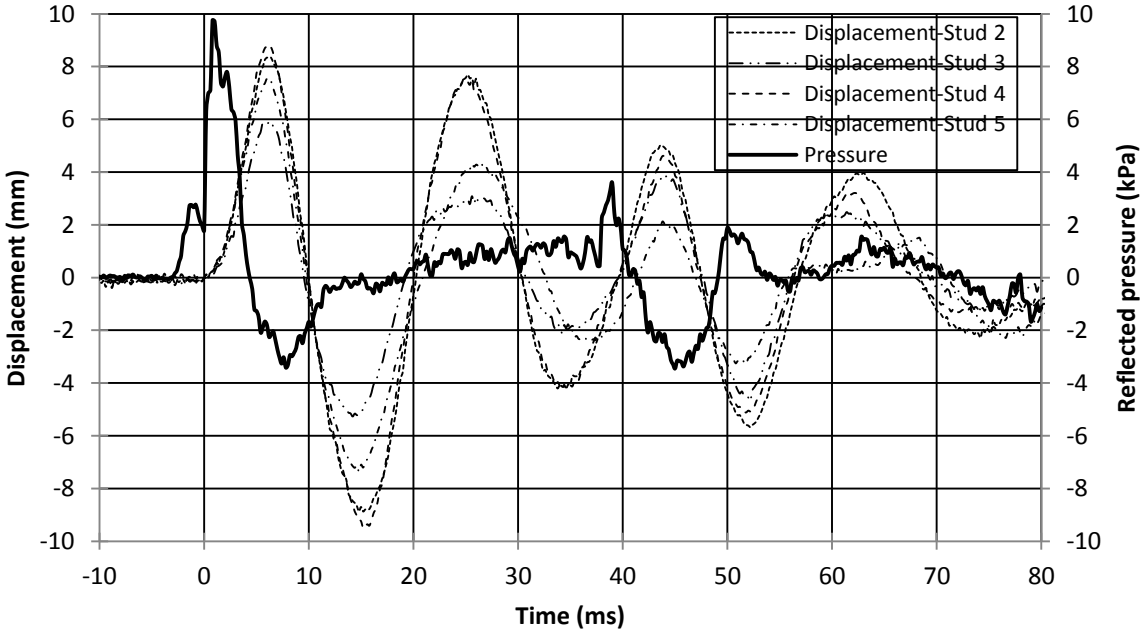

Figure B8-1.2: Displacement and pressure time histories for Wall 8 Shot 1

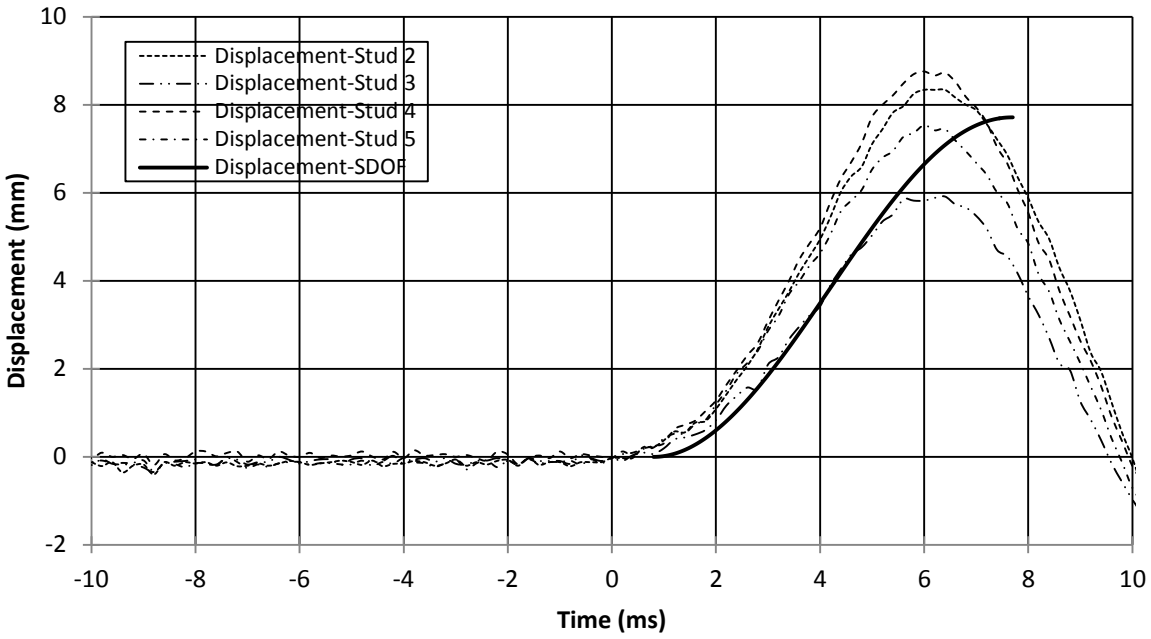

Figure B8-1.3: SDOF prediction for Wall 8 Shot 1

Wall 8, Pressure-Impulse Combination Number 2

Table B8-2: Wall 8, Shot 2-Test result summary

Light-Frame Stud Wall Dynamic Tests: Wall 8, Pressure-Impulse Combination Number 2

Test name:	Wall_8_Shot_2	**Test date:**	17/12/2012
Driver length:	305 **mm**	**Driver pressure:**	568.8 **kPa**

Test specimen description:

-6-38 mm x 140 mm MSR studs @ 406.4 mm o/c. -11 mm OSB

-Nails, 64 mm x 3.50 mm @150 mm o/c (field and edge)

-2,159 mm total height of wall -2,083 mm long studs -2,032 mm clear span

Average maximum reflected pressure:	52.6	**kPa**	**Wall mass:**	71.7	**kg**
Average maximum reflected impulse:	163.0	**kPa-ms**			
Experimental positive phase:	8.0	**ms**			
Theoretical positive phase:	6.2	**ms**			
Average deflection of wall studs:	45	**mm**			
Average time to maximum deflection:	7.9	**ms**			
Quantified wall damage:	**Moderate**				

Stud number	Stud reference name	Max. Disp.	Time to max.	Stud damage
		mm	ms	
1	63A	-	-	Cracked
2	108A	46	7.6	Failed
3	121A	39	7.6	No damage
4	23A	55	8.6	Cracked
5	47A	42	7.6	Severe Cracking
6	95A	-	-	Cracked

General comments and response description:

Stud 2 and 5 cracked, thus initiating a failure, at mid-span upon reaching first positive peak. Upon reaching the first negative peak, Stud 2, 4 and 5 cracked and during the return to the second positive peak Stud 2 failed completely. The damage was amplified for the other studs between the oscillations of positive to negative peaks. Due to the high pressure experienced during the negative phase, a portion of the sheathing between Studs 5 and 6 was sucked in the shock tube. Nail withdrawal was observed.

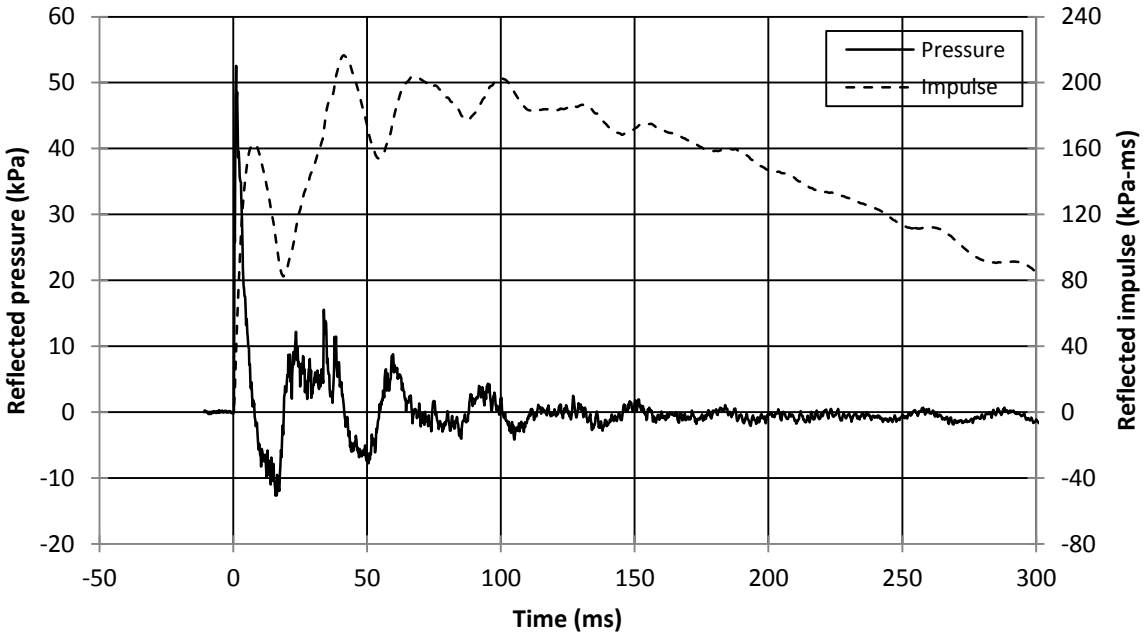

Figure B8-2.1: Reflected pressure and impulse time histories for Wall 8 Shot 2

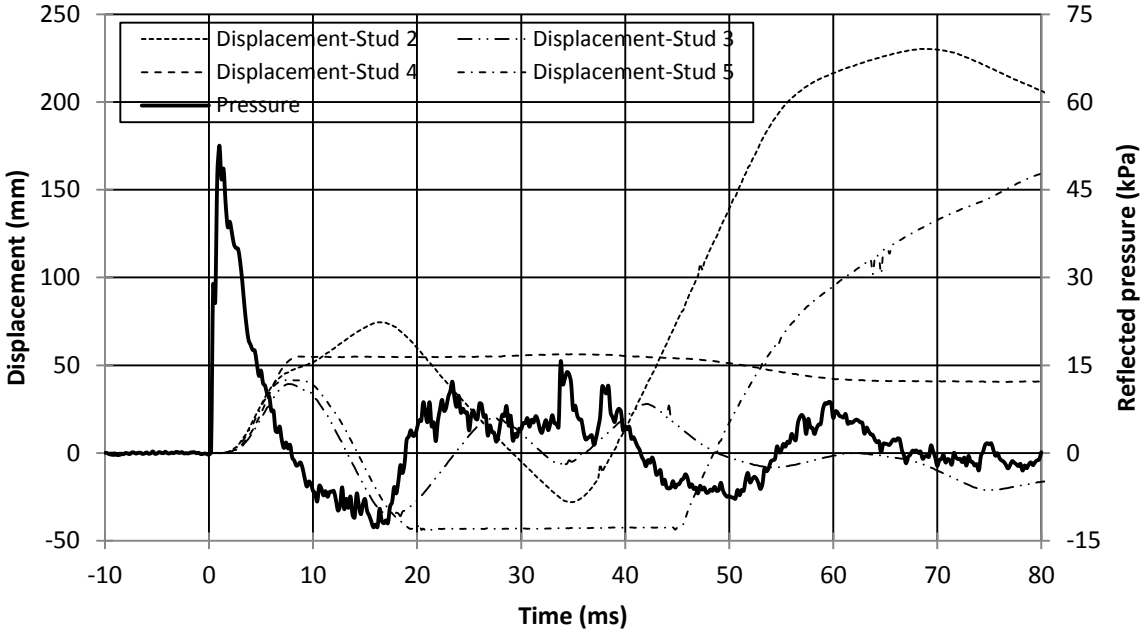

Figure B8-2.2: Displacement and pressure time histories for Wall 8 Shot 2

(a) t=0 ms (b) t=6 ms (c) t=12 ms

(d) t=20 ms (e) t=50 ms (f) t=60 ms

Figure B8-2.3: Evolution of damage with time for Wall 8 Shot 2

(a) View of entire wall (right side)

(b) View of entire wall (left side)

(c) Local damage

(d) Sheathing damage

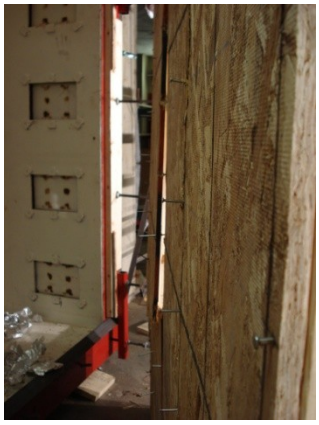

(e) Nail withdrawal

Figure B8-2.4: Damage of Wall 8 after shot 2

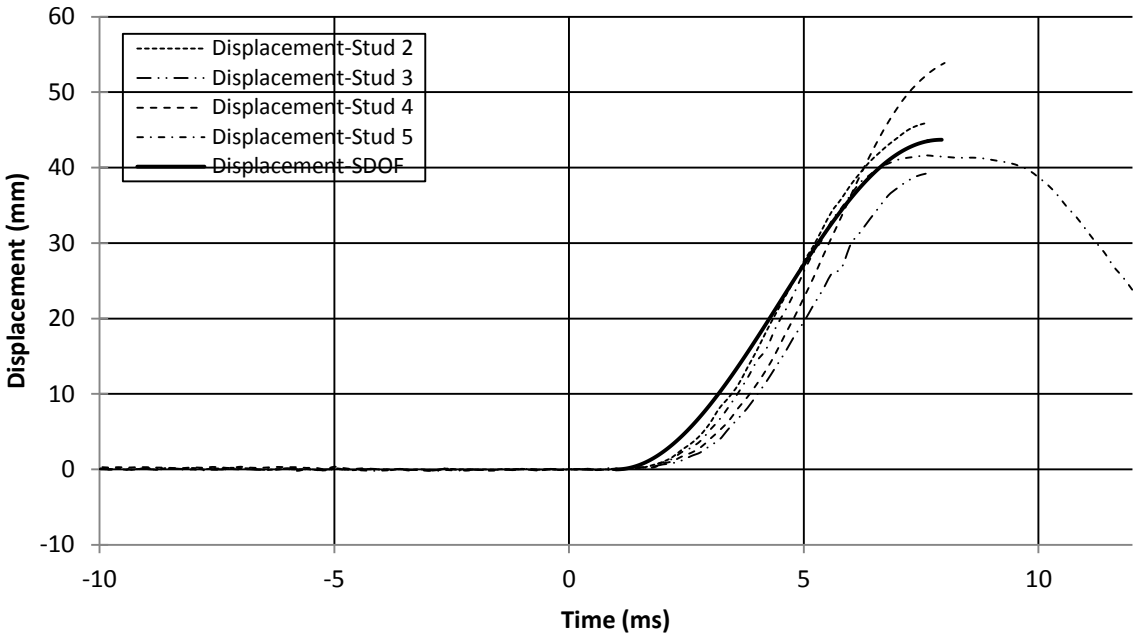

Figure B8-2.5: SDOF prediction for Wall 8 Shot 2

Wall 9, Pressure-Impulse Combination Number 1

Table B9-1: Wall 9, Shot 1-Test result summary

Light-Frame Stud Wall Dynamic Tests: Wall 9, Pressure-Impulse Combination Number 1

Test name:	Wall_9_Shot_1	**Test date:**	13/12/2012
Driver length:	2,745 **mm**	**Driver pressure:**	40.7 **kPa**

Test specimen description:

-6-38 mm x 140 mm MSR studs @ 406.4 mm o/c. -11 mm OSB

-Nails, 64 mm x 3.50 mm @150 mm o/c (field and edge)

-2,159 mm total height of wall -2,083 mm long studs -2,032 mm clear span

Average maximum reflected pressure:	6.6	**kPa**	**Wall mass:**	77.5	**kg**
Average maximum reflected impulse:	76.1	**kPa-ms**			
Experimental positive phase:	23.5	**ms**			
Theoretical positive phase:	23.1	**ms**			
Average deflection of wall studs:	8	**mm**			
Average time to maximum deflection:	10.6	**ms**			
Quantified wall damage:	**Superficial**				

Stud number	Stud reference name	Max. Disp.	Time to max.	Stud damage
		mm	ms	
1	110A	-	-	No damage
2	68A	9	10.7	No damage
3	7A	8	11.7	No damage
4	94A	8	9.8	No damage
5	21A	8	10.0	No damage
6	58A	-	-	No damage

General comments and response description:

The wall did not suffer any damage and remained elastic throughout its displacement history. Due to an instrumentation problem, signal interference or "noisy" data was recorded; therefore the curves are not as smooth.

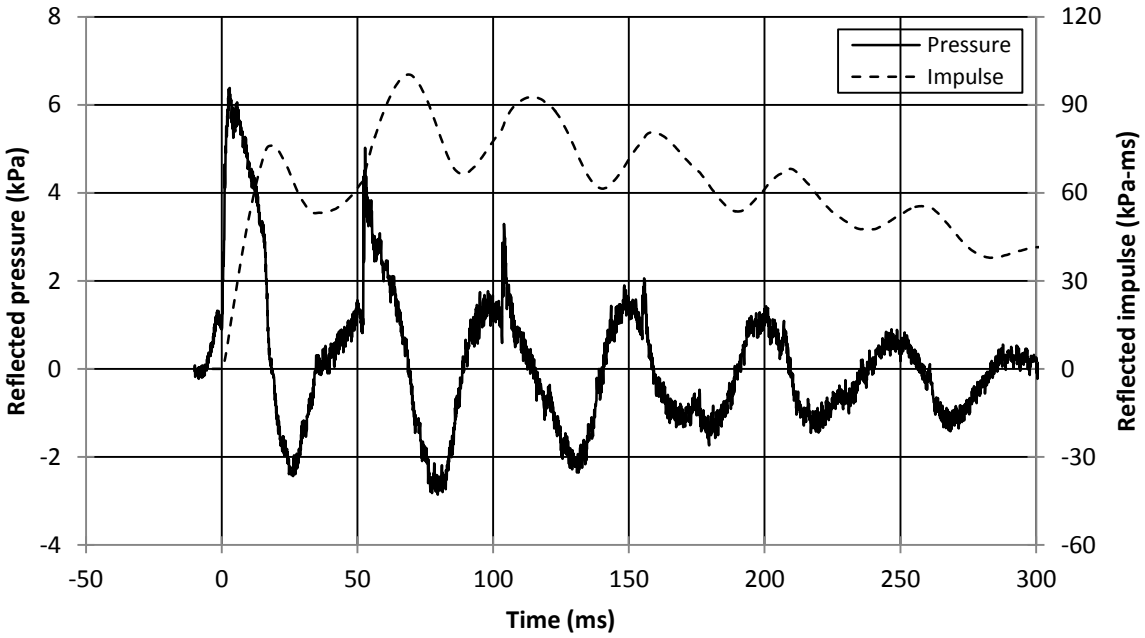

Figure B9-1.1: Reflected pressure and impulse histories for Wall 9 Shot 1

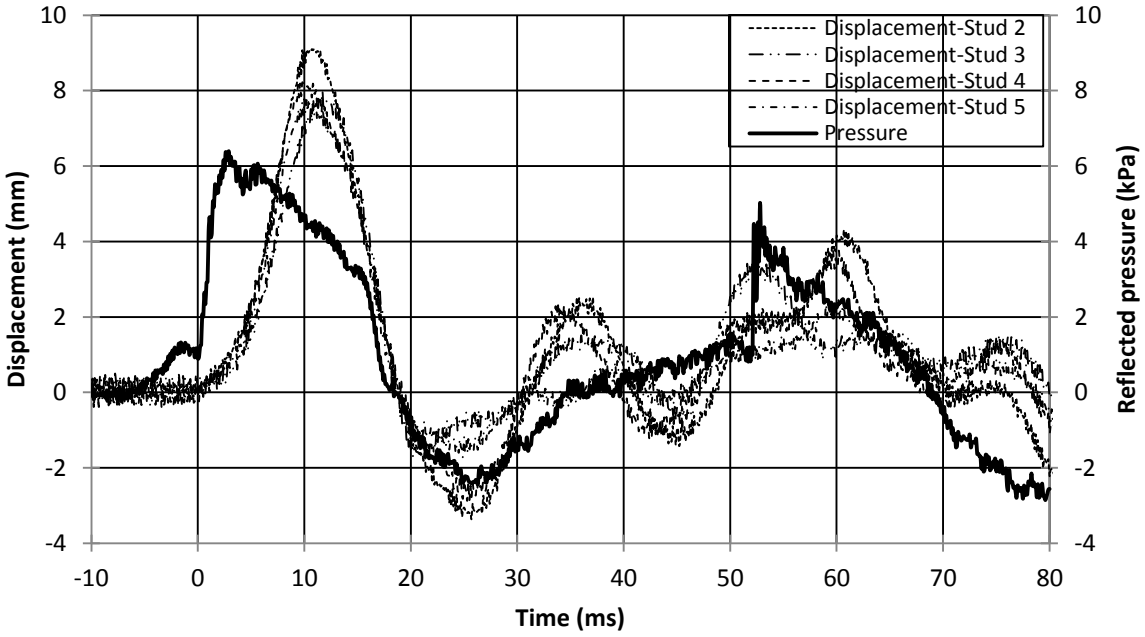

Figure B9-1.2: Displacement and pressure time histories for Wall 9 Shot 1

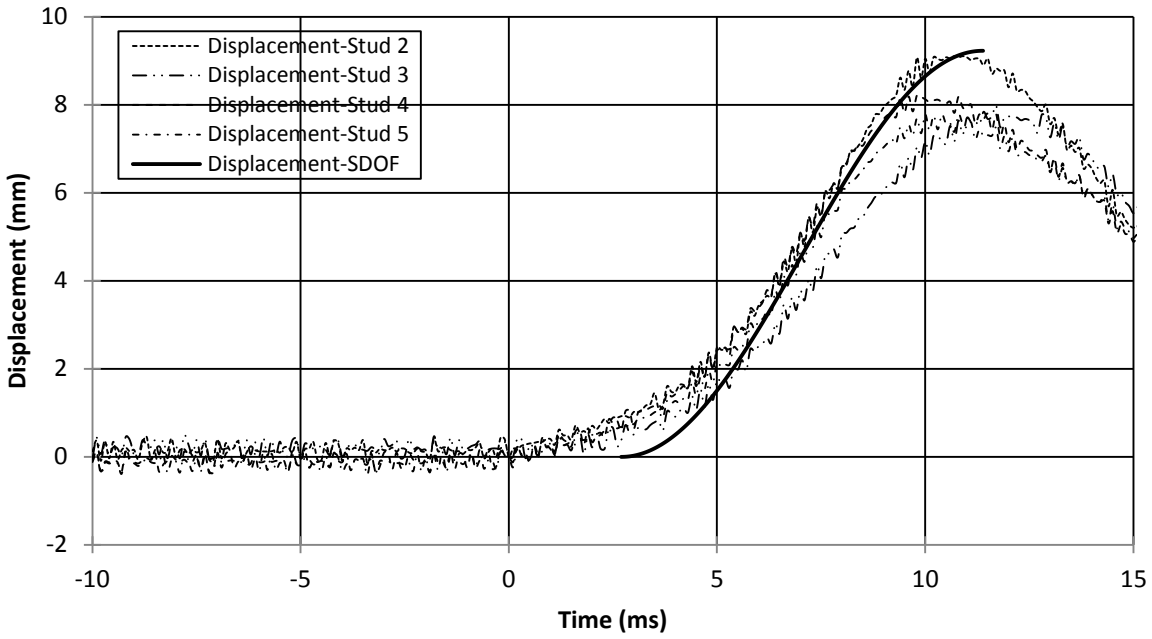

Figure B9-1.3: SDOF prediction for Wall 9 Shot 1

Wall 9, Pressure-Impulse Combination Number 2

Table B9-2: Wall 9, Shot 2-Test result summary

Light-Frame Stud Wall Dynamic Tests: Wall 9, Pressure-Impulse Combination Number 2

Test name:	Wall_9_Shot_2	**Test date:**	13/12/2012
Driver length:	2,745 **mm**	**Driver pressure:**	138.6 **kPa**

Test specimen description:

-6-38 mm x 140 mm MSR studs @ 406.4 mm o/c. -11 mm OSB

-Nails, 64 mm x 3.50 mm @150 mm o/c (field and edge)

-2,159 mm total height of wall -2,083 mm long studs -2,032 mm clear span

Average maximum reflected pressure:	28.9	**kPa**	**Wall mass:**	77.5	**kg**
Average maximum reflected impulse:	282.3	**kPa-ms**			
Experimental positive phase:	21.5	**ms**			
Theoretical positive phase:	19.6	**ms**			
Average deflection of wall studs:	39	**mm**			
Average time to maximum deflection:	11.7	**ms**			
Quantified wall damage:	**Superficial**				

Stud number	Stud reference name	Max. Disp.	Time to max.	Stud damage
		mm	ms	
1	110A	-	-	No damage
2	68A	42	11.0	No damage
3	7A	32	11.2	No damage
4	94A	43	12.6	Cracked
5	21A	39	11.8	No damage
6	58A	-	-	No damage

General comments and response description:

With the exception of Stud 4, the wall did not suffer any damage and remained elastic throughout its displacement time history. Damage of Stud 4 initiated on the first positive peak. Although a portion of Stud 4 cracked, the stud had no residual displacement. No sheathing failure, nor nail withdrawal.

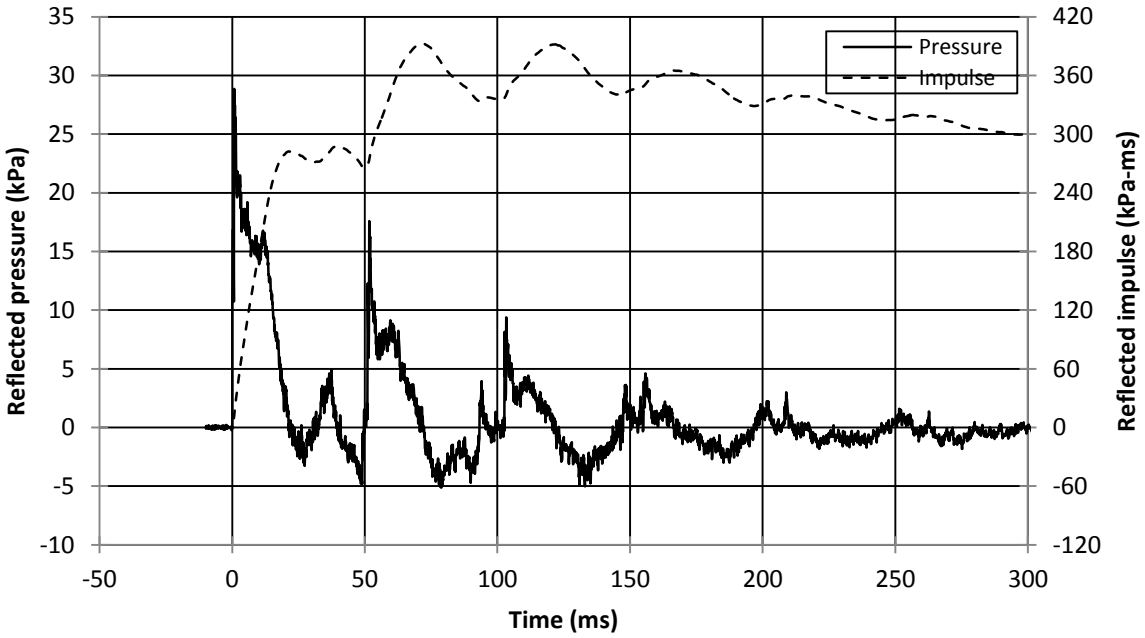

Figure B9-2.1: Reflected pressure and impulse time histories for Wall 9 Shot 2

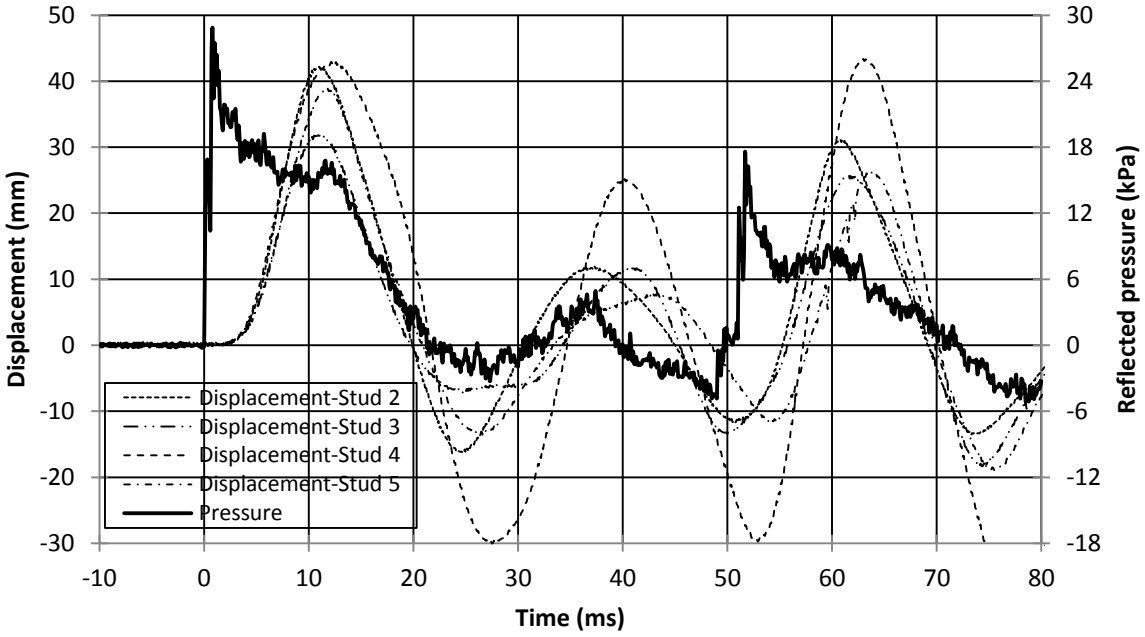

Figure B9-2.2: Displacement and pressure time histories for Wall 9 Shot 2

(a) t=0 ms (b) t=8 ms (c) t=20 ms

(d) t=28 ms (e) t=40 ms (f) t=100 ms

Figure B9-2.3: Evolution of damage with time for Wall 9 Shot 2

(a) View of entire wall

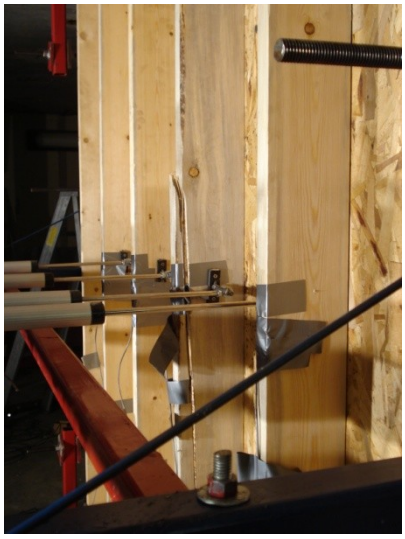

(b) Localized damage stud 4-Upper half

(c)Localize damage stud 4-Lower half

Figure B9-2.4: Damage of Wall 9 after shot 2

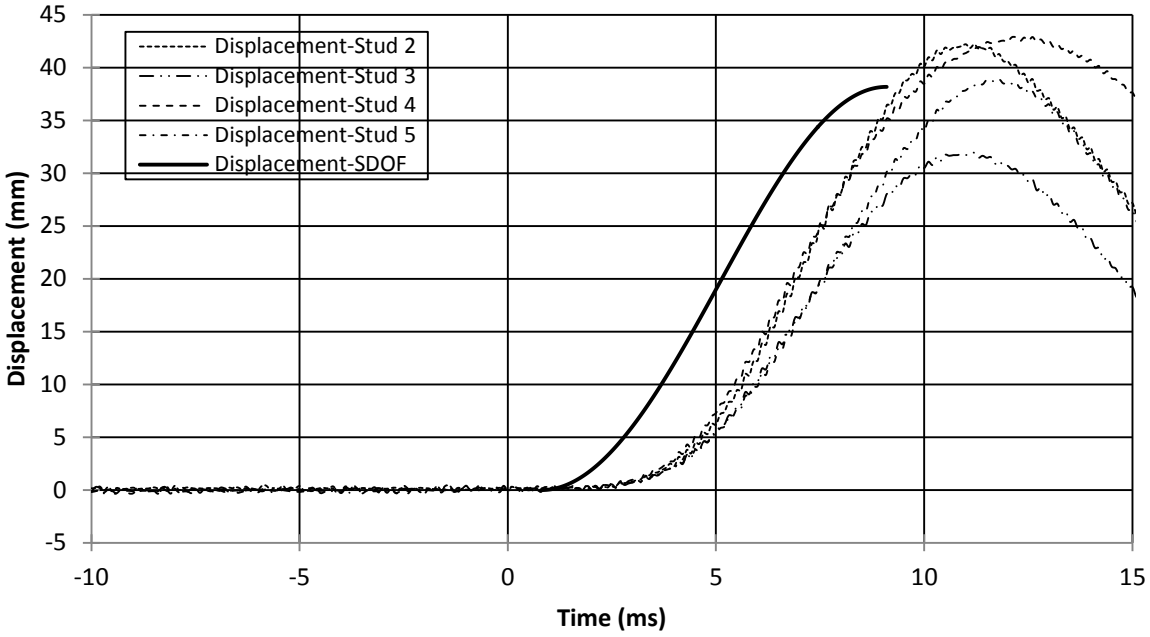

Figure B9-2.5: SDOF prediction for Wall 9 Shot 2

Wall 9, Pressure-Impulse Combination Number 3

Table B9-3: Wall 9, Shot 3-Test result summary

Light-Frame Stud Wall Dynamic Tests: Wall 9, Pressure-Impulse Combination Number 3

Test name:	Wall_9_Shot_3	**Test date:**	13/12/2012
Driver length:	2,745 **mm**	**Driver pressure:**	241.3 **kPa**

Test specimen description:

-6-38 mm x 140 mm MSR studs @ 406.4 mm o/c. -11 mm OSB

-Nails, 64 mm x 3.50 mm @150 mm o/c (field and edge)

-2,159 mm total height of wall -2,083 mm long studs -2,032 mm clear span

Average maximum reflected pressure:	41.9	**kPa**	**Wall mass:**	77.5	**kg**
Average maximum reflected impulse:	386.5	**kPa-ms**			
Experimental positive phase:	21.5	**ms**			
Theoretical positive phase:	18.5	**ms**			
Average deflection of wall studs:	60	**mm**			
Average time to maximum deflection:	11.7	**ms**			
Quantified wall damage:	**Moderate**				

Stud number	Stud reference name	Max. Disp.	Time to max.	Stud damage
		mm	ms	
1	110A	-	-	No damage
2	68A	65	11.2	Minor Cracking
3	7A	51	11.0	Minor Cracking
4	94A	-	-	Failed
5	21A	65	12.8	Failed
6	58A	-	-	No damage

General comments and response description::

Initial damage of studs occurred during first positive peak to maximum displacement and was exasperated on the rebound displacements. Stud 2 was slightly cracked on the tension side while Stud 3 was cracked at mid-span towards the bottom plate. Failure of the sheathing occurred between Studs 3 and 4 as well as Studs 5 and 6. There was no sheathing debris. Some nail withdrawal was observed. Data was not recorded for Stud 4 to protect the LVDT device as the stud was cracked in the previous test and failure was expected.

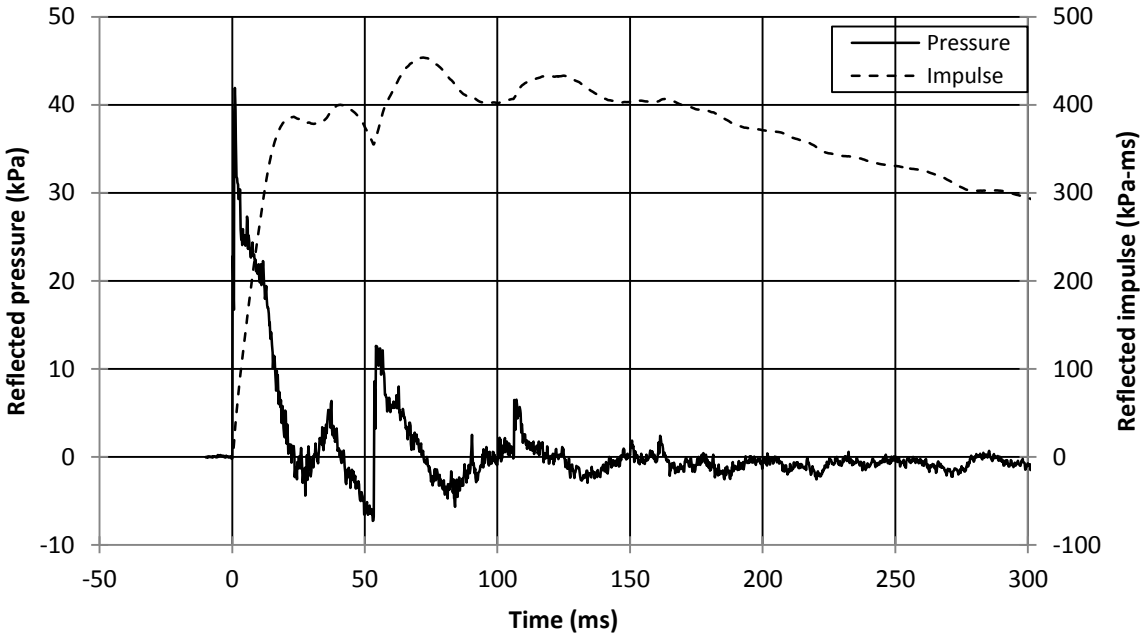

Figure B9-3.1: Reflected pressure and impulse for Wall 9 Shot 3

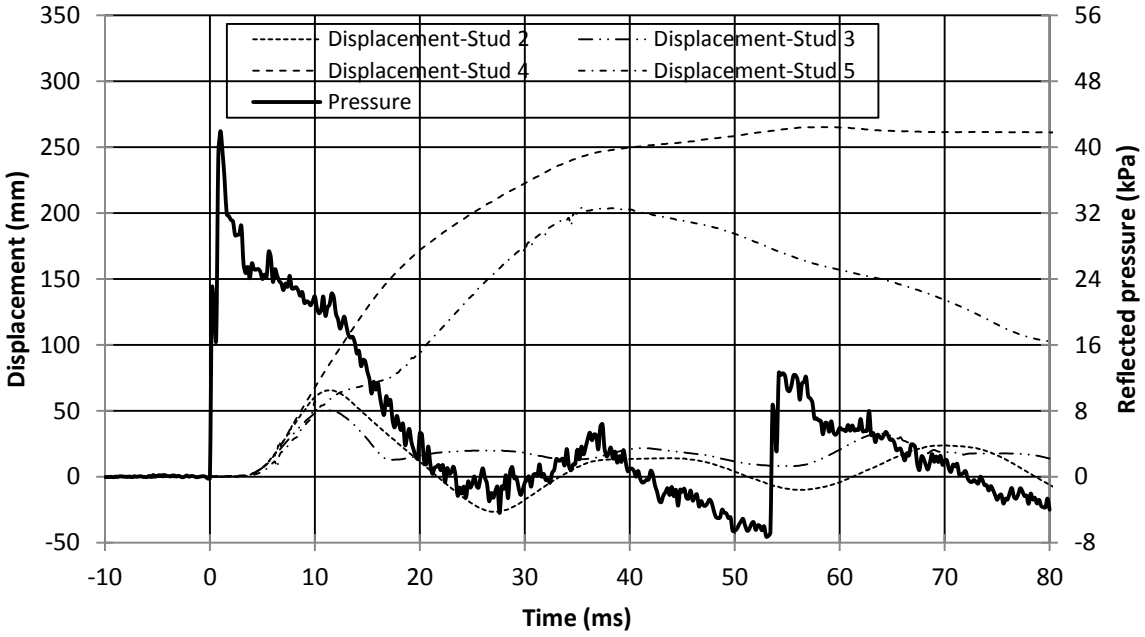

Figure B9-3.2: Displacement and pressure time histories for Wall 9 Shot 2

(a) t=0 ms (b) t=8 ms (c) t=14 ms

(d) t=20 ms (e) t=26 ms (f) t=130 ms

Figure B9-3.3: Evolution of damage with time for Wall 9 Shot 3

(a) View of entire wall

(b) View of sheathing failure

(c) Close-up of stud damage

Figure B9-3.4: Damage of Wall 9 after shot 3

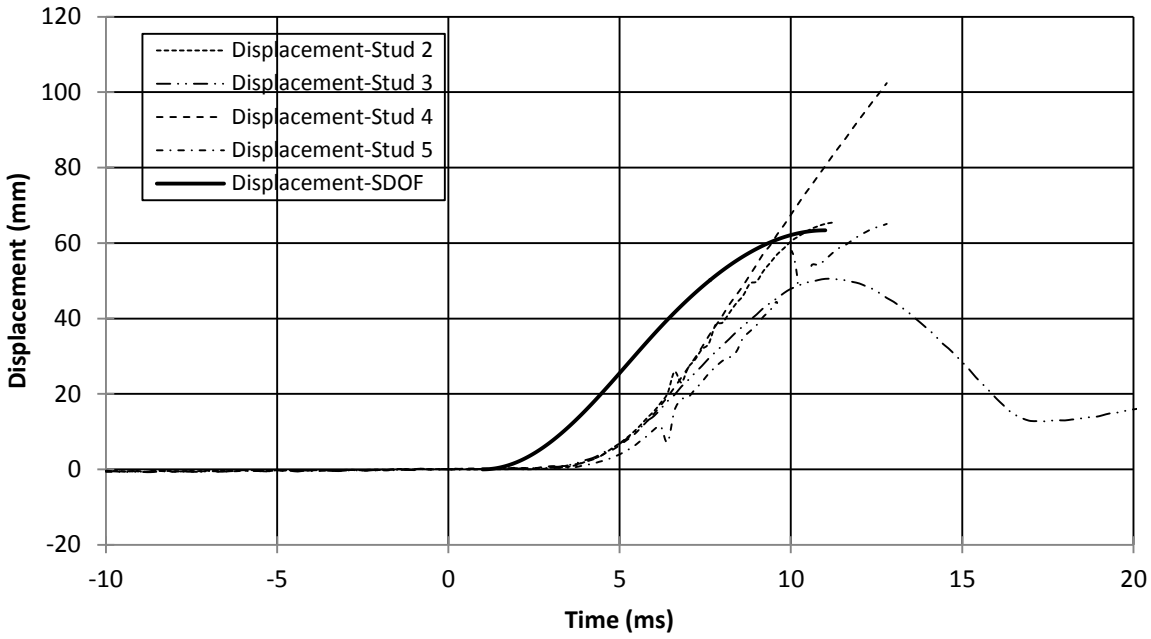

Figure B9-3.5: SDOF prediction for Wall 9 Shot 3

Wall 10, Pressure-Impulse Combination Number 1

Table B10-1: Wall 10, Shot 1-Test result summary

Light-Frame Stud Wall Dynamic Tests: Wall 10, Pressure-Impulse Combination Number 1

Test name:	Wall_10_Shot_1	**Test date:**	18/12/2012
Driver length:	4,880 **mm**	**Driver pressure:**	71.7 **kPa**

Test specimen description:

-6-38 mm x 140 mm MSR studs @ 406.4 mm o/c. -11 mm OSB

-Nails, 64 mm x 3.50 mm @150 mm o/c (field and edge)

-2,159 mm total height of wall -2,083 mm long studs -2,032 mm clear span

Average maximum reflected pressure:	11.6 **kPa**	**Wall mass:**	73.5 **kg**
Average maximum reflected impulse:	207.0 **kPa-ms**		
Experimental positive phase:	35.0 **ms**		
Theoretical positive phase:	35.8 **ms**		
Average deflection of wall studs:	9 **mm**		
Average time to maximum deflection:	9.0 **ms**		
Quantified wall damage:	**Superficial**		

Stud number	Stud reference name	Max. Disp.	Time to max.	Stud damage
		mm	ms	
1	48A	-	-	No damage
2	19A	-	-	No damage
3	13A	-	-	No damage
4	87A	9	9.0	No damage
5	62A	-	-	No damage
6	42A	-	-	No damage

General comments and response description::

The wall did not suffer any damage and remained elastic throughout its displacement history. Recorded displacement data was only available for Stud 4 due to an instrumental problem.

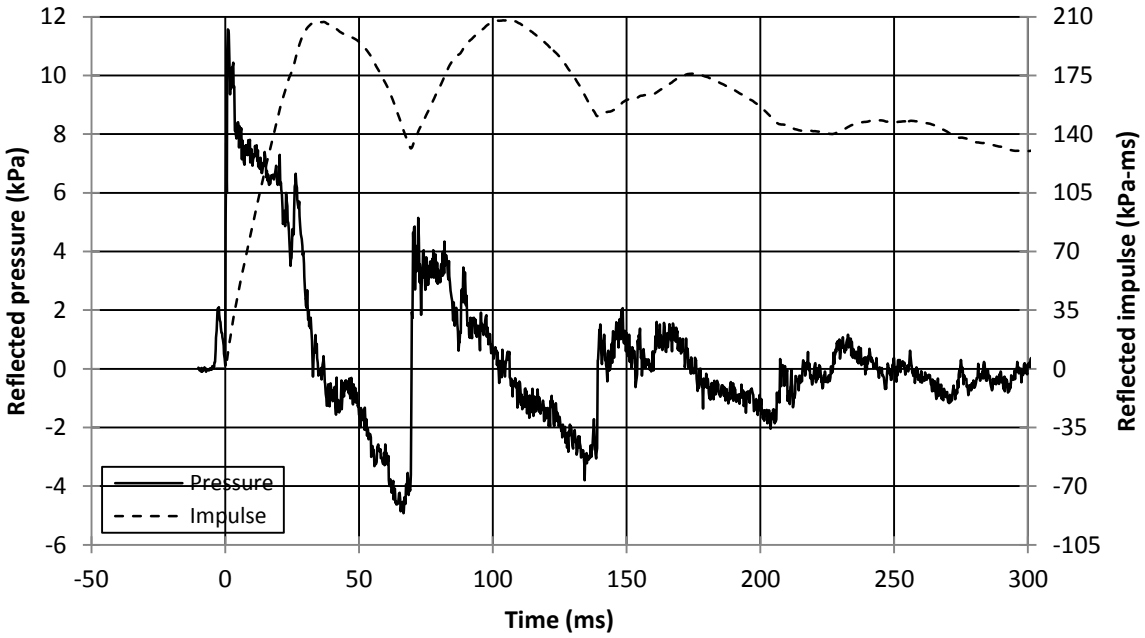

Figure B10-1.1: Reflected pressure and impulse time histories for Wall 10 Shot 1

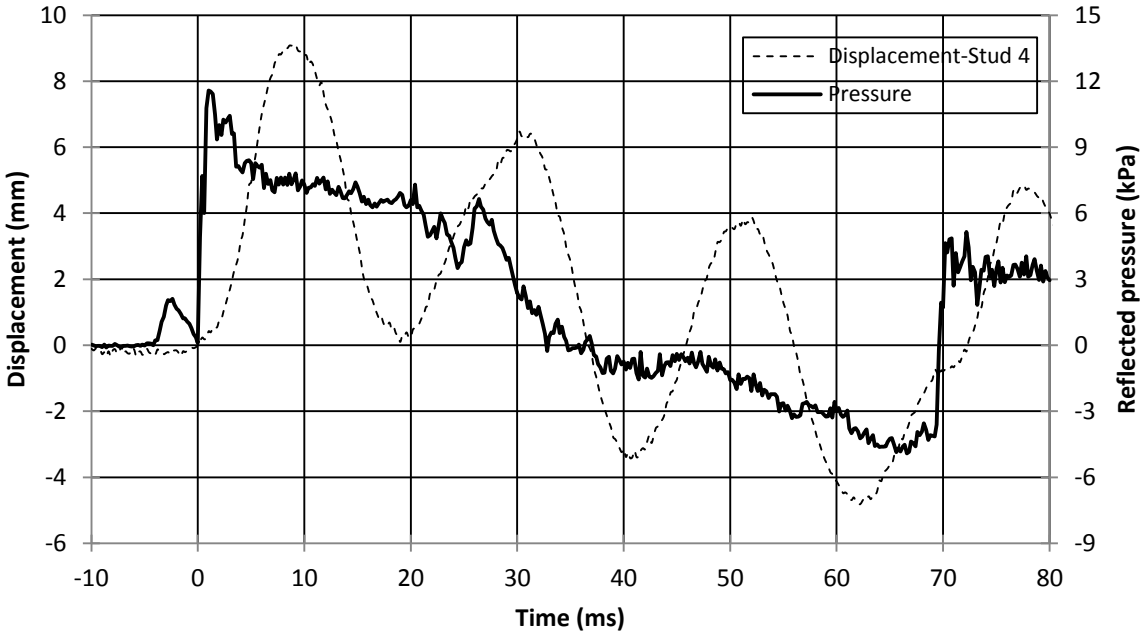

Figure B10-1.2: Displacement and pressure time histories for Wall 10 Shot 1

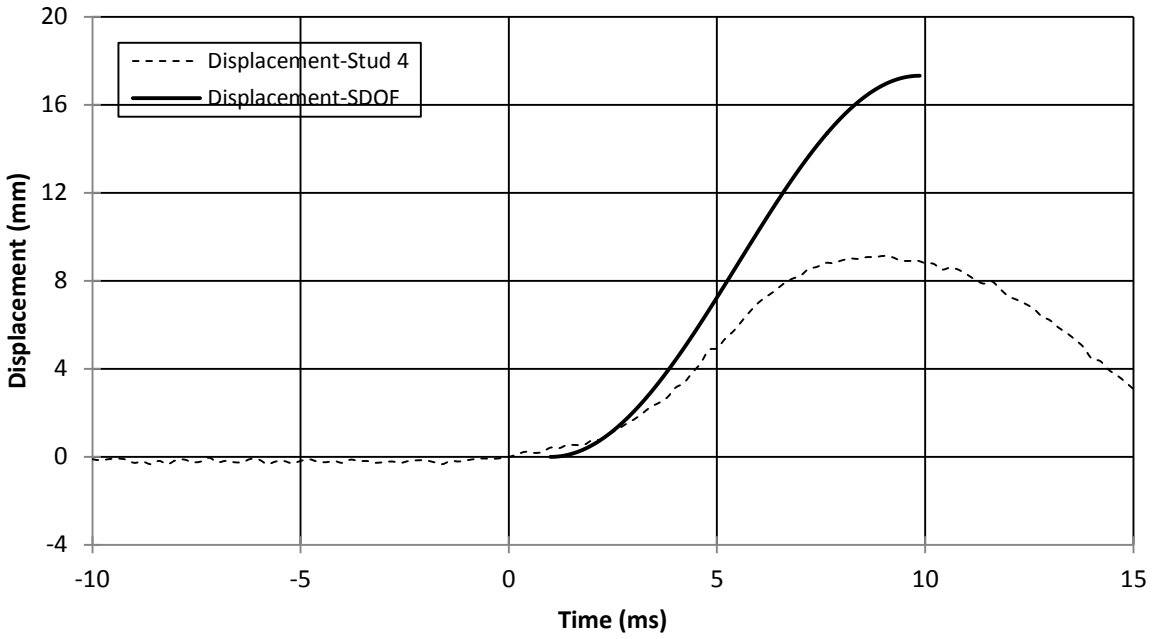

Figure B10-1.3: SDOF prediction for Wall 10 Shot 1

Wall 10, Pressure-Impulse Combination Number 2

Table B10-2: Wall 10, Shot 2-Test result summary

Light-Frame Stud Wall Dynamic Tests: Wall 10, Pressure-Impulse Combination Number 2

Test name:	Wall_10_Shot_2	**Test date:**	18/12/2012
Driver length:	4,880 **mm**	**Driver pressure:**	208.2 **kPa**

Test specimen description:

-6-38 mm x 140 mm MSR studs @ 406.4 mm o/c. -11 mm OSB

-Nails, 64 mm x 3.50 mm @150 mm o/c (field and edge)

-2,159 mm total height of wall -2,083 mm long studs -2,032 mm clear span

Average maximum reflected pressure:	31.3	**kPa**	**Wall mass:**	73.5	**kg**
Average maximum reflected impulse:	495.1	**kPa-ms**			
Experimental positive phase:	44	**ms**			
Theoretical positive phase:	31.6	**ms**			
Average deflection of wall studs:	48.1	**mm**			
Average time to maximum deflection:	12.0	**ms**			
Quantified wall damage:	**Moderate**				

Stud number	Stud reference name	Max. Disp.	Time to max.	Stud damage
		mm	ms	
1	48A	-	-	No damage
2	19A	73	15.2	Cracked
3	13A	40	11.4	Minor Cracking
4	87A	32	9.4	Minor Cracking
5	62A	-	-	No damage
6	42A	-	-	No damage

General comments and response description::

The damage observed occurred during the first peak to maximum displacement. Stud 3 and 4 had very minor cracking on the tension side while Stud 2 had a more pronounced crack initiating at mid-span on the tension side toward the top plate. The sheathing cracked in the upper portion of the wall between Studs 1 and 2. No nail withdrawal observed. Due to an instrumentation problem, data was not available for Stud 5.

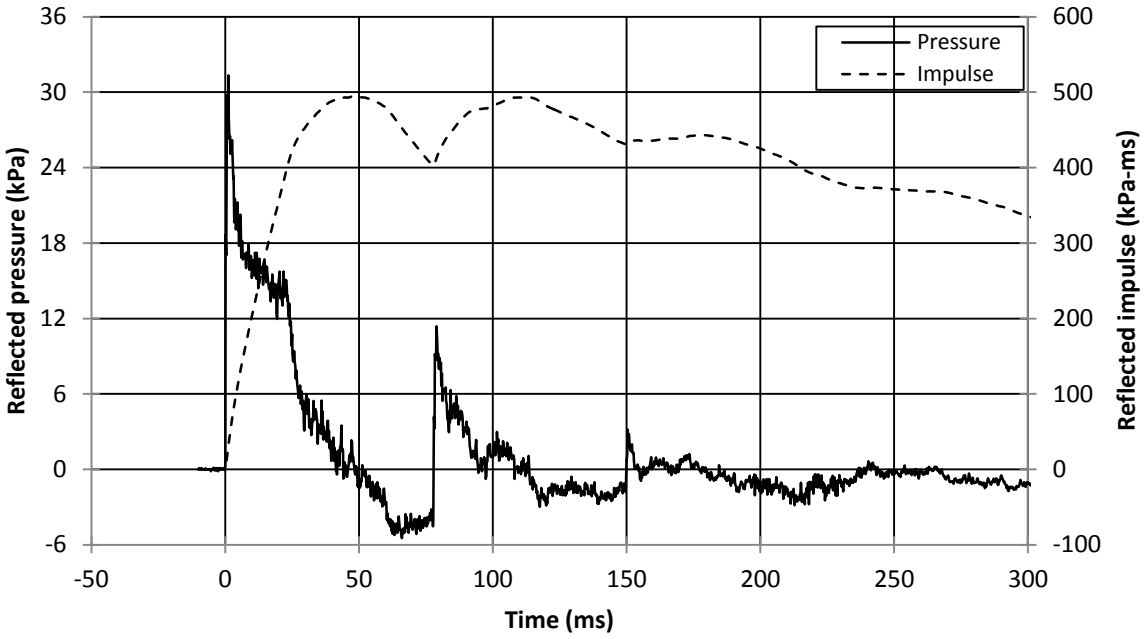

Figure B10-2.1: Reflected pressure and impulse for Wall 10 Shot 2

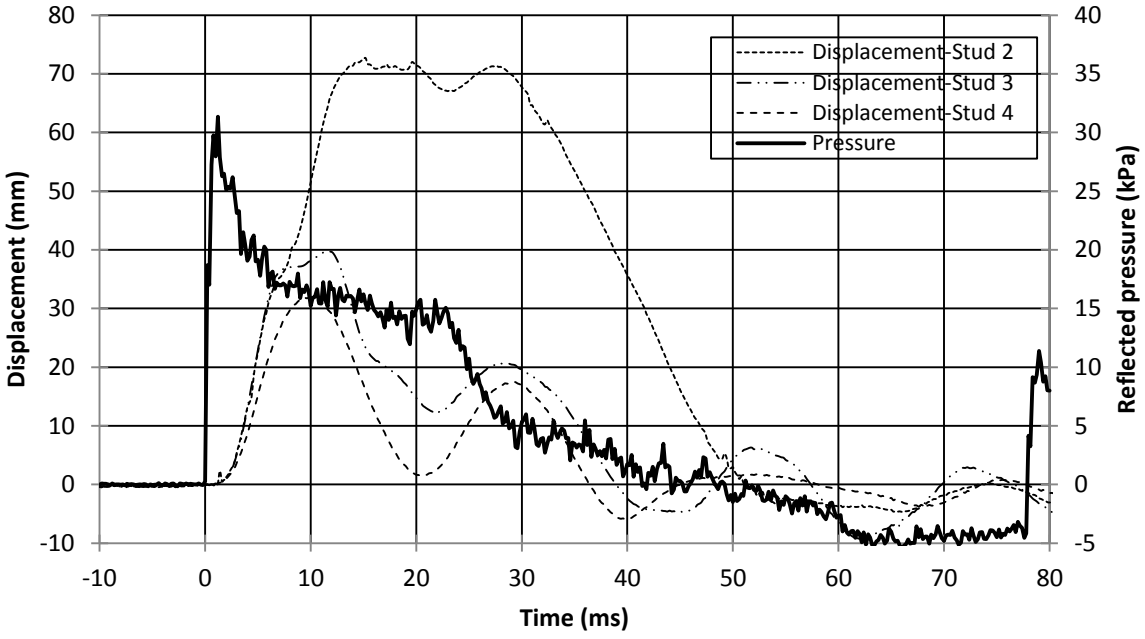

Figure B10-2.2: Displacement and pressure time histories for Wall 10 Shot 2

(a) t=0 ms (b) t=12 ms (c) t=20 ms

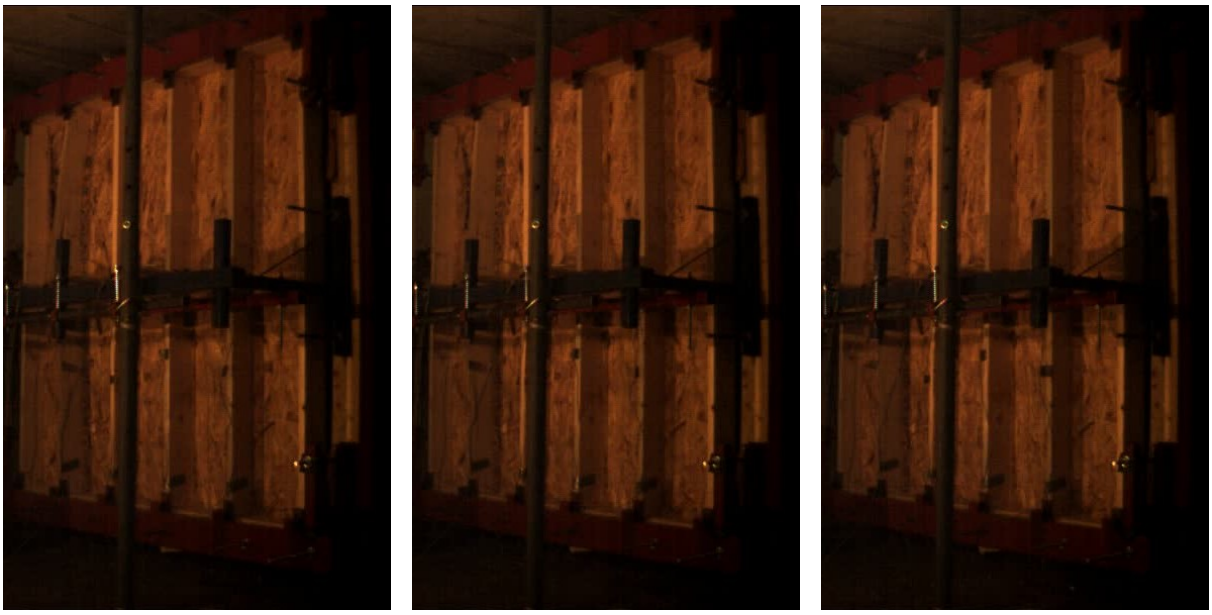

(d) t=30 ms (e) t=40 ms (f) t=90 ms

Figure B10-2.3: Evolution of damage with time for Wall 10 Shot 2

(a) View of entire wall

(b) View of sheathing failure

(c) Close-up of stud damage

Figure B10-2.4: Damage of Wall 10 after shot 2

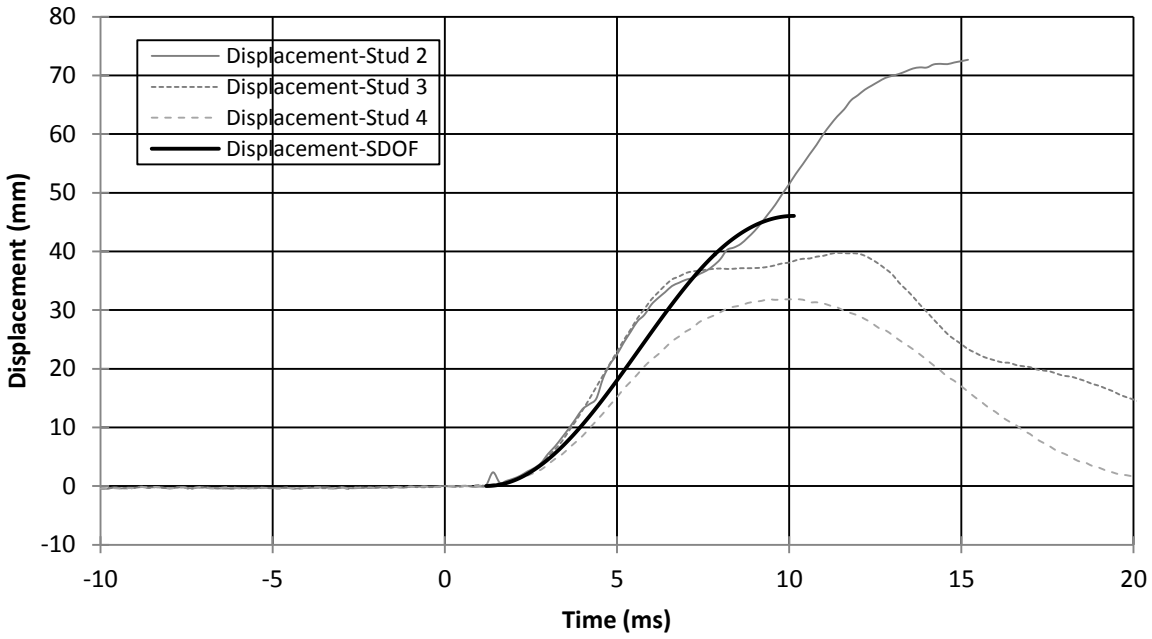

Figure B10-2.5: SDOF prediction for Wall 10 Shot 2

Wall 16, Pressure-Impulse Combination Number 1

Table B16-1: Wall 16, Shot 1-Test result summary

Light-Frame Stud Wall Dynamic Tests: Wall 16, Pressure-Impulse Combination Number 1

Test name:	Wall_16_Shot_1	**Test date:**	15/12/2012
Driver length:	2,745 **mm**	**Driver pressure:**	68.9 **kPa**

Test specimen description:

-6-38 mm x 140 mm MSR studs @ 406.4 mm o/c. -18.5 mm plywood

-Nails, 89 mm x 4.24 mm @150 mm o/c (field and edge)

-2,159 mm total height of wall -2,083 mm long studs -2,032 mm clear span

Average maximum reflected pressure:	11.5	**kPa**	**Wall mass:**	85.3	**kg**
Average maximum reflected impulse:	128.1	**kPa-ms**			
Experimental positive phase:	19.5	**ms**			
Theoretical positive phase:	22.3	**ms**			
Average deflection of wall studs:	11	**mm**			
Average time to maximum deflection:	9.8	**ms**			
Quantified wall damage:	**Superficial**				

Stud number	Stud reference name	Max. Disp.	Time to max.	Stud damage
		mm	ms	
1	52A	-	-	No damage
2	34A	13	10.4	No damage
3	61A	12	10.8	No damage
4	106A	8	8.6	No damage
5	92A	12	9.4	No damage
6	25A	-	-	No damage

General comments and response description::

The wall did not suffer any damage and remained elastic throughout its displacement history.

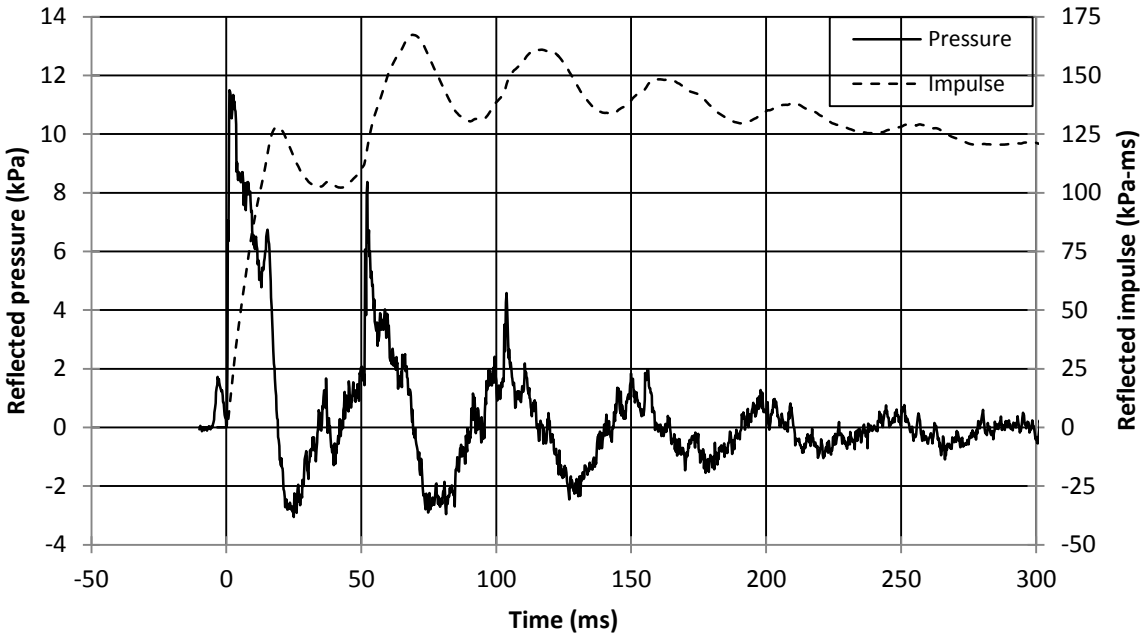

Figure B16-1.1: Reflected pressure and impulse time histories for Wall 16 Shot 1

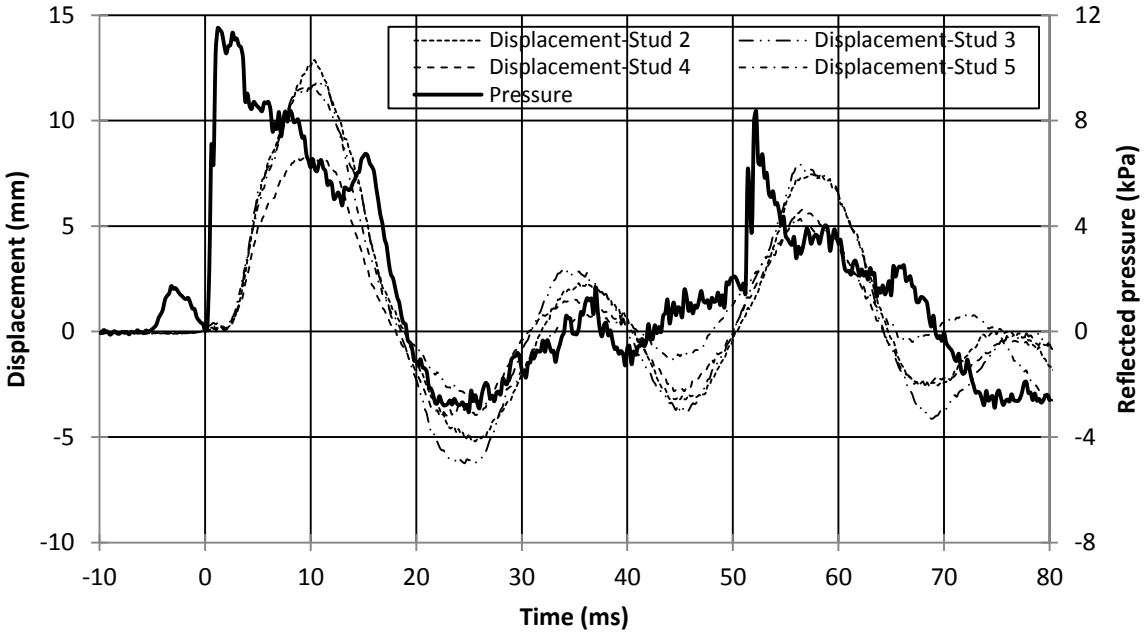

Figure B16-1.2: Displacement and pressure time histories for Wall 16 Shot 1

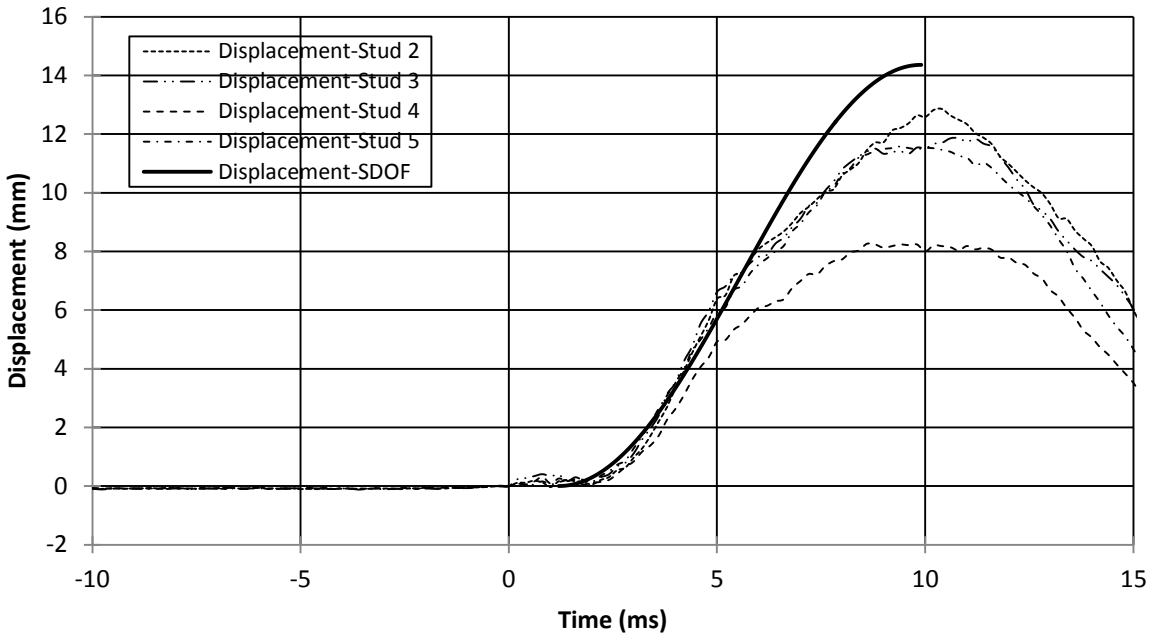

Figure B16-1.3: SDOF prediction for Wall 16 Shot 1

Wall 16, Pressure-Impulse Combination Number 2

Table B16-2: Wall 16, Shot 2-Test result summary

Light-Frame Stud Wall Dynamic Tests: Wall 16, Pressure-Impulse Combination Number 2

Test name:	Wall_16_Shot_2	**Test date:**	15/12/2012
Driver length:	2,745 **mm**	**Driver pressure:**	216.5 **kPa**

Test specimen description:

-6-38 mm x 140 mm MSR studs @ 406.4 mm o/c. -18.5 mm plywood

-Nails, 89 mm x 4.24 mm @150 mm o/c (field and edge)

-2,159 mm total height of wall -2,083 mm long studs -2,032 mm clear span

Average maximum reflected pressure:	32.6	**kPa**	**Wall mass:**	85.3	**kg**
Average maximum reflected impulse:	331.5	**kPa-ms**			
Experimental positive phase:	21.8	**ms**			
Theoretical positive phase:	20.3	**ms**			
Average deflection of wall studs:	37	**mm**			
Average time to maximum deflection:	9.9	**ms**			
Quantified wall damage:	**Moderate**				

Stud number	Stud reference name	Max. Disp.	Time to max.	Stud damage
		mm	ms	
1	52A	-	-	No damage
2	34A	38	8.4	Failed
3	61A	41	10.8	Minor Cracking
4	106A	30	10.4	No damage
5	92A	38	10.0	No damage
6	25A	-	-	No damage

General comments and response description::

Stud 2 failed during the first positive peak to maximum displacement while cracks initiated in Stud 3. Stud 2 was cracked lengthwise while a piece of it fell down. Studs 1, 4, 5, and 6 remained elastic. No sheathing failure. Nail withdrawal was observed.

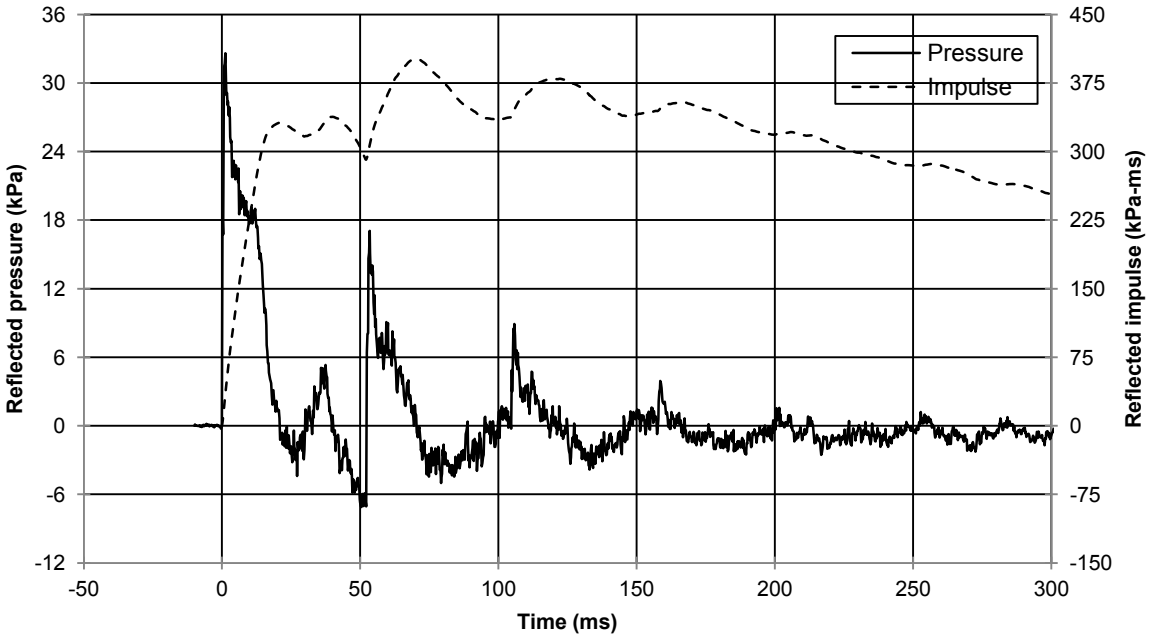

Figure B16-2.1: Reflected pressure and impulse time histories for Wall 16 Shot 2

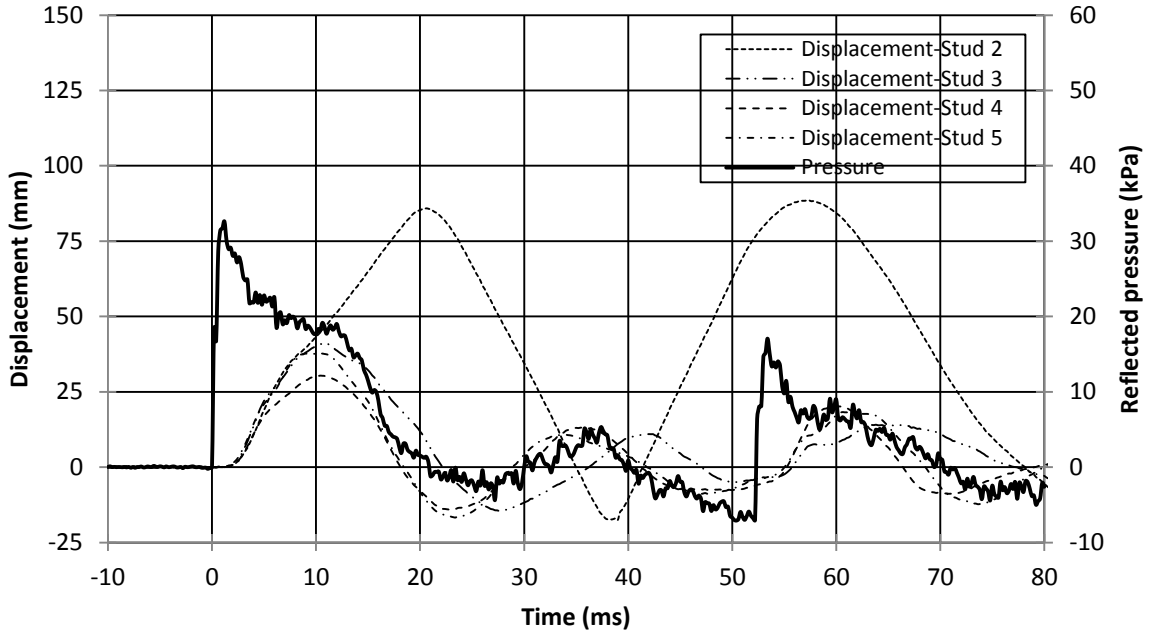

Figure B16-2.2: Displacement and pressure time histories for Wall 16 Shot 2

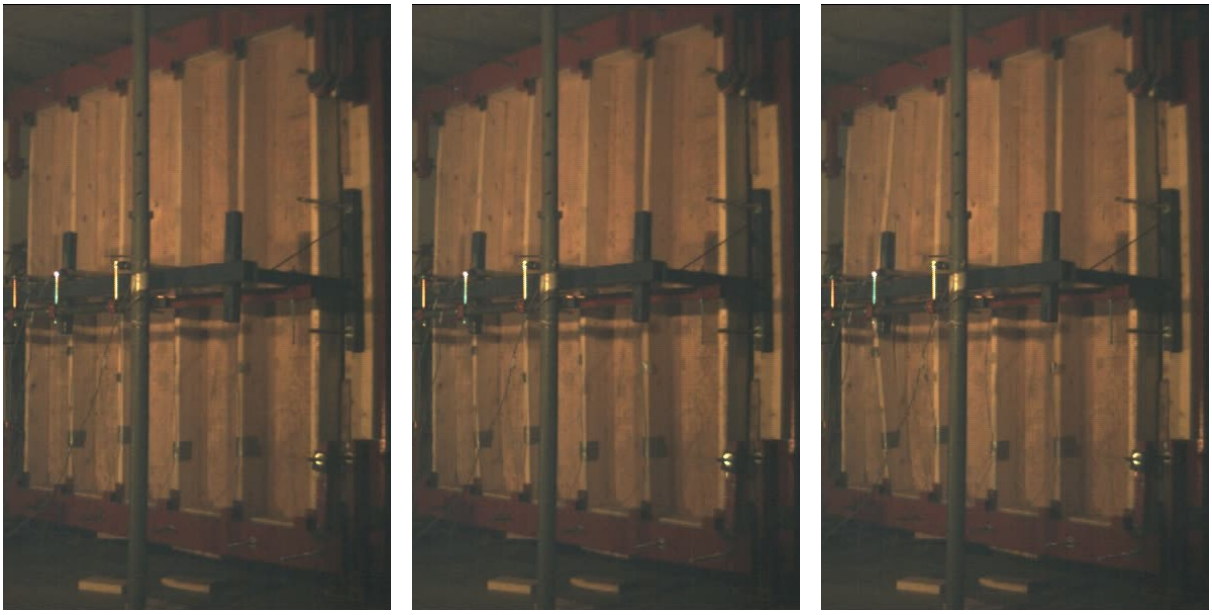

(a) t=0 ms (b) t=6 ms (c) t=14 ms

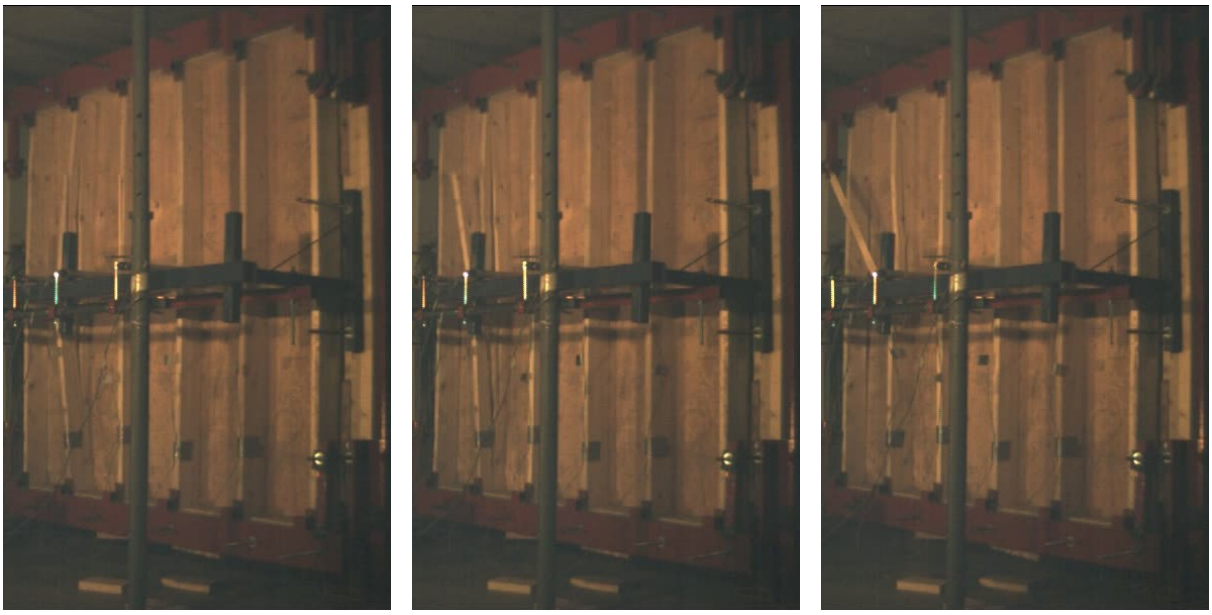

(d) t=18 ms (e) t=28 ms (f) t=90 ms

Figure B16-2.3: Evolution of damage with time for Wall 16 Shot 2

(a) View of entire wall

(b) Localized damage stud 2 and 3-Upper half

(c)Localize damage stud 2-Lower half

Figure B16-2.4: Damage of Wall 16 after shot 2

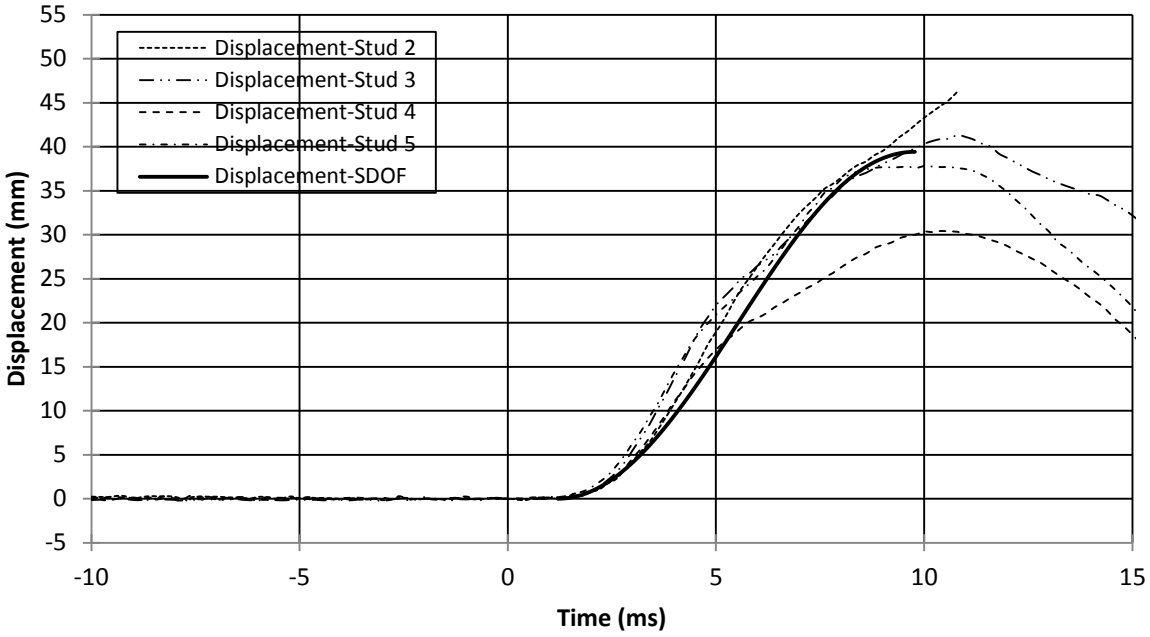

Figure B16-2.5: SDOF prediction for Wall 16 Shot 2

Wall 16, Pressure-Impulse Combination Number 3

Table B16-3: Wall 16, Shot 3-Test result summary

Light-Frame Stud Wall Dynamic Tests: Wall 16, Pressure-Impulse Combination Number 3

Test name:	Wall_16_Shot_3	**Test date:**	15/12/2012
Driver length:	2,750 **mm**	**Driver pressure:**	247.5 **kPa**

Test specimen description:

-6-38 mm x 140 mm MSR studs @ 406.4 mm o/c. -18.5 mm plywood

-Nails, 89 mm x 4.24 mm @150 mm o/c (field and edge)

-2,159 mm total height of wall -2,083 mm long studs -2,032 mm clear span

Average maximum reflected pressure:	34.1	**kPa**	**Wall mass:**	85.3	**kg**
Average maximum reflected impulse:	377.6	**kPa-ms**			
Experimental positive phase:	22.0	**ms**			
Theoretical positive phase:	22.2	**ms**			
Average deflection of wall studs:	45	**mm**			
Average time to maximum deflection:	11.4	**ms**			
Quantified wall damage:	**Heavy**				

Stud number	Stud reference name	Max. Disp.	Time to max.	Stud damage
		mm	ms	
1	52A	-	-	Failed
2	34A	-	-	Failed
3	61A	54	11.6	Failed
4	106A	36	11.0	No damage
5	92A	44	11.6	No damage
6	25A	-	-	No damage

Response description:

Studs number 1 to 3 failed during the first positive peak and the damage was exasperated during the successive peaks. No sheathing failure was observed. No sheathing failure. Nail withdrawal was observed. Due to previous failure, data for Stud 2 was not recorded.

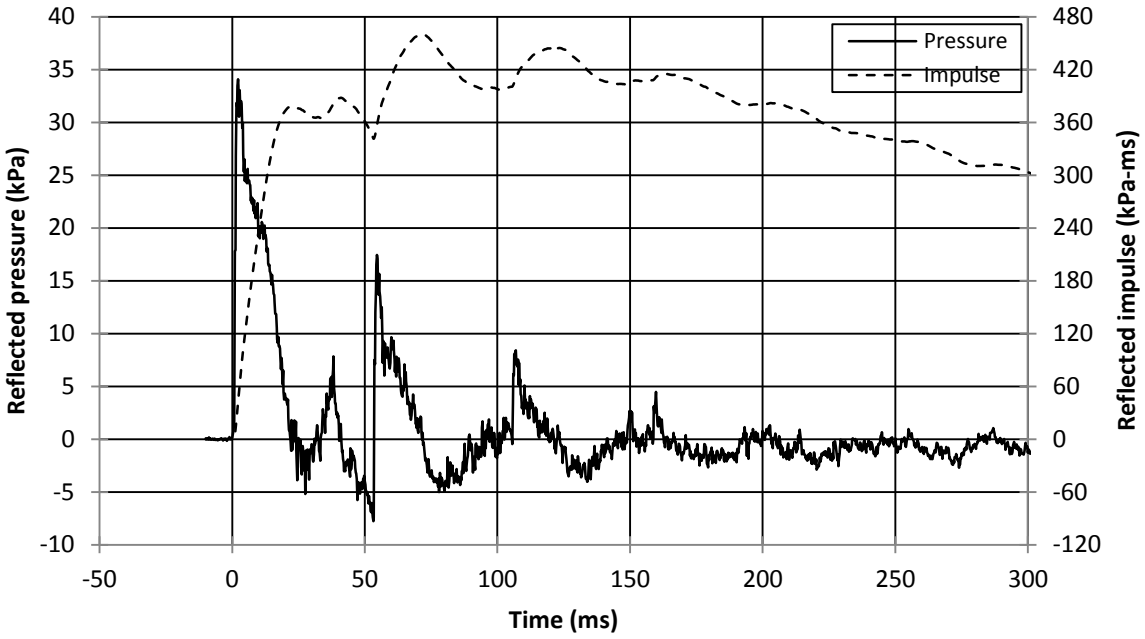

Figure B16-3.1: Reflected pressure and impulse time histories for Wall 16 Shot 3

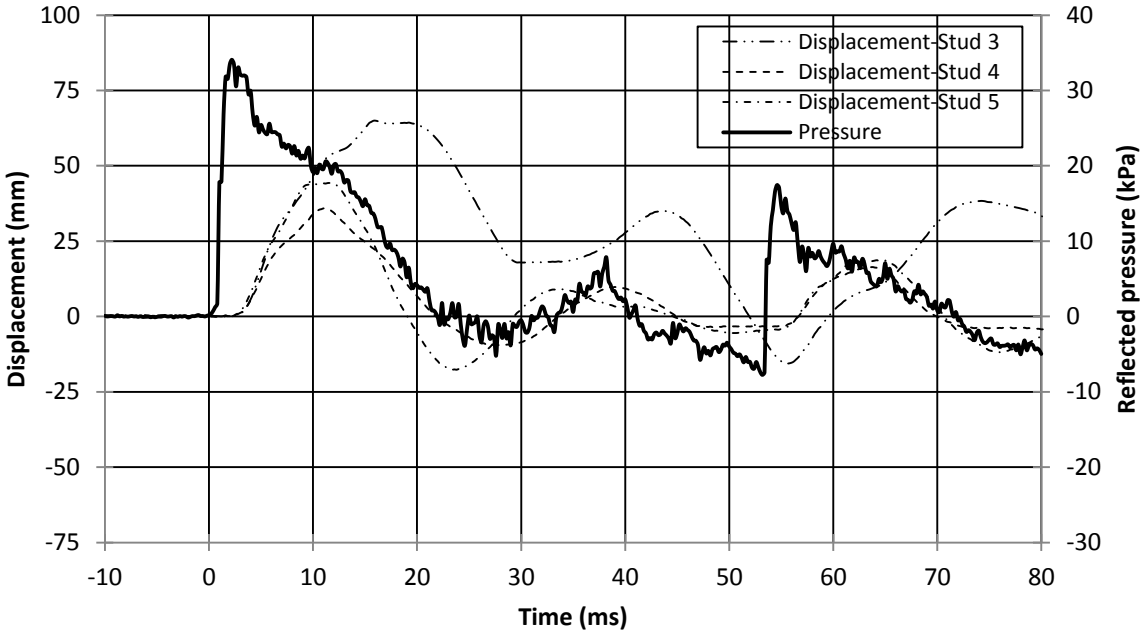

Figure B16-3.2: Displacement and pressure time histories for Wall 16 Shot 3

(a) t=0 ms (b) t=8 ms (c) t=14 ms

(d) t=18 ms (e) t=28 ms (f) t=100 ms

Figure B16-3.3: Evolution of damage with time for Wall 16 Shot 3

(a) View of entire wall

(b) Localized damage stud 1 to 3-Upper half

(c) Localized damage stud 1 to 3-Lower half

Figure B16-3.4: Damage of Wall 16 after shot 3

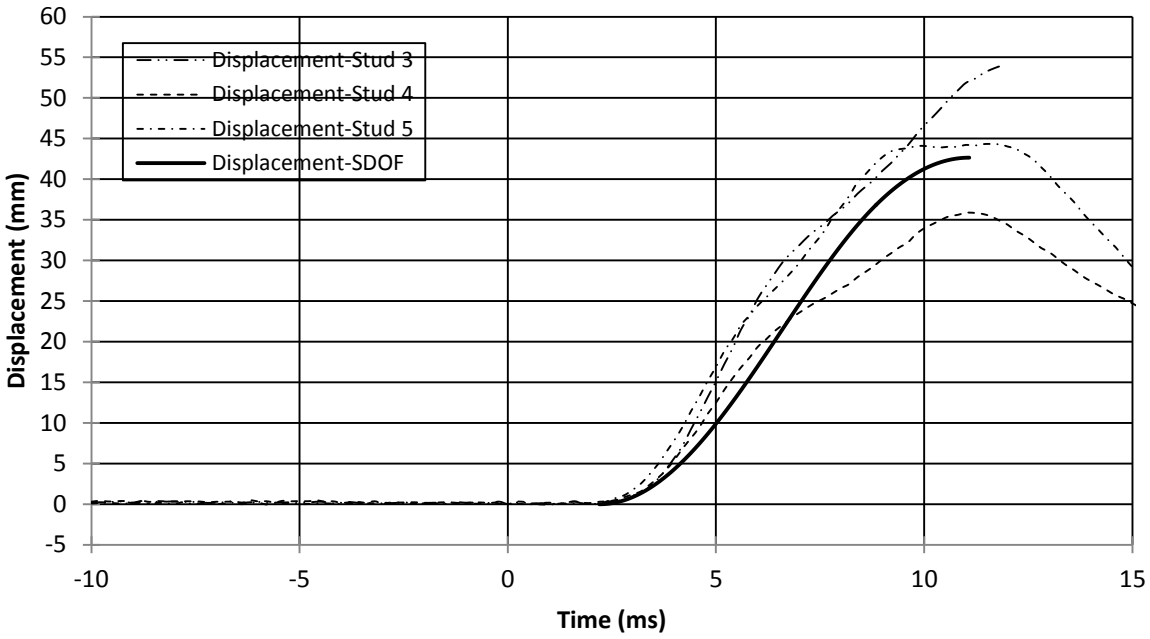

Figure B16-3.5: SDOF prediction for Wall 16 Shot 3

Wall 17, Pressure-Impulse Combination Number 1

Table B17-1: Wall 17, Shot 1-Test result summary

Light-Frame Stud Wall Dynamic Tests: Wall 17, Pressure-Impulse Combination Number 1

Test name:	Wall_17_Shot_1	**Test date:**	19/12/2012
Driver length:	4,880 **mm**	**Driver pressure:**	70.3 **kPa**

Test specimen description:

-6-38 mm x 140 mm MSR studs @ 406.4 mm o/c. -18.5 mm plywood

-Nails, 89 mm x 4.24 mm @150 mm o/c (field and edge)

-2,159 mm total height of wall -2,083 mm long studs -2,032 mm clear span

Average maximum reflected pressure:	12.6	**kPa**	**Wall mass:**	84.0	**kg**
Average maximum reflected impulse:	245.7	**kPa-ms**			
Experimental positive phase:	38.5	**ms**			
Theoretical positive phase:	39.0	**ms**			
Average deflection of wall studs:	13	**mm**			
Average time to maximum deflection:	9.9	**ms**			
Quantified wall damage:	**Superficial**				

Stud number	Stud reference name	Max. Disp.	Time to max.	Stud damage
		mm	ms	
1	113A	-	-	No damage
2	85A	12	10.6	No damage
3	8A	14	10.2	No damage
4	12A	11	9.8	No damage
5	56A	15	8.8	No damage
6	89A	-	-	No damage

Response description:

The wall did not suffer any damage and remained elastic throughout its displacement history.

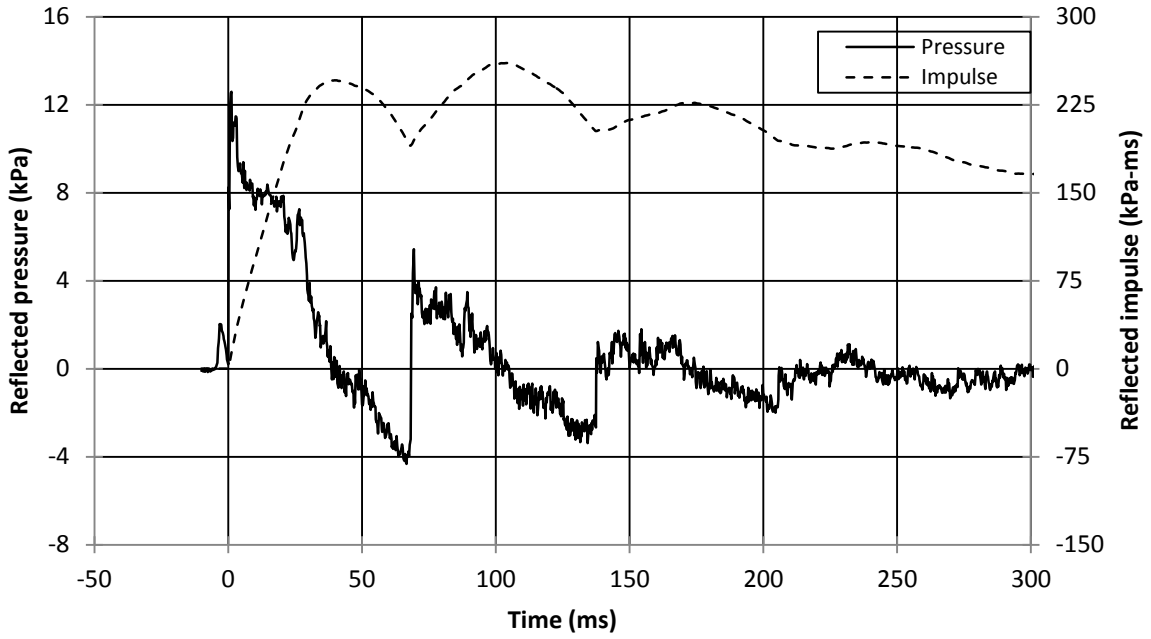

Figure B17-1.1: Reflected pressure and impulse time histories for Wall 17 Shot 1

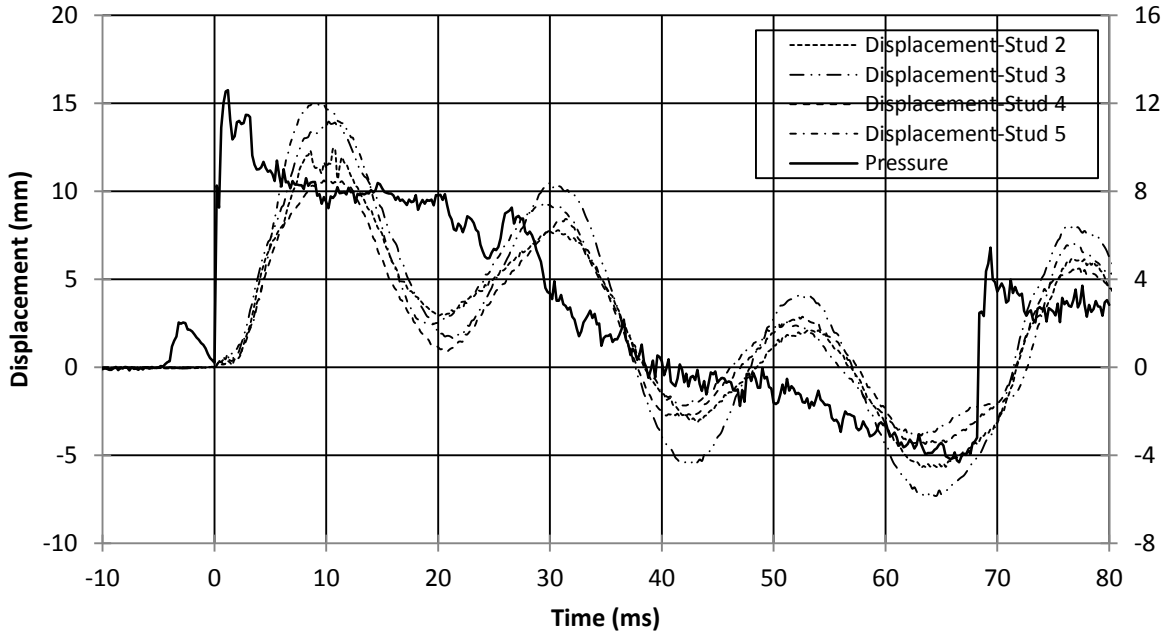

Figure B17-1.2: Displacement and pressure time histories for Wall 17 Shot 1

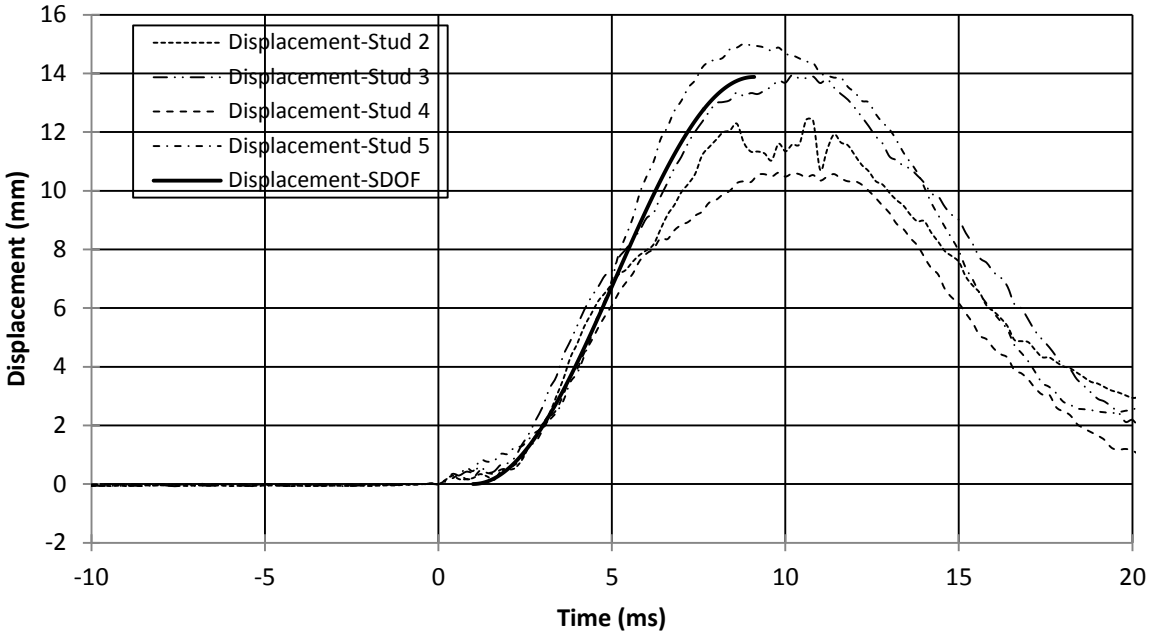

Figure B17-1.3: SDOF prediction for Wall 17 Shot 1

Wall 17, Pressure-Impulse Combination Number 2

Table B17-2: Wall 17, Shot 2-Test result summary

Light-Frame Stud Wall Dynamic Tests: Wall 17, Pressure-Impulse Combination Number 2

Test name:	Wall_17_Shot_2	**Test date:**	19/12/2012
Driver length:	4,880 **mm**	**Driver pressure:**	266.1 **kPa**

Test specimen description:

-6-38 mm x 140 mm MSR studs @ 406.4 mm o/c. -18.5 mm plywood

-Nails, 89 mm x 4.24 mm @150 mm o/c (field and edge)

-2,159 mm total height of wall -2,083 mm long studs -2,032 mm clear span

Average maximum reflected pressure:	40.1	**kPa**	**Wall mass:**	84.0	**kg**
Average maximum reflected impulse:	813.12	**kPa-ms**			
Experimental positive phase:	56.0	**ms**			
Theoretical positive phase:	40.5	**ms**			
Average deflection of wall studs:	51	**mm**			
Average time to maximum deflection:	9.9	**ms**			
Quantified wall damage:	**Moderate**				

Stud number	Stud reference name	Max. Disp.	Time to max.	Stud damage
		mm	ms	
1	113A	-	-	Failed
2	85A	48	8.6	Failed
3	8A	58	10.0	Failed
4	12A	44	11.2	No damage
5	56A	54	9.6	Minor Cracking
6	89A	-	-	No damage

Response description:

Studs number 1 to 3 failed during the first positive peak to maximum displacement while the damage was exasperated during the successive peaks. Minor cracks were observed on the tension face of Stud 5. No sheathing failure was observed. No nail withdrawal.

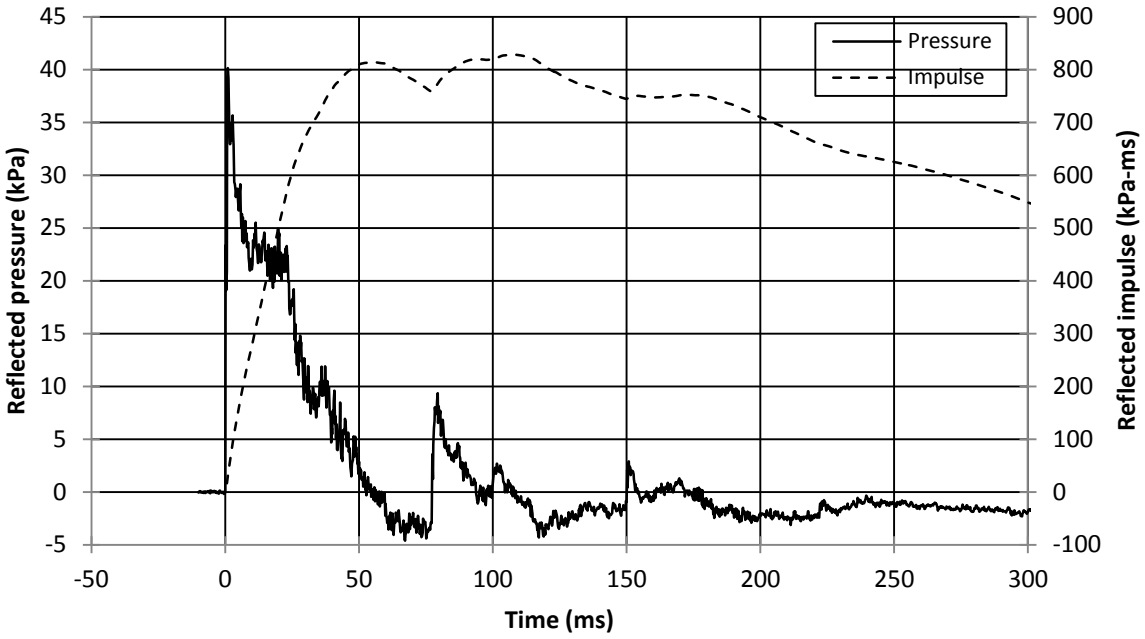

Figure B17-2.1: Reflected pressure and impulse time history for Wall 17 Shot 2

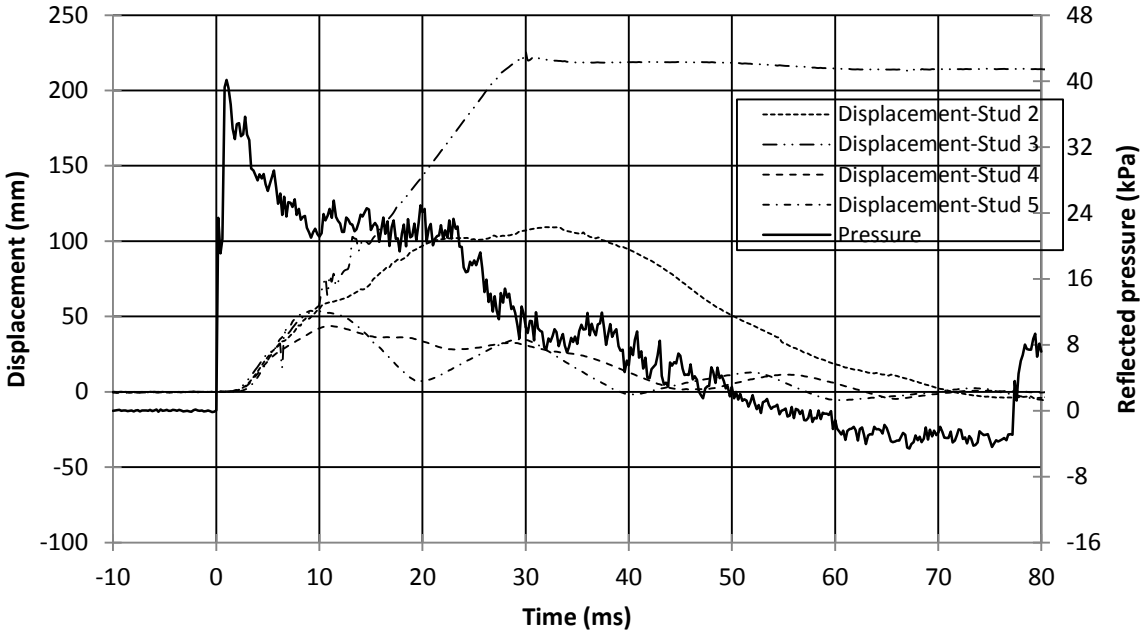

Figure B17-2.2: Displacement and pressure time histories for Wall 17 Shot 2

(a) t=0 ms (b) t=10 ms (c) t=16 ms

(d) t=24 ms (e) t=30 ms (f) t=120 ms

Figure B17-2.3: Evolution of damage with time for Wall 17 Shot 2

(a) View of entire wall

(b) Localized damage stud 1 to 3-Upper half

(c) Localized damage stud 1 to 3-Lower half

Figure B17-2.4: Damage of Wall 17 after shot 2

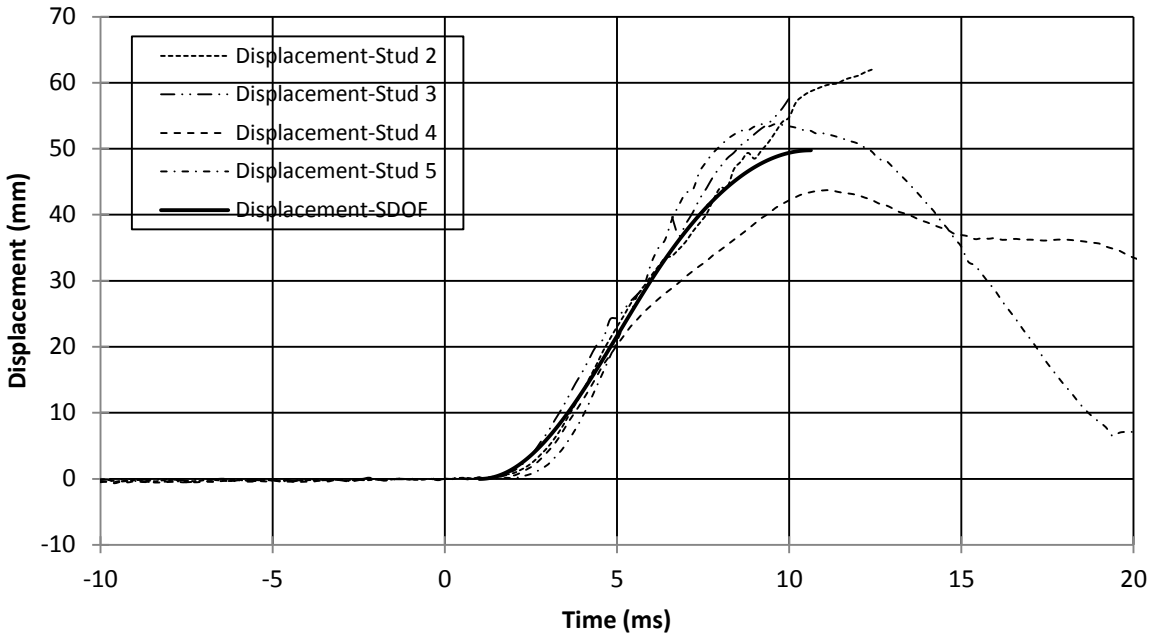

Figure B17-2.5: SDOF prediction for Wall 17 Shot 2

Wall 18, Pressure-Impulse Combination Number 1

Table B18-1: Wall 18, Shot 1-Test result summary

Light-Frame Stud Wall Dynamic Tests: Wall 18, Pressure-Impulse Combination Number 1

Test name:	Wall_18_Shot_1	**Test date:**	17/12/2012
Driver length:	305 **mm**	**Driver pressure:**	82.7 **kPa**

Test specimen description:

-6-38 mm x 140 mm MSR studs @ 406.4 mm o/c. -18.5 mm plywood

-Nails, 89 mm x 4.24 mm @150 mm o/c (field and edge)

-2,159 mm total height of wall -2,083 mm long studs -2,032 mm clear span

Average maximum reflected pressure:	9.5	**kPa**	**Wall mass:**	83.8	**kg**
Average maximum reflected impulse:	27.3	**kPa-ms**			
Experimental positive phase:	5.8	**ms**			
Theoretical positive phase:	5.8	**ms**			
Average deflection of wall studs:	5	**mm**			
Average time to maximum deflection:	5.6	**ms**			
Quantified wall damage:	**Superficial**				

Stud number	Stud reference name	Max. Disp.	Time to max.	Stud damage
		mm	ms	
1	43A	-	-	No damage
2	115A	5	5.6	No damage
3	122A	-	-	No damage
4	22A	-	-	No damage
5	28A	-	-	No damage
6	29A	-	-	No damage

Response description:

The wall did not suffer any damage and remained elastic throughout its displacement history. Due to an instrumentation error, displacement data was only available for Stud 2.

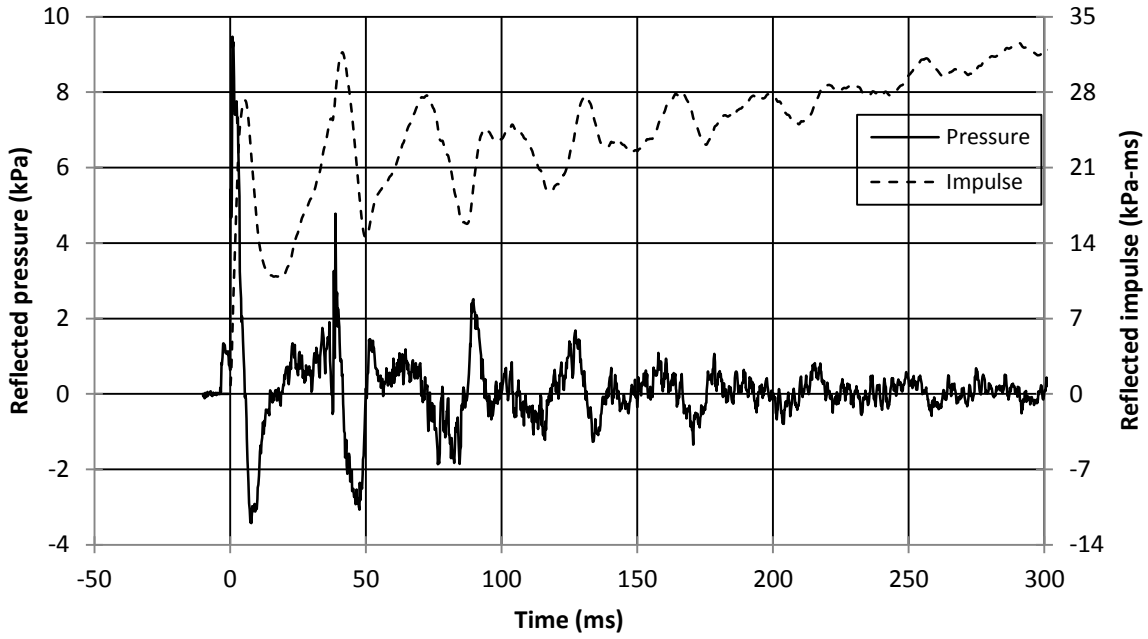

Figure B18-1.1: Reflected pressure and impulse time histories for Wall 18 Shot 1

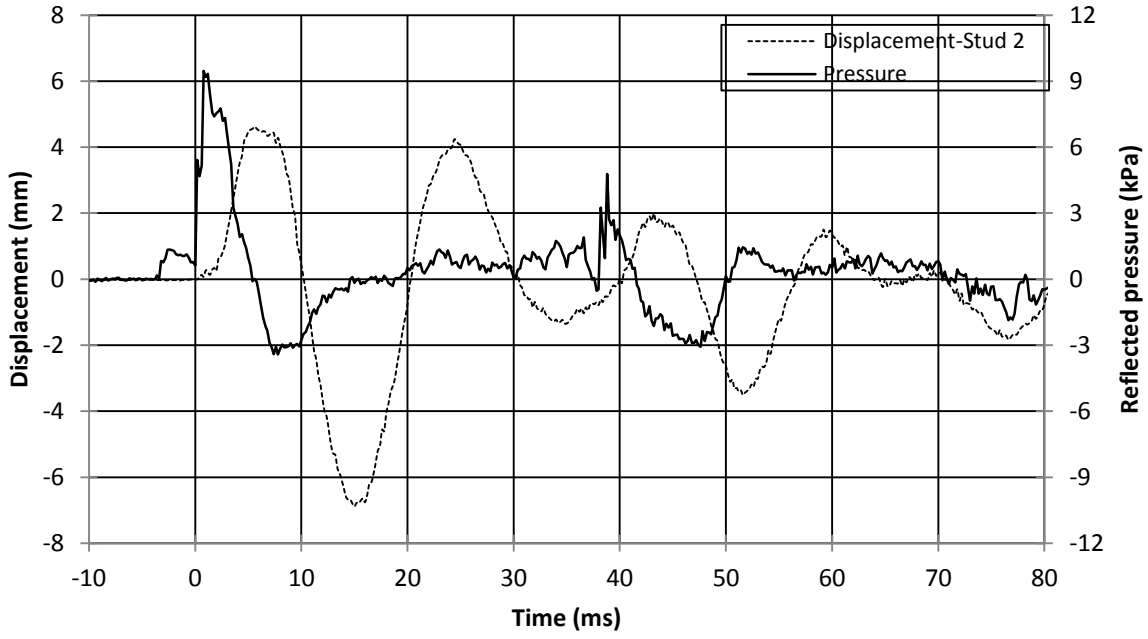

Figure B18-1.2: Displacement and pressure time histories for Wall 18 Shot 1

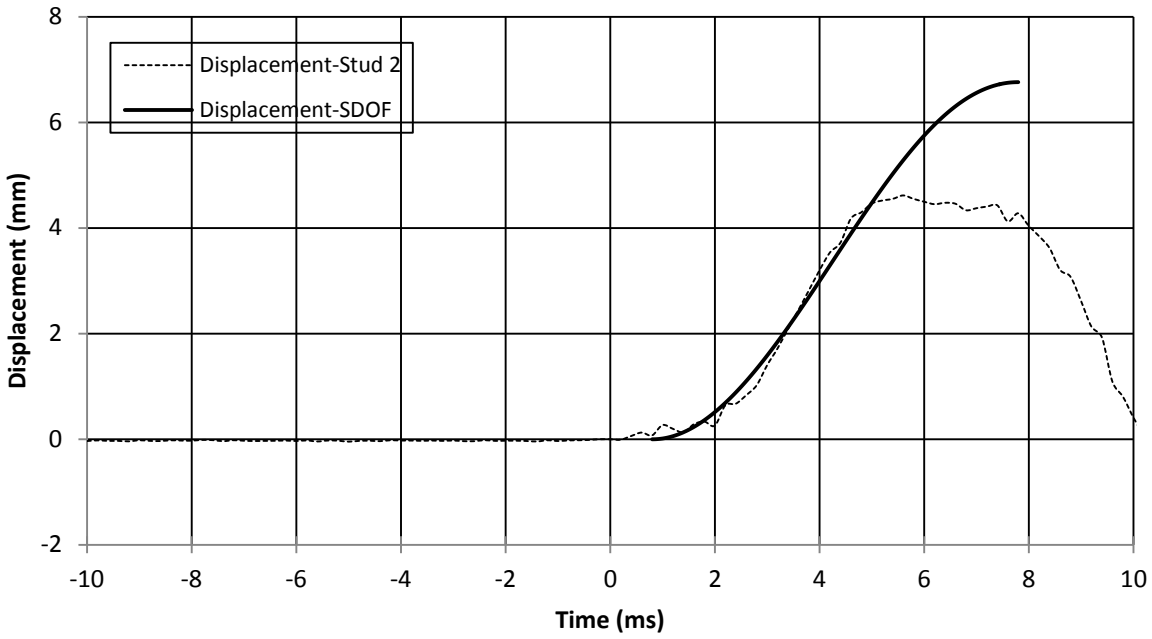

Figure B18-1.3: SDOF prediction for Wall 18 Shot 1

Wall 18, Pressure-Impulse Combination Number 2

Table B18-2: Wall 18, Shot 2-Test result summary

Light-Frame Stud Wall Dynamic Tests: Wall 18, Pressure-Impulse Combination Number 2

Test name:	Wall_18_Shot_2	**Test date:**	17/12/2012
Driver length:	305 **mm**	**Driver pressure:**	613.6 **kPa**

Test specimen description:

-6-38 mm x 140 mm MSR studs @ 406.4 mm o/c. -18.5 mm plywood

-Nails, 89 mm x 4.24 mm @150 mm o/c (field and edge)

-2,159 mm total height of wall -2,083 mm long studs -2,032 mm clear span

Average maximum reflected pressure:	55.0	**kPa**	**Wall mass:**	83.8	**kg**
Average maximum reflected impulse:	172.6	**kPa-ms**			
Experimental positive phase:	8.0	**ms**			
Theoretical positive phase:	6.3	**ms**			
Average deflection of wall studs:	45	**mm**			
Average time to maximum deflection:	8.7	**ms**			
Quantified wall damage:	**Moderate**				

Stud number	Stud reference name	Max. Disp.	Time to max.	Stud damage
		mm	ms	
1	43A	-	-	No damage
2	115A	53	9.2	Minor Cracking
3	122A	-	-	Failed
4	22A	37	8.2	Failed
5	28A	-	-	Failed
6	29A	-	-	No damage

Response description:

No studs failed during the first positive peak although cracks initiated. Due to the high pressure experienced during the negative phase, the change from compression to tension observed in the oscillations of positive to negative peaks led to failure of Studs 3, 4 and 5. A longitudinal crack was observed in Stud 2. No sheathing failure was observed. No nail withdrawal. Due to an instrumentation error, displacement data was not available for Studs 3 and 5

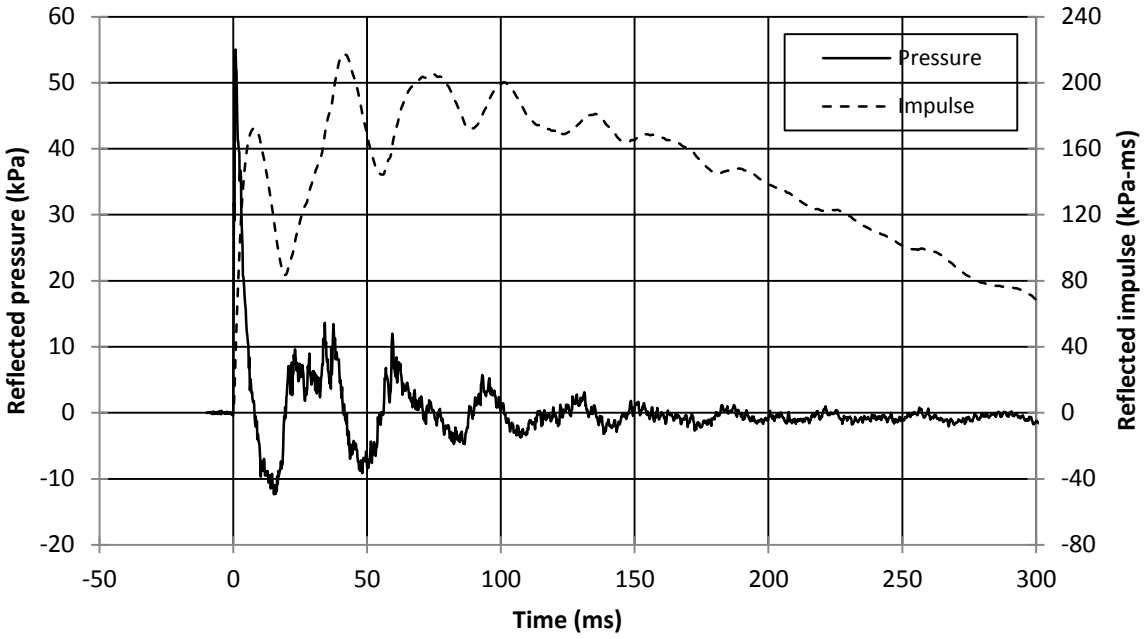

Figure B18-2.1: Reflected pressure and impulse time histories for Wall 18 Shot 2

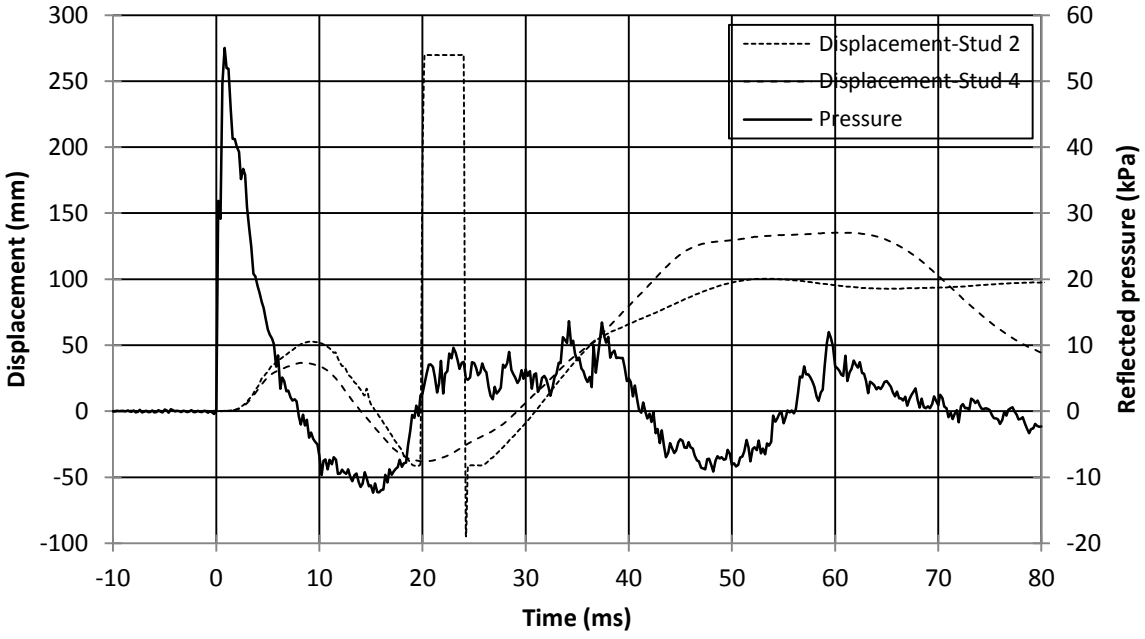

Figure B18-2.2: Displacement and pressure time histories for Wall 18 Shot 2

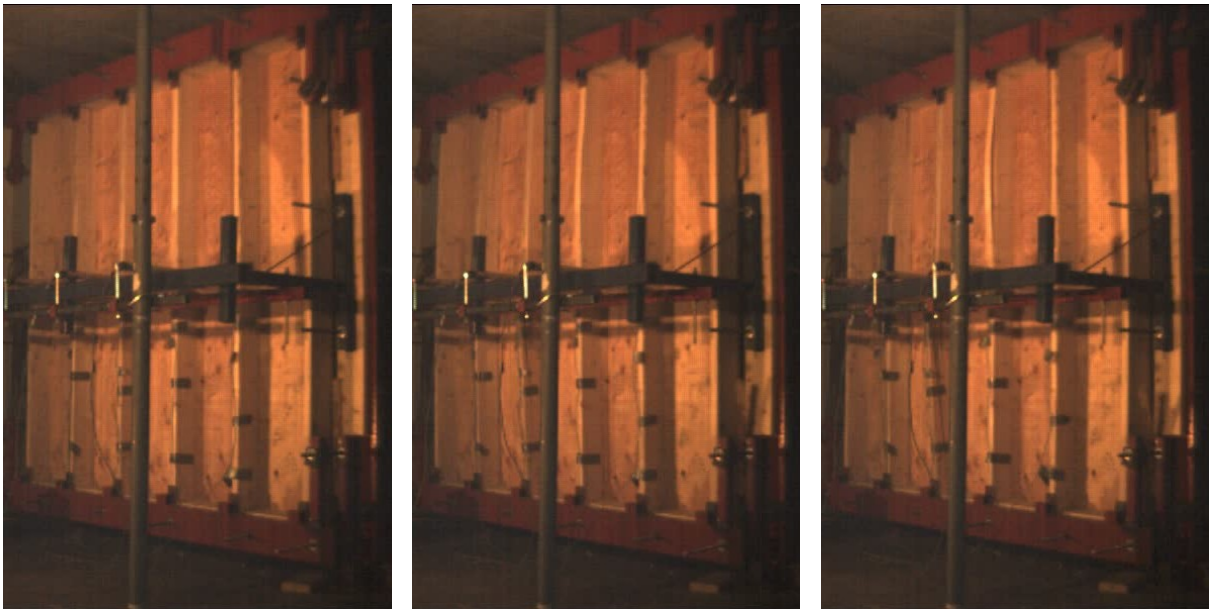

(a) t=0 ms (b) t=8 ms (c) t=12 ms

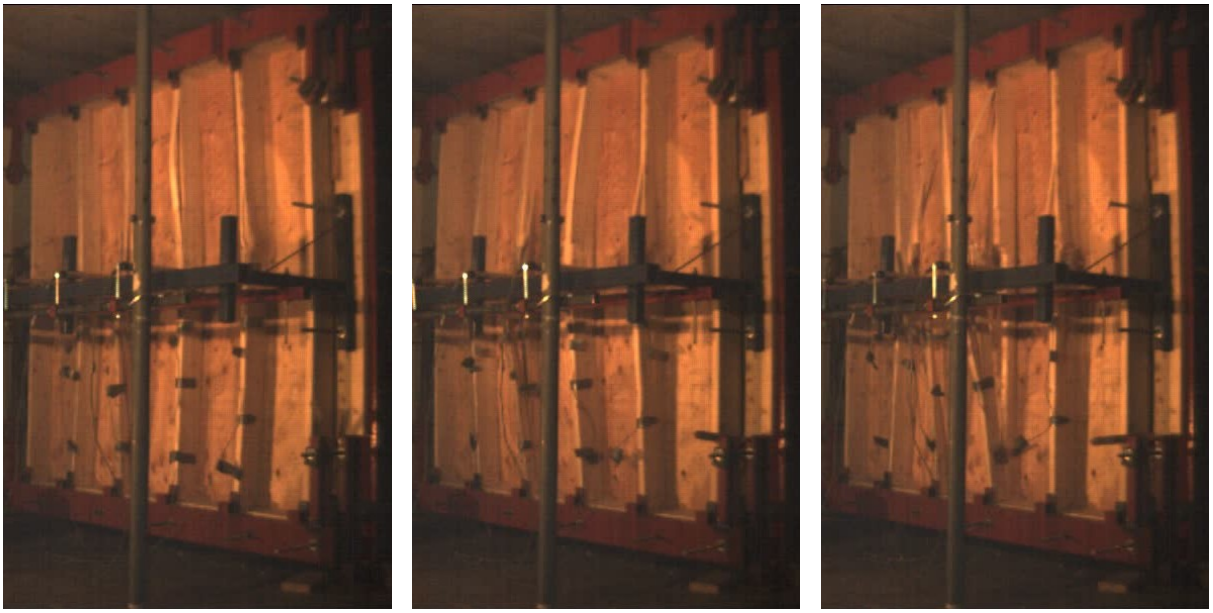

(d) t=18 ms (e) t=40 ms (f) t=56 ms

Figure B18-2.3: Evolution of damage with time for Wall 18 Shot 2

(a) View of entire wall

(b) Localized damage stud 1 to 5-Upper half

(c) Localized damage stud 1 to 5-Lower half

Figure B18-2.4: Damage of Wall 18 after shot 2

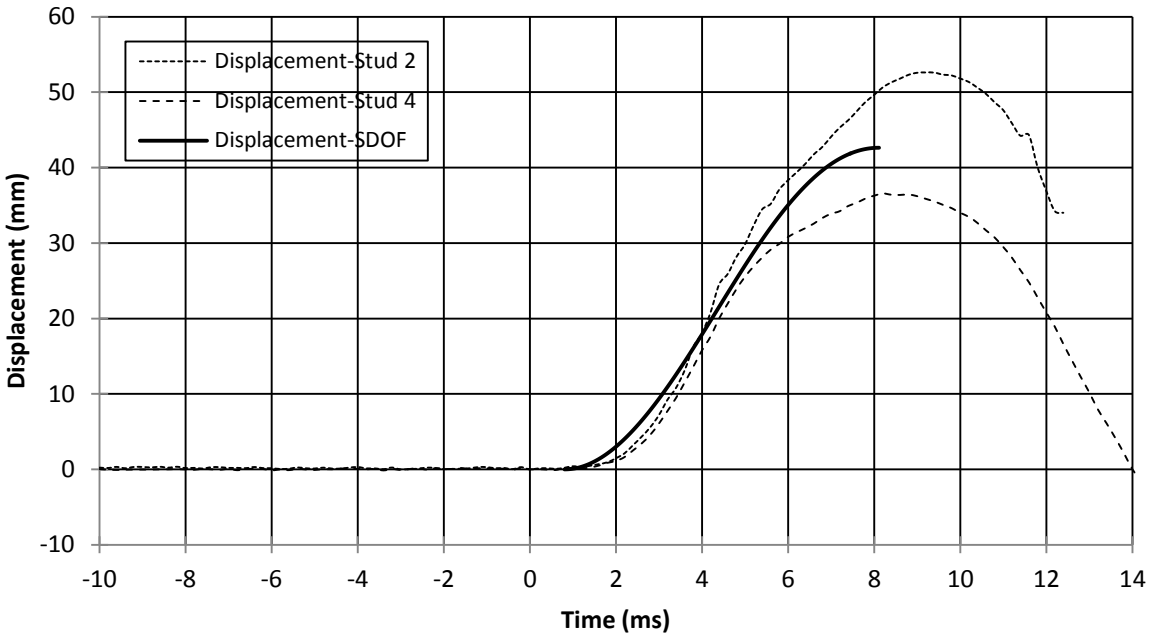

Figure B18-2.5: SDOF prediction for Wall 18 Shot 2

Wall 19, Pressure-Impulse Combination Number 1

Table B19-1: Wall 19, Shot 1-Test result summary

Light-Frame Stud Wall Dynamic Tests: Wall 19, Pressure-Impulse Combination Number 1

Test name:	Wall_19_Shot_1	**Test date:**	16/12/2012
Driver length:	2,745 **mm**	**Driver pressure:**	64.8 **kPa**

Test specimen description:

-6-38 mm x 140 mm MSR studs @ 406.4 mm o/c. -18.5 mm plywood

-Nails, 89 mm x 4.24 mm @150 mm o/c (field and edge)

-2,159 mm total height of wall -2,083 mm long studs -2,032 mm clear span

Average maximum reflected pressure:	11.0	**kPa**	**Wall mass:**	83.1	**kg**
Average maximum reflected impulse:	122.2	**kPa-ms**			
Experimental positive phase:	19.0	**ms**			
Theoretical positive phase:	22.2	**ms**			
Average deflection of wall studs:	11	**mm**			
Average time to maximum deflection:	9.8	**ms**			
Quantified wall damage:	**Superficial**				

Stud number	Stud reference name	Max. Disp.	Time to max.	Stud damage
		mm	ms	
1	77A	-	-	No damage
2	66A	10	9.8	No damage
3	55A	11	9.6	No damage
4	18A	12	10.0	No damage
5	80A	11	9.6	No damage
6	14A	-	-	No damage

Response description:

The wall did not suffer any damage and remained elastic throughout its displacement history.

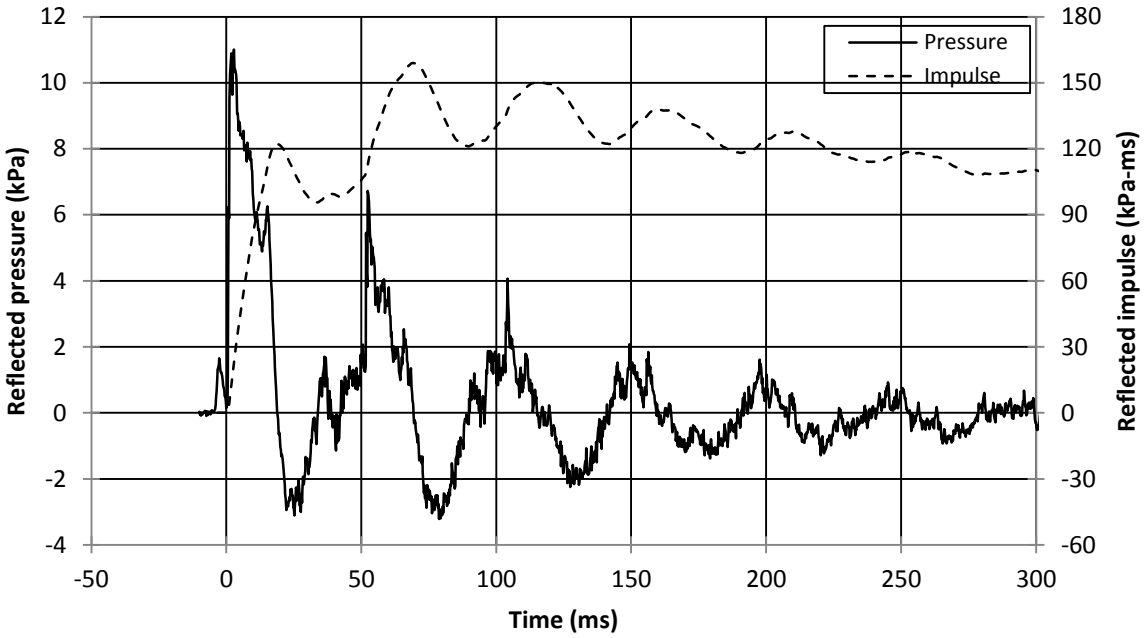

Figure B19-1.1: Reflected pressure and impulse time histories for Wall 19 Shot 1

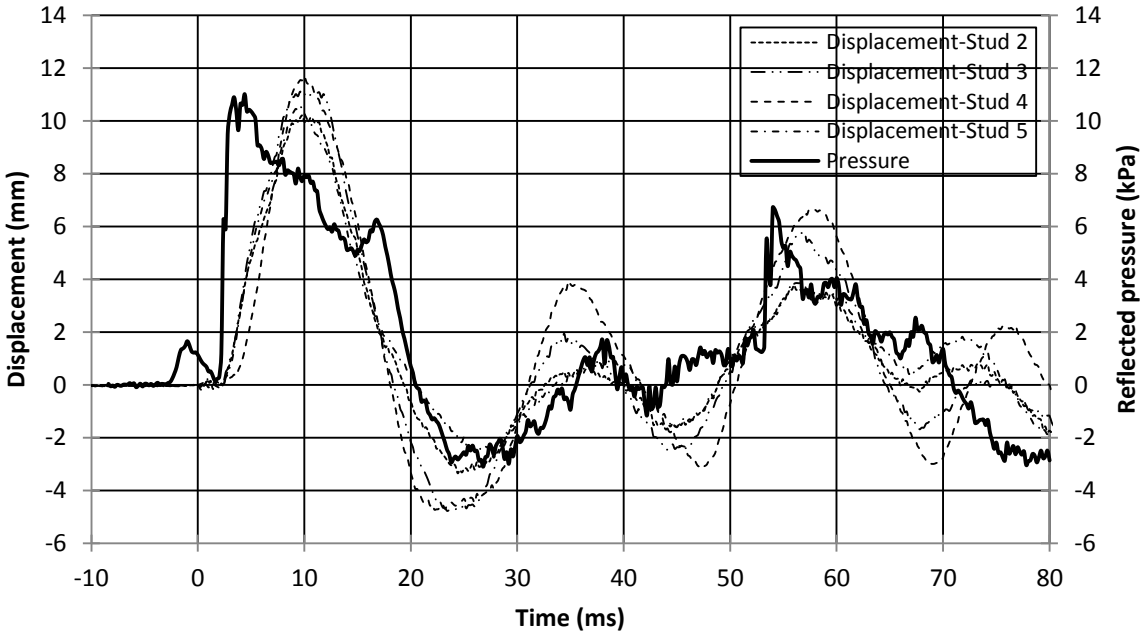

Figure B19-2.3: Displacement and pressure time histories for Wall 19 Shot 1

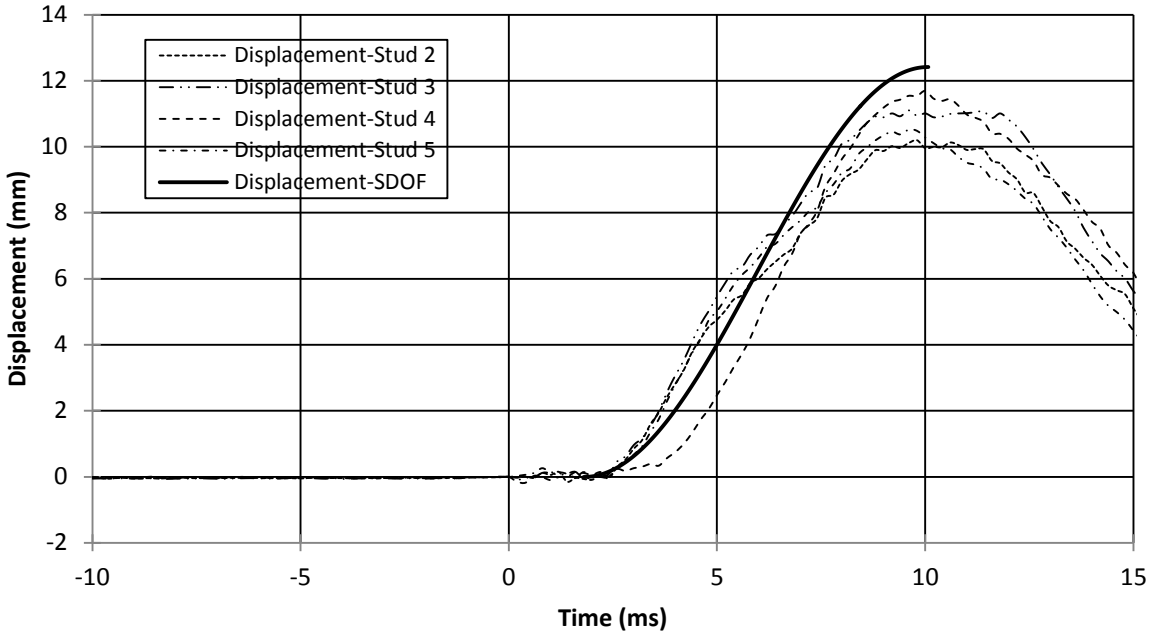

Figure B19-1.3: SDOF prediction for Wall 19 Shot1

Wall 19, Pressure-Impulse Combination Number 2

Table B19-2: Wall 19, Shot 2-Test result summary

Light-Frame Stud Wall Dynamic Tests: Wall 19, Pressure-Impulse Combination Number 2

Test name:	Wall_19_Shot_2	**Test date:**	16/12/2012
Driver length:	2,745 **mm**	**Driver pressure:**	264.0 **kPa**

Test specimen description:

-6-38 mm x 140 mm MSR studs @ 406.4 mm o/c. -18.5 mm plywood

-Nails, 89 mm x 4.24 mm @150 mm o/c (field and edge)

-2,159 mm total height of wall -2,083 mm long studs -2,032 mm clear span

Average maximum reflected pressure:	42.1	**kPa**	**Wall mass:**	83.1	**kg**
Average maximum reflected impulse:	450.4	**kPa-ms**			
Experimental positive phase:	24.0	**ms**			
Theoretical positive phase:	21.4	**ms**			
Average deflection of wall studs:	56	**mm**			
Average time to maximum deflection:	10.3	**ms**			
Quantified wall damage:	**Moderate**				

Stud number	Stud reference name	Max. Disp.	Time to max.	Stud damage
		mm	ms	
1	77A	-	-	Cracked
2	66A	68	10.0	Failed
3	55A	-	-	Failed
4	18A	48	11.6	Minor Cracks
5	80A	52	9.4	Minor Cracks
6	14A	-	-	No damage

Response description:

The Studs 2 and 3 failed during the first positive peak while the damage was exasperated in the successive peaks. Stud 1 had a considerable crack on the tension side leaving a piece of wood hanging free from one end. Minor cracks were observed in Studs 4 and 5. No sheathing failure was observed. No nail withdrawal. Due to an instrumentation error, displacement data was not available for Stud 3

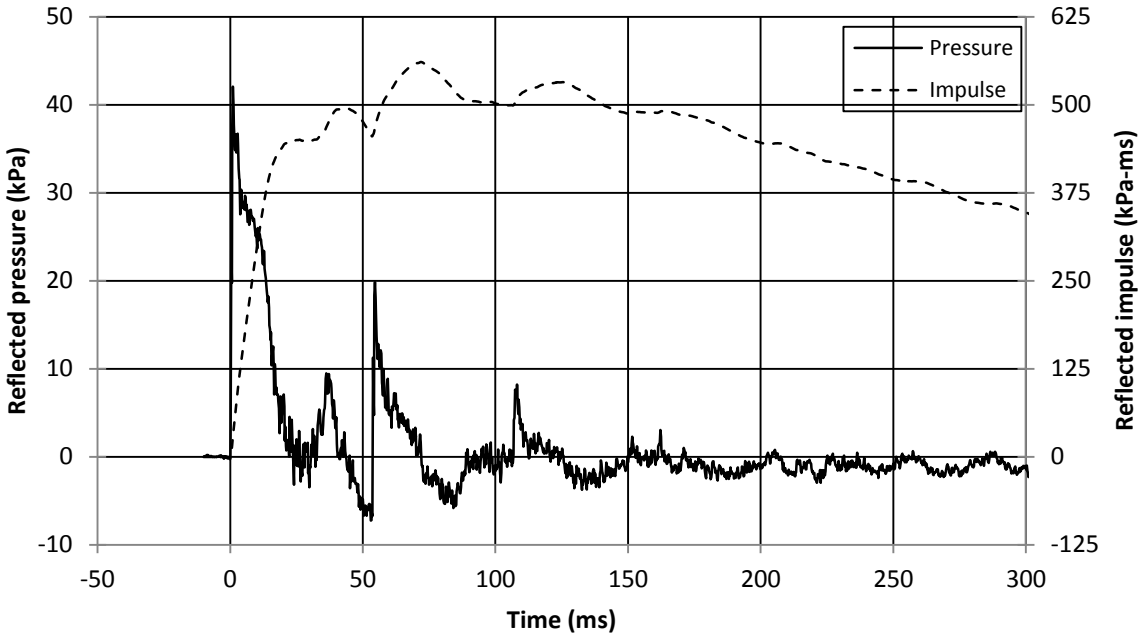

Figure B19-2.1: Reflected pressure and impulse time histories for Wall 19 Shot 2

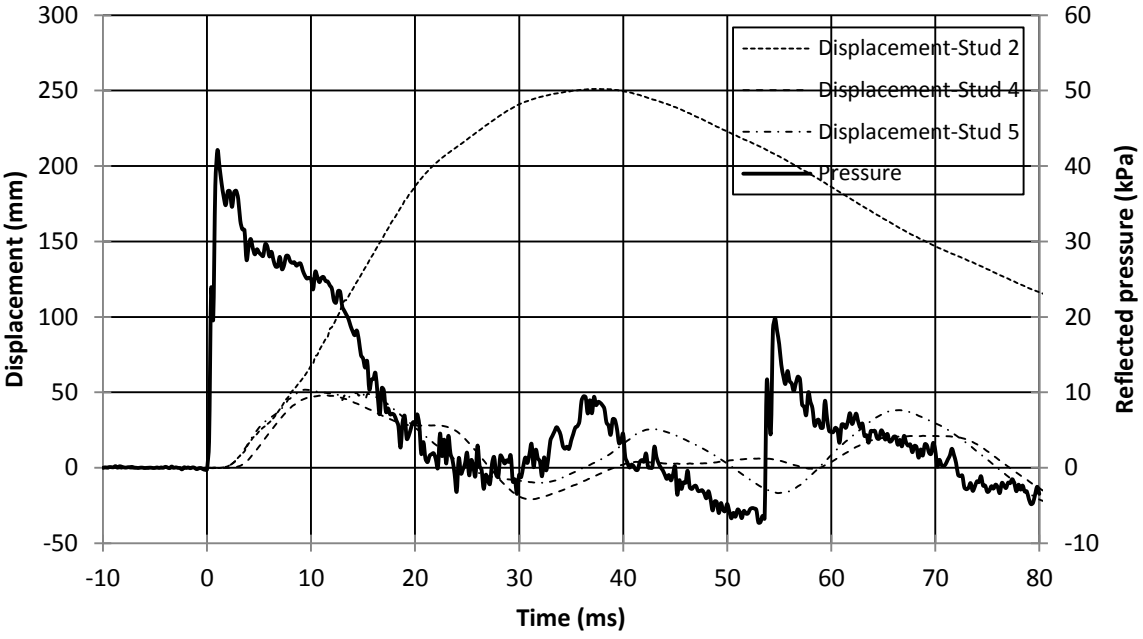

Figure B19-2.2: Displacement and pressure time histories for Wall 19 Shot 2

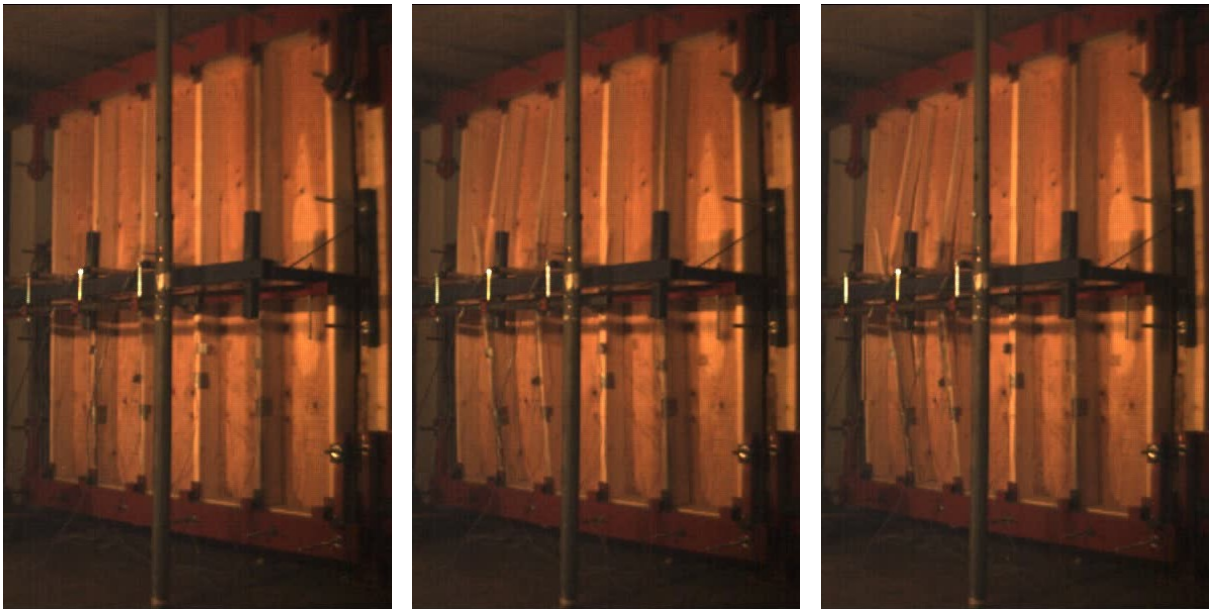

(a) t=0 ms (b) t=12 ms (c) t=16 ms

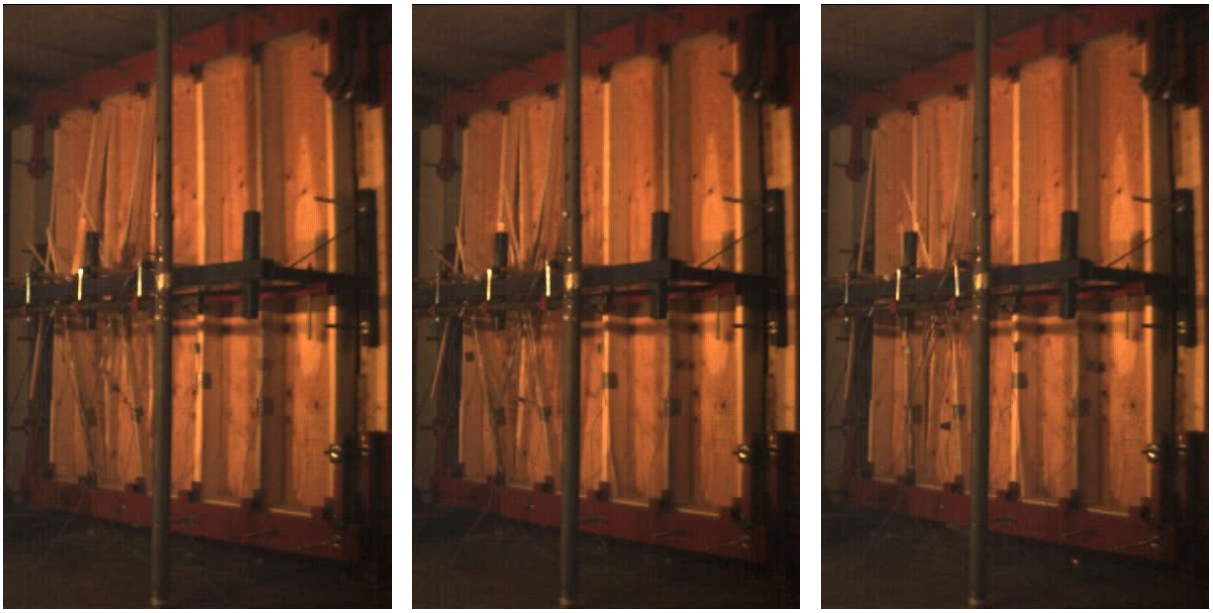

(d) t=26 ms (e) t=34 ms (f) t=90 ms

Figure B19-2.3: Evolution of damage with time for Wall 19 Shot 2

(a) View of entire wall from right side

(b) View of entire wall from left side

Figure B19-2.4: Damage of Wall 19 after shot 2

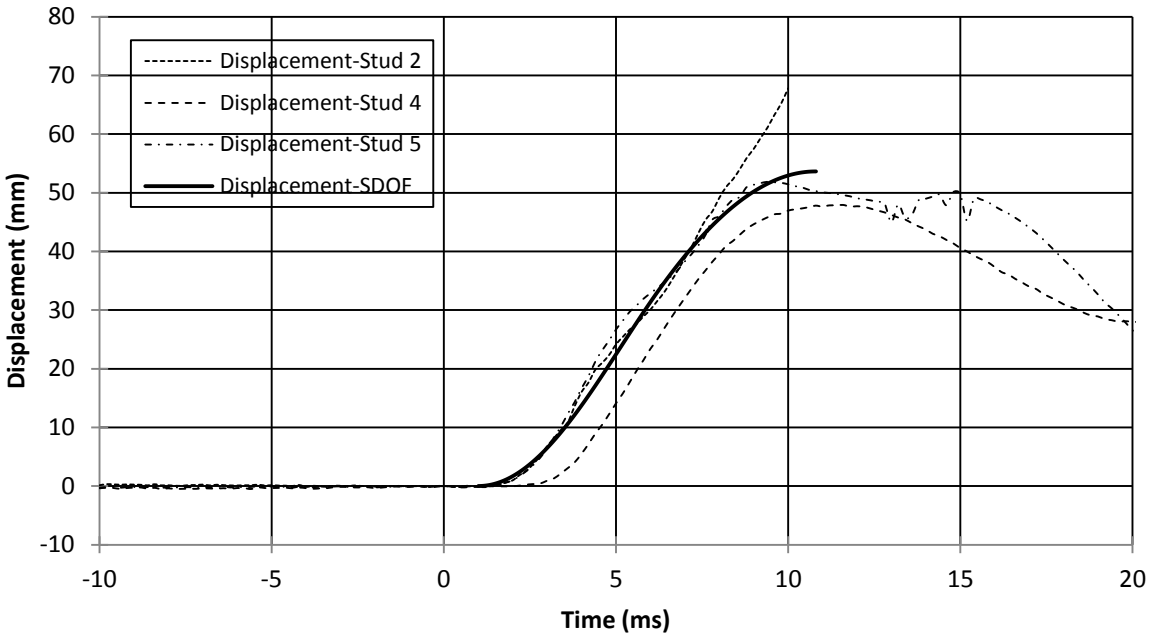

Figure B19-2.5: SDOF prediction for Wall 19 Shot 2

Wall 20, Pressure-Impulse Combination Number 1

Table B20-1: Wall 20, Shot 1-Test result summary

Light-Frame Stud Wall Dynamic Tests: Wall 20, Pressure-Impulse Combination Number 1

Test name:	Wall_20_Shot_1	**Test date:**	14/12/2012
Driver length:	2,745 **mm**	**Driver pressure:**	76.5 **kPa**

Test specimen description:

-6-38 mm x 140 mm MSR studs @ 406.4 mm o/c. -18.5 mm plywood

-Nails, 89 mm x 4.24 mm @150 mm o/c (field and edge)

-2,159 mm total height of wall -2,083 mm long studs -2,032 mm clear span

Average maximum reflected pressure:	12.5	**kPa**	**Wall mass:**	85.2	**kg**
Average maximum reflected impulse:	160.3	**kPa-ms**			
Experimental positive phase:	22.0	**ms**			
Theoretical positive phase:	25.6	**ms**			
Average deflection of wall studs:	16	**mm**			
Average time to maximum deflection:	12.1	**ms**			
Quantified wall damage:	**Superficial**				

Stud number	Stud reference name	Max. Disp.	Time to max.	Stud damage
		mm	ms	
1	54A	-	-	No damage
2	15A	16	11.4	No damage
3	17A	17	12.0	No damage
4	75A	15	12.8	No damage
5	10A	16	12.0	No damage
6	83A	-	-	No damage

Response description:

The wall did not suffer any damage and remained elastic throughout its displacement history.

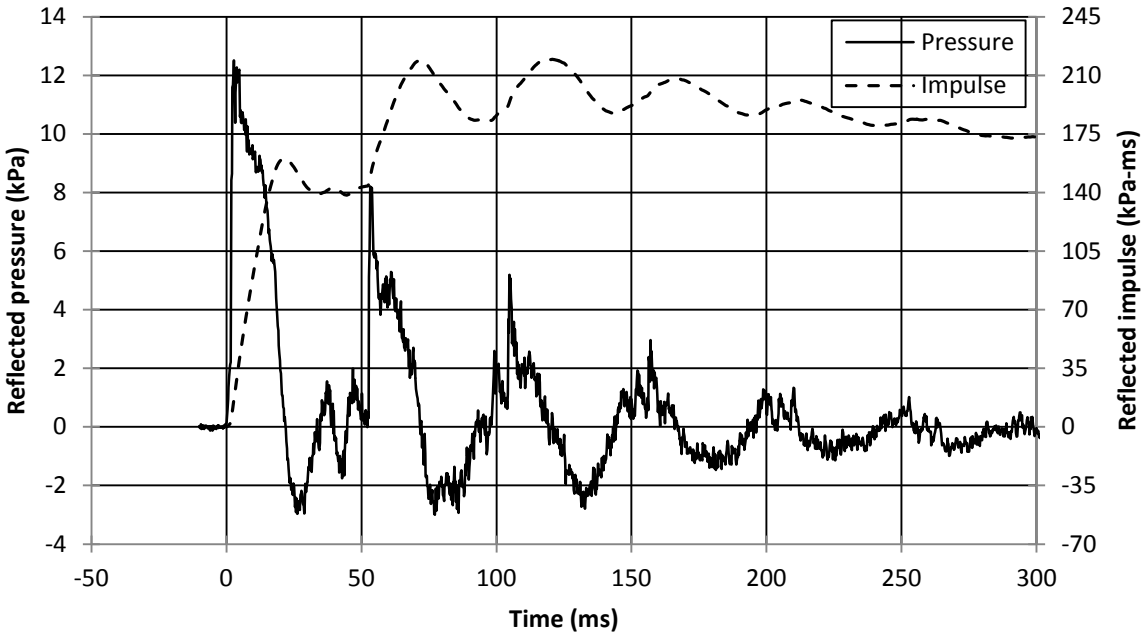

Figure B20-1.1: Reflected pressure and impulse time histories for Wall 20 Shot 1

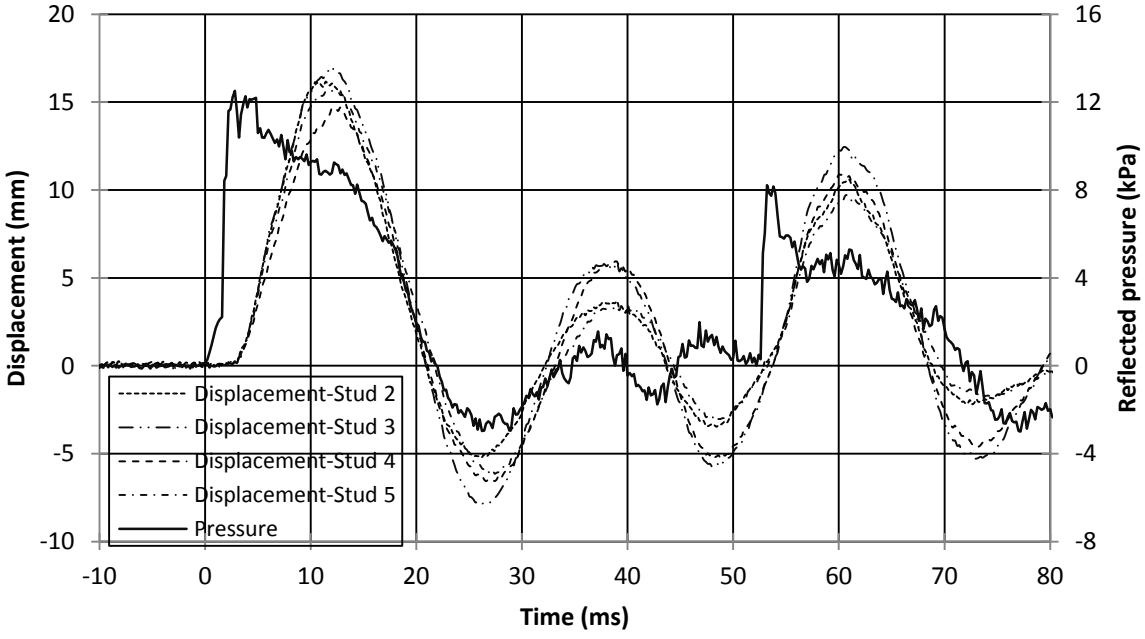

Figure B20-1.2: Displacement and pressure time histories for Wall 20 Shot 1

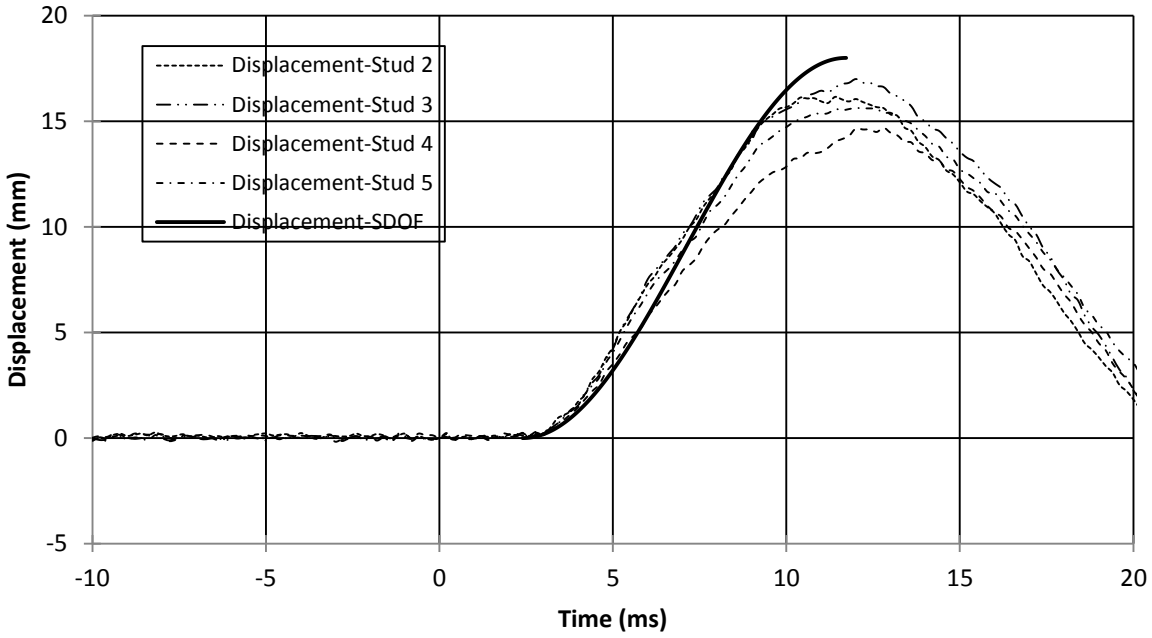

Figure B20-1.3: SDOF prediction for Wall 20 Shot 1

Wall 20, Pressure-Impulse Combination Number 2

Table B20-2: Wall 20, Shot 2-Test result summary

Light-Frame Stud Wall Dynamic Tests: Wall 20, Pressure-Impulse Combination Number 2

Test name:	Wall_20_Shot_2	**Test date:**	14/12/2012
Driver length:	2,745 **mm**	**Driver pressure:**	200.6 **kPa**

Test specimen description:

-6-38 mm x 140 mm MSR studs @ 406.4 mm o/c. -18.5 mm plywood

-Nails, 89 mm x 4.24 mm @150 mm o/c (field and edge)

-2,159 mm total height of wall -2,083 mm long studs -2,032 mm clear span

Average maximum reflected pressure:	31.0	**kPa**	**Wall mass:**	85.2	**kg**
Average maximum reflected impulse:	302.0	**kPa-ms**			
Experimental positive phase:	23.0	**ms**			
Theoretical positive phase:	19.5	**ms**			
Average deflection of wall studs:	41	**mm**			
Average time to maximum deflection:	11.7	**ms**			
Quantified wall damage:	**Superficial**				

Stud number	Stud reference name	Max. Disp.	Time to max.	Stud damage
		mm	ms	
1	54A	-	-	No damage
2	15A	38	9.2	No damage
3	17A	40	11.0	No damage
4	75A	34	10.8	No damage
5	10A	54	15.8	Cracked
6	83A	-	-	No damage

Response description:

Apart from Stud 5, the wall did not suffer any damage and remained elastic throughout its displacement history. Stud 5 was split lengthwise with an additional crack above mid-span initiating towards the top plate. No permanent deflection was observed in Stud 5. No sheathing failure. No nail withdrawal.

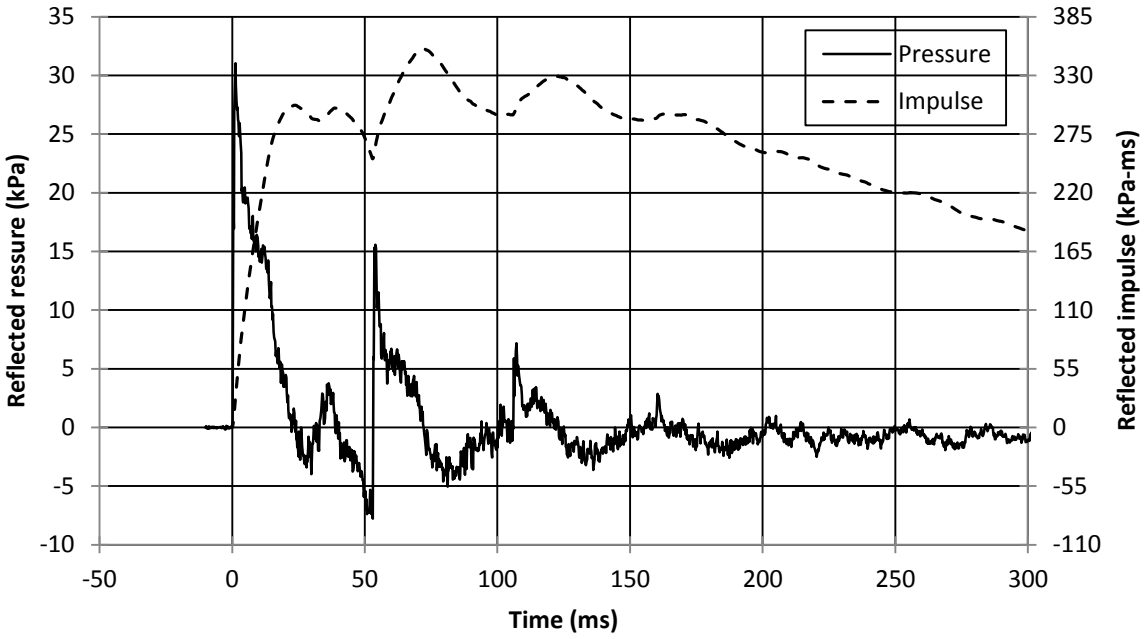

Figure B20-2.1: Reflected pressure and impulse time histories for Wall 20 Shot 2

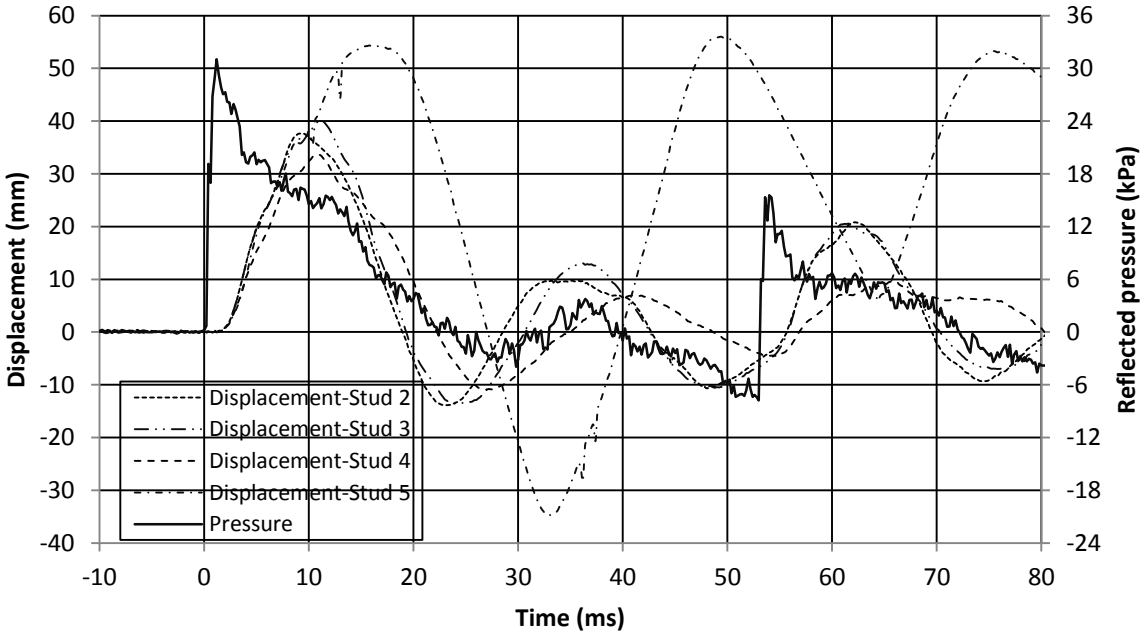

Figure 20B-2.2: Displacement an pressure time histories for Wall 20 Shot 2

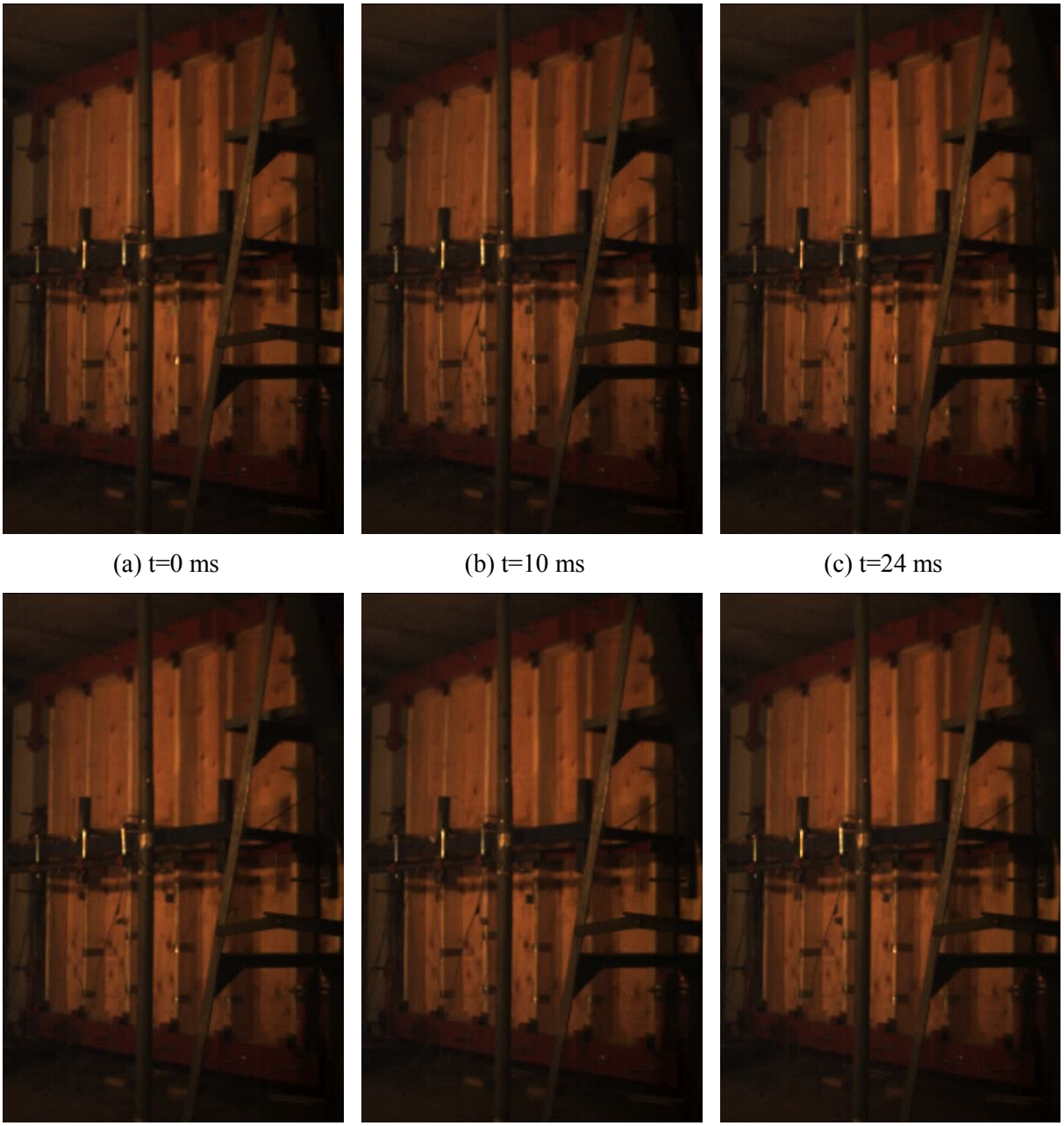

(a) t=0 ms (b) t=10 ms (c) t=24 ms

(d) t=40 ms (e) t=60 ms (f) t=100 ms

Figure B20-2.3: Evolution of damage with time for Wall 20 Shot 2

(a) View of entire wall

(b) Localized damage stud 5-Upper half

(c)Localize damage stud 5-Lower half

Figure B20-2.4: Damage of Wall 20 after shot 2

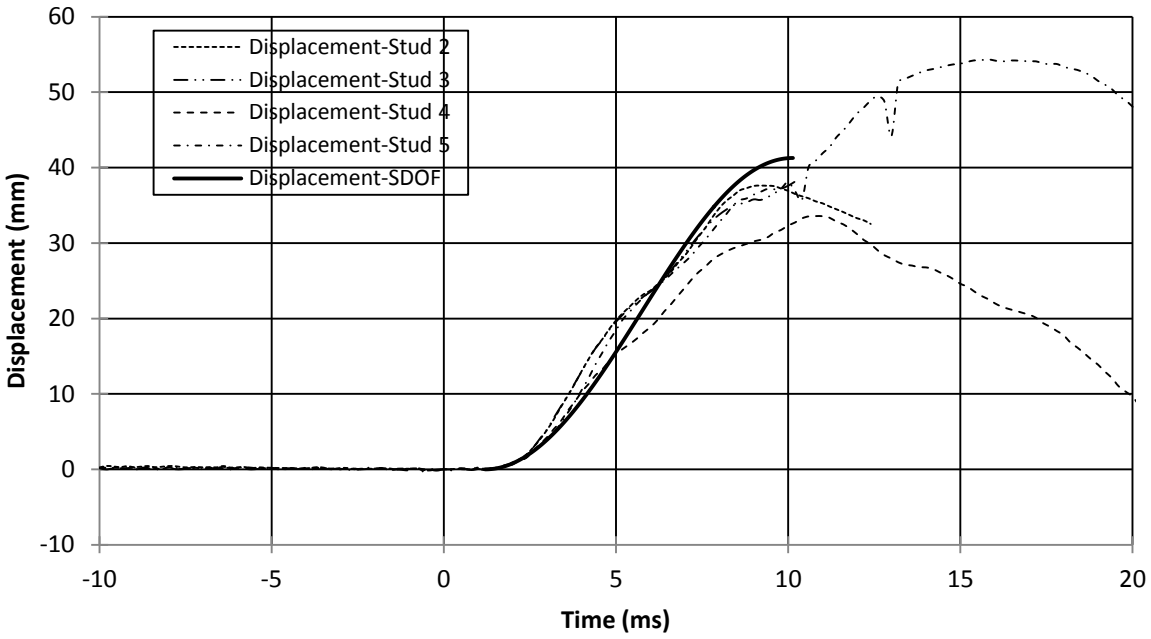

Figure B20-2.5: SDOF prediction for Wall 20 Shot 2

Wall 20, Pressure-Impulse Combination Number 3

Table B20-3: Wall 20, Shot 3-Test result summary

Light-Frame Stud Wall Dynamic Tests: Wall 20, Pressure-Impulse Combination Number 3

Test name:	Wall_20_Shot_3	**Test date:**	14/12/2012
Driver length:	2,745 **mm**	**Driver pressure:**	269.6 **kPa**

Test specimen description:

-6-38 mm x 140 mm MSR studs @ 406.4 mm o/c. -18.5 mm plywood

-Nails, 89 mm x 4.24 mm @150 mm o/c (field and edge)

-2,159 mm total height of wall -2,083 mm long studs -2,032 mm clear span

Average maximum reflected pressure:	38.7	**kPa**	**Wall mass:**	85.2	**kg**
Average maximum reflected impulse:	427.9	**kPa-ms**			
Experimental positive phase:	23.0	**ms**			
Theoretical positive phase:	22.1	**ms**			
Average deflection of wall studs:	61	**mm**			
Average time to maximum deflection:	11.9	**ms**			
Quantified wall damage:	**Heavy**				

Stud number	Stud reference name	Max. Disp.	Time to max.	Stud damage
		mm	ms	
1	54A	-	-	No damage
2	15A	54	9.8	No damage
3	17A	75	14.4	Failed
4	75A	55	11.6	Failed
5	10A	-	-	Failed
6	83A	-	-	No damage

Response description:

Studs 3, 4 and 5 failed during the first positive peak to maximum displacement. Sheathing failure is observed between Stud 4 and 5 as well as 5 and 6 which were sheathed with the half of the full size plywood sheet compared to Studs 1 to 4 which were covered by a full sheet. Nail withdrawal along Stud 4 was observed on both panel edges. Data was not recorded for Stud 5 as damage was already observed and to protect the LVDT from experiencing any damage.

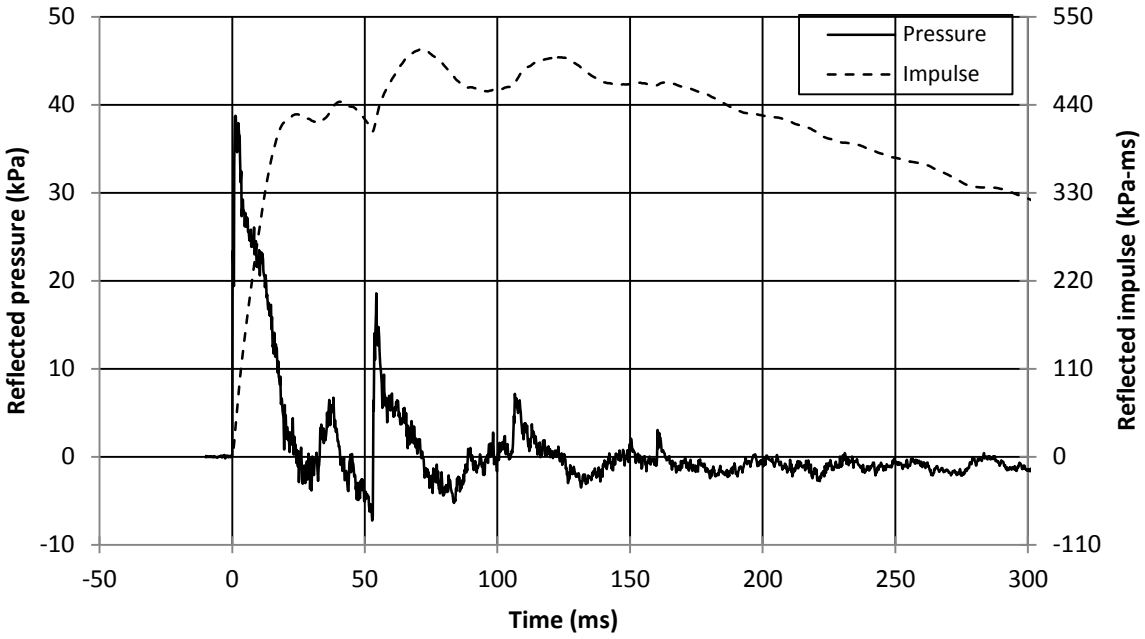

Figure B20-3.1: Reflected pressure and impulse time histories for Wall 20 Shot 3

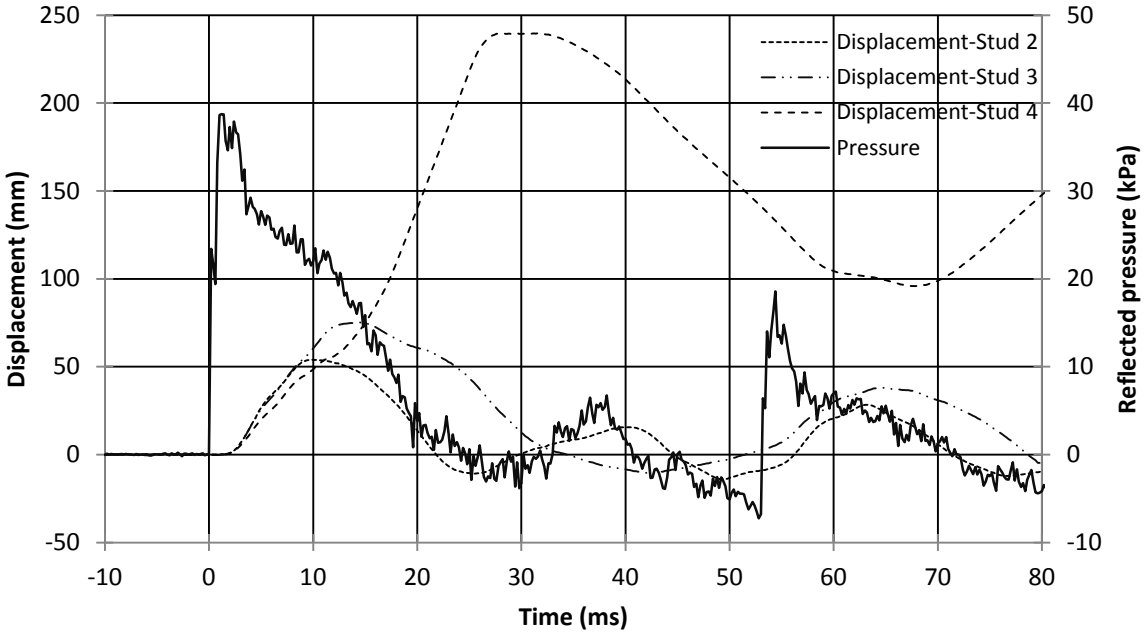

Figure B20-3.2: Displacement and pressure time histories for Wall 20 Shot 3

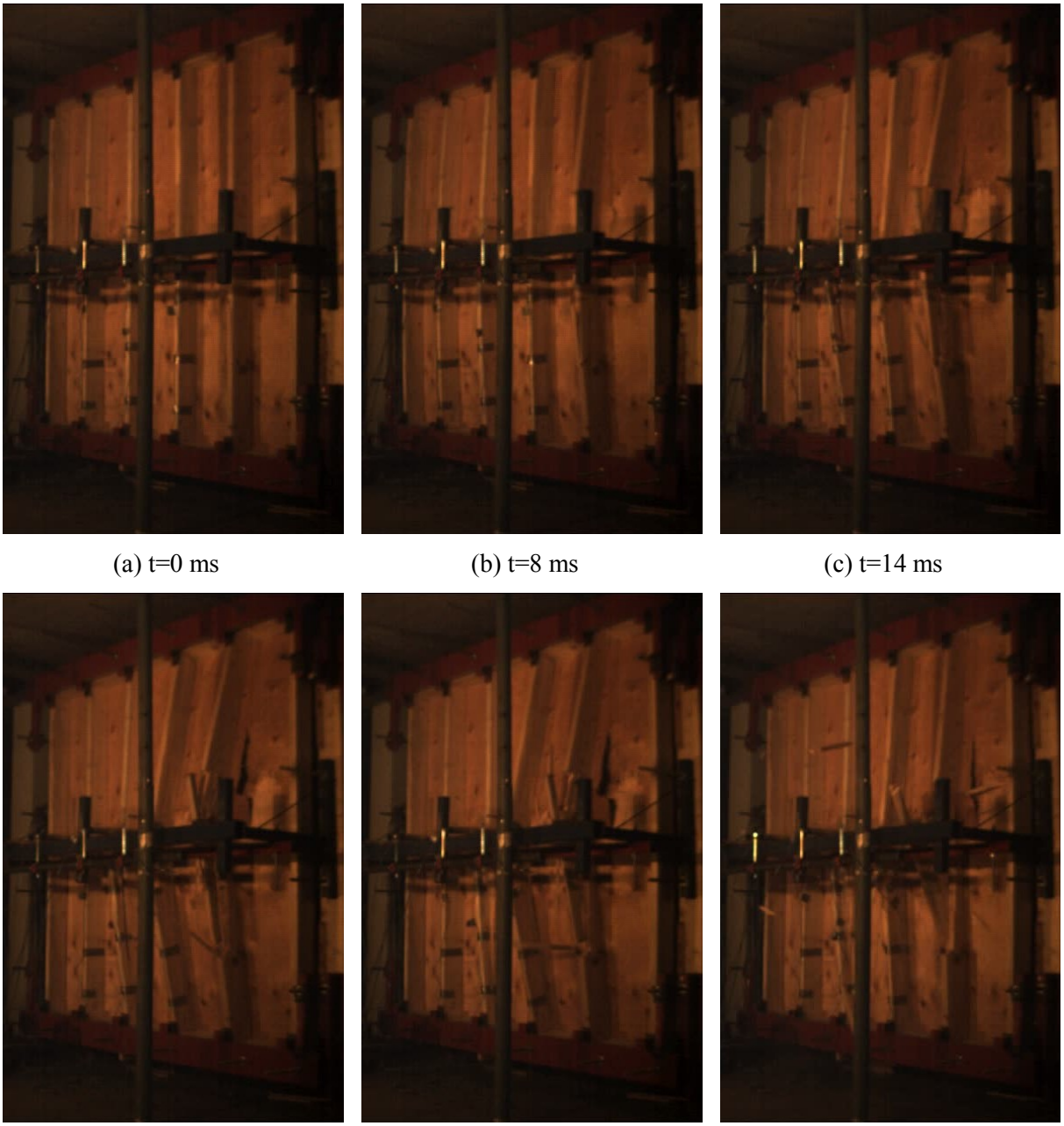

(a) t=0 ms (b) t=8 ms (c) t=14 ms

(d) t=22 ms (e) t=30 ms (f) t=100 ms

Figure B20-3.3: Evolution of damage with time for Wall 20 Shot 3

(a) View of entire wall from the right side

(b) View of entire wall from the left side

Figure B20-3.4: Damage of Wall 20 after shot 3

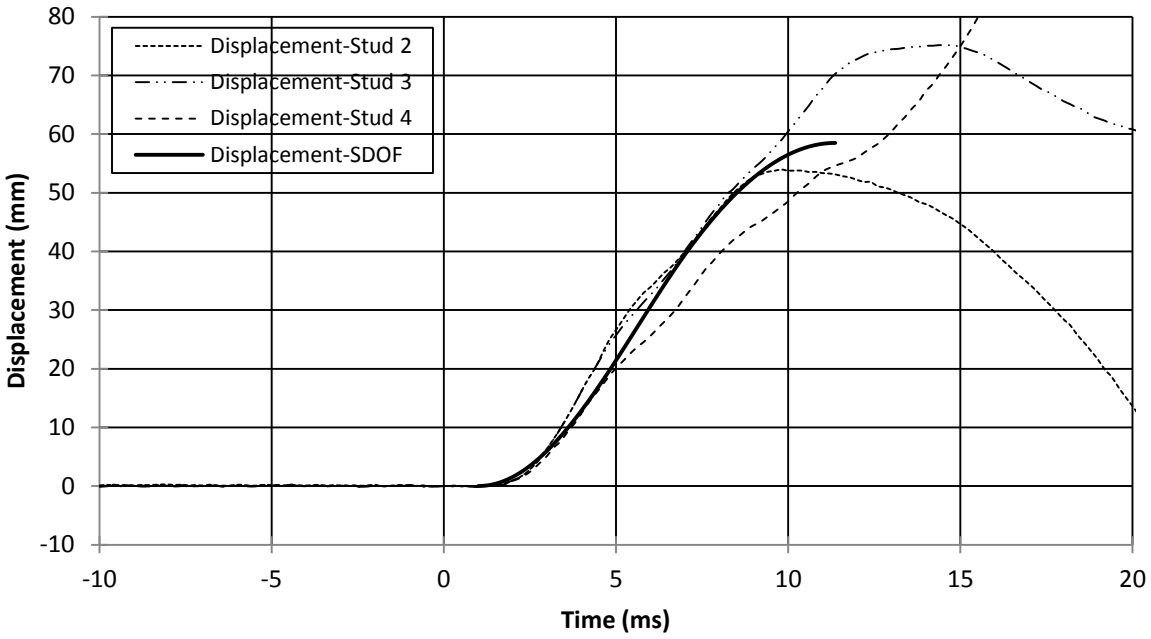

Figure B20-3.5: SDOF prediction for Wall 20 Shot 3